School of Physical Sciences
Department of Exploration Geophysics

Seismic Imaging of Sandbox Models

Donald H. Sherlock B.Sc. (Hons) U.W.A.

This thesis is presented as part of the requirements for the degree of Doctor of Philosophy of Curtin University of Technology

December 1999

ACKNOWLEDGEMENTS

This project was supervised by Dr Brian Evans of the Department of Exploration Geophysics, Curtin University of Technology, who I thank for his guidance, endless enthusiasm and above all, his friendship. I would like to thank my associate supervisor, Associate Professor Bruce Hartley, for his technical input and alternate perspective on many issues.

I thank MERIWA and WMC Petroleum, which initially funded this research, and particularly Dr. William French, former Vice President of Petroleum Geo-Services, for his initiative to continue support for this project after WMC Petroleum ceased to exist.

I would like to thank Milovan Urosevic, for always giving more information than was asked for and for encouraging me to question accepted wisdom. I also thank our computer systems manager, Murray Hill, for always making room for me at the front of a very long queue for his assistance.

I would also like to thank Anthony Gartrell and Richard Higgins from the Structural Geology and Analogue Modelling Laboratory at the University of Western Australia, for their input on sandbox modelling.

Special thanks go to my wife, Delice, for her unconditional patience and support through the hard times.

Abstract

Analogue sandbox models are important in the study of reservoir geology because they can offer insight into geological processes that we are rarely able to observe in nature. Seismic physical modelling is used to study the effects of seismic wave propagation in isotropic and anisotropic media and is particularly suited to isolating the effects of a single parameter independently from all others in an infinitely complex geological system. Seismic physical modelling has also been used for the testing of numerical processing algorithms, and to evaluate interpretations of field seismic sections with scaled representations of geological formations. For this project, I set about developing methods to combine these two independent modelling techniques for the first time. However, previous attempts to use sand as a seismic modelling material failed due mainly to problems with understanding and controlling the distribution of the grain packing.

This research has addressed a number of these problems through systematic laboratory experimentation that has provided new insight into the factors that affect unconsolidated sediment acoustics. An innovative technique of recording seismic physical modelling surveys has been developed so that it is now possible to successfully record ultrasonic reflections within analogue sandbox models in three-dimensions (3-D), providing benefits for both analogue sandbox and seismic modelling disciplines. For sandbox modelling, the recording of seismic images allows more detailed analyses of the structures than previously possible. For seismic modelling, more geologically realistic settings can be modelled at a fraction of the cost and construction time of conventional models. However, the greatest benefit of this new technology is that it is now possible to build seismic physical models from porous media, rather than solid, non-porous materials that are conventionally used. This scientific advance allows different fluids to be incorporated into physical models for the first time.

Time-lapse 3-D seismic is becoming increasingly important in the management of hydrocarbon production, yet there is a lack of model data to support some of the conclusions being deduced. The controlled physical modelling laboratory environment

combined with the ability to consistently repeat the 3-D seismic survey process now allows time-lapse seismic experiments to be performed without the need for the costly and time consuming data processing that is necessary to match legacy 3-D field data. This subsequently avoids any pitfalls that may be associated with the process, such as the masking of true fluid flow anomalies or the generation of false anomalies from data acquisition footprints.

A series of time-lapse models are presented where the three-dimensional movement of fluids through the models is remotely monitored using time-lapse 3-D seismic data. These models demonstrate the true seismic response that comes from recording real data from models that undergo real changes representative of reservoir environments. Such models are inexpensive and allow rapid data turn around in a matter of days. The techniques developed here provide a new research tool that can be used to improve our understanding of the dynamics of fluid flow within porous sediments, or to study the seismic response of reservoirs as they change with time.

TABLE OF CONTENTS

CHAPTER FOUR

LIST OF FIGURES

FIGURE **Page No.**

LIST OF TABLES

CHAPTER ONE

INTRODUCTION

1.1 Characteristics of reservoirs

Hydrocarbon reservoirs rarely have constant thickness, shape or internal characteristics. It is, therefore, essential to estimate reservoir and constituent facies architecture and geometry in order to optimise volume estimations and to assess reservoir connectivity and flow path tortuosity. Reservoirs are heterogeneous with respect to porosity and permeability. Internal variations result from the inherent sediment variability of depositional processes, localization of diagenetic effects and deformation after burial. An appreciation of fluid flow through sand requires an understanding of the scale, density, distribution, geometry and inter-relationships between various heterogeneities. This is required to assess their relative importance to hydrocarbon accumulation, distribution and recovery. Production well spacing is rarely sufficiently close to quantitatively evaluate these parameters in any given oil field.

Analogues are of great importance in the study of reservoir geology because it is not possible to observe the development of rocks and structures first hand. Alexander (1993) provides a comprehensive discussion on the use of analogues for reservoir geology. There are three types of analogues used to help our understanding of geology, namely

i) comparisons with modern depositional systems,

ii) rock record analogues, and

iii) experimental simulations in the laboratory.

Each of these methods has limitations and scaling problems in both the physical and temporal sense. Modern depositional analogues are based on the premise that 'the present is the key to the past', which is not necessarily a valid assumption. These types of comparisons are effective for getting a 'feel' of the geology, but are seldom adequate

for quantitative data. Rock record analogues are comparisons with data, such as core or outcrop, from other geological settings. These data may be used to describe a sedimentary succession, but using such data to predict sedimentary facies, diagenetic features or fracture distribution in unsampled areas can be misleading if the analogue is inaccurate or stretched beyond reasonable limits.

Laboratory simulations, which are the focus of this thesis, can offer valuable insight into the geological processes that we are unable to observe in nature. They are particularly suited to isolating the effects of a single parameter independently from all others in an infinitely complex geological system. A reservoir simulation that gives valuable results does not necessarily have to be geologically correct. The aim of reservoir simulation models is to help estimate recoverable hydrocarbons and production characteristics, not to reproduce the geology. However, models that are more geologically realistic and closer to the truth will, in general, give more reliable results.

1.2 Overview of the Use of Models

Scaled models of geological processes, using analogue materials, have proved to be very powerful tools in the study of structural processes produced in nature, especially where the phenomena are poorly understood (Vendeville *et al.*, 1987). Such modelling has proved to be particularly successful in the structural analysis of extensional fault systems (Harris *et al.*, 1994; Cockshell *et al.*, 1995; Gartrell, 1997; Higgins and Harris, 1997).

Analogue sandbox models offer cheap, concise data and allow the evolution of structures to be observed, leading to a better interpretation of structural systems. The model builder can control the boundary conditions, and then compare the results of modelling to natural geological examples, in order to either negate or substantiate possible mechanisms for the development of geological structures. Analogue models offer significant advantages over numerical models. For example, discontinuous behaviour, such as reactivation, can be modelled in three dimensions (McClay, 1989),

and can be directly compared with geological structures for improved conceptual visualization of the processes involved. This type of modelling is very difficult to simulate numerically.

Seismic methods to produce an image of geological structures evolved during the 1920s. Now, reflection seismology is the key method in mapping subsurface geology for petroleum exploration. Three-dimensional (3-D) seismic surveying was developed to understand the full 3-D structure of geology. French (1974) simulated the 3-D seismic method, using simple plastic physical models to explain how two-dimensional (2-D) methods were inadequate to describe 3-D geology. The collection of seismic data over physical models, known as 'seismic physical modelling', has two great advantages over working with field data. That is, it is orders of magnitude cheaper than performing field surveys, and the 'geology' is known so its effects on wave propagation can be directly measured and understood. Physical modelling experiments have been performed at Curtin University since 1991, to study the 3-D effects of seismic wave propagation in isotropic and anisotropic media.

Seismic reflections detected in physical models are most often based on velocity contrasts alone. The construction of a conventional 3-D model is a complicated task, and takes months of testing of the plastics and resins used to model sedimentary sequences (Evans *et al.*, 1995). Once a model has been poured and solidified, it is placed under water. Ultrasonic transducers are then used to record 2-D and 3-D seismic data under computer control in a known x, y and z coordinate system. This capability offers great potential as a scientific tool, to understand the seismic expression of various structural styles, and offers insight into future methods of 2-D and 3-D seismic acquisition and processing for improved target mapping.

Prior to this research, all seismic physical modelling has had to be performed using solid models, which are constructed with pre-determined structures built into the model. This restriction imposes constraints on the realism or 'natural variation' within the model. The ability to apply this technology to cohesionless sand analogue models would dramatically reduce the cost and time involved in construction of the model.

Sandbox modelling is a dynamic process, developing structures that form with many of the idiosyncrasies of natural systems. Hence, the production of seismic profiles from such models would provide a new modelling concept in understanding three-dimensional geology.

A major problem in the past that has prevented the application of seismic imaging methods to sandbox models has been the severe energy attenuation of sonic waves as they travel through the sand matrices (Purnell, 1986). This is due to a number of factors such as energy loss due to friction between grains in the unconsolidated matrix, an unrealistic ratio of grain size to seismic pulse wavelength, and problems of uneven grain packing and pore space distribution. This prompted seismic experiments on the testing of grain mixes within consolidated matrices, such as silicon rubber (Purnell, 1986), and resins (Zhang *et al.*, 1996), where grain distribution was controllable. However, a fundamental goal of this work was to overcome such problems, and move the technology forward.

1.3 Aims of the Research

The petroleum industry adopts two approaches to interpreting geological formations in the search for hydrocarbons. One is the seismic method, which provides an image of the subsurface geology, and the other is the geological approach, which tries to understand the three-dimensional evolution of the structures, and hence predict the presence of hydrocarbons. Physical models provide an alternative that can combine many aspects of both approaches. This project was aimed at developing the modelling and seismic techniques required to provide 2-D and 3-D images from analogue sandbox models of geological settings.

The path taken to achieve the aims of this project was to firstly identify and understand the factors that affect the acoustic properties of unconsolidated sand through systematic experimentation in the laboratory. The results from these experiments would then be

used to guide the development of techniques to alter the acoustic properties of different layers within sandbox models, thereby allowing the subsequent ultrasonic 3-D imaging of analogue geological systems. The second part of this project, developed in parallel with the first, was to address some of the limitations inherent with the seismic physical modelling system, such as problems with recording data at variable offsets. This combined approach would hopefully lead to the development of geophysical techniques to provide more accurate seismic images of model structures, eventually resulting in better methods for seismic acquisition, processing and interpretation.

Once the techniques of imaging sandbox models reached an adequate level of refinement, the final goal of this research was to develop time-lapse seismic imaging of sandbox models that have undergone changes caused by fluid movement through them. This would take advantage of two fundamental benefits of seismic physical modelling. That is, the ability to build seismic physical models from porous media, developed for this project, combined with the repeatability of data acquisition that is inherent with the physical modelling system.

The development of techniques to build physical models from porous media would allow different fluids to be incorporated into physical models for the first time. The acquisition repeatability that is possible with the physical modelling system would permit direct comparisons between seismic images recorded at different stages as fluids flow through the model. These time-lapse comparisons could be performed without the complex data processing and compromises that accompany such exercises in the field. This would also provide rapid data turn around in a matter of days, rather than having to revisit an area years later, and provide time-lapse data for analysis at a fraction of the cost of acquiring field data. The end result would be the development of a new research tool that could be used to better understand the mechanisms of hydrocarbon fluid flow and the subsequent effects on the acoustic properties of reservoirs.

1.4 Importance of this Research

The development of the techniques to enable seismic images to be recorded from analogue sandbox models provides benefits for both analogue sandbox modelling and seismic physical modelling. For sandbox modelling, the recording of seismic images allows more detailed analysis of the structures than previously possible and can provide the missing link between comparing structures within a model and seismic data from the field. For seismic physical modelling, the main advantages are that the data collected contain natural features that cannot be built into conventional physical models, resulting in a more realistic image, and the cost and construction time of the models is dramatically reduced. However, the biggest potential for seismic sandbox modelling is to use the time-varying characteristics of the models to better understand changes that take place within reservoirs as a function of fluid flow. Seismic monitoring of subsurface fluid flow has potential impact in the enhanced recovery of hydrocarbons, groundwater and environmental studies, and in a broader context, global climate issues and improved understanding of plate tectonic mechanisms.

Time-lapse 3-D surveys of producing reservoirs are becoming increasingly common in the petroleum production industry for mapping changes in fluid movement that occur with the extraction of hydrocarbons. The most powerful application for time-lapse seismic data is its use as an interactive diagnostic tool. Coupled with fluid flow simulation and hydrocarbon production history matching, time-lapse seismic can potentially help to better understand the dynamics of fluid flow and ultimately improve the efficiency of hydrocarbon extraction from the subsurface. However, many of the changes observed on time-lapse 3-D surveys cannot be interpreted with any confidence due to a multitude of problems involved with the imprecise duplication of the acquisition parameters and the complex data processing that is required to allow valid comparisons. Physical modelling provides an ideal environment for studying these changes because surveys can easily be repeated with the same parameters. In this way, most of the problems that plague field studies can be avoided and it is known that any changes seen on later seismic surveys must be a result of changes within the model.

1.4.1 The Need for Laboratory Measurements

The acoustic properties derived from laboratory measurements of unconsolidated sands vary widely in the literature and the measured velocities do not match those predicted from empirical models based on porosity. The disparity occurs because the acoustic properties of sediments at low pressure depend mainly on the nature of the grain contacts, which are highly sensitive to small changes in grain sorting, compaction and saturation. Differences will exist not only between similar sands, but also between different samples of the same sand. For these reasons, it is not feasible to rely on published data on the acoustic properties of unconsolidated sand to predict the response of the sands used in this thesis. A comprehensive series of acoustic measurements were required to establish the behaviour of the sand used under the exact conditions that they would be subjected to in the models. I will show with these tests that the methods used to build the models are just as significant as the actual physical properties of the sands.

1.5 Organisation of the Thesis

This research combines two distinctly different modelling methods, namely seismic physical modelling and analogue sandbox modelling. Before each of these concepts is discussed, a brief introduction to the seismic method is provided in Chapter Two, with an emphasis on the principles of time-lapse 3-D seismic. An overview of modelling techniques is provided in Chapter Three. This includes a detailed analysis of some of the inherent limitations involved with seismic physical modelling which are demonstrated with a series of experiments. I have included a number of innovations, devised as part of this research to address these limitations, in this Chapter.

The theory of unconsolidated sediment acoustics is discussed in Chapter Four, which includes a breakdown of the individual parameters that affect the seismic velocity and rate of attenuation within unconsolidated sand. This is followed by a comprehensive

series of laboratory experiments on the testing of the acoustic properties of unconsolidated materials in Chapter Five, which also includes the development of methods to record ultrasonic reflections from within sandbox models.

All of the techniques I developed to that point are then combined in a series of models that I present in the first half of Chapter Six. The lessons I learnt from these models, together with results from acquisition repeatability tests, culminate in a final set of three time-lapse models that are presented along with a discussion to complete the chapter. Conclusions and recommendations for future work are presented in Chapter Seven, followed by the References to complete the thesis.

The nature of this project is one of progressive refinement, where I developed improvements in fundamental techniques for several key areas of the research. For example, improvements in data acquisition techniques evolved simultaneously with, but independently of, improvements made to model building methods. As such, progressive examples presented in the data acquisition chapter utilised any improvements made in model building as they evolved. This should to be taken into account when comparing results between different vintages of data. Hence, although I present this thesis as discrete chapters which each cover a specific aspect of the research, improvements made in one area may manifest themselves in examples presented in other chapters.

The seismic images presented in this thesis represent only a small fraction of those recorded over hundreds of models during this research. Data from every experiment performed have been archived and catalogued, and are being held at the Department of Exploration Geophysics, Curtin University of Technology.

CHAPTER TWO

THE SEISMIC METHOD

2.1 Introduction

This section presents a brief overview of the basic terms and concepts of seismic surveying to image the subsurface. It is not within the scope of this thesis to comprehensively cover all of the theory involved. Readers wanting more detail than that provided here should refer to textbooks such as those by Evans (1997) for seismic data acquisition, Yilmaz (1987) for data processing and Brown (1996) for interpretation. Readers already familiar with the general concepts may prefer to move on to time-lapse seismic methods in Chapter 2.2.

Seismic reflection simply involves the release of an energy impulse, which causes a pressure wave to radiate outwards from a source located near the Earth's surface, and the recording of reflected energy arriving later at the Earth's surface. Reflection seismic surveying is the dominant method of understanding the three dimensional (3-D) geometry of geological structures in petroleum exploration and also has applications in mineral exploration (Evans, 1997). Deep reflection seismic profiling is also used to provide information of the lithospheric-scale structure of orogenic belts with associated applications to mineral exploration (Clowes, 1994).

Many millions of dollars are spent by the petroleum exploration industry to obtain drilling and seismic data in an attempt to resolve the geology of the subsurface. Much of the mapping interpretation is 'best guess accuracy', using seismic profiles that have many possible alternative interpretations and in some cases contain 'ghost' structures that are not present in the actual geology (Tucker and Yorston, 1973). Additional costs are then incurred to check if reservoir conditions are favourable. The locations for drilling are determined from the seismic interpretation, with only a low probability of

actually intersecting a significant hydrocarbon reserve. In deep reflection seismic profiling, interpretation problems are exacerbated, as it is not possible to check interpretations by drilling to the base of the crust.

The seismic reflection method is based on observing the time it takes for energy (which is created artificially at a known location or 'shot-point') to be reflected from geological boundaries within the Earth back to a line, or lines, of known receiver-points at the surface (Sheriff and Geldart, 1982). If the shot-points and receiver-points lie along the same line, the survey is said to be two-dimensional (2-D). A 2-D survey creates a representation of a vertical section of the Earth. If the receiver-points lie along lines other than those of the shot-points, the survey is said to be three-dimensional (3-D). 3-D surveys create data cubes, from which seismic information may be extracted in any vertical or horizontal direction. Vertical sections that are parallel to the shot-points in a 3-D survey are said to be 'in-line', while sections perpendicular to the shot lines are referred to as 'cross-lines'.

2.1.1 Data Acquisition

There are many differences in the methods of acquiring seismic data between land and marine surveys, however the principles remain the same.

2.1.1.1 Source and Receiver

The ideal seismic source emits a waveform with a wide bandwidth and short duration. On land, vibrators are commonly used, while marine surveys generally use air guns. The application of a source depends on a compromise between a number of factors such as reflected frequency range, energy content, safety and operational cost. Other important features of a good source are that it is quickly and consistently repeatable, and has a pulse of known shape.

In marine work, seismic receivers convert pressure differences associated with the reflected seismic pulse into an electrical signal and are known as 'hydrophones'. On land, 'geophones' are used, which convert mechanical movement into an electrical signal. Many of the factors that make up a good source also apply to receivers. A good seismic wave detector must be able to receive a wide frequency band with a high signal-to-noise ratio (SNR). Receivers should also be light, small, robust and require a minimum of maintenance.

2.1.1.2 Survey Design

The type of survey and the nature of the geology under examination determine line spacing. For reconnaissance work, large line spacings may be used to give a regional picture (eg. 50 km), and in-fill lines with smaller spacing (500 m) may be added later. As a rule of thumb, if the geological horizons from one line cannot be followed onto the next, then the lines are too far apart. In 3-D surveying, a line spacing as short as 25 m may be used to provide a detailed geological image. Logistical and economic constraints must also be considered when designing a survey, and these factors may have as much bearing on the quality of the final image as does the subsurface geology.

2.1.2 Processing

The position from which the energy is reflected is assumed to be halfway between the shot-point and receiver location, which is commonly referred to as the common mid-point (CMP). In a 3-D survey, the CMP is replaced with a CMP bin, which contains data reflected from a given area. Reflections from the same CMP are recorded by using a number of source and receiver positions, and these repeated traces are summed together or 'stacked' in order to improve the signal-to-noise ratio. This is the ratio between the reflection data recorded and other unwanted events, which are referred to as noise. The number of traces gathered together in a CMP defines the 'fold' of coverage. The recorded data is then 'processed' to remove unwanted noise and to correct for all changes in reflection amplitude which are not results of the interaction

between the seismic wave and the boundary of interest. Correcting for these other factors that affect amplitudes is called 'True Amplitude Processing' or 'TAR' (Sheriff and Geldart, 1983). The data are then re-sorted so that all traces recorded from the same CMP are contained in a single file or 'CMP-gather'. Corrections for the arrival time differences for different source-receiver distances, which are called 'normal move-out' (NMO) corrections, are then made, and all of the traces within the same CMP gather are summed or 'stacked'. This creates a stacked section that represents an image of the geology beneath the line along which the shots and receivers are placed. Once the data has been stacked it is referred to as being in the 'post-stack' domain, whereas prior to stacking it is referred to as being in the 'pre-stack' domain.

2.1.2.1 Migration

On seismic sections, the reflection points are only located directly beneath the source and receiver when the reflecting layer is horizontal. Migration is the process of reconstructing a seismic section so that reflection events from dipping beds are repositioned to their correct location and reflection time (Yilmaz, 1987). It also has the effect of collapsing diffractions back to their point source and thereby improves the SNR. The success of migration depends on both the accuracy of velocity information and spatial sampling. The recording area must be greater than the subsurface area of interest, and must be extended over areas of steepest dip (Lynn and Deregowski, 1981).

2.1.3 Interpretation

Reflection events are traced across a seismic section by correlating arrivals from trace to trace, and in this way the distribution of subsurface reflections are mapped. It is important to note that, while seismic sections appear similar to a geological cross-section, the vertical axis is usually time, not depth, and so the images are distorted from their true geometry. Conversion of data from the time domain to the depth domain is becoming increasingly common when the velocity information is of sufficient accuracy.

There are two major benefits of 3-D data over 2-D data. These are greater resolution and more accurate reflector positioning. There are a number of other benefits as well. With 2-D data, interpretations are correlated from line to line by comparing events at profile intersections. With 3-D data, the interpreter has all the reflection data contained within the seismic data volume, and is able to use a computer to select various types of data for display, such as vertical sections in any orientation or horizontal time slices.

2-D profiles from a 3-D data set can be displayed in any orientation, and this gives the interpreter more insight into the geometry of structures. Time slices are horizontal sections through the time scale and highlight features such as lateral variations of fault positions. If the 3-D data are of high enough quality to allow accurate interpretation of reflecting horizons, maps of each horizon can be generated as topographical contour maps, amplitude contour maps, or as a 3-D volume, and can be oriented to highlight particular structures of interest. However, 3-D surveys are much more expensive to acquire than 2-D and are therefore used for detailed mapping, whereas 2-D is considered a regional survey tool.

The hydrocarbon industry currently uses a number of visual signatures on seismic sections to assist in the search for hydrocarbons. These are called 'direct hydrocarbon indicators' (DHIs), which have significantly increased the success ratio for drilling wildcat wells. Some common DHIs are high amplitude anomalies or 'bright spots', phase changes, flat spots, time sags, frequency shadow zones and chimney effects (Yu, 1985). Fluid interfaces may also be recognisable as 'flat spots' which are horizontal events in areas where the local geology is dipping (Brown, 1996). Bright spots occur because of the large acoustic impedance contrast at the top and bottom of gas zones. Unfortunately, amplitude anomalies may also be due to a number of geological features, such as high-velocity lenses or low velocity gas-sands. In recent times, the industry has turned to examining the amplitude variation with offset in pre-stack CMP gathers to determine the presence of gas-sands (Castagna and Backus, 1993) and infer the presence of fracture zones (Urosevic *et al.*, 1995).

2.1.3.1 *Structural Analysis*

Structural analysis involves determining the reflector geometries on the basis of reflection arrival times. The major application of this type of analysis is in the search for structural traps containing hydrocarbons. Time-structure maps can be constructed with contours of equal reflection time. These maps are very similar in appearance to structural contour maps (which can be produced from time-structure maps if the appropriate velocity information is available). However, they may be subject to distortion associated with lateral or vertical changes in the velocity of waves through the subsurface.

Problems often arise when producing these maps due to difficulty in correlating reflection events across areas that suffer from a poor SNR, structural complexities, or rapid stratigraphic transition that is beyond the resolution of the data. In some cases, reprocessing of the data may be able to overcome these problems. Additional in-fill seismic lines are sometimes needed to resolve problems with an initial interpretation.

2.1.3.2 *Stratigraphic Analysis*

Stratigraphic analysis using seismic stratigraphy methods identifies distinct depositional sequences as seismic expressions of the lithology. Reflection packages are used to define chronostratigraphic units, typically bounded by angular unconformities such as onlap, downlap, toplap or erosion on a regional scale (Keary and Brooks, 1991). Diachronous lithological units tend to be transitional and not produce reflections.

Once a seismic section has been subdivided into its constituent sequences, each sequence may be analysed in terms of its character, which is a method known as 'seismic facies analysis'. On a regional scale, parallel reflections characterise some shallow marine depositional conditions, while sigmoidal or oblique cross-bedded reflectors indicate deep marine conditions (Sheriff, 1980). Methods of seismic stratigraphy applied to sedimentary basins with little geological control often enable

correlation of locally recognized depositional sequences with a worldwide pattern of sea-level changes (Mitchem and Vail, 1977).

Identifying the sedimentary environments is extremely important in locating hydrocarbon traps, since they indicate the suitability of the conditions for potential source, reservoir and/or seal rocks. Organic-rich basinal muds represent potential source rocks, sand bodies formed in shelf environments represent potential reservoir rocks, and evaporite sequences make ideal seals.

The interpretation of field data of fault and fracture zones cannot be unique. Different geological configurations can produce similar results, and most seismic profiles can lead to non-unique interpretations. Correlation of reflections between adjacent profiles can be difficult when the horizons are not continuous. Steeply dipping reflectors are not able to be imaged because the signal is reflected away from the survey area. Physical modelling of such geology offers significant assistance to interpretation as there is no way of checking the real results in field data (other than from wells, which is barely adequate for extrapolation across an entire section). Many of the characteristics mentioned above can be built into physical models of geology to allow an inexpensive method of testing interpretation techniques.

2.1.4 Seismic Wave Propagation

Seismic wave transmission through an elastic solid, such as the Earth's crust, is known as 'elastic wave propagation'. Several kinds of waves can occur, and each type is classified according to how the seismic energy vibrates the rock matrix particles, as the wave travels through it. Of the many types of seismic wave, the two fundamental types are the compressional and shear waves.

2.1.4.1 *Compressional Waves (P-Waves)*

When a seismic energy source is fired, there is an initial volume decrease of the medium upon which the force acts, followed by an immediate rebound or expansion. This develops into a seismic wave, which is referred to as a primary compressional wave, or 'P-wave'. In this case, the particles of the rock move back and forth in the direction of wave propagation. Unless specified otherwise, the use of the term velocity in this thesis refers to the P-wave velocity.

2.1.4.2 *Shear Waves (S-Waves)*

When an energy source is fired, secondary waves are also produced, known as shear waves (S-waves). These waves travel in the same direction as the P-waves, but in this case their particle motion is perpendicular to the direction of wave propagation. The velocity of S-waves is a function of the resistance to shear stress of the material through which the wave is travelling and is often around half of the material's P-wave velocity. S-waves do not occur in water because shear stresses do not propagate in fluids, except when the viscosity is very high.

2.1.5 Velocity

Velocity is a function of the rigidity and density of a medium, and can range from around 500 ms^{-1} in some sands, up to 7500 ms^{-1} in dense ultramafic rock (Carmichael, 1989). For a wide range of sedimentary rocks the P-wave velocity is related to the density, and established velocity-density curves have been published (Sheriff and Geldart, 1982). The velocity increases very rapidly with confining pressure over the first 100 MPa. The velocity in unconsolidated sand (the most relevant sediments to this thesis) increases with depth of burial and age, due to progressive compaction and cementation. The factors that influence the velocity in unconsolidated sand are discussed more fully in Chapter Four.

2.1.6 Seismic Reflections in Layered Media

The acoustic impedance of a rock is defined as the density multiplied by the sonic velocity of the rock. At a layered interface in the subsurface, there is often a contrast in the acoustic impedance between the rocks on either side of the interface. Seismic energy incident on this interface is partitioned into transmitted and reflected energy and the relative proportion of each is determined by the acoustic impedance contrast across the boundary. Consider the boundary between two layers of velocities V_1 and V_2, and densities of ρ_1 and ρ_2. The reflection coefficient (R_C) provides the relative amplitude of a normally incident wave reflected from a boundary between two rocks where,

$$R_c = \frac{\rho_2.V_2 - \rho_1.V_1}{\rho_2.V_2 + \rho_1.V_1} \quad . \tag{2.1}$$

2.1.6.1 Multiple Reflections

'Sea-bed' or 'water-bottom' multiples are caused by the high acoustic impedance contrasts between the air and sea, and between the sea and sea-bed, where the seismic energy rebounds from one interface to the other. Interbed or 'peg-leg' multiples can occur when a portion of the incident wavefront energy becomes internally reflected within a layer. Both of these multiple types are illustrated in Figure 2.1.

Multiples are not always easy to recognize and could be mistaken for reflected events. The problem is that they are unwanted signal that has the same appearance and similar travel times to normal reflections. They are therefore treated as coherent noise events. If multiples are generated, there are several data processing techniques that can remove or at least partially attenuate them.

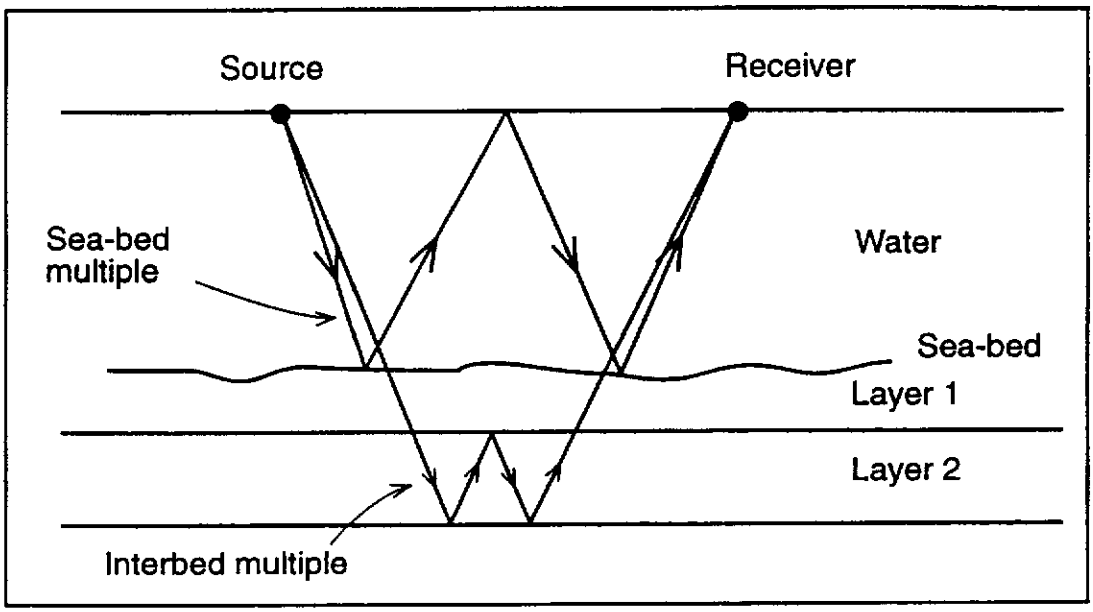

Figure 2.1: Ray paths for sea-bed (or water-bottom) and interbed (or peg-leg) multiples.

2.1.7 Attenuation of Energy

Wavefront energy gradually decreases in amplitude as it passes through a rock for two reasons - spreading loss and attenuation. As a seismic wave expands outwards from the source, the energy (which remains constant if absorption is ignored) has to spread over an increasingly larger area. Attenuation occurs because rocks are not perfectly elastic and the rate of attenuation is particularly high in unconsolidated sands. In general, high frequencies are attenuated more than low frequencies. The mechanisms of attenuation are discussed more fully in Chapter Four.

2.1.8 Resolution

Resolution is the ability to distinguish individual features contributing to an observed effect and depends largely on the frequency of the signal. Seismic surveys are designed for specific geology at varying depths. Different limiting factors apply to vertical and horizontal resolution and will be discussed separately.

2.1.8.1 Vertical Resolution

Since high frequencies are more readily absorbed than low frequencies during wave transmission, the high frequency content of seismic waves decreases with depth. Resolution is related to the frequency component, and hence, resolution also deteriorates with depth. The typical resolution of field seismic surveys is a few metres for shallow reflections, and a few tens of metres for deep reflections.

When the distance between two reflectors is less than $^1/_4$ of the wavelength, interference between the two reflected waves is destructive and distinction of the two reflectors becomes increasingly difficult. Reflections from the top and base of a thin bed interfere to produce amplitude variations known as 'tuning' effects. The definition of the absolute limit of vertical resolution is between $^1/_8$ and $^1/_4$ of the wavelength depending

on the criteria for ascertaining (Sheriff, 1994). The Rayleigh (1945) limit is $\lambda/4$ where λ is the dominant wavelength. The Widess (1973) limit is defined as $\lambda/8$. All of these limits assume that the data is essentially noise free and that changes in the waveform are not a result of the geology. The practical resolvable limit is accepted as $\lambda/4$ but beds thinner than this can sometimes be resolved from amplitude information provided that the variation in amplitude is purely a result of variations in thickness (Kallweit and Wood, 1982).

Resolution is also decreased if the signal is resonant (or 'ringy') and this is a major problem with seismic physical modelling because the ultrasonic transducers used for the source do not generate simple pulses, but rather a long wavetrain that resonates for several cycles. Koefoed (1981) showed that with zero phase signals, vertical resolution is also controlled by the side lobe ratio, which is defined as the ratio of the amplitudes of the side lobes to that of the central lobe. The signal emitted from the ultrasonic transducers is not zero phase but has strong side lobes, which effectively limits the resolution for the seismic physical models in this thesis to around one wavelength.

2.1.8.2 Horizontal Resolution

According to ray theory, a reflection is assumed to emanate from a 'point'. However, from wave theory we know that seismic energy travels as wavefronts and subsequently a reflection does not come from a point, but rather is generated by integration over an area called the Fresnel Zone (Lindsey, 1989). The centre of this area is the point we generally consider as the reflection point (Figure 2.2). Within the Fresnel Zone, constructive interference of the reflected seismic energy occurs. The size of the first Fresnel Zone defines the lateral resolution obtained by seismic reflection data and is a function of velocity, frequency and reflector depth (Sheriff, 1977).

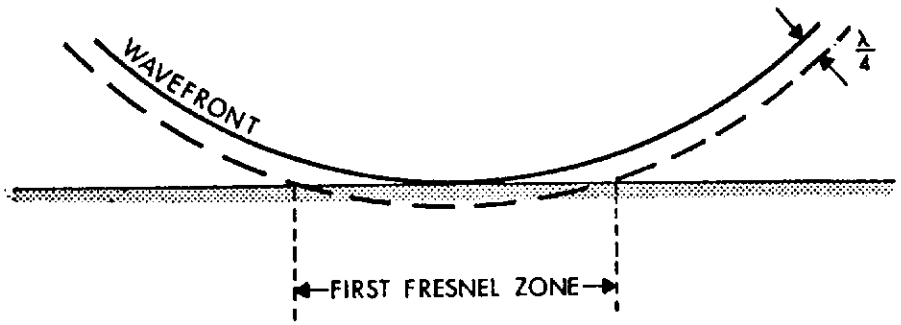

(a)

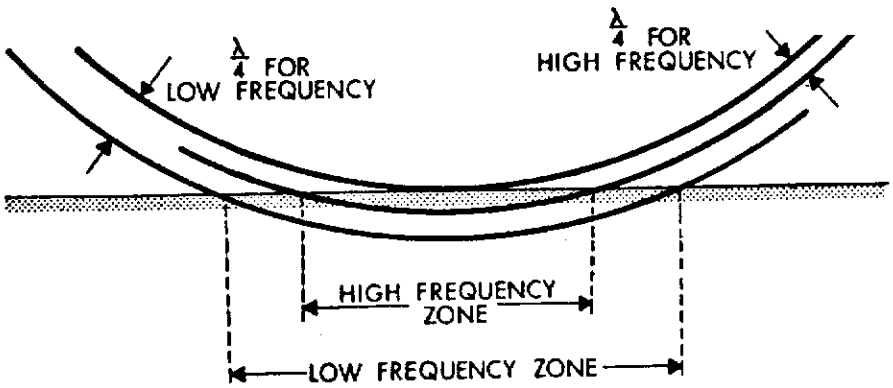

(b)

Figure 2.2: First Fresnel Zone for (a) Spherical waves reflected from the plane interface. (b) The Fresnel Zone size as a function of frequency (after Sheriff, 1977).

2.2 Time-Lapse 3-D Seismic

Time-lapse 3-D seismic (or '4-D') is used to monitor fluid movements in the subsurface by recording multiple seismic surveys over the same area at different calendar times. One seismic image is subtracted from a second image acquired at a different time to produce a seismic 'difference image'. Assuming the two data sets are identical other than any changes in the seismic response resulting from production related fluid movements, the seismic difference section should have zero amplitude everywhere except where the fluid content has changed. Unfortunately, it is impossible to perfectly repeat a seismic survey and environmental changes also occur in the time between repeated surveys such that simple subtraction of one data set from another will yield meaningless results. Great care must be taken to 'equalize' the data sets with data processing before a successful difference section can be produced.

Time-lapse 3-D seismic is becoming increasingly important in the management of hydrocarbon production, yet there is a distinct lack of model data to support some of the fundamental interpretations being made. The method relies on the ability to make valid comparisons between different vintages of seismic data that have been recorded over the same area. However, subtle anomalies on difference sections may in fact be artifacts of the different acquisition footprints or manufactured from the complex data processing that is necessary to allow comparison of legacy data sets. The two most significant issues to resolve are the repeatability of multiple seismic surveys and the credibility of the difference anomalies (Eastwood *et al.*, 1999).

In production geophysics, detecting zones of production or constraining in-situ conditions within a reservoir are often of greater importance than obtaining a highly resolved structural image (Schmitt, 1999). Most existing methods of monitoring fluid flow in hydrocarbon reservoirs are based on data measured at wells. This includes data such as pressure, production rate, injection rate, and produced water/oil ratio (WOR) and gas/oil ratio (GOR). This dynamic production information is used to boost the overall recovery level. However, the major limitation of these data is that it is one-

dimensional and cannot be used to indicate fluid movements beyond the immediate vicinity of the well. Time-lapse seismic can provide the link between wells and is becoming an integrated part of reservoir characterization. Coupled with fluid-flow simulation, geology and rock physics, time-lapse seismic data can be used to infer flow paths and fluid phase-front movements within a reservoir.

2.2.1 Reservoir Changes with Production – Fluid Flow

The seismic properties of a hydrocarbon reservoir can change significantly over time as a result of changes in saturation, temperature and pressure that occur with production. Reservoirs typically contain three fluid phases, that is, water (or brine), oil and gas. During production, pore pressure decreases where fluids are withdrawn at a producing well. Injection wells are commonly used to maintain reservoir pressure during depletion of hydrocarbons, and the pore pressure will increase around these injection wells. Pressure variations cause three-phase fluid flow in three dimensions which is controlled by the geology. Variations in temperature alter the viscosity and composition of the hydrocarbons, which adds to the complexity of the environment.

Hydrocarbon production typically causes changes in both saturation and pressure. The changes in the seismic response from each of these fluid parameters can either add up or cancel each other depending on the situation (Wang *et al.*, 1998). The effect of fluid flow on the seismic response depends on the lithology. In short, if the rock frame is stiff, it will be relatively insensitive to the fluid type in the pores but if the rock is 'soft' or poorly consolidated, the influence of fluids will be much greater.

The most obvious change that occurs with production is the relative saturation levels of the different fluid phases as hydrocarbons are extracted. Production by depletion methods will cause a reduction in pore pressure. Subsequently, the overburden will not be supported by the pore pressure resulting in an effective pressure increase, possibly causing reservoir compaction, which in turn changes the porosity and density of the formation. Fluid flow barriers may also cause complex pressure gradients throughout a

reservoir. Production of hydrocarbons can cause micro-seismic earthquakes and induce fractures, which may alter the seismic properties substantially. Temperature changes will occur in cases where reservoirs are injected with water or steam and the movement of temperature fronts may be observable in time-lapse data (Eastwood *et al.*, 1994).

In terms of the observable changes in seismic data, the ideal case is where the velocity in the reservoir changes such that the interval travel time within the reservoir will change. Such changes manifest themselves as pull-up or push-down reflections from the underlying interfaces. More subtle changes may be observed as changes in amplitudes within a seismic section, although variations in amplitude can be caused by any number of data processing steps and interpretations based on these alone can be seriously incorrect (Jack, 1998). Many other attributes can be used to identify more subtle changes in the seismic data but they are all derived from the fundamental attributes of travel time and amplitude.

2.2.2 Feasibility of Time-lapse Seismic

Before a decision can be made to record a time-lapse seismic survey, a feasibility analysis must be performed to determine the likelihood of seismically detecting changes in rock properties due to fluid flow. Repeating seismic surveys is expensive and it is often difficult to determine if subtle fluid movements will be visible in the seismic data, or what the best time interval for repeating the seismic survey should be (Lumley *et al.*, 1997). The most favourable reservoir conditions for a successful time-lapse study in the field are shallow, poorly consolidated reservoirs that undergo large changes in fluid saturation with production. These conditions allow for the greatest changes in seismic response and subsequently the best possible signal-to-noise ratio in the resulting difference sections.

Figure 2.3 shows the steps involved in performing a feasibility study to determine if time-lapse seismic is a viable option for a particular reservoir. The analysis begins with a reservoir model where the lithology, porosity and permeability are defined at every

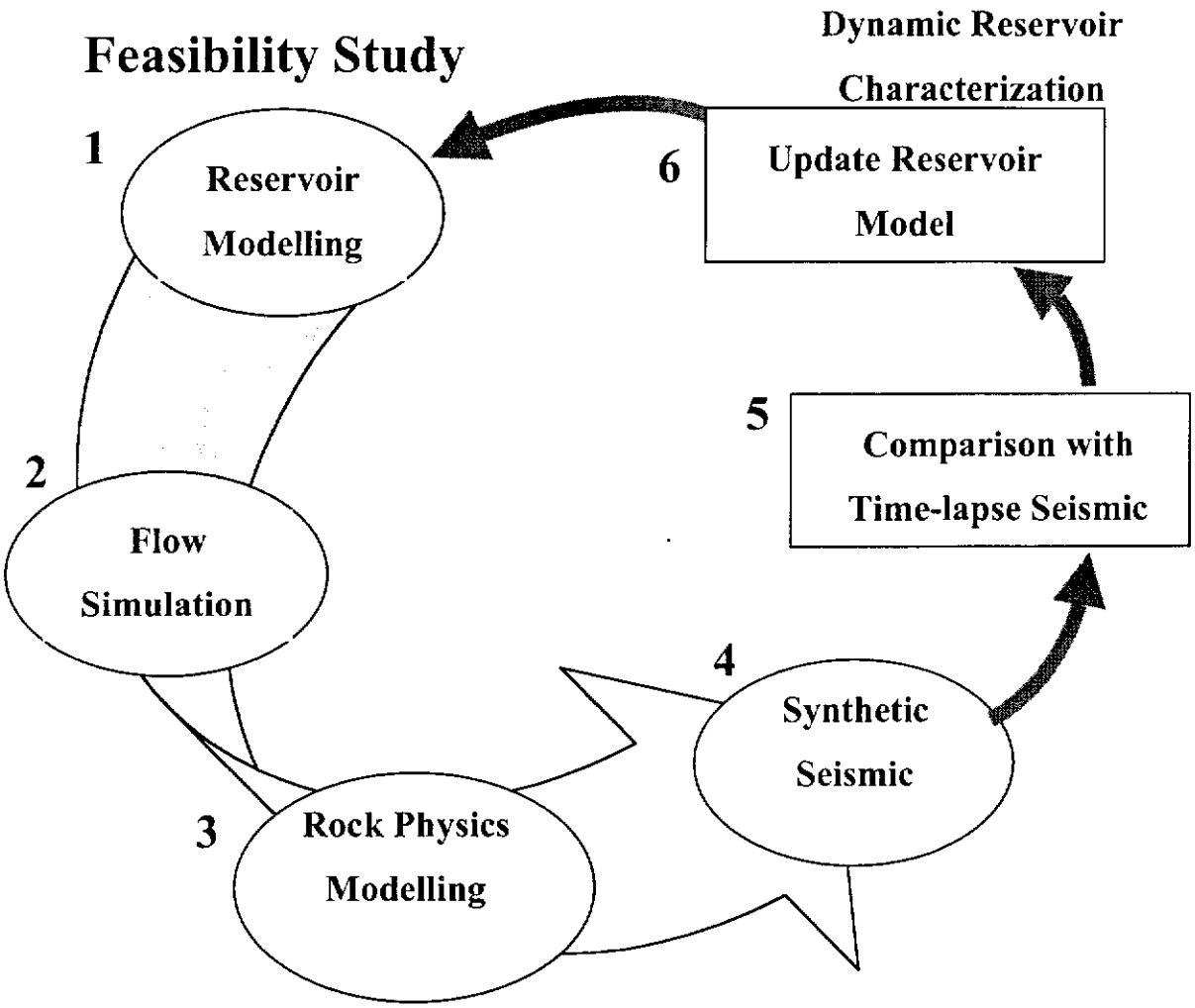

Figure 2.3: Steps involved in monitoring reservoir performance. Steps one to four are part of the feasibility study to determine if time-lapse seismic is viable. Steps five and six complete a continuous 'dynamic reservoir characterization' loop whereby the model is updated and parameters are constrained further as new data becomes available (modified after Mavko, 1998).

pixel within the three-dimensional model (Mavko, 1998). Such models may typically comprise several million voxels (volume pixels). Reservoir fluid properties are specified and a value for density and P- and S-wave velocity is assigned to each pixel. Upscaling is then necessary to reduce the complexity of the model for the fluid flow simulation. This is typically in the order of 100:1 and can be a major problem as changes in the reservoir may be below this resolution. Fluid flow simulations are used to predict the spatial distribution of flow pressure, temperature and fluid saturation. Rock physics transformations are then used to model the elastic properties so that a synthetic seismic image may be generated. Repeat surveys may be simulated from the base survey where the expected changes are estimated and then assessed to determine if they will be visible over the noise in the difference surveys (Blonk *et al.*, 1999).

The properties for numerical modelling are often derived from petrophysical studies in the laboratory. For example, Wang *et al* (1991) measured the properties of core samples that were flushed with different fluids (water, pentane and air) at different temperatures to determine what rock types and conditions might be suitable for monitoring of water floods. In addition to petrophysical factors, there are a number of other issues to consider, such as survey repeatability, SNR issues, and data processing. Multiple surveys acquired with different acquisition parameters such as fold, offset coverage and azimuth, may lead to artifacts that dominate the time-lapse comparisons and cover up subtle difference anomalies. Reservoir simulation software has been developed for modelling fluid flow and hydrocarbon recovery processes. However, the recovery process is complex and such models are oversimplified for modelling subtle temporal responses (Christiansen and Batzle, 1998).

Once a time-lapse survey has been recorded, the data is compared with the predicted response from the numerical simulation. Unexpected differences between the modelled and observed seismic data are analysed and used in conjunction with production data to constrain the parameters and update the reservoir model (Mavko, 1998). The updated reservoir model is then used to repeat the whole process in an iterative loop known as 'dynamic reservoir characterization' (Figure 2.3).

2.2.3 Dynamic Reservoir Characterization

Reservoirs are heterogeneous in terms of lithology, porosity, permeability and pore-fluid composition. Knowledge of the spatial variation of these reservoir parameters is vital to evaluate the total recoverable hydrocarbons and to predict fluid flow pathways and associated processes such as heat and pressure transfer.

Reservoir characterization is used to forecast the hydrocarbon recovery performance. Uncertainty is measured by the difference in outcomes between different, but equally valid, geological models. Time-lapse data can be used to continually update the reservoir model and reduce uncertainty (Guerin *et al.*, 1998). Constraining the parameters in the model is very important and time-lapse data can be very useful for this if integrated into a multidisciplinary study (Biondi *et al.*, 1998). Dynamic reservoir characterization can maximize incremental recovery without a large increase in cost (Talley *et al.*, 1998).

2.2.4 The Importance of Fluid Flow Monitoring

The main driving force for the development of fluid flow monitoring technology is the potential for enhanced recovery of hydrocarbons and more efficient reservoir management, but there is also potential to apply these techniques in other areas such as groundwater, environmental studies and global climate issues (Lumley, 1993).

The ability to monitor fluid flow allows real-time reservoir management. It is estimated that 65% to 75% of discovered oil is potentially recoverable, but the average recovery rate is around 25% (Nur, 1997). The poor recovery rate is due to subsurface heterogeneities and compartments of hydrocarbons that are left behind 'unswept' by the recovery process. For example, water-flooding in the Gullfaks Field in the North Sea flushed the top of the reservoir but left deeper zones undrained (Digranes *et al.*, 1999). Mapping the fluid flow was vital to assist planning for in-fill wells to drain the bypassed zones. Time-lapse seismic is a potentially powerful tool for improving reservoir

characterization (Hwang *et al.*, 1998). It should play a major role in declining fields that have large amount of hydrocarbons still to be recovered.

2.2.5 Previous Work

Most early time-lapse projects were performed in areas where it was determined that large changes in seismic velocity would occur, such as areas where production was driven by steam or fire-floods. Steam-floods are ideal for time-lapse surveys because they are typically shallow, poorly consolidated reservoirs that are sensitive to changes in pore fluid and pressure (Batzle *et al.*, 1998). Successful case studies of monitoring more subtle fluid changes are less common.

Pullin *et al* (1987), were able to qualitatively map the location of heated zones in the Athabasca tar sands reservoir by comparing time delay and amplitude variation maps between two stacked surveys. A similar analysis was performed by Eastwood *et al* (1994) on time-lapse data from the Alberta cyclic steam stimulation (CSS) project. The time-lapse data was part of an integrated study including crosswell data, thermal reservoir simulations and rock physics measurements in the laboratory.

Hirsche (1998) showed that production by pressure depletion can cause seismic anomalies if the pressure drops below the 'bubble point', that is, when gas comes out of solution and changes the saturation level within the reservoir. Pressure depletion may close micro-cracks in stress-sensitive reservoirs, which is a very important factor for permeability and also affects the seismic response (Lorenz, 1999).

Time-lapse data was combined with 3-D elastic modelling, reservoir characterization and fluid-flow simulation to understand drainage patterns and identify areas of bypassed pay in a turbidite reservoir in offshore Louisiana (Anderson *et al.*, 1998). Wang *et al* (1998) showed with a time-lapse study of crosswell data that the effects of saturation and pore pressure changes may potentially be separated if P-wave and S-wave data are

available. The P-wave velocity is sensitive to both pressure and saturation changes while the S-wave velocity is sensitive only to changes in pore pressure.

Dyer *et al* (1999) used permanent monitoring of micro-seismic earthquakes generated in the Valhall reservoir in the North Sea as a result of hydrocarbon production. Downhole geophones were able to monitor micro-seismic earthquakes, which were clustered along fault planes, and these data were used to help delineate the structure, compartmentalization and fluid flow within the reservoir.

2.2.6 Data Acquisition Repeatability

Data acquisition repeatability is a measure of the degree to which the identical seismic survey can be repeated without incurring differences in the unprocessed field data. This includes all aspects of acquisition such as source signature repeatability, offsets, azimuths, recording instrument response, navigation, receiver coupling, plus climate and seasonal variations. Changes to any one of these factors can be so severe as to make time-lapse monitoring of fluid flow impossible. Johnstad *et al* (1993) found that small navigational errors alone were serious enough to almost completely mask a seismic fluid-flow anomaly. Rozemond and Simensen (1999) suggest that time-lapse surveys have to be compatible, but not necessarily identical, to achieve good results, and identified sail-line and source array repeatability as the most important parameters. Inadequate acquisition repeatability can result in patterns of high amplitudes in the seismic difference volumes known as 'acquisition footprints'.

A consistent source signature (ie. waveform) is very important. In cases where two surveys have different spectral content, it may be necessary to reduce both data sets to the portion of the spectra that overlaps. This effectively reduces the data to the lowest common denominator. Amplitude variations between subsequent surveys can harm seismic difference sections even if time-difference errors are negligible. Such changes in amplitudes are often not indicative of true changes in the reservoir but rather a factor of source and receiver coupling with the surface. Even permanent deployment of

geophones cannot guarantee that coupling will not change between surveys (Meunier and Huguet, 1998). Non-repeatability of amplitudes is not necessarily an indication of non-repeatability in source signature (Aritman, 1997).

The effect of changing acquisition parameters was investigated with numerical models by Gullaksen *et al* (1999) where the effect of changes in parameters were modelled individually. The seismic physical modelling techniques developed within this thesis are also perfectly suited to this style of application.

2.2.7 Data Processing

Careful attention to data processing, known as 'crossequalization' is needed to ensure that a valid comparison can be made between two data sets. Even near-identical and short time-lapse surveys need careful processing to be of any value (Jack, 1998). Crossequalization of two data sets involves convolving the field data with an impulse response function, or matching filter. This function can be computed on either a surface consistent trace by trace basis, or globally from the base to monitor survey (Ross *et al.*, 1996). It includes timing changes, energy balancing, bandwidth normalising and phase matching. It has been shown that producing difference sections from seismic lines that are identical other than a minimal change to just one of the above parameters will often result in residual amplitudes equal to around 30% of the primary amplitudes (Jack, 1998). These amplitudes are noise on seismic difference sections and can completely obscure seismic fluid flow anomalies (Lumley, 1993). Without crossequalization, differencing of field seismic surveys would produce a volume of data with meaningless amplitudes equal to or greater than the amplitudes on either primary survey.

Amplitude changes within small reservoir compartments can be masked by the stacking process, which may sum traces that have been affected by fluid movement with traces from larger offsets that undershoot the target area and remain unaffected (Bacharach and Nur, 1997). In this case, the range of offsets used for analysis should be restricted.

Timing corrections are necessary to correct the effects of seasonal variations in water temperature and salinity. Timing errors of just one or two samples will result in high amplitudes on difference sections. The difference wavelet looks like a phase-rotated wavelet from the primary survey. Errors increase with timing delay and the higher the bandwidth the quicker this occurs (Ross et al., 1996). A phase difference of 15 degrees between time-lapse data sets will result in residual amplitudes on the difference section of around 20% of the primary survey (Jack, 1998). A difference in bandwidth between seismic surveys of just 2.5 Hz will result in residual energy of 7% on the difference section and 40% residual energy will result from a typical bandwidth difference of 12.5 Hz.

Statistical signal enhancement processes, such as deconvolution, are useful for improving seismic images but can be harmful to repeatability (Eiken *et al.*, 1999). Migration processing is very good for improving repeatability but requires an accurate velocity model and the same velocity model and migration algorithm must be used on both data sets (Eastwood *et al.*, 1998). Navigational errors require the data to be repositioned. Williams *et al* (1999) achieved substantial improvement with a bulk shift of the whole 3-D data volume, which involved both rotation and translation components that were determined by statistical analysis.

Matching filters are generally designed over static reflectors that exclude the reservoir and, therefore, are not expected to change with production over time. While this method is sound in principle, it is not perfect in practice. The somewhat contradictory aim of making data the same to see what is different may diminish the extent that true changes are highlighted or possibly create subtle false anomalies where no change has occurred. Clearly further research is needed. However, the huge expense of repeating a 3-D seismic survey in the field, when the value of such an exercise is unknown beforehand, is difficult to justify in all but the most favourable conditions. If Time-lapse 3-D seismic could be established under controlled conditions, then the merit of performing such surveys can be quantified for the first time.

CHAPTER THREE

MODELLING

This research draws on a wide range of modelling concepts for its inspiration. Therefore, it is necessary to spend some time introducing the many variations of each technique to appreciate the potential impact of developing this seismic imaging technology further.

3.1 Seismic Physical Modelling

Any improvement in seismic survey design, data acquisition, processing or interpretation techniques are going to be of great benefit for predicting where to drill for hydrocarbons. Ways to improve methods of exploration have traditionally been approached from two directions. That is, using forward numerical wave theory modelling, or using a geological approach trying to understand the evolution of structures and their form. The use of seismic physical models is the alternative approach, as presented here.

3.1.1 Introduction

Seismic modelling was first considered in the 1920s, but was limited by a lack of adequate instrumentation. After World War Two, Soviet scientists took advantage of the major improvements in electronics to become the first to experiment with seismic physical modelling. The first 2-D plate model was tested by Kaufman and Roever (1951). The Russians dominated seismic physical modelling for the next ten years, their efforts driven by the quest for knowledge of the deep Earth structure from

earthquakes, which was driven by the need for the detection of nuclear tests (Ivakin, 1966). The language barrier slowed the spread of this approach to the West.

Much of the early work was focused on refracted events, which are very important in the study of earthquakes, the major field for seismologists in the early years. The limited dynamic range of early recording instruments, which made it difficult to record reflections in the presence of Rayleigh waves, restricted seismic reflection modelling. Refracted waves arrive before the Rayleigh wave and so do not suffer from this problem. The introduction of digital computers into exploration geophysics in the late 1960s led to physical models being used to test seismic data processing algorithms (Donato, 1960a). Numerical modelling methods were not well advanced and computers were too slow to make numerical modelling a viable alternative.

Experiments on the seismic effects of complex geology have been performed over the last 20 years in the Allied Geophysical Laboratories (AGL) at the University of Houston, where much work has been carried out into understanding the effects of fault patterns of producing oil fields (Ass'ad *et al.*, 1992a; Ebrom and Sheriff, 1992). In 1991, a new physical modelling system was built at the AGL and shipped to Curtin University, where it was reconstructed and is being used for studying the 3-D effects of seismic wave propagation in isotropic and anisotropic media.

The collection of seismic data over physical models has two great advantages over working with field data. That is, it is orders of magnitude cheaper than performing field surveys, and the 'geology' is known so its effects on wave propagation can be directly measured and understood. This capability offers great potential as a scientific tool to understand the seismic expression of various structural styles, and offers insight into future methods of 2-D and 3-D seismic acquisition and processing for improved target mapping. However, such models incorporate a number of simplifications and, at this stage, are restricted in their complexity.

Seismic reflections detected in physical models are most often based on velocity contrasts alone. The construction of a conventional 3-D model is a complicated task,

and takes months of testing of the plastics and resins used to model sedimentary sequences (Evans *et al.*, 1995). Prior to the work reported herein, all seismic physical modelling has had to be performed using solid models, which are constructed with pre-determined structures built into the model. This restriction imposes constraints on the realism or 'natural variation' within the model. The ability to apply this technology to cohesionless sand analogue models would dramatically reduce the cost and time involved in the construction of a physical model. Sandbox modelling is a dynamic process, developing structures that form with many of the idiosyncrasies of natural systems. Hence, the production of seismic profiles from such models would provide a new modelling concept in understanding 3-D geology.

3.1.1.1 Examples

Seismic physical modelling has long been used as a means of testing fundamental wave theory. Early experiments were performed to compare observed reflection amplitudes from a simple plane-layer model with those predicted from reflection theory (Clay and McNiel, 1955). The critical refraction of elastic waves has been tested (O'Brien, 1955), and the shape and amplitudes of refracted waves have been studied (Donato, 1960b). Physical models have also been used to study the effects of P-wave anisotropy in stratified media (Melia and Carson, 1984), and anisotropy induced by fracturing (Hsu and Schoenberg, 1990; Ass'ad *et al.*, 1992b).

Physical modelling has proven to be an ideal medium for testing seismic data processing algorithms because the structure of the model is pre-determined, which allows the processed seismic data to be directly compared with the known structure of the model. A wide range of these experiments can be found in the literature, such as the testing of crosshole imaging software (East *et al.*, 1988), inversion algorithms (Macdonald *et al.*, 1987), the analysis of dip moveout (Forel and Gardner, 1988), and the testing of migration algorithms (Uren *et al.*, 1991).

Seismic physical modelling experiments by French (1974) were the first to show that 3-D seismic surveys were necessary to map 3-D geological structure. His models were

also used to prove new 3-D data processing transforms, such as migration processing, were necessary to correctly image geological features in three dimensions (Figure 3.1).

The use of seismic modelling is not limited to simplistic models. Physical models have also been widely used to study wave propagation in complex media, such as the effects of scattering (Levin and Robinson, 1968), the identification of the slow P-wave (Plona, 1980), and the effects of sideswipe (Ebrom and McDonald, 1992). Interpretation of conventional seismic data uses only a single compressional (acoustic) component of the reflected seismic energy. Physical modelling studies have shown that if the full elastic wavefield is recorded, the data can more readily be used to indicate the presence of fractures (Tatham *et al.*, 1983). This type of modelling research led to the seismic recognition of fractures in field experiments (Mueller, 1992), the presence of which was later corroborated by horizontal drilling.

Other examples of the benefits of seismic physical modelling research were demonstrated with scaled experiments of the Oliver field in the Timor Sea by Evans *et al.* (1995). They showed an interpretation of 2-D data recorded over the offshore Oliver field that indicated the presence of faulting. However, a scaled model of the geology of the field, built without faulting, showed an identical seismic response to that observed in the field data. The 'ghost' faulting interpreted on the field data proved to be due to the juxtaposition of large acoustic impedances across small throw faults in the shallow section. 2-D and 3-D seismic data recorded over the model also provided proof that the 3-D structure of the field could be properly imaged using cost-effective 3-D seismic data collected in the strike direction only. These results highlighted the fact that the interpretation of field data for the presence of fracturing and faulting cannot be unique.

The use of ultrasonics in the laboratory is not limited to the study of seismic effects. Experiments of two-phase fluid flow such as those by Thomas and Clouse (1995) utilized ultrasonic transducers to monitor the progress of oil migrating through a 2-D water saturated sand pack. In addition to visual monitoring, travel times between

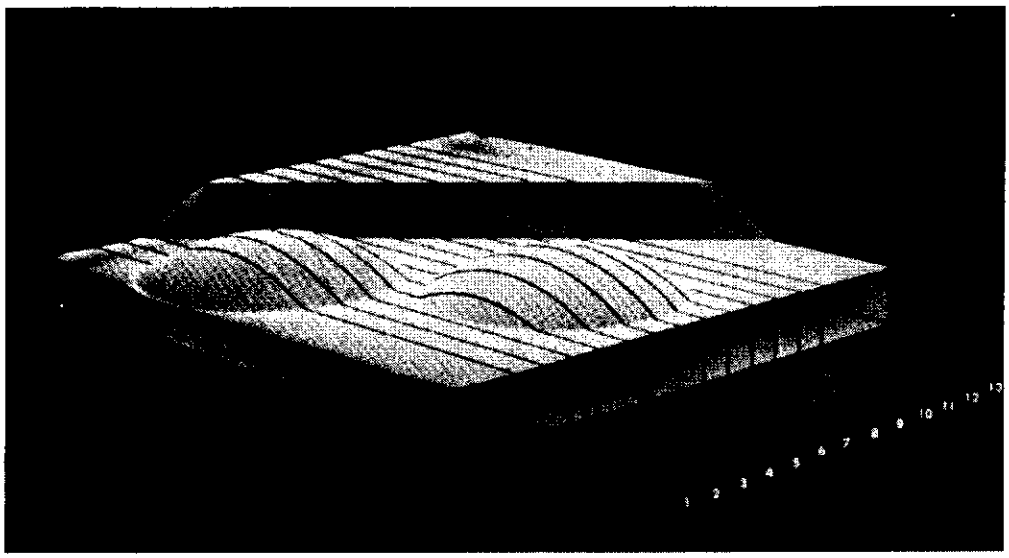

(a)

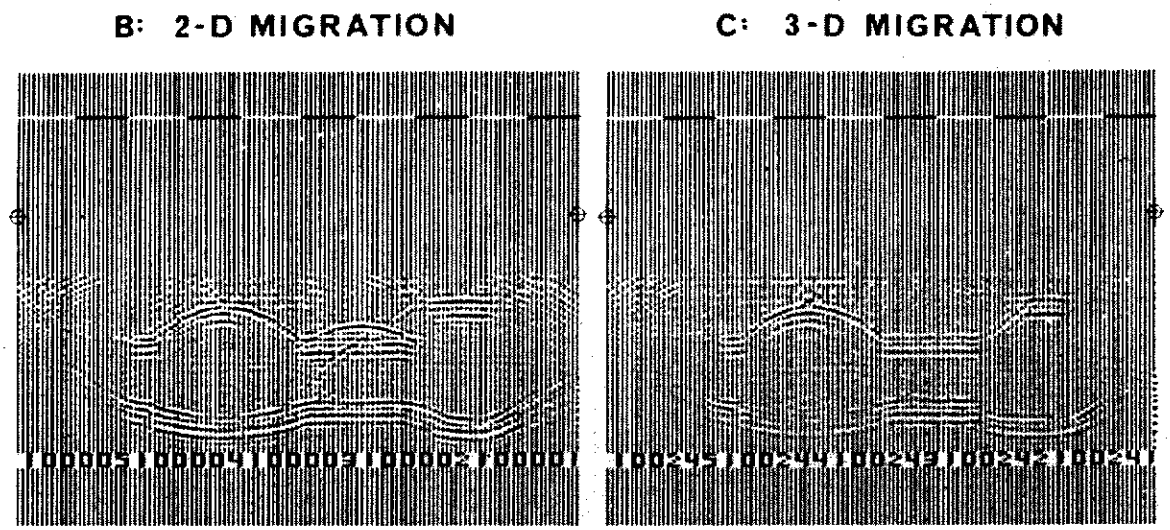

(b)

Figure 3.1: (a) Photograph of the physical model used by French (1974) to demonstrate the importance of recording 3-D seismic data to image a 3-D structure. (b) 2-D and 3-D migrated seismic sections recorded over line seven on the model. Reflections from the second anticline feature are evident on the middle traces of the 2-D migrated section. These reflections, known as sideswipe, are from outside the plane of the seismic section. French showed that 3-D migration is necessary to remove these sideswipe reflections.

source and receiver were used to estimate the relative oil saturations over different regions of the sand pack.

3.1.1.2 *Solid versus Unconsolidated Models*

Many different materials have been used in seismic physical models, such as rocks, metals, plastics, glass, concrete and pitch, various aqueous solutions and organic fluids (O'Brien and Symes, 1971). Purnell (1986) did a series of experiments on wave velocity and attenuation in two-phase (solid and liquid) media, to investigate their possible use in seismic physical models. He found that variables such as the elastic constants and the distribution of pore space in unconsolidated, fluid-filled sand packs were too difficult to determine and control. He concluded that an unconsolidated grain framework, with fluid-filled pores, was not suitable for physical modelling, and that two-phase media are better modelled using suspensions of grains in a fluid-like matrix, such as silicone rubber. The research undertaken for this project addressed the shortcomings of unconsolidated models and offers a number of solutions to overcome them.

The major benefits of solid physical models are that the rate of energy attenuation is far less than in unconsolidated grain matrices, and a particular structural configuration can be precisely modelled. However, construction of conventional solid physical models is a lengthy process and inherently comprises simplistic structural configurations limited by conventional understanding of deformation processes and structural geometries. The structural configuration and the velocity of each layer within the model are derived from an interpretation of field data from the particular area of interest. Various mixes of the modelling materials are then exhaustively tested so that the velocity of the material used for each layer is correctly scaled. Once the mix for each layer has been finalised, each layer is poured and solidified, and then machined to the predetermined structural configuration before the next layer is added.

Analogue sandbox models, by contrast, are not used to simulate a particular structure from the field, but a style of structures that are generated dynamically within the model

as it is deformed. The main advantage of this is that the models contain a degree of natural variation within each layer that cannot be built into a solid model, which means the resulting seismic data contain all the natural characteristics that make processing and interpretation of field data difficult. In short, sandbox models provide a more realistic seismic response than solid models, but suffer from the relative lack of control over the structures produced.

In conventional physical models, reflections are received as a result of acoustic impedance contrasts that are produced by altering the chemical mixture of each layer within a solid model. In sedimentary sequences, the contrasts are mainly a result of changes in porosity and the degree of consolidation. With this in mind, the impedance contrasts within the models presented in this report were mainly achieved with changes in porosity from variations in grain size and sorting, and by adding cohesion to the matrix of some layers in an otherwise cohesionless sand model.

3.1.1.3 Numerical Versus Physical Modelling

As computer technology has evolved and increased in speed of operation, numerical models have begun to become an alternative to physical modelling in many areas, but there is still plenty of potential for physical models because numerical models assume simplicity that does not exist in nature. Physical models are very useful for studies of wave mechanisms and 2-D or 3-D responses of isotropic or anisotropic models because they produce natural results rather than contrived results (which respond to the particular waveform required by the computer user). Physical models can also provide relatively inexpensive data for evaluating proposed geological models related to hydrocarbon prospects.

Seismic physical models have frequently been used as an independent check on predictions of mathematical models of wave propagation (O'Brien, 1955; Melia and Carson, 1984). They are also useful for providing inexpensive data for educational purposes (eg. Walton, 1996; Davis, 1997).

One advantage of numerical modelling is their versatility, that is, it is very easy to change parameters. True 3-D computation, however, uses a huge amount of computer time. More significantly, numerical models involve gross simplifications of the geometry of the structures and approximations on the elasticity and isotropy of the media of propagation. Physical models can far more easily simulate complex 3-D geological structures, and are able to incorporate the fundamental seismic properties of absorption, dispersion and diffractions, but lack the versatility of numerical models. To change parameters means a new model has to be built. There are coupling problems with simulating land surveys, but marine surveys overcome this.

The major restrictions of seismic physical modelling are as follows;

i) to produce realistic acoustic impedance, or velocity contrasts within the models requires months of testing of materials;

ii) amplitudes are difficult to reproduce to scale, due to energy attenuation problems of the materials and the directionality of the source and receiver; and

iii) it is difficult to scale down the source and receiver dimensions with respect to the wavelength.

It is not appropriate to label one method superior to the other, as both physical and numerical modelling offer insight into many of the same problems, but from different approaches. They are complementary rather than competing methods of modelling. Both physical and numerical models have the same goals, that is, to understand the phenomena of wave propagation in complex media, and to improve methods of seismic data acquisition, processing and interpretation to obtain the best possible image of the subsurface, leading to improved mapping of hydrocarbon reservoirs.

3.1.2 Physical Modelling System

Figures 3.2 and 3.3 are, respectively, a photograph of the physical modelling system and a schematic diagram of the system components. Piezoelectric transducers used for the ultrasound source and receiver have a flat round face and an active element with a

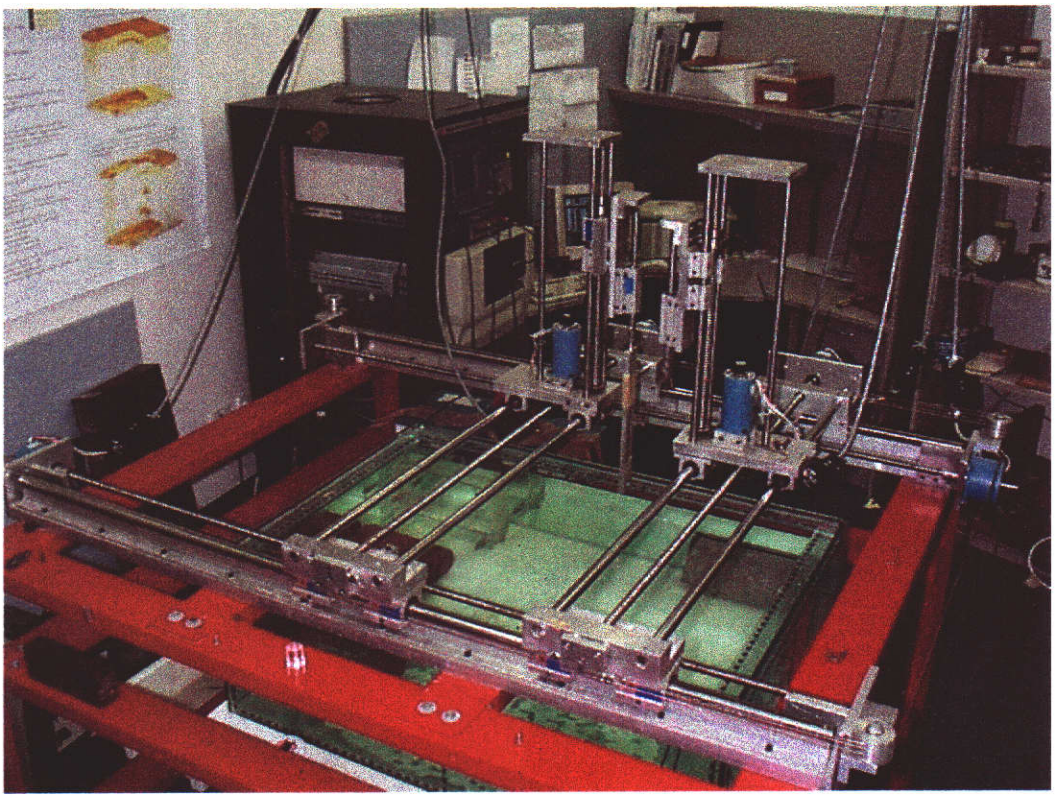

Figure 3.2: Photograph of the physical modelling system at Curtin University of Technology.

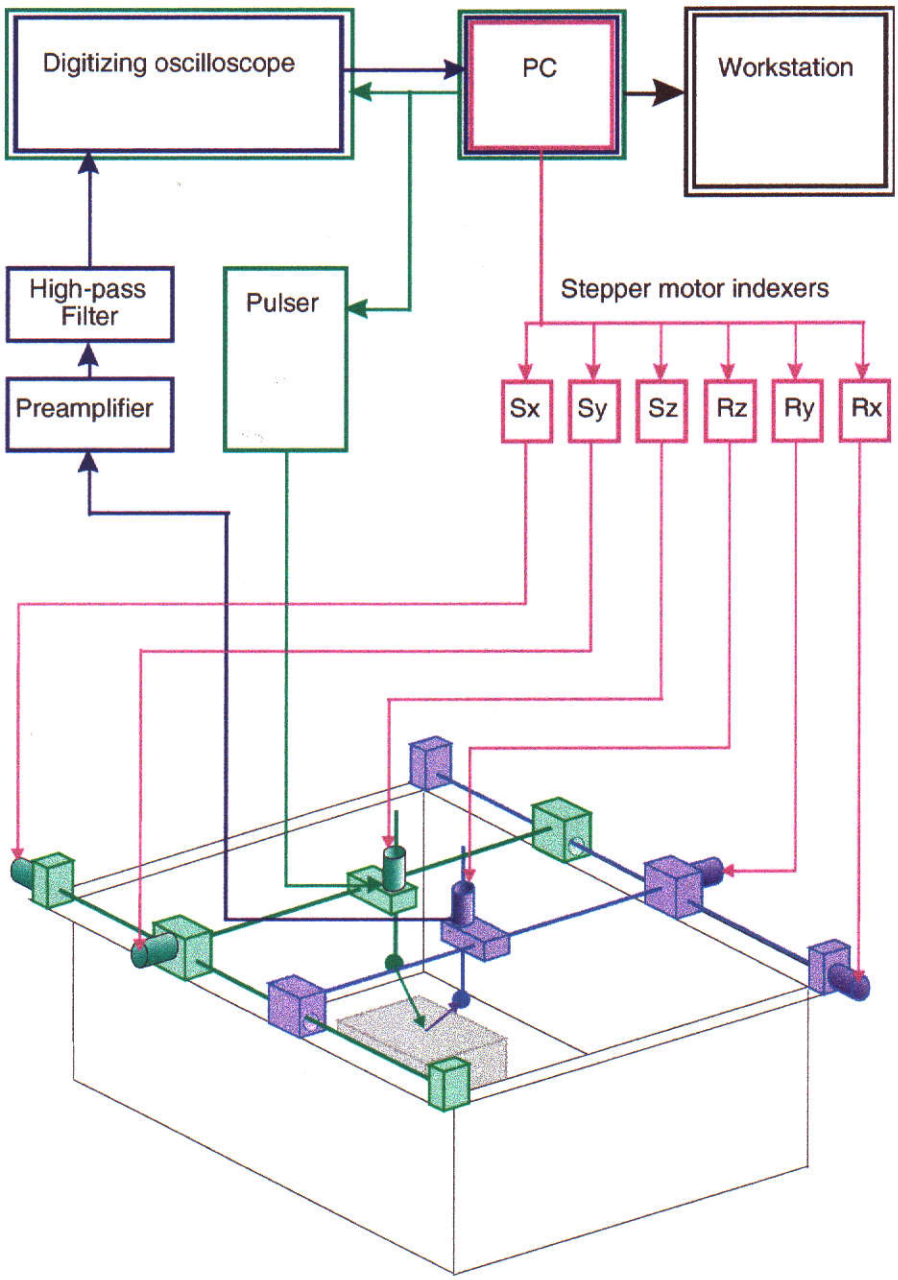

Figure 3.3: Schematic diagram of physical modelling system components.

diameter of 13 mm. The Panametrics V303S transducers used for the majority of the experiments in this thesis are sensitive to displacement normal to the contact face, and generate and receive compressional waves (P-waves). A single transducer can be used as both a source and receiver to record zero-offset surveys. Shear wave (S-wave) transducers which have displacement tangential to the contact face are available but are not used for marine surveys as water will not transmit S-waves.

Marine surveys are performed in a glass water tank that is 1 m by 800 mm wide and 700 mm high. Movement of each transducer is controlled in three-dimensions by six Superior Electric SLO-SYN stepper motors (three co-ordinates for each transducer). The six stepper motors are individually controlled by SLO-SYN 430-PI indexer motor drives. The electrical input for the source transducer comes from a Panametrics 5055PR pulser/receiver. These have a maximum pulse of 250 volts and an output adjustable in four steps to between 18 and 220 μjoules, with a rise time of less than 10 ns.

The received signals have a maximum frequency of 10 MHz with the bandwidth controlled by an analogue high-pass filter that is selectable between 0.01 and 1 MHz. The output from the V303S transducer has a narrow bandwidth between around 0.6 and 1.4 MHz. The high-pass filter is usually set to 0.3 MHz on the assumption that noise will dominate outside the signal band. Filtering these frequencies reduces overall noise but preserves most of the signal. This filtering is done before analogue-to-digital (a/d) conversion to prevent the low frequency amplitudes from saturating the a/d converter. A preamplifier then boosts the analogue signal with a voltage gain of 40dB or 60dB.

The signal is digitized using a Nicolet 430 digital oscilloscope, which is a two channel, 12 bit system with a sample interval of 100 ns (10 Megasamples per second). The dynamic range of the recorded signal can be adjusted between 30 mV and 120 V to optimize the SNR. For many of the models in this thesis, the range is set such that the strongest amplitudes, which are reflections from the model surface, exceed the maximum (usually 3 V). These events are then squared off or 'clipped' as a trade off for better resolution of important low amplitude events from within the model. Source

signature repeatability and the SNR can be improved by summing a number of shots in the one location. Triggering is controlled with a Pentium personal computer (PC) through the parallel printer port. The oscilloscope and stepper motor indexers are controlled through the IEEE-488 interface bus and the serial interface respectively.

3.1.2.1 Data Recording and Transcription

The data acquisition software, called SAM, was originally developed for the Allied Geophysical Laboratories at the University of Houston, and has since been modified by staff at Curtin University. This software can be used to perform any configuration of 2-D or 3-D, land or marine seismic survey. The choice between zero-offset or variable offset data acquisition is significant, and many of the experiments in this thesis were conducted to determine the benefits and limitations associated with each configuration. Once a model has been built, it is placed in the water tank and the ultrasonic transducers are set up over the model. The survey acquisition parameters are then entered into SAM, ready to record acoustic waves in a simulated marine environment.

The data is scaled by a predetermined factor of up to 80 000:1, although 10 000:1 is used throughout this thesis. The output is downloaded directly onto an Exabyte magnetic tape in SEG-Y format or stored on disk ready for processing. From this point on, the data is treated as normal field seismic data.

The volume of data collected is similar in size to that collected in the field. Hence, a large disk and tape capacity is a prerequisite plus the requirement of processing data on fast computers. 2-D data processing is performed using interactive workstations, networked to a Sun 1000E processor within the Department of Exploration Geophysics at Curtin University, and uses the commercially available software 'Promax'. 3-D interpretation and visualisation is performed on a Silicon Graphics workstation, and uses the Paradigm software 'SeisX' and 'VoxelGeo'.

3.1.2.2 *Scaling Physical Models*

Most field seismic data are within the frequency range of 10 to 100 Hz. Therefore, a scale of between 1:10 000 and 1: 100 000 is realistic for the 1 MHz transducer used for most of this research. When scaling physical models, the main rule that must be followed is that the ratio of geological feature size to wavelength must be the same in both field and model. The larger end of this range (1:10 000) was chosen for the sandbox models presented in this thesis due to the relatively large grain size to wavelength ratio. The implications and limitations of upscaling ultrasonic data to represent field seismic data are discussed in the following Chapter.

Many modelling materials have sound velocities much lower than true rock velocities, and because of this the time scale is often specified independently of the distance scale. It is worth noting that both the distance and time scales are, in a sense, arbitrary. This is because both the horizontal and vertical axes can be 'stretched' or 'squeezed' when displaying the seismic section by resampling.

3.1.3 Transducer Types

A transducer is a device that converts one form of energy into another. There are many types of transducers, such as the electrodynamic geophone which converts mechanical motion into an electrical voltage and vice versa. Other types include electrostatic, magnetostrictive and piezoelectric. Piezoelectric is the property of a dielectric which generates a voltage across it in response to a stress (Sheriff, 1994). Piezoelectric transducers are used to convert elastic or acoustical energy into electric energy and vice versa. Transducers used in this study are made from barium titanate or zirconate.

The ideal ultrasonic source for use in seismic physical modelling would have the same characteristics as a field seismic source, that is, it would have a large bandwidth, high energy output and an omni-directional source signature. Unfortunately, with piezoelectric transducers, these three characteristics are mutually conflicting (Savic,

1995). The energy output of a transducer is directly proportional to the area of the crystal face. The bandwidth of a transducer is controlled by the element diameter to thickness ratio and also the presence (or not) of a physical backing to the crystal. Without a backing the piezoelectric element oscillates around its resonant frequency which produces a very narrow bandwidth and results in several strong cycles instead of the desired one. A backing can reduce this 'ringing' effect to a degree but as will be seen, the output still comprises several cycles, which serves to limit the bandwidth and degrade the vertical resolution.

A compromise is necessary between these mutually conflicting aims. For high frequencies, a small diameter crystal is required, but this limits the energy output that is possible. A large diameter element will provide high energy, which is very important for the SNR in physical modelling, but also results in unwanted source directivity. The waves generated are neither plane nor spherical but rather a directional pattern of waves that vary considerably with emergent angle. It is vital to understand the nature of this to be able to understand the phenomena observed and to determine any corrections needed. If realistic amplitudes are desired, they must be corrected to allow for these effects. Changes in temperature will also affect the waveform as the piezoelectric element changes volume.

If the frequency is too low, the resolution will be inadequate and the signal may overlap with the instrument noise, which means it cannot be filtered out with an analogue high-pass filter. If the frequency is too high, there will be serious problems with scattering, which begins to dominate as the wavelength approaches the geological feature size (ie. grain size of the sand). The size of the transducers means that the source and receiver are not scaled correctly with respect to the model. The source and receiver become very large with respect to the geology, which imposes restrictions on the nearest offset possible when recording variable offset surveys and also limits the horizontal resolution. One of the approaches to overcome the drawback of the size of the source and receiver with respect to the wavelength is to use laser ultrasonics, which also provides a cleaner, less resonant pulse (Poet and Rasolofosaan, 1993). However, this

technology is in its infancy and has its own drawbacks, and was not available for this research.

3.1.3.1 *Plane wave (directional) and spherical wave (omni-directional) transducers*

Several different transducer types, with different source frequencies and focal lengths, are used on physical models at Curtin University. The transducers differ in the way the energy spreads from the source. These can be divided into two basic types: omni-directional transducers where the energy spreads spherically in the same way that it does from a field source, and directional transducers, which direct most of the energy towards the direction they are facing. Directional transducers can be focussed to deliver the majority of their energy to one point location, but this variation is rarely used in physical modelling because it is only useful over a very narrow distance range. The energy spreading characteristics of the two transducer types is schematically shown in Figure 3.4.

Omni-directional transducers output a more realistic seismic source. The energy output is equal, or very close to being equal, in all directions, which means that the relative amplitudes recorded in a variable offset shot record in the laboratory will be a more realistic simulation of shot records recorded in field surveys. The waveform itself is also very stable over a wide range of angles, so there are no problems involved with stacking the data. However, when recording seismic surveys over sand models, which have very high rates of attenuation, the energy output from this type of transducer is too low to allow reflections to be recorded from layers deeper than about 30 mm, and this will be inadequate in most cases.

Directional transducers have a flat face and are designed to transmit most of the energy in one direction. This provides enough energy for use with sand models and so is the preferred type used in this research. Directional transducers are also much less

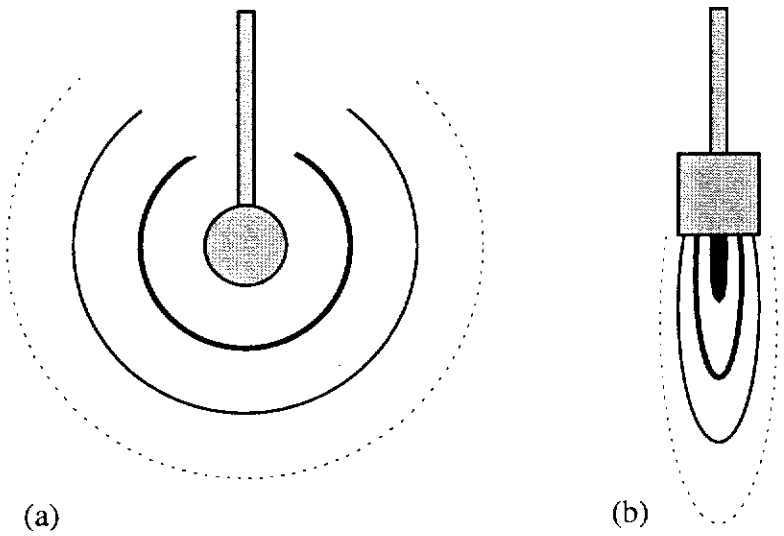

Figure 3.4: Radiation pattern of the two main piezoelectric transducer types. (a) Omni-directional transducer. Spherical element produces energy that spreads spherically from source. (b) Directional transducer. Flat element produces energy that is focussed towards the direction the transducer is facing to give higher output.

susceptible to sideswipe energy, which results from reflections from structures outside the 2-D plane of the seismic line, or the recording of diffracted arrivals from the edges of structures within the model. This can be an advantage in terms of image quality, but is essentially a disadvantage in that it is not simulating a realistic field source. An example of the differences in energy output and the diffractions that are recorded with each transducer type is shown in Figure 3.5.

The sideswipe reflections recorded with omni-directional transducers can present other problems that are a result of reflections from the sides of the water tank and the edges of the model itself. These unwanted edge effects can be potentially overcome with the use of a larger water tank and models that are much larger laterally. However, this would require a significant increase in the use of materials and time taken to build the models, with a subsequent increase in expense. Unless stated otherwise, the transducers used for all of the data in this thesis were Panametrics type V303S. These transducers are directional and have a dominant frequency of 1 MHz.

3.1.3.2 Bender elements

Bender elements are a special kind of transducer that comprises two piezoelectric elements of opposite polarity bonded together. When a voltage is applied, one side contracts while the other expands, which causes flexure and generates elastic waves. The same effect works in reverse when the element is used as a receiver. These elements tend to be lower frequency than conventional transducers as the frequency is inversely proportional to the square of the length of the element (rather than the length for conventional transducers). Bender elements have been used to successfully record elastic waves (compressional and shear) in unconsolidated sands (Butler *et al.*, 1997), but this type of application is limited as the elements must be buried in the sand and kept stationary. Measurements can be taken while the sand undergoes changes from fluid saturation for example, but the transducers cannot be moved in or around a model to simulate a seismic survey.

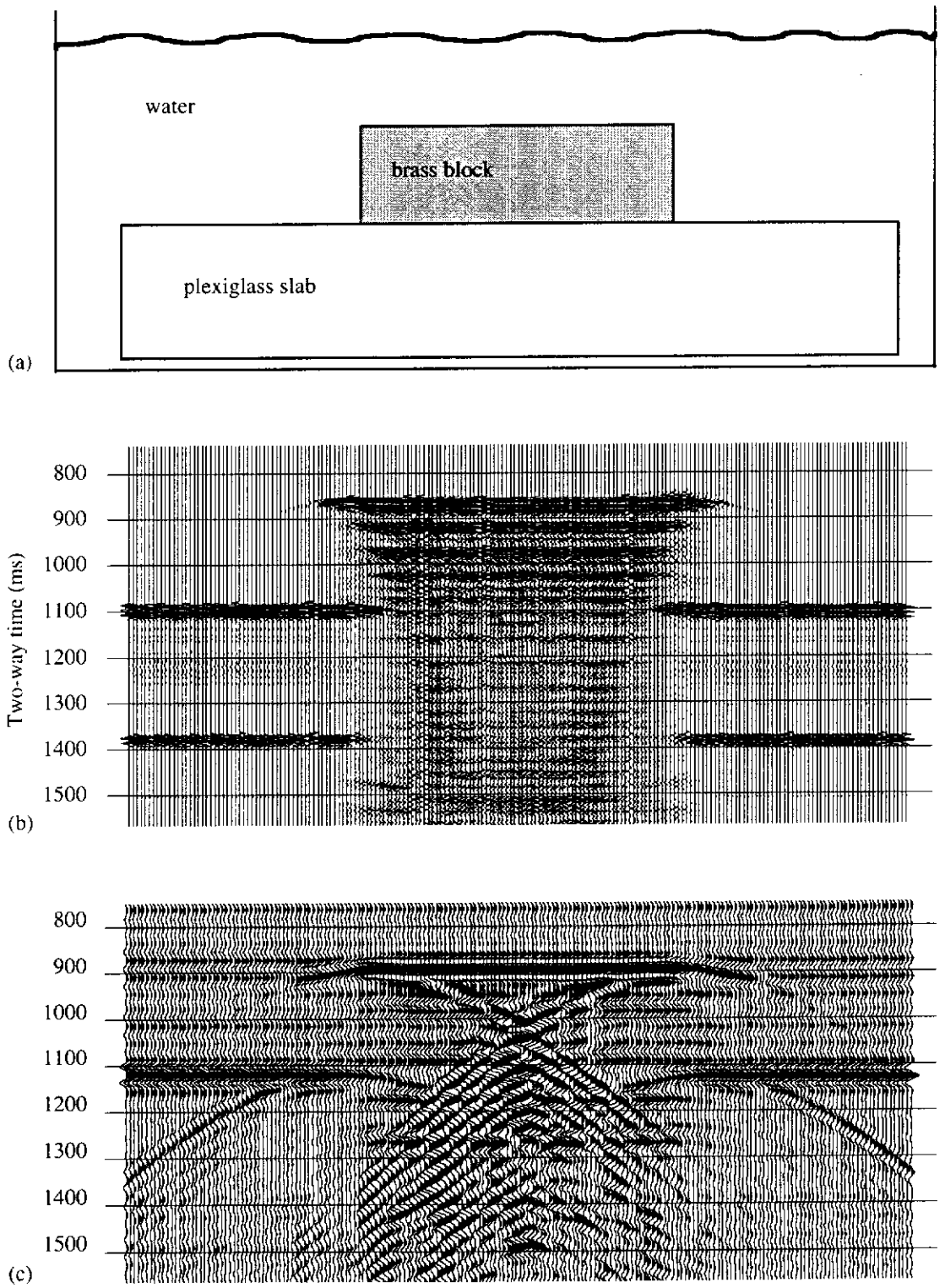

Figure 3.5: (a) Schematic diagram of a physical model designed to produce strong diffractions from the edges of a brass block overlying a slab of Plexiglas. (b) Zero-offset seismic section recorded over the model with a directional transducer. (c) Seismic section from the same model recorded with an omni-directional transducer.

Conventional transducers can be used in contact with a physical model to produce and record elastic waves, or suspended in water to produce acoustic waves, as is the case in this thesis. However, these transducers are unable to generate elastic waves when used in contact with unconsolidated sand models due to poor coupling which is a result of the large contrast in stiffness between the element and the sand surface (Shirley, 1978). The coupling can be improved by increasing the applied pressure but this will also change the elastic properties that are being measured. In the case of unconsolidated models this would also destroy the surface of the models. For this reason only acoustic waves have been recorded in this thesis.

3.1.4 First Break Picking for Velocity Measurements

Correct picking of first breaks is vital for accurate velocity measurements and for determining the elastic parameters of a laboratory sample or model. This seemingly trivial task can be the difference between the success and failure of an experiment and is frequently overlooked or poorly documented. When comparing results from different acoustic studies it is very important to understand the implications of the possible differences in first break picking methods.

The problems are a result of one or more of the following factors:

i) the definition of the first break,
ii) the method used to pick it,
iii) the kind of arrival that the first break represents, and
iv) the travel path that is assumed for the event.

The most room for error in actually picking the onset of an arrival is when there is a poor SNR. However, for physical modelling with directional transducers this is the least serious of a number of potential problems, particularly when the data has been recorded at variable offsets, or when the model material is highly attenuating (ie.

unconsolidated sand). It will be shown here that the arrival times of the first breaks are significantly affected by the unrealistic size of the source (ie. they are not point sources).

The travel path for the first break is often calculated assuming it's the distance between the centres of the transducers. However, as will be shown, the first arrival is actually the one that has taken the shortest path between the near edges of the transducer. This can lead to serious errors in velocity estimations. With variable offset data there are several distinct events that are from different parts of the transducer face that could all be termed 'first breaks'.

3.1.4.1 Velocity types

The term velocity can mean different things in different situations. The concepts of group, phase, signal and energy velocities are described in Brillouin (1960). Depending on the type of seismic source and the media that the waves are travelling in, these velocities may be significantly different. Group velocity is the velocity that energy travels away from a point source, while the phase velocity is the velocity perpendicular to the wavefront (Figure 3.6). In the isotropic case, or along the symmetry axis in the anisotropic case, these velocities are equivalent.

In the laboratory, to measure the group velocity a point source is required, but to measure the phase velocity data must be recorded at normal incidence to a plane wave source (Dellinger and Vernik, 1992). Directional piezoelectric transducers can be used to record either velocity type depending on their relative separation and width. At normal incidence, the wavefront from a directional transducer is flat like a plane wave, while at offsets greater than the element diameter the wavefront represents the group velocity surface (Vestrum, 1994). Theoretically, an infinite width transducer is required to generate the true plane waves necessary to measure the phase velocity when the axis of anisotropy is tilted relative to the transducers. However, it has been shown that a

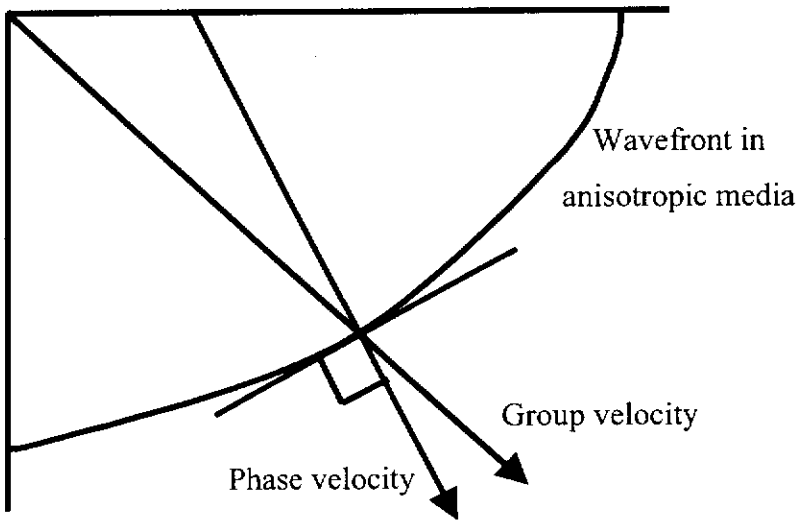

Figure 3.6: Schematic diagram representing group and phase velocities in anisotropic media, where the wavefront is not spherical. The group velocity is the velocity of the wavefront away from the source. The phase velocity is the velocity normal to the wavefront.

typical 12 mm diameter transducer will yield velocities very close to the phase velocity as long as consideration is given to the true travel path taken (Dellinger and Vernik, 1994). There is a high concentration of the energy in the plane-wave portion of the wavefront because it does not share the same geometrical spreading relationship that is associated with a point source. This last point is most important when using laboratory data to estimate rates of attenuation.

3.1.4.2 *Velocity in highly attenuating media*

In media where there is strong attenuation, the physical meaning of group velocity breaks down as the wave packet spreads. Carcione (1998) argues that group velocity only describes the wavefront for values of Q greater than 100. For Q less than 100, velocity dispersion becomes significant. The effects of attenuation and velocity dispersion are discussed in Chapter Four.

Using the travel times of first breaks to compare velocities in media with different rates of attenuation is hazardous as the measurements are most likely from different parts of the waveform (Wyllie *et al.*, 1958). This may be because either the true first arrival is imperceptible over the instrument noise or the dynamic range of the recording instruments is inadequate to record the absolute first arrival. There are some cases in this thesis where what appears to be the onset of the first peak in one sample actually corresponds to the second peak in another sample from the same series of experiments. Even more common is the case where the first arrival for some experiments is a peak, while for others the first detectable onset of energy is the trough from the same wave.

3.1.4.3 *Picking methods*

There are a number of methods of first break picking and it is difficult to say which one should be used for laboratory measurements of ultrasonics. While the particular method chosen is not necessarily a major concern when measuring relative changes in velocity, it can be serious if comparisons are to be made with other published results. It is,

therefore, imperative to state which method is used. This is most significant at low confining pressures where velocity variations between methods can be as high as 5%.

The first break has been defined as the point where amplitudes reach 1% of the maximum peak amplitude (Dellinger and Vernik, 1994), or when they reach 5% of the average amplitude (Rio *et al.*, 1996), which is approximately where it might be manually picked by eye depending on the SNR. Picking the first extremum amplitude (peak or trough) rather than the onset of energy, is a more consistent method although dispersion is again significant when attenuation is high. In many of the experiments in this thesis the time separation between the first break, the first peak and the maximum amplitude peak is not constant between samples, so it is important to consider the implications of this when picking arrival times. In most cases in this thesis the maximum amplitude peak is picked manually. The reasons for this will be discussed further in the section on velocity measurements in the following Chapter.

Other methods used to pick first breaks are cross-correlation of the recorded arrival with the input source signal (Peraldi and Clement, 1972). This method is sensitive to the time window used and this can be serious when attenuation is high. A similar concept has been devised by Molyneux and Schmitt (1997), that relies on finding the maximum correlation between a portion of an observed and an appropriate reference waveform. In this case it is the signal velocity, rather than the usual group velocity that is measured. This method is unique in that it is the only one developed specifically for physical modelling ultrasonic data. It is claimed that it does not suffer from dispersion effects as it only samples around one eighth of the waveform and therefore is most applicable when the waveforms evolve slowly as a result of changing conditions, pressure effects or attenuation. However, the accuracy of this method deteriorates rapidly as the SNR decreases and it can also be ineffective at low (room) pressures due to waveform inconsistency. Boschetti *et al* (1996) developed a fractal-based technique that is slow but effective in areas where the SNR is too low for other methods to be successful.

3.1.5 Waveform Changes with Offset

The following discussion relates to the far field energy pattern of directional transducers, which is when the distance from the transducer face is greater than the diameter of the active element. For an analysis of the near field behaviour the reader is referred to Savic (1995)

3.1.5.1 Amplitude changes with offset

The directional characteristics of the transducers that ensure sufficient energy output in a desired direction involve a large sacrifice in signal quality laterally from the direction in which they are focussed. Two problems result. These are changes in the amplitude and shape of the waveform with offset. Figure 3.7 shows the results of direct transmission tests of a similar transducer used by Tadepalli (1995). The receiving transducer directly faced the source transducer and was rotated around 180° to record the changes with offset. A solution to the problem of amplitude changes with offset was offered by Tadepalli, using a directivity function derived by Waters (1987). This correction treats the large flat face of the transducer element as a finite set of linear arrays, each subdivided into a finite set of omni-directional sources (or receivers). The directionality effects are produced by the constructive and destructive interference between the component waves of the individual source-receiver elements of the array.

The Waters correction will restore amplitudes to what would be expected from a truly omni-directional source and receiver configuration, with the trade-off being that a large reduction in signal-to-noise ratio (SNR) would be expected at large offsets. This solution is adequate for many physical modelling studies when the first break amplitudes are the only part of the data that is of interest. However, when the data are required to be stacked and treated as any other field data set with wide offsets, the changes that occur to the waveform cause the biggest problem. It also makes no allowance for the apparent changes in source and receiver location that occurs when recording variable offsets, and affects the relative travel time relationships.

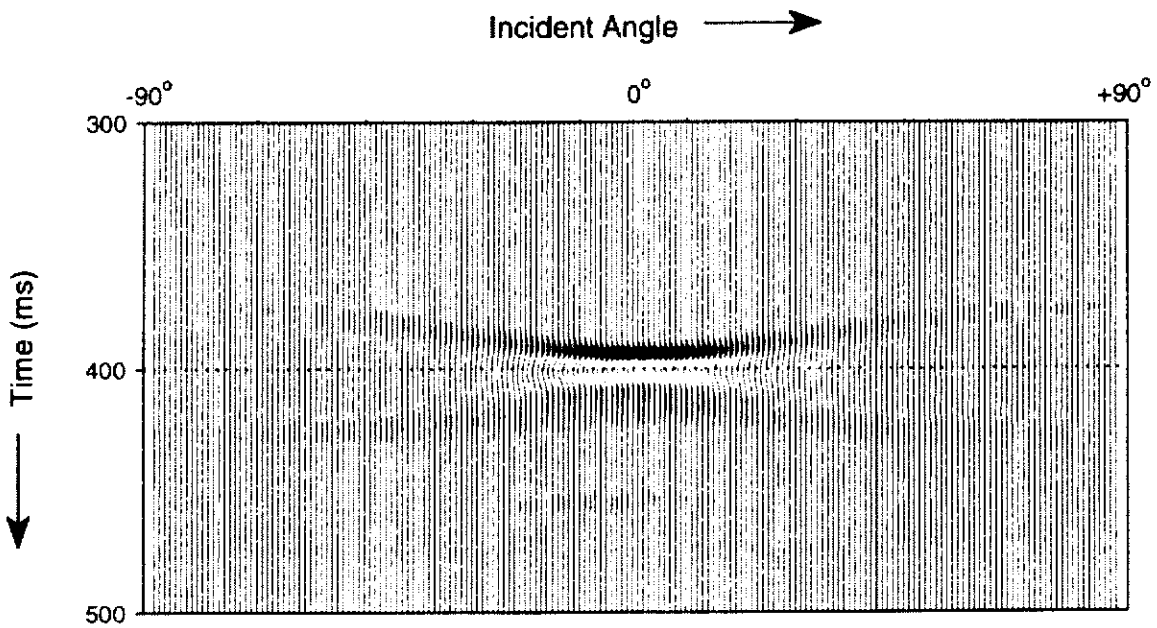

Figure 3.7: P-wave transmission record showing how the waveform and amplitudes recorded with directional transducers varies with incident angle (after Tadepalli, 1995).

3.1.5.2 *Waveform and frequency changes with offset*

The data from a variable offset physical modelling survey have been sorted into four constant offset sections with the same CMP in Figure 3.8, to show the changes that occur to the surface reflection of a flat layered sand model with offset, along with the associated frequency spectra. As the offset is increased, the waveform of the surface reflection changes dramatically and the frequency content is also reduced from a central frequency close to 100 Hz (scaled) at zero offset, to around 60 Hz at 20° offset. This effect means that it is very hard to achieve a reasonable stack of variable offset data without degradation of the near offset, higher frequency data.

3.1.5.3 *Diverging arrivals*

Another problem with variable offset acquisition becomes apparent when velocity analysis is performed. The velocity required to achieve an adequate stack of the surface reflection (sea bed) is in fact higher than the known velocity of water (1500 m/s). It appears as though the first arrival does not originate from the centre of the transducer face, as assumed, but rather from the nearest edge of the transducer. This apparently incorrect assumption about the position of the source means that the travel paths are actually shorter than the calculated distance between the transducer's centres, which subsequently results in a higher than expected velocity to perform normal move-out (NMO) corrections. At larger offsets the surface reflection separates into three diverging arrivals with different moveouts (Figure 3.9). The directional characteristics result in interference of the wave with itself at non-normal emergent angles. This can also be seen on other physical modelling data sets not related to this project although, to the best of the author's knowledge, this is the first time it has been documented. The three arrivals are all clearly water-bottom reflections, but each one requires a different moveout velocity to stack effectively. The first one requires a higher than expected velocity to stack (source is the near side of the transducer which has a shorter offset). The second, or middle, arrival stacks correctly using the velocity of water and, therefore, could have originated from the middle of the transducer face as

(a) Zero offset

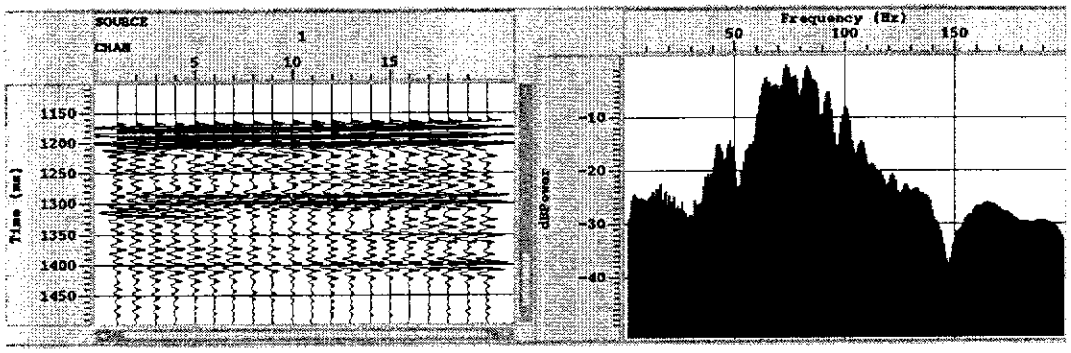

(b) Near offset (6°)

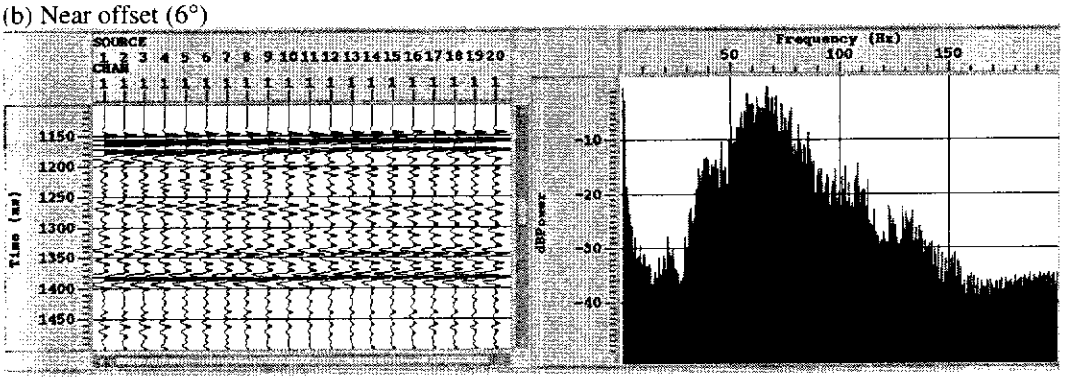

(c) Mid offset (13°)

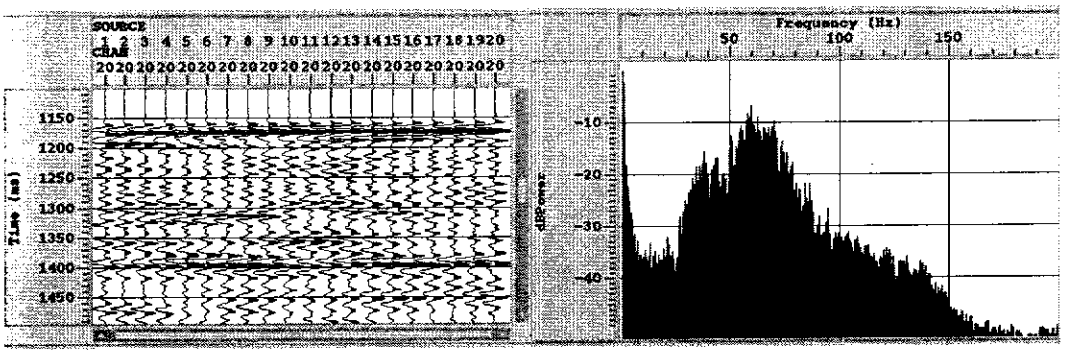

(d) Far offset (20°)

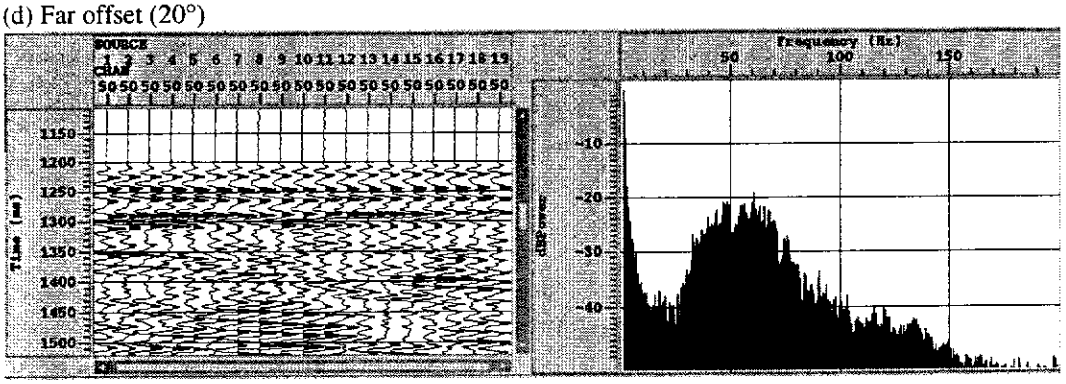

Figure 3.8: Constant offset seismic sections and corresponding frequency spectra recorded at progressively increasing offsets. Note how the reflections deteriorate and the frequency content is reduced at larger offsets.

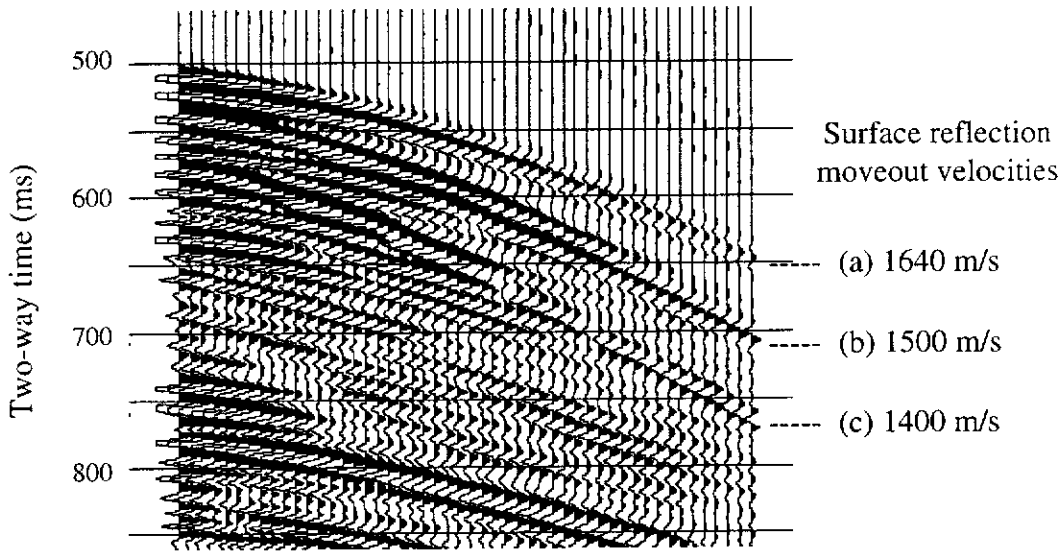

Figure 3.9: Physical modelling shot record showing how the model surface reflection recorded with directional transducers diverges into three discrete arrivals with different moveout velocities.

originally assumed. The third arrival can be stacked effectively using a slower velocity than that of water, and so it is suggested that this signal originates from the far side of the transducer face where the offsets are larger than the centre-to-centre distance. As the velocity of water is clearly constant over the shot record, the diverging arrival times must correspond to different travel paths. Simple calculations to quantify the changes in travel time that correspond to the near and far sides of the transducers with increasing offset confirms that the transducer size is the source of the phenomenon.

Deeper reflections involve less variation in travel path lengths between the near and far transducer edges, so the difference in moveout is less dramatic. This reduction in moveout distance with increasing depth is shown in Figure 3.10, where the depth of the surface reflection is progressively increased. The variation in the waveform that occurs both spatially and temporally is one reason why waveform shaping processes such as deconvolution yield poor results.

While it has been recognised elsewhere that the first arrivals are waves that travel the shortest path (eg. Brown *et al.*, 1991), which is from the edges of the transducers that are nearest to each other, the existence of the extra two diverging 'first' arrivals has not. This is probably due to the fact that the majority of physical modelling studies are only interested in first arrivals, and the studies that record multi-offset data usually use the less powerful omni-directional transducers, which do not suffer from this problem.

If only the first arrival from the near edges of the transducers is of interest, a reasonably effective stack can be achieved using the appropriate (but incorrect) stacking velocity, as indicated in Figure 3.9. A simple and more appropriate solution is to alter the apparent offset between transducers such that the source and receiver locations are treated as the near edges of the transducers. This way the first arrivals will stack together using the true velocity (alternatively, the third 'first' arrival could also be successfully stacked using the same true velocity by modifying the offsets to correspond with the far edges of the transducers). The quality of the final stack will still suffer from changes that occur to the waveform with increasing offset.

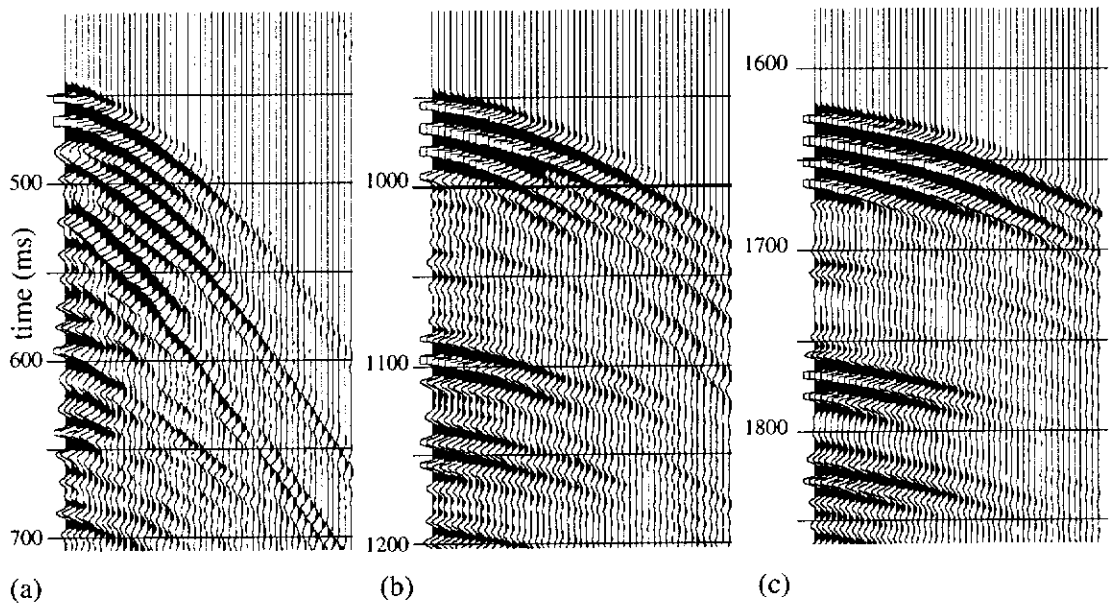

Figure 3.10: Comparison of three shot records from the same model, recorded at progressively increasing depth. The divergence of the three surface reflections with increasing offset is greatest at shallow depths where there is the largest difference in travel paths between the near and far edges of the transducers.

Altering the offsets to force the first reflection to stack with the true velocities is not a valid method when the objective is to stack data that contains several reflections from different depths within the model. This would result in all of the first 'near-side-of-the-transducer' reflections stacking successfully while the related second and third events should stack out and instead contribute to the noise within the data. However, this soon breaks down. The second of the three 'first' arrivals has the highest amplitudes and corresponds to the true centre-to-centre distance between the transducers. This arrival soon becomes the dominant event as the depth to a reflector within a model increases. This occurs particularly rapidly in unconsolidated sand models because the rate of attenuation is extremely high. To understand why this occurs, one needs to consider the geometry of the problem and how it affects the three diverging arrivals.

As mentioned earlier, the flat face of the transducer acts as a finite set of omni-directional point sources in a linear array. The first arrival travels from the nearest point source to the nearest point receiver (Figure 3.11). Similarly, the third event corresponds to the distance between the furthest points on the source and receiver. In terms of energy, these waves are effectively generated by just one point on the transducer face. The second or middle series of arrivals corresponds to the distance between the centres of each transducer. This distance is constant between every point source in the linear array and its respective point receiver. Hence, this wave is effectively the sum of all the points in the array and as such the energy is much greater than the arrivals from each edge. An unfortunate side effect is that the Fresnel zone is effectively widened, which reduces the horizontal resolution. There are of course an infinite number of alternate ray paths that would yield arrival times somewhere between the first and third events but their effect is presumably diminished by destructive interference.

3.1.6 Waveform Shaping

A major limitation to all seismic physical models is the resonant signal emitted from the source. The waveform is usually generated by a short, sharp (spike) input signal.

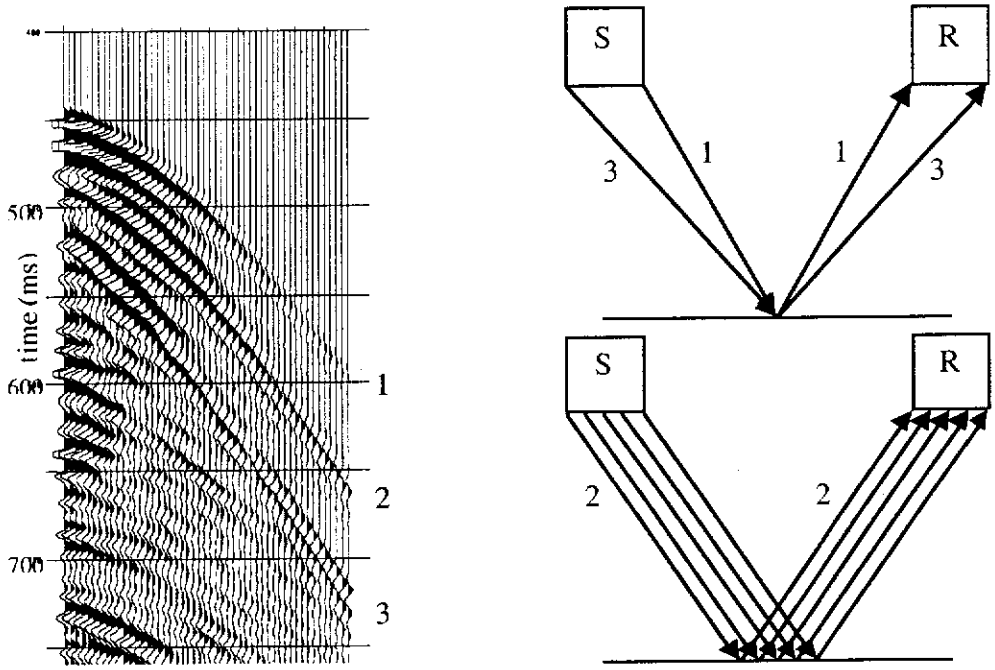

Shot record

Travel paths of three arrivals

Figure 3.11: Schematic representation of the different travel paths associated with the three diverging surface reflections. The second arrival corresponds to the distance between the centres of the transducers and has the highest amplitude because it is the sum of all in-phase arrivals with the same travel times.

However, as previously mentioned, the characteristic of a piezoelectric transducer is such that the crystal resonates for several cycles after the initial outgoing pulse. Consequently, the signal appears on the seismic section as three or four strong peaks over a time span of about 30 ms (scaled). This equates to a scaled depth of around 40 m in sand and effectively imposes restrictions on the best possible vertical resolution for all physical models, regardless of other problems associated with sandbox models.

The resonance of the transducers can be overcome to some degree with the use of a specially tailored waveform as the input rather than a simple spike. The waveform used for this is designed to cancel out the extra peaks and troughs that arrive after the first primary spike. The procedure used to generate a wave is to firstly record the ringy wavelet that is transmitted when a spike waveform is used as the input. The inverse of this waveform is then calculated (using software written at Curtin University) which is based on convolving the recorded output waveform with a fixed operator. This resulting inverse waveform is then used as the input signal for the transducers and should, in principle, result in a zero-phase spike output. Figure 3.12 demonstrates that this technique is fairly successful at damping the oscillations.

However, this process alone is not enough to solve the problems with variable offset acquisition as it does not allow for the changes that occur with offset. To do this, a method was developed by the author where a different inverse wavelet is used for every different incident angle within the shot record.

A range of different inverse wavelets was calculated for incident angles from 0 to 20°. A variable-offset shot record could then be built by using the appropriate waveform for each offset. This process is time consuming but effective in terms of achieving a consistent waveform with offset. The use of different inverse wavelets tailored for each particular offset is also reasonably effective in cancelling out the problem of the diverging arrivals mentioned in the previous section at near to mid-offsets. However,

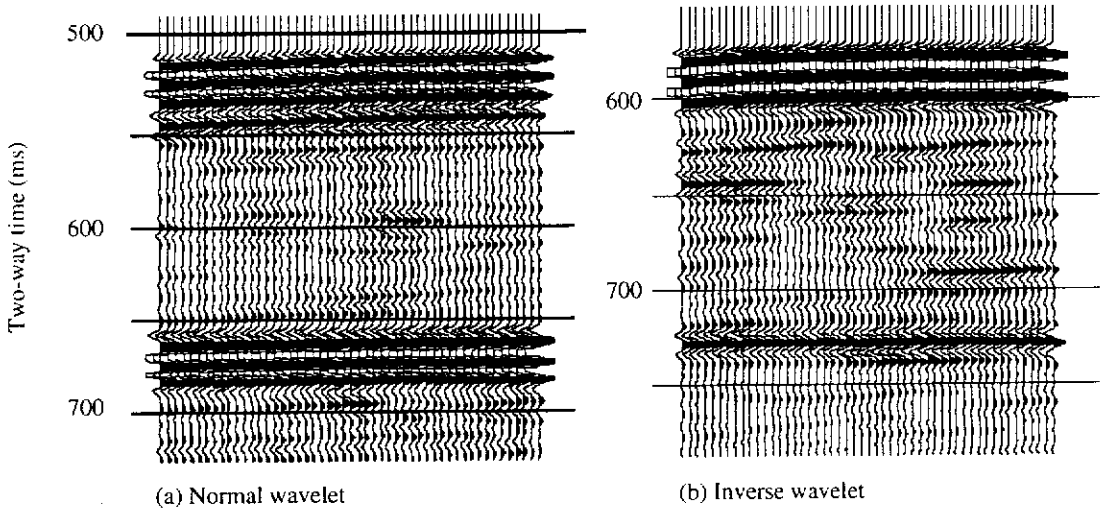

Figure 3.12: Comparison of seismic sections recorded with different input signal (a) Resonant signal produced from normal 'spike' input. (b) Compressed output signal from a tailored 'inverse filtered' input waveform.

the inverse filtered waveform has a maximum period of 25 μs (250 ms scaled). As the time separation of the diverging arrivals increases at larger offsets, the inverse waveform is no longer able to cancel out these effects. Another limitation is the fact that the waveform is designed for a certain incidence angle, and is therefore only valid over a certain pre-determined depth within any model. This is because the angle of incidence for any particular offset will reduce as the depth to any reflector increases. It also does not deal with the severe reduction in energy that occurs at significant offsets.

While this time consuming method of tailoring waveforms is a vast improvement, an even better technique has since been developed by the author that addresses these problems as well as producing much greater and more consistent signal energy at larger offsets. This new technique is described in the next section.

3.1.7 Transducer Rotation with Offset

Two transducer brackets were designed where the transducers could be rotated about the apparent point source of the energy (ie, the centre of the crystal face). This way, surveys could be recorded with the transducers rotating as the offset is increased, such that they are always directed at the same CMP (Figure 3.13).

To ensure that the location of the point source of the energy remains constant as the transducers are rotated, it was necessary to calculate exactly where the energy appears to originate from within the transducer. This was tested by directing the transducers at each other and firing a signal from one to the other at different distances. The different arrival times were then used to extrapolate back to the apparent source location, which was found to be 1.2 mm behind the protective cover of the transducer face. The actual distance may be less due to some inherent delay between firing the source in the acquisition program (SAM) and the actual output from the transducer. However, this makes no difference as long as the transducers are rotated about the apparent source location.

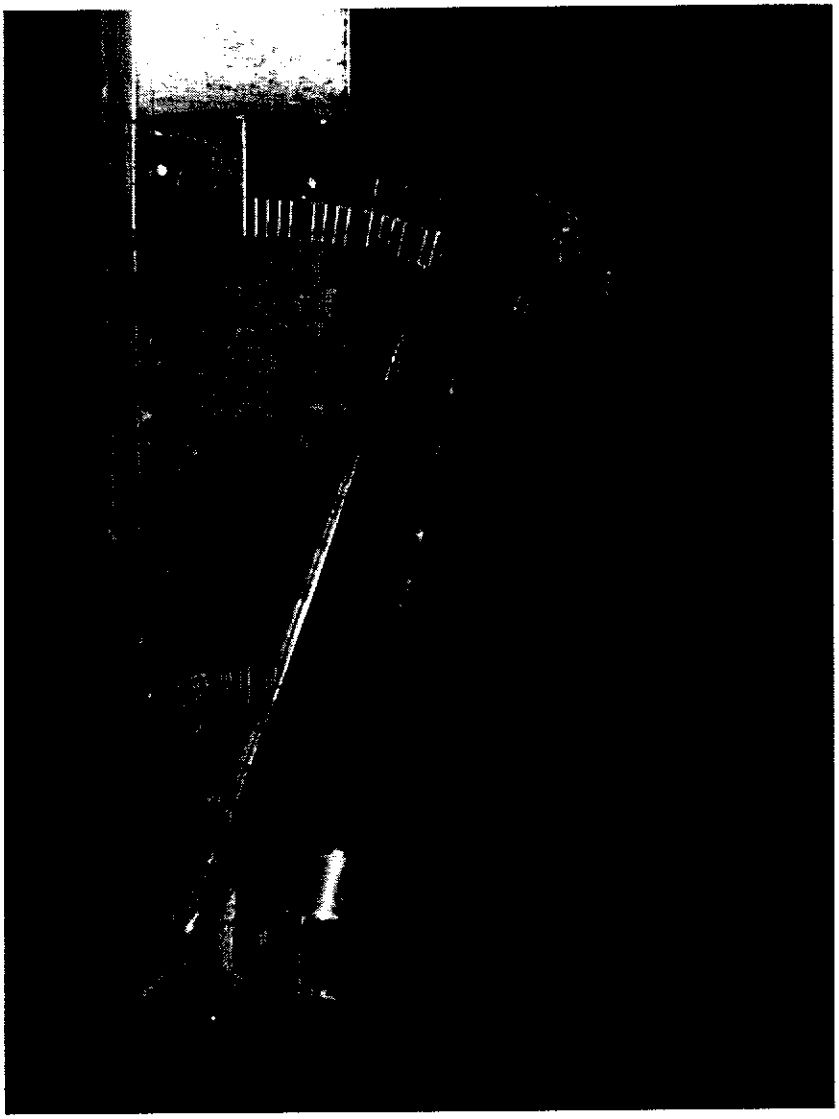

Figure 3.13: Photograph of brackets used to rotate the transducers as the offset is increased. The axis of rotation is about the apparent point source of the energy, which is 1.2 mm behind the centre of the transducer face.

Variable offset surveys are recorded as a series of constant offset surveys with the transducers fixed at the appropriate angle for each offset. The data are then rearranged into shot gathers sharing the same shot point, or CMP gathers ready for processing and stacking. Preliminary tests of this method over models comprising only horizontal reflections showed that this is perhaps the best solution to the drawbacks of using transducers to simulate a scaled seismic source.

It is clear that both zero-offset and the angled transducer offset are superior to variable offset surveys collected with the transducers held at a fixed angle. However, this does not solve all problems as there are two other effects to take into consideration:

1. When transducers are directed at a CMP on the model surface, the angle of incidence at horizons below that CMP will be decreased and therefore some change in source signal will occur.
2. Ray path bending (Snell's Law) means that the angle of incidence to horizons below the surface will be increased, again resulting in a change in source signature.

The combined effects of these two problems cancel each other to some extent, but calculations using a simple velocity field considered representative of a typical sandbox model (water = 1500 ms^{-1}, over sand = 1700 ms^{-1} , with a 'shale' horizon at 20 mm depth = 1800 ms^{-1}) reveal that the combined effects are such that there is a 0.4° decrease in incident angle at a depth of 25 mm for near offsets, and a total combined effect of 2.3° decrease in incidence angle at far offsets (20°).

These effects, while undesirable, can be mostly overcome with some careful planning at the acquisition stage. Firstly, it is an easy matter to set the angle of the transducers such that they allow for these effects. Secondly, there is no need to focus the transducers at a CMP on the model surface. By focussing the transducers at a certain depth within the model, say 25 mm (250 m scaled), a better image of the interior reflections can be produced, with the tradeoff being an inferior stack of the surface reflection. The surface of the model will still be imaged clearly due to the very large acoustic impedance

contrast and the fact that it is always a (near) horizontal surface. As the surface reflection is the least important reflection from the model, a slight deterioration of the quality of this horizon's image is of no consequence. This is illustrated in Figure 3.14, which compares two shot records recorded over the same model. The transducers for the first record (Figure 3.14a) were directed at a CMP on the model surface, and for the second record (Figure 3.14b) they were lowered by 25 mm so they were directed at the same lateral position, but at a depth of 25 mm within the same model.

If the transducers are focussed at a depth of 25 mm in a model with a total depth of 60 mm, the change in incident angle above and below the focal point at any CMP will be no more than 2° at large offsets, and much less at mid and near offsets. Significant changes in waveform do not occur at angles below 2° and so the quality of the stack should not be affected greatly. The stacked sections of the two cases shown in Figure 3.14 are shown in Figure 3.15.

While these results suggest that this method has potential, with such a simple model comprising only horizontal reflections, it is not clearly superior to zero-offset acquisition. To prove the worth of this acquisition set-up, it is necessary to record a survey over a model containing some sort of geological structure, where the benefit of stacking waves with different ray-paths can be realised. An example of this will be shown in Chapter Six after the methodology of building reflecting horizons into sandbox models is presented in Chapter Five. The technique of rotating the transducers with increasing offset developed here led directly to another physical modelling project on the effects of high velocity layering on seismic wave propagation (Leslie, 1998).

It is important to note that this style of acquisition is labour intensive and much slower to record than a zero-offset survey. To record a 20-fold survey takes 20 times longer to record than a corresponding zero-offset survey. While this is a small price to pay for a superior image, it becomes significant if a 3-D survey is required. The time taken to record a small 3-D survey can easily add up to a week, compared with a few hours for a zero-offset 3-D survey. The extra time required is particularly significant if time-lapse changes are occurring within a model because these changes may take place over a

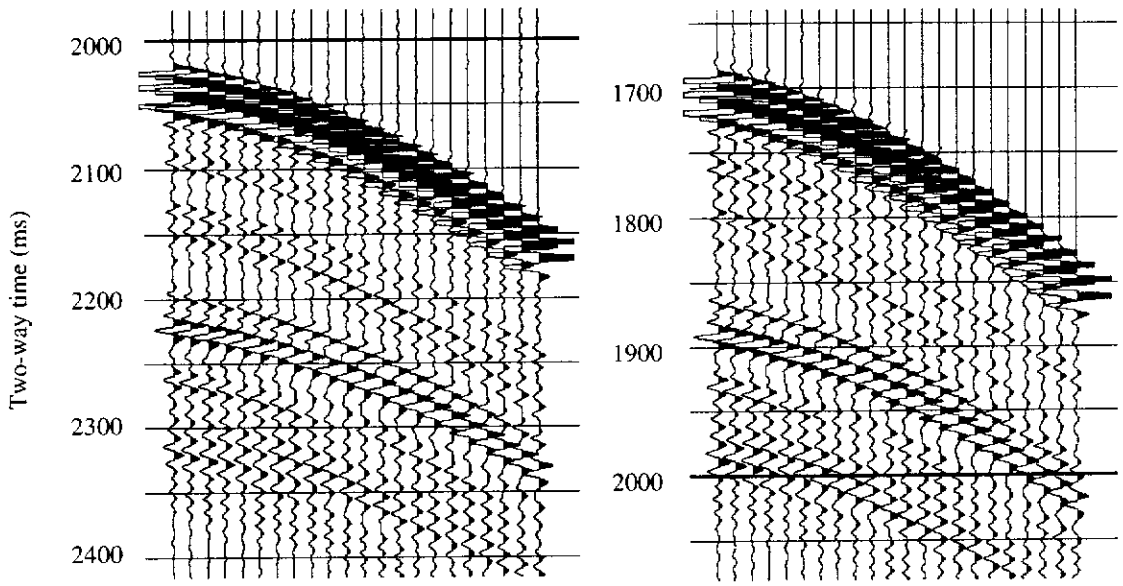

Figure 3.14: Comparison of shot records where the angle of the transducers is changed with increasing offset such that they are focussed on the same CMP on (a) the surface, and (b) 25 mm depth.

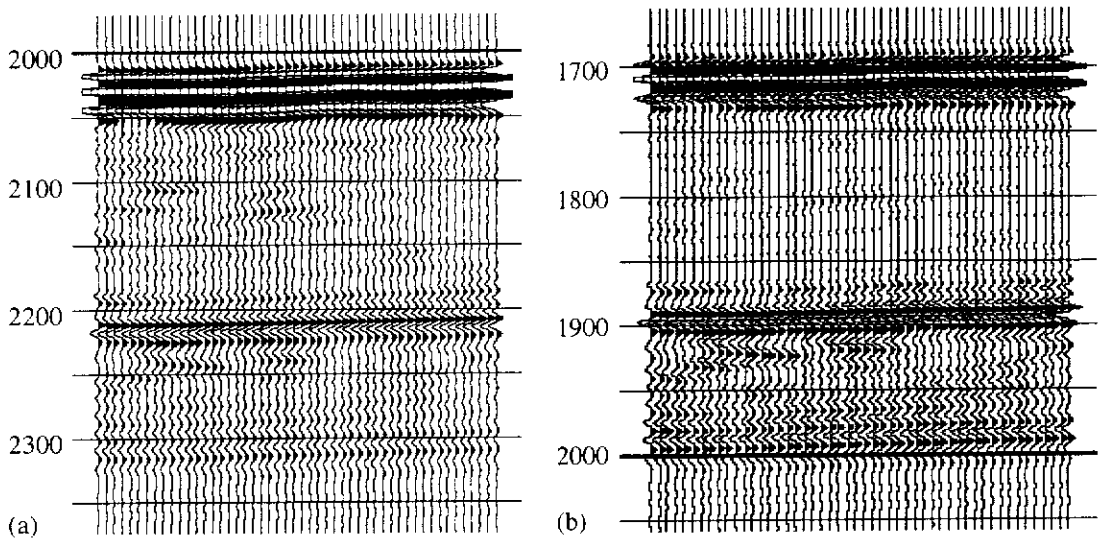

Figure 3.15: Stacked seismic sections of shot records in Figure 3.14. (a) Transducers focussed at surface. (b) Transducers focussed at 25 mm depth.

similar time span. This means that the changes are happening during the survey, so the final stack will be affected and time-lapse comparison surveys will not be successful.

The obvious solution to reduce the amount of extra time required to record a full-fold 3-D survey is to automate the mechanism of rotating the transducers and development of this is currently underway. Brackets have been made that house an extra stepper motor for each transducer. The motors are held above the water level and control the transducer rotation via shafts that are connected by right-angled reduction gears. The brackets have been tested and shown to work reasonably well although further refinement is necessary to improve the precision of the movements. The acquisition software SAM would have to be modified to incorporate the appropriate transducer rotations during acquisition.

3.1.8 Transducer Positioning

3.1.8.1 Positional Accuracy

It was noticed, when moving the transducers in discrete steps between source and receiver locations, that there was an amount of vibration or 'wobble' of the transducers caused as the brackets holding the transducers are jerked between positions. The modelling system incorporates cables and shafts that are designed to allow precise control of the movements in three-dimensions. It was found, due to the nature of the system, that movements along the arbitrarily named y-axis are more precise and have less backlash than movements along the x-axis.

For this reason, whenever possible, the 2-D surveys were recorded along the y-axis and when recording 3-D surveys, the in-lines were also along the y-axis. However, there are alternative ways to control the movement of the transducers and these were tested to find the fastest and most accurate way to acquire the data without compromising the time required to record large surveys.

3.1.8.2 *Discrete-Step Acquisition Versus Continuous Motion*

When recording seismic surveys on the physical modelling system, there is some trade-off between positional accuracy, acquisition speed, and the amount of unwanted 'wobble' of the transducers, depending on the configuration used. The computer-controlled positioning system for the source and receiver transducers can be set to any predetermined speed and acceleration between one shot location and the next. When the transducers are moved to each subsequent location, there is a degree of oscillation that requires a small amount of time to settle down.

After the transducers are moved between locations in discrete steps, it is possible to include a delay between the time that the transducer reaches the next location and when the source signal is fired. This option for a delay is to allow time for the transducers to come closer to complete rest before the source is fired, and subsequently should result in a cleaner, more consistent source signature. A comparison was made between two surveys where the only difference was the amount of 'wait' time between shots. It was found that for surveys along the y-axis there was no discernible difference between one second wait time and no wait time. Hence, the time saved by removing the wait time, especially on long surveys, was worthwhile.

Another option available when acquiring data is to move the transducers along the survey line in one continuous motion, firing shots at predetermined time intervals that coincide with the desired transducer locations. The time saved when recording large surveys this way is significant, especially if recording a 3-D survey. However, when recording variable offset CMP records, it was found that the positional accuracy suffered and, subsequently, moveouts were not perfectly hyperbolic, and this is a necessary requirement if the best possible stack is to be produced. This method also precludes the option of vertical summing, which later will prove to be an important factor for source repeatability.

3.1.9 Multiple Identification and Removal

3.1.9.1 Water-Bottom Multiples

A series of experiments was conducted to observe the effect that changing the transducer depth within the tank of water had on energy attenuation and the timing of the multiple arrivals. It was found that the typical sea-bed multiple that was internally reflected back from the water-air interface could be removed easily by increasing the depth of water in the tank. The result was that the travel path of this multiple was extended such that its arrival time was later than the reflections from the layer boundaries within the models, where it did not obscure any useful information. This method is obviously much easier to implement in modelling experiments than it is in the field.

3.1.9.2 Transducer-Face Multiples

The transducers used as source and receiver have a flat face with a diameter of 13 mm. In scaled terms this is 130 m, which means that they effectively provide a large surface from which incident seismic waves may reflect. It was found that this resulted in a multiple reflection that is unique to seismic physical modelling. The signal had reflected off the model surface (sea-bed), then off the flat face of the source and/or receiver, down to the surface and back again. This multiple must occur with all zero-offset or near-offset physical models using this system, but a literature search on experiments of this kind showed that this had not previously been published, or was ignored.

While this multiple had previously gone unrecognized, its existence was readily proven with models where there was a change in the distance between the model surface and the transducer. As the travel time for the surface reflection was increased with depth,

the multiple had its travel time extended by exactly double. Calculations of the travel times from all other possible reflected ray paths, such as those from the sides and base of the water tank, and the edges of the model container, showed that there was no other reflecting surface that could have produced these reflections.

To demonstrate this, a two-layer model was used in a series of experiments with progressively increased offset between the source and receiver. A zero-offset experiment, where the same transducer is used for both the source and receiver, was also recorded over the same model. Increasing the offset was found to have the predicted effect of attenuating the multiple from the transducer faces, by moving the reflecting face of the transducers further away from a midpoint position where the signal could reflect from it and back again (Figure 3.16).

This could be observed in real time on the oscilloscope. The offset was manually increased while repeatedly firing the source, and the amplitude of the multiple reflection decreased very quickly relative to the primary reflection. However, the strength of the primary reflection was also affected and so this was not the preferred option for most experiments. The zero-offset experiment (same transducer for source and receiver) produced both the strongest primary and multiple reflections. As the multiples could be easily removed with thoughtful positioning of the transducer with respect to both the depth in the water and to the model surface, zero offset was used for many of the models in this thesis.

3.2 Analogue Sandbox Modelling

3.2.1 Introduction

Consider a box filled with sand, within which there are thin horizontal sand layers of contrasting colours. By progressively altering the dimensions of the box, the sand

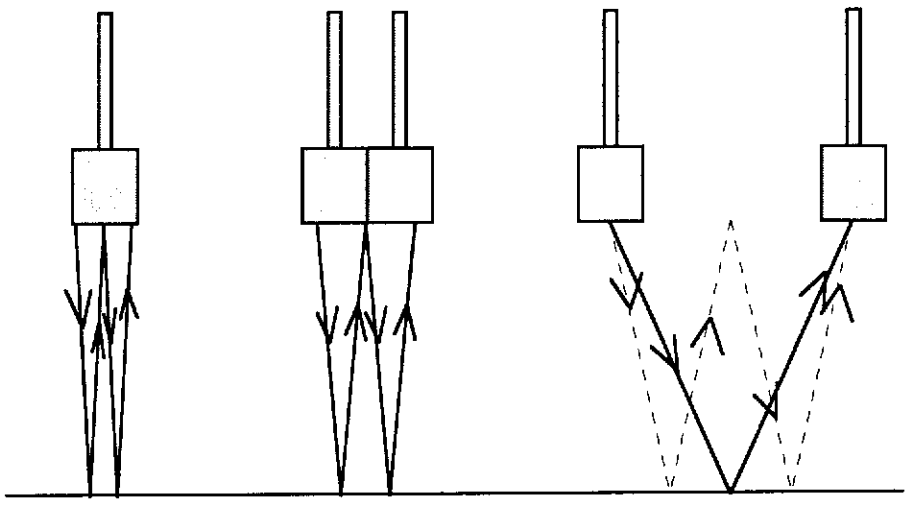

(a) Zero offset (b) Near offset (c) Far offset

Figure 3.16: Ray paths for multiple reflections from the face of the transducers. The multiple is not generated at far offsets.

grains are rearranged. The coloured layers act as markers, illustrating the pattern of deformation of the sand within the box. This is the principle behind sandbox modelling experiments - begin with undeformed coloured sand layers, impose a known stress regime, and then observe the deformation patterns that result.

Analogue sandbox models are scale models of the Earth's crust. They attempt to mimic the deformation response from tectonic forces and the resulting structural styles observed in nature. A sandbox model's design is based on a limited knowledge of the natural example or structural style that is to be modelled. By imposing known or presumed boundary conditions on a model, the behaviour of the material can be tested for comparison with the natural example. Principal stress directions applied to the model are based on those hypothesised from field or geophysical data (such as the orientation and inferred displacement senses of folds, faults and shears). Features that appear consistently and repeatedly in the modelling provide an indication of deformation processes and the sequential evolution of structures.

The key benefit in using analogue sandbox models is that information inaccessible in nature, due to limited seismic or mapping information (which may be ambiguous or of limited extent due to survey constraints), can be obtained by observing structures in detail from plan views or sections through the model. Previous modelling studies have aided the interpretation of map or geophysical data, especially seismic sections, where several alternative interpretations are often possible (Gartrell, 1993; Lemon and Mahmood, 1994). However, prior to this study, analogue models had not been used to test the correspondence of a seismic image of geological structures with actual geological sections. A series of simple sandbox models was used in this research, and models were mostly kept as structurally simple as possible to assist the development of techniques for advancing the seismic modelling technology.

Sandbox modelling is well suited to modelling extensional systems, and since these systems are often associated with subsidence and burial beneath sediments or the sea or both, they are also particularly relevant to reflection seismology. The deformation style

of such models is, however, of no great significance in this thesis, since the focus is on developing techniques to enable seismic imaging of the models.

Criticism of analogue modelling is usually aimed at the fundamental assumptions of geological developments and subsequent simplifications involved. There are usually too many unknown variables to attempt to accurately model individual geological structures. However, by removing some of the complications found in natural systems, the key elements are highlighted for investigation of the concepts of stratigraphic deformation. Analogue models not only reproduce structures recognised in nature, but also structures that were previously unrecognized (Vendeville *et al.*, 1987).

3.2.2 Rheology and Scaling of Sandbox Models

Rheology refers to the flow and deformation response of a material to an imposed stress. Sandbox models commonly focus on brittle deformation in the upper crust, using dry cohesionless sand grains. However, they can also incorporate materials such as silicone putty or honey, analogous to the ductile lower crust and upper mantle. For laboratory results to be considered true analogues of natural structures, it is important that the materials and tectonic processes are accurately scaled (Ramberg, 1967).

Horsefield (1977) showed that the rheological properties of moderately cohesive sediments, with frictional plastic behaviour at the time of faulting, can be simulated with dry sand after scaling down by a factor of between 1:10 000 and 1:100 000. Dry sand has an angle of internal friction ϕ = 30-32°, which is similar to that determined for brittle sedimentary rocks in the upper continental crust (Bryerlee, 1978). However, this value can vary significantly depending on the handling technique employed (Krantz, 1991) and, as shown later, also has a significant effect on seismic transmission properties. The deformation process obeys the Mohr-Coulomb failure criterion for faulting, in accordance with deformation mechanisms in the brittle upper crust (Jaeger and Cook, 1979). The characteristics of granular material mean that faults develop as

dilational shear zones (Mandle *et al.*, 1977), and the width of these is governed by the size and packing distribution of the grains.

The very low cohesive strength of dry sand makes the models essentially strain-rate independent, and allows deformation experiments to be performed over a reasonable length of time. Millions of years of tectonic deformation in sedimentary rocks are usually simulated in less than a day. Although the cohesion between the sand grains is very small (most publications refer to it as 'negligible') it may be important in models involving fault reactivation (Richard and Krantz, 1991).

A scale factor of 1:10 000 was chosen for the models presented here, for reasons relating to the seismic response that is discussed later. Thus a typical model area of 300 mm by 200 mm and depth of around 100 mm represents field dimensions of 3 km by 2 km and a depth of 1 km. The quartz sand used in most of these models has a mean grain size of 200 μm and a maximum of 300 μm, which, although a good analogue for sedimentary rocks in terms of its deformational behaviour, later experimentation will show is not ideal in terms of the seismic response. This is because an actual grain size of 200 μm represents the equivalent of a 2 m diameter boulder.

3.2.3 Examples

Perhaps the most common style of analogue model is one that is used to simulate normal faults and their hanging-wall deformation. Such models have guided the structural interpretation of field and seismic data for more than 60 years (Cloos, 1928; Vendeville and Cobbold, 1988; McClay, 1989; Withjack *et al.*, 1995). They have also provided data for testing and calibrating geometric models of normal faults (Dula, 1991; Kerr and White, 1992; White, 1992; Xiau and Suppe, 1992).

More recent models of extensional rift systems have been extended to include multiphase systems, where faults are reactivated by later extension in an oblique orientation (Keep and McClay, 1997). The orientation of each phase of deformation

can be tailored to help understand a particular geological setting where the maximum stress directions are deduced from field studies and palaeostress analysis (Harris *et al.*, 1994).

Analogue models have been used to gain insight into pure strike-slip faulting (Emmons, 1969; Gapais *et al.*, 1991; Richards *et al.*, 1991; Tron and Brun, 1991; Schruers, 1994) and also their development with pull-apart basins in complex extensional settings (Hempton and Neher, 1986; McClay and Dooley, 1995; Richard *et al.*, 1995). A recent innovation in pull-apart modelling is the use of a mobile and ductile sheet within the model to act as a decollement (detachment surface) (Sims *et al.*, 1999).

Much work has been carried out at The University of Texas at Austin on modelling the kinematics and dynamics involved with salt tectonics (Ge *et al.*, 1997; Guglielmo *et al.*, 1997) and salt dissolution (Ge and Jackson, 1998). Models simulating inversion tectonics have also been dealt with (Koopman *et al.*, 1987; Buchanan and McClay, 1991; McClay and Buchanan, 1992) although they have received relatively little attention.

Sandbox models have been used to examine rheological anisotropy (Cobbold *et al.*, 1971; Harris and Cobbold, 1985; Hanmer *et al.*, 1996). Rheological stratification induced by temperature variations within the crust has recently been modelled with paraffin wax (Rossetti *et al.*, 1999) which has temperature sensitive viscosity. Lithospheric-scale analogue models have also utilized silicone putties to simulate the Newtonian flow characteristics of the ductile mantle been performed (Davy and Cobbold, 1991; Gartrell, 1997). Cobbold and Castro (1999) are developing ways to couple fluid migration with deformation in sandbox models of tectonic structures. Their idea is that detachments in sedimentary basins associated with gravity gliding, thrusting or rifting could be modelled by injecting air through a sieve under the model.

A different style of sand modelling is used to replicate depositional processes such as turbidity currents. As the number of undrilled structural hydrocarbon traps decreases, stratigraphic traps become more important. However these are generally undervalued in

most portfolios because of uncertainties in factors such as the seismic definition, hydrocarbon volumes and migration pathways (Meckel, 1999). Turbidite modelling involves visual observation of the depositional patterns that result as volumes of sand are released down underwater ramps. Some examples of variations on this theme are turbidity currents incident upon a ramp type flow barrier (Edwards *et al.*, 1994), multi-layer turbidites around obstacles (Alexander and Morris, 1994), and turbidity currents in density-stratified water (Rimoldi *et al.*, 1996). Seismic imaging of these models would allow improved interpretations of the relationship between successive flows.

3.2.4 Limitations

The nature of modelling means that assumptions and simplifications are inevitable (Vendeville and Cobbold, 1988). Many limitations can be overcome with more complicated and expensive model designs, but it is important to consider the main aims of the model building and the various effects that each physical property have on the desired outcome of the particular model. The complexity of structures in most of the models used for this research has been kept to a minimum, as the primary focus has been to develop techniques to enable the recording of seismic images of the models.

The main limitations to the style of models in this thesis are as follows:

i) non-perfect scaling of modelling materials;
ii) factors such as pore fluid pressure, temperature and differential compaction are absent; and
iii) cohesionless sand is unable to accommodate folds.

There are other limitations that apply to different types of analogue modelling of reservoirs. Reservoir heterogeneity is hierarchical in nature (Van De Graaff and Ealey, 1989) from the intergrain scale (Morrow, 1971), to basin or formation scale (Bridge and Leeder, 1979). No single analogue study can cover all of these scales. However, these limitations are largely irrelevant to the simplistic nature of the models presented in this

thesis, where the emphasis is on the seismic characteristics of the materials, rather than the deformation response.

3.2.5 Current Methods of Structural Analysis

3.2.5.1 Sectioning

The fundamental approach for the analysis of the structures formed in analogue models is the manual sectioning of the model with a knife after deformation has been taken to completion. The most common means of consolidating the sand sufficiently to prevent the model collapsing when sectioned is to saturate it with a water and gelatine mix. This process provides enough cohesion between the sand grains to allow sections of the model to be cut and photographed for later analysis without affecting the internal structure.

Sections can be cut in any orientation, even horizontally, but are typically cut vertically in the prevailing dip direction to reveal as much information as possible. In this orientation fault throws are at their maximum, and features such as antithetic faults, rollovers and block rotations are revealed (eg. Figure 3.17, after Buchanan and McClay, 1991). The orientation of the sections must be decided beforehand, and is based on the known applied stress fields and any information inferred from observations of the surface expression of the model as it is being run.

Typically, sections are cut as closely together as possible to enable the 3-D geometry to be inferred from the 2-D sections. Most publications cite section spacings of 10 mm, with smaller spacings very difficult to cut by hand. This equates to scaled dimensions of 100 m to 1 km between sections, which is sometimes barely adequate to map even the gross structure in 3-D if the model contains complex faulting. Nevertheless, having multiple sections from the one geological setting is a luxury unavailable in the field, and is the fundamental aspect of sandbox model analysis that makes it so powerful.

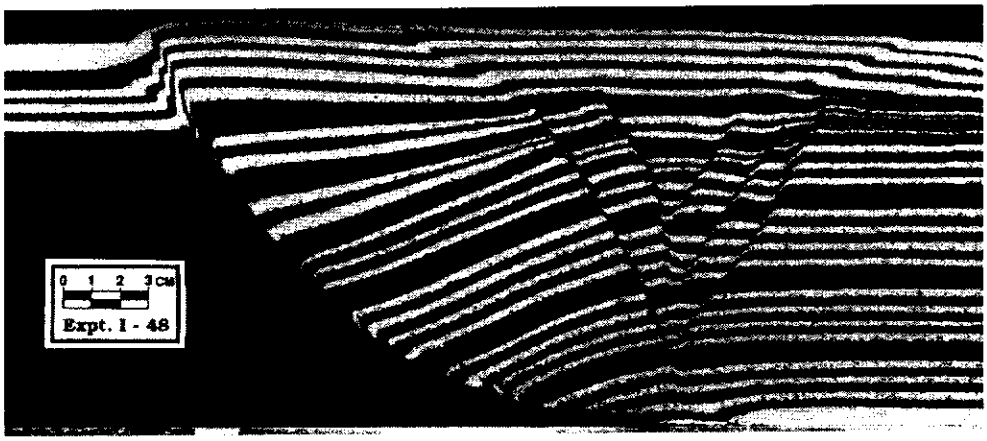

Figure 3.17: An example of an analogue sandbox model section. The section was cut along the main dip direction of the faults to capture the maximum fault throw and block rotations (after Buchanan and McClay, 1991).

3.2.5.2 *Surface Expression*

Time-lapse photography is often used to record progressive stages of deformation as the model is being run. There is often only limited information to be gained from this as it can only record the surface expression of the model, and syn-deformational layers of sand are usually added to the model at progressive stages, covering up the faults visible on the surface. However, the use of lighting at low angles to the surface highlights any visible faults, and photographs of this can be very helpful in establishing the order that faults are initiated within the model. Although most experiments are analyzed predominately from section-views, an example where a plan-view approach was used for the basis of the structural interpretation is provided by Dooley and McClay (1997) in Figure 3.18.

3.2.5.3 *3-D Computer Visualization.*

Improvements in the acquisition and processing of 3-D seismic data are probably the oil industry's most significant technological advance in recent times. Interpretation of these data has been influenced by the analysis of analogue models. However, such models have been analyzed almost entirely by traditional 2-D methods employing mostly cross-sections, which often makes it impossible to understand the full 3-D geometry of complex models.

Newly developed computer visualization software, EarthVision®, enables serial cross-sections from a sandbox model to be digitized, interpolated and rendered in 3-D to aid in visualizing structurally complex geology. This technology has been used to great effect with salt-related analogue models by Guglielmo *et al.* (1997) (Figure 3.19). However, it is important to note that this is purely a visualization tool, and does not provide any information that is not already available from the cross-sections of the model. The final result is still limited by the relatively large spacings required between each section, which the software must interpolate to fill the gaps. To visualize more subtle structures that may exist between each section, finer spatial sampling is

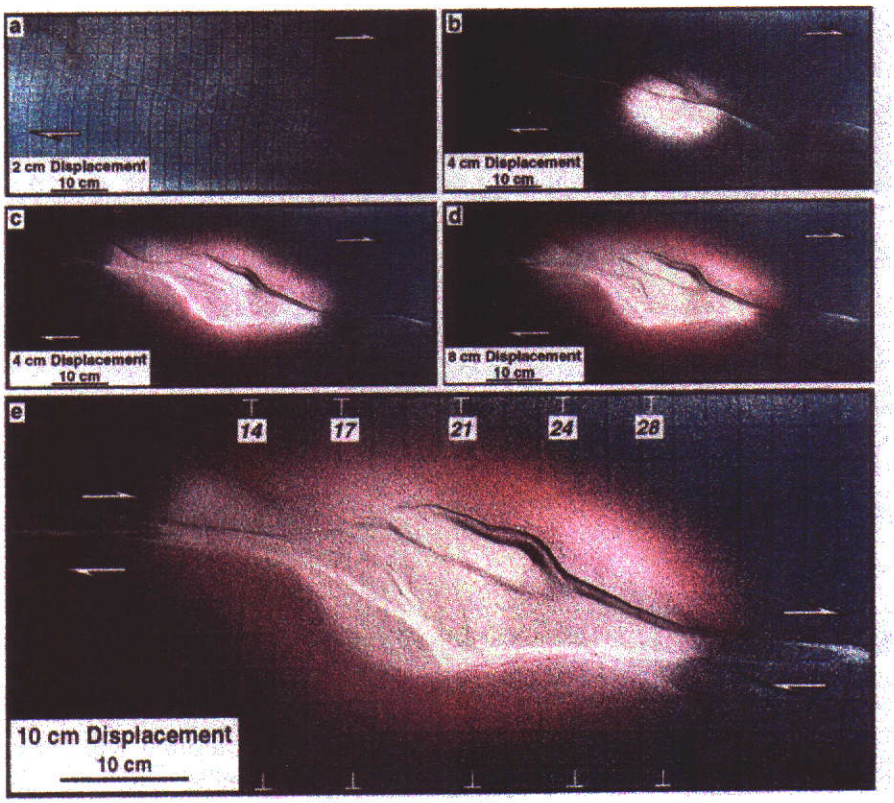

Figure 3.18: Plan view photographs of a pull-apart basin model. Time-lapse photography allows the evolution of the faults to be observed (after Dooley and McClay, 1997).

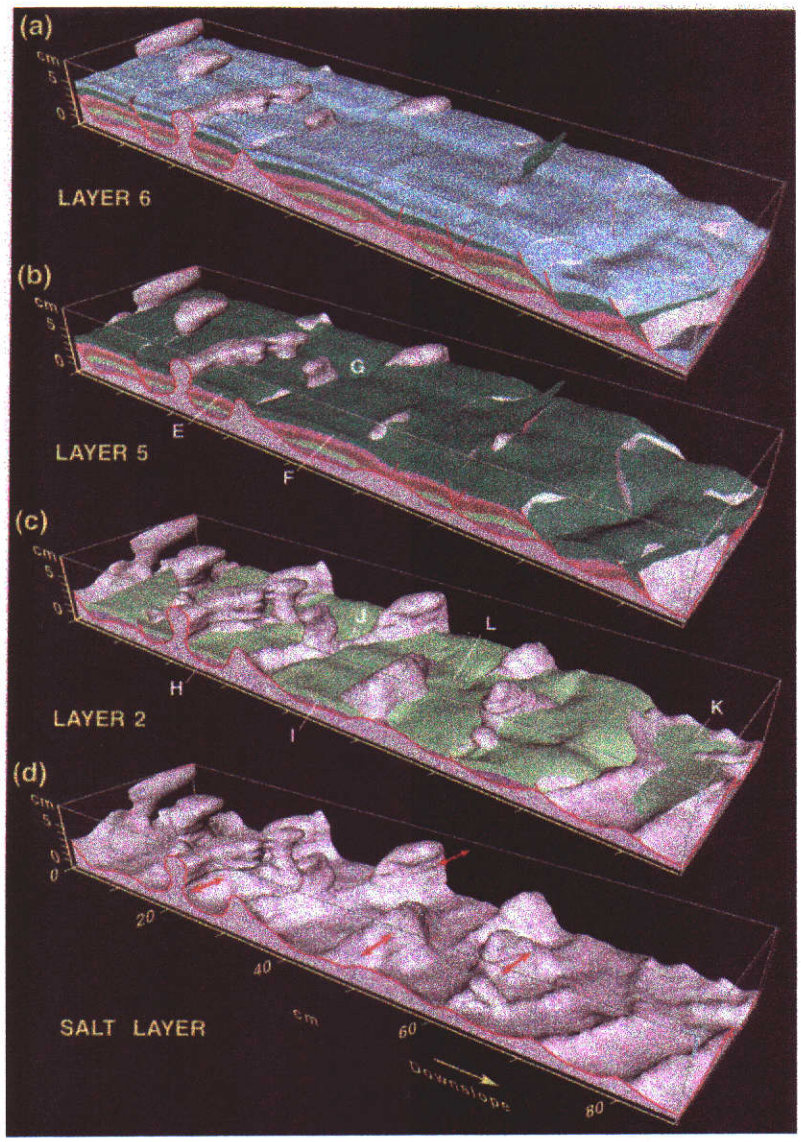

Figure 3.19: An analogue sandbox model of salt-related structures produced during gravity spreading and gliding. Computer visualisation software is used to progressively peel away the strata to reveal the subsurface structures in three dimensions (after Guglielmo *et al*, 1997).

required, which is one of the biggest potential benefits of developing the seismic imaging techniques in this thesis.

3.2.5.4 *Computerized X-Ray Tomography*

A recent innovation in non-destructive imaging of structures within sandbox models has been the adaptation of computerized X-ray tomography, or CT scans, for use with dry granular media. Manual sectioning of sandbox models means that the model is destroyed and only allows one orientation of sections to be made. CT scans have the advantage of being non-destructive, and therefore they allow sections to be imaged in a number of orientations. Another key benefit of this technique is that it allows the evolution of structures to be observed at progressive stages of deformation.

The CT technique was originally developed for medical imaging (Hounsfield, 1973). It was first adapted for use in geology to analyse rock properties and fractures in core samples (Vinegar, 1986; Raynaud *et al.*, 1989). Its use in analyzing analogue sandbox models was pioneered in Shell Oil Company laboratories (Mandl, 1988).

CT is based on the recording of a set of attenuation profiles recorded from an X-ray beam. Absorption of X-radiation by any substance depends on its bulk density and atomic number. The lower the density of the material, the more transparent it is to X-rays. If the materials used are relatively homogeneous, the resultant attenuation is roughly proportional to the local density (Desrues *et al.*, 1996). Faults develop in granular materials as dilational zones and can result in a density contrast of around 30% (Colletta *et al.*, 1991), and so they show up as areas of lower attenuation in the CT scan. Old faults that die out tend to recover their initial density, and so it is possible to visualize the fault chronology and emphasize out-of sequence mechanisms.

Recording a successful CT image from a sandbox model is far from simple. The resultant images contain considerable noise that is a result of density variations that inevitably occur from the non-uniform sorting of the sand (Figure 3.20, after Mahmood, 1996). As shown in this study, this is a problem that also affects the seismic response in

Figure 3.20: Computerised tomography (CT) image of normal faults developed during extension of an analogue sandbox model. The faults develop as dilational shear zones with lower density than the surrounding sand and show up as light colours in the CT scan (after Mahmood, 1996).

sandbox models. It should be possible to visualize the scans in 3-D using computer graphics systems similar to those used for 3-D seismic data, although the author knows of no examples of this to date.

3.3 Other Laboratory Modelling Techniques

3.3.1 Fluid flow models

Fluid flow models are designed to aid our understanding of how hydrocarbons move through water saturated sediments. These models can have applications in either a geological context, such as studying mechanisms of how oil moves from source rock to reservoir (secondary oil migration), or in a reservoir engineering context such as developing ways to improve enhanced oil recovery (EOR) methods. There is potential to apply the seismic modelling techniques developed in this thesis to either of these purposes.

3.3.1.1 Secondary oil migration models

Experiments with one-dimensional flow of oil in water saturated sands by Dembicki and Anderson (1989) involved visually monitoring the progress of oil as it migrated up through vertical or tilted glass columns. Similar models by Catalan *et al* (1992) studied the effects of changing parameters such as grain size, oil density and the oil-water interfacial tension. The gravity and capillary-controlled flow of oil in water saturated sand has also been studied in two-dimensional models by Thomas and Clouse (1995) (Figure 3.21). In this case the oil migration pathways were monitored visually and also with ultrasonic travel times to estimate relative saturations in different regions of the model.

The acoustic visibility of immiscible fluids (dodecane and water) in unconsolidated sands was examined by Kowalski *et al* (1998). The distribution of dodecane was

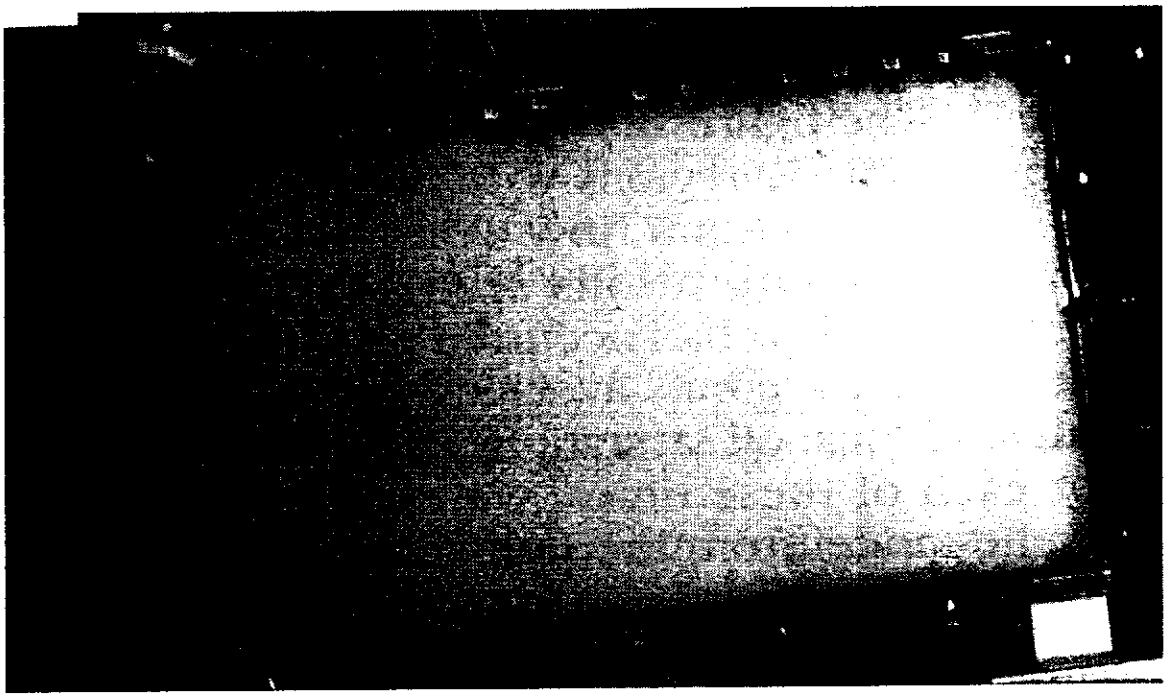

Figure 3.21: Photograph of 2-D oil migration through a sand pack model. The oil was injected at the bottom left of the model and migrates upwards and along the top surface of the model towards the outlet at the top right. The migration was monitored visually and with ultrasonic travel times. The ultrasonic data was recorded across the 25 mm thick model at periodic stages throughout the 231 day model run. Scale marks along the top are approximately 25 mm increments. (after Thomas and Clouse, 1995).

mapped in two-dimensions from changes in one-way ultrasonic transmission times. While in this case the model was three-dimensional, only an approximate estimation of the fluid distribution in 3-D was possible. This was done by excavating the sand from the model in a grid-wise fashion after the data was recorded and then separating the immiscible fluids.

Miscible and immiscible fluid displacement in porous media was mapped with ultrasonic transmission data by Soucemarianandin *et al* (1989). The method involved the use of a fixed array of transducers to monitor the progression of the fluid movement in 2-D from changes in one-way travel time. The spatial resolution of the fixed array was too large to resolve the fine 'fingers' of immiscible fluid that were observed visually.

3.3.1.2 Enhanced oil recovery models

Enhanced oil recovery methods are processes that are designed to flush out larger volumes of hydrocarbons from within a reservoir. These processes involve injection of other fluids that help mobilize the oil trapped within the sediment pores. Fluids commonly used for this are steam, carbon dioxide or water, depending on the geological conditions. Petroleum engineers have used physical models to help them understand and evaluate the mechanisms involved. For example, the processes of pressure cycling and steam injection were modelled with unconsolidated sand models under high confining pressure by Kimber (1991). The effects of injection rate and the oil-to-water viscosity ratio on recovery were investigated in models of water-flooding by Rapoport (1958). Similar models of carbon dioxide floods were performed by Farouq Ali *et al* (1991) to test the effectiveness of carbon dioxide injection as an enhanced recovery method in heavy oil reservoirs.

All of the examples above are 'pseudo' 2-D models. Ultrasonic one-way transmission travel times cannot be used to infer the fluid distribution in 3-D. However, two-way reflection methods developed herein can be used to map the areal distribution of fluids

and also potentially constrain the location of fluid movements in 3-D from changes in reflection travel times and amplitudes.

3.3.2 Turbidite models

Turbidites are thought to contain a large proportion of the world's hydrocarbons, but their complex architecture makes them a high-risk proposition for drilling. Abrupt sand terminations on pre-existing bathymetry, such as continental slopes, can make excellent traps that do not require structural closure. It is estimated that around 75% of the world's giant turbidite fields are at least partially stratigraphically trapped (Pettingill, 1998). However, if thin sands are draped over the slope they can create a 'thief zone' that bleeds off the hydrocarbons (Meckel, 1999). These are seldom resolvable in seismic data and therefore represent a major risk for drilling.

Sand rich turbidite reservoirs commonly have sandstones interbedded with genetically related shales from hemipelagic deposition between discrete turbidite depositional events. Lateral variability is related to successive flows that can preserve or partially erode mud caps to produce amalgamated turbidite beds. These beds can have very different vertical to horizontal permeability, which is extremely important in terms of sweep efficiency in hydrocarbon production (Stephen and Clark, 1999). Anisotropic permeability can also result from the alignment of grains to the flow direction.

Laboratory models are required to understand turbidite depositional processes because they are not observed directly in nature. Recent turbidites do not outcrop and have not been cored for analysis, while older turbidites are generally lithified and deformed (Hughes *et al.*, 1995). To determine the nature of the onlap, a detailed analysis of sub-seismic scale reservoir architecture is required, by outcrop and reservoir modelling of uncertainties.

Underwater turbidite models are used to better understand the structure and mechanisms of formation (Edwards *et al.*, 1994). Seismic imaging could help in the interpretation of

such physical models. Building the models underwater is also a more realistic analogue of marine deposition, although it is difficult to provide the compaction and subsequent seismic velocity increase that comes with increased burial depth. The lack of compaction would be the biggest limitation for recording seismic images of multi-layer turbidites. However, it would be an ideal technique for mapping the bathymetry of such models, and it should be possible to image at least one interface with an underlying turbidite flow, or to record multiple seismic images after successive turbidite flows. This would be a major advancement on current techniques, which at this stage rely solely on visual observations.

The techniques to record 3-D seismic images from models of unconsolidated sand presented in this thesis provide an opportunity to extract more information from all of the model types discussed in this Chapter. In the following Chapter, the theory of seismic wave propagation in unconsolidated sands is reviewed. The experiments that were performed to establish the techniques required to successfully record seismic images from sandbox models are then presented in Chapter Five.

CHAPTER FOUR

THEORY OF UNCONSOLIDATED SEDIMENT ACOUSTICS

There are many unresolved questions about acoustic velocity in unconsolidated sediments. The purpose of this section is to illustrate two main points of significance in this research. Firstly, it is aimed at providing an appreciation of the complexity of the subject and also to show that, while much is known, even more is yet to be understood. Secondly, it is presented to illustrate the profound effect that even the most subtle of changes can have on the velocity in a sediment, changes that we are usually unable to control or even determine. These problems are not only confined to unconsolidated sediments, but also affect sedimentary rocks to a lesser degree. The relationship between rock properties established for one geological environment will certainly not be the same for another (Shatilo, 1996).

A large proportion of the published rock physics data for poorly consolidated or unconsolidated sands are based on laboratory measurements for "Ottawa Sand", which is a clean, poorly consolidated sand with porosity ranging from 22-38%. However, the acoustic properties derived from these measurements vary widely in the literature. This occurs not only between separate studies by different workers, but also between different samples in the same series of experiments. A typical example is the laboratory measurements taken from three supposedly identical samples of Ottawa sand by Dvorkin and Nur (1996), who found that... "There is a large disparity not only between the theoretical and the experimental values for Ottawa sand but also among the experimental values for the three samples". The disparity occurs because the acoustic properties of sediments at low pressure depend mainly on the nature of the grain contacts, which are highly sensitive to small changes in grain sorting, compaction and saturation. Differences will exist not only between similar sands, but also between different samples of the same sand. The problem is compounded by the fact that laboratory samples are handled and prepared by humans, such that it would be

impossible to exactly duplicate measurements from two samples even if they were initially identical.

While the focus of this section is on unconsolidated sands, reference is made to the velocity of sound through rocks in order to highlight the differences between the two cases, particularly the different influences of the main controlling parameters, and to show that rock theory is largely inapplicable. For example, the velocity of sound in consolidated rocks is mainly influenced by density (which is dependent on mineralogy, porosity and fluid type), the degree of cementation, pressure and temperature. However, in the case of loose, uncemented sands, the influence of all of these factors is less clear. Density no longer plays a significant role and the major factors are now pressure, temperature and frame (or matrix) rigidity. This research was carried out at room temperatures and pressures so the focus is on understanding what controls the frame rigidity, and how it can be measured or estimated under those conditions.

All research in this area revolves around two underlying theories, the Gassman theory (Gassman, 1951), and the Biot theory (Biot, 1956a, b). The Gassman theory coincides with the low-frequency limit of the Biot equations. The common relationship that links all velocity theories, ignoring frequency effects, is that the square of the velocity is proportional to the appropriate elastic moduli divided by the density. Before these theories are introduced, the parameters of elastic constants are defined. The nomenclature and units used in this thesis are consistent throughout, although there is considerable variation in the literature.

4.1 Elastic Moduli

Elasticity can be described as deformations that vanish entirely upon removal of the stresses (Sheriff, 1994). The elastic moduli of a material express the linear relationship between an imposed stress and the resultant strain. In isotropic media, where properties are the same regardless of the direction they are measured, there are two independent elastic constants. There are a number of different types of elastic moduli depending on

the type of stress applied, but for the purpose of this research we are really only concerned with the Bulk Modulus (K), and shear modulus (μ). K expresses the ratio of hydrostatic pressure (P) to resultant volume strain ($\Delta V/V$) and is defined as:

$$K = \frac{P}{\Delta V/V} \quad . \tag{4.1}$$

However, the Bulk Modulus of a sediment comprises three components, Bulk Modulus of the grains (K_s), of the fluid (K_w), and of the matrix or frame (K_f). Of these parameters, K_f proves to be the most illusive and the very definition of the frame itself is uncertain. The underlying controversy lies in the definition of the boundary between the frame and fluid (Chotiros, 1998).

The shear modulus (or rigidity modulus, or Lame's constant - μ) is the stress strain ratio for simple shear:

$$\mu = \frac{\Delta F/A}{\Delta L/L} \quad , \tag{4.2}$$

where ΔF is the shearing (tangential) force, A is the cross-sectional area, ΔL is the shear displacement, and L is the distance between shear planes.

4.2 Gassman Theory

Gassman's theory (Gassman, 1951) was derived to describe the propagation of an elastic wave through a packing of spheres. He related V_p in porous sediment to the moduli of the grain material, pore fluid and sedimentary frame. The form of Gassman's equations has been modified over time and is usually expressed as:

$$V_p^2 = \frac{(K + 4\mu/3)}{\rho} \quad , \tag{4.3}$$

$$V_s^2 = \frac{\mu}{\rho} \quad , \tag{4.4}$$

with

$$K = \frac{K_s(K_f + Q)}{K_s + Q} \quad , \tag{4.5}$$

and

$$Q = \frac{K_w(K_s - K_f)}{\phi(K_s - K_w)} \quad , \tag{4.6}$$

where ρ is the density, ϕ is the porosity and Q is the quality factor, which is related to the rigidity of the sediment frame, or matrix. Q is a measure of how dissipative the material is and can be thought of as the ability of the sediment to transmit energy. The lower the Q, the larger the dissipation.

An underlying assumption of these equations is that there is elastic wave propagation, and effects due to viscoelastic properties are ignored. Because of this, later publications question the validity of these equations. Weakly cemented sands are not elastic, as the elastic properties are controlled by cementation, and are not at all sensitive to the actual modulus of the grains (Han, 1994). Other assumptions are that the rock is isotropic, the mineral moduli are homogeneous (if more than one mineral is present, an 'average' mineral must be derived) and the frequency is low.

Gassman's relations are most useful for calculating the expected change in velocities as a result of a change in pore fluid. Gassman's relations can be used to describe the moduli of a saturated rock (K_{sat} and μ_{sat}) in terms of the dry rock moduli (K_{dry} and μ_{dry}) and the fluid modulus (K_f) as follows:

$$\frac{K_{sat}}{K_s - K_{sat}} = \frac{K_{dry}}{K_s - K_{dry}} + \frac{K_f}{\phi(K_s - K_f)} \quad , \tag{4.7}$$

and

$$\mu_{sat} = \mu_{dry} \quad . \tag{4.8}$$

These equations are transformations and require no assumptions about pore space geometry or stiffness. The effect of substituting, say, brine for oil, can be predicted

with these equations without the need to measure the dry rock velocity or derive the dry rock moduli. However, this formula is only valid at low frequencies and is not applicable to ultrasonic laboratory measurements. A problem with Gassman's relations, which applies to all elastic wave theories, is that the shear wave velocity is needed to extract the bulk and shear moduli. The shear wave velocity is often estimated from an empirical V_p/V_s relationship, or inverted from an assumed dry rock Poisson's ratio. Mavko (1995) found that a reasonable approximation to Gassman is to replace the bulk modulus with the P-wave modulus (M) which is:

$$M = \rho V_p^2 \ . \tag{4.9}$$

4.3 Biot Theory

Biot (Biot, 1956a, b) proposed a set of coupled differential equations to describe the frequency-dependent propagation of sound waves in fluid-filled porous media. It incorporates some, but not all, of the mechanisms of viscous and inertial interaction between pore fluid and matrix. However, the elastic parameters were not clearly defined in terms of measurable quantities. Constraints on the possible values were published later by Biot and Willis (1957). The Biot model is very sensitive to the input parameters which are either not well defined (eg. the 'wet frame' moduli) or not easily measured (eg. the tortuosity parameter) (Boyle and Chotiros, 1992). A major problem with using Biot theory to model sound in water saturated sediments is that it assumes the sediment is equivalent to a homogeneous solid (Hickey and Sabatier, 1997). Hence, its applicability to uncemented sands is questionable.

Biot theory does not provide a direct link from microstructure to macroscopic behaviour, but rather requires the user to input a consistent and physically realistic model for both the porous medium and the fluid, as well as certain coupling 'factors' that are inherently difficult to quantify (Stoll, 1998). Some formulations of Biot theory have an implicit assumption that porosity is independent of pore pressure, an issue of

some debate. Biot's original theory used two parameters to represent K_s, one of which allows a change in porosity with pore pressure.

When applying the Biot model, often the case is that the measured data points are significantly different from the model predictions. Chotiros (1995) argued that there is no need to doubt the underlying theory as the equations have been checked by eminent scientists since they were first put forward, and he concludes that the problems lie in the definition of the input parameters and the wide range of values used. Sound speeds and attenuations are not well modelled by current theories as they treat the sediment as either a fluid or a solid medium (Boyle and Chotiros, 1992).

4.4 Velocity Bounds

4.4.1 Wyllie Time-Average

The velocity of water-saturated sediment is often estimated using the Wyllie 'time-average' equation (Wyllie *et al.*, 1956), which is:

$$\frac{1}{V} = \frac{\phi}{V_f} + \frac{1-\phi}{V_s} \quad , \tag{4.10}$$

where ϕ is the porosity. This formula is simply the volume weighted average of the travel time through each component. The relationship was derived for sands at depth, where there is significant overburden pressure holding the grains in contact. Blangy, *et al.*, (1993) found this relationship was valid at 30 MPa and with 100% water saturation, but for low pressures the effect of porosity on velocity was much less obvious. Another problem with this relationship is that it does not hold when there is partial gas saturation because it ignores the sensitivity to differential pressure (Elliott and Wiley, 1975).

4.4.2 Voigt-Reuss

To predict the effective elastic moduli of a mixture of grains and pores theoretically, three things need to be specified:

i) the volume fractions of the various solid and fluid phases,
ii) the elastic moduli of each phase, and
iii) the geometric details of how the phases are arranged.

The geometric details can only be estimated. Terms such as 'soft pores' and 'stiff pores' are used to explain the large variations in properties between sediments with similar compositions. In terms of predicting the elastic moduli or velocity of sediments, the best that can be done is to constrain the range of possible values between bounds.

The Voigt (upper) and Reuss (lower) bounds are the simplest and most robust bounds. Measurements will never exceed these. The Voigt upper bound of the effective elastic modulus (M_V) is the linear weighted average of the elastic moduli of each phase.

$$M_V = \sum_{i=1}^{N} f_i M_i \quad , \tag{4.11}$$

where f_i and M_i are the volume fraction and elastic modulus of the ith medium respectively. The Voigt average is sometimes referred to as the 'isostrain average' because it gives the ratio of average stress to strain when all constituents are assumed to have equal strain. Real isotropic mixtures can never be as stiff as the Voigt bound, except for the single-phase end members.

The Reuss lower bound of the effective elastic modulus (M_R) is

$$\frac{1}{M_R} = \sum_{i=1}^{N} \frac{f_i}{M_i} \quad . \tag{4.12}$$

The Reuss average is sometimes referred to as the 'isostress average' as it gives the ratio of average stress to strain assuming uniform stress. When all phases have zero shear modulus (ie. gases and liquids) the Reuss average gives the effective moduli exactly. The Reuss average is sometimes referred to as the Wood's relation when expressed in terms of velocity (Figure 4.1, from Marion, 1990).

Critical porosity refers to the transition between grains in suspension and grains in contact (Figure 4.2 from Nur *et al*, 1998). Above the critical porosity, which is usually around 40%, grains are suspended in a fluid and the Reuss average exactly describes the effective moduli. Below the critical porosity, the moduli may rise slightly above the Reuss bound depending on the nature of the grain packing and the grain shape. Larger deviations from this bound only occur if the sediment frame is stiffened by cementation or confining pressure.

Sometimes when a simple estimate of the moduli or velocity is needed, rather than a range, the arithmetic mean of the Voigt and Reuss bounds is used, which is known as the Voigt-Reuss-Hill average. The Reuss average is more appropriate for the sands used in this thesis as they are not cemented and have moderate to high porosities. As rocks rarely approach the Voigt upper bound, the modified Voigt bound is sometimes used (Nur *et al.*, 1998). This simply involves moving the end-point from 100% porosity to the critical porosity. The end points are connected by a straight line in terms of the bulk modulus, or a curved line in terms of velocity.

There are other more complex theories that attempt to better constrain the velocity bounds, such as the Hashin-Shtrikman bounds (Hashin and Shtrikman, 1963). It is unnecessary to expand on them here as all of the sands used in this thesis are uncemented and, hence, fall very closely to the Reuss lower bound.

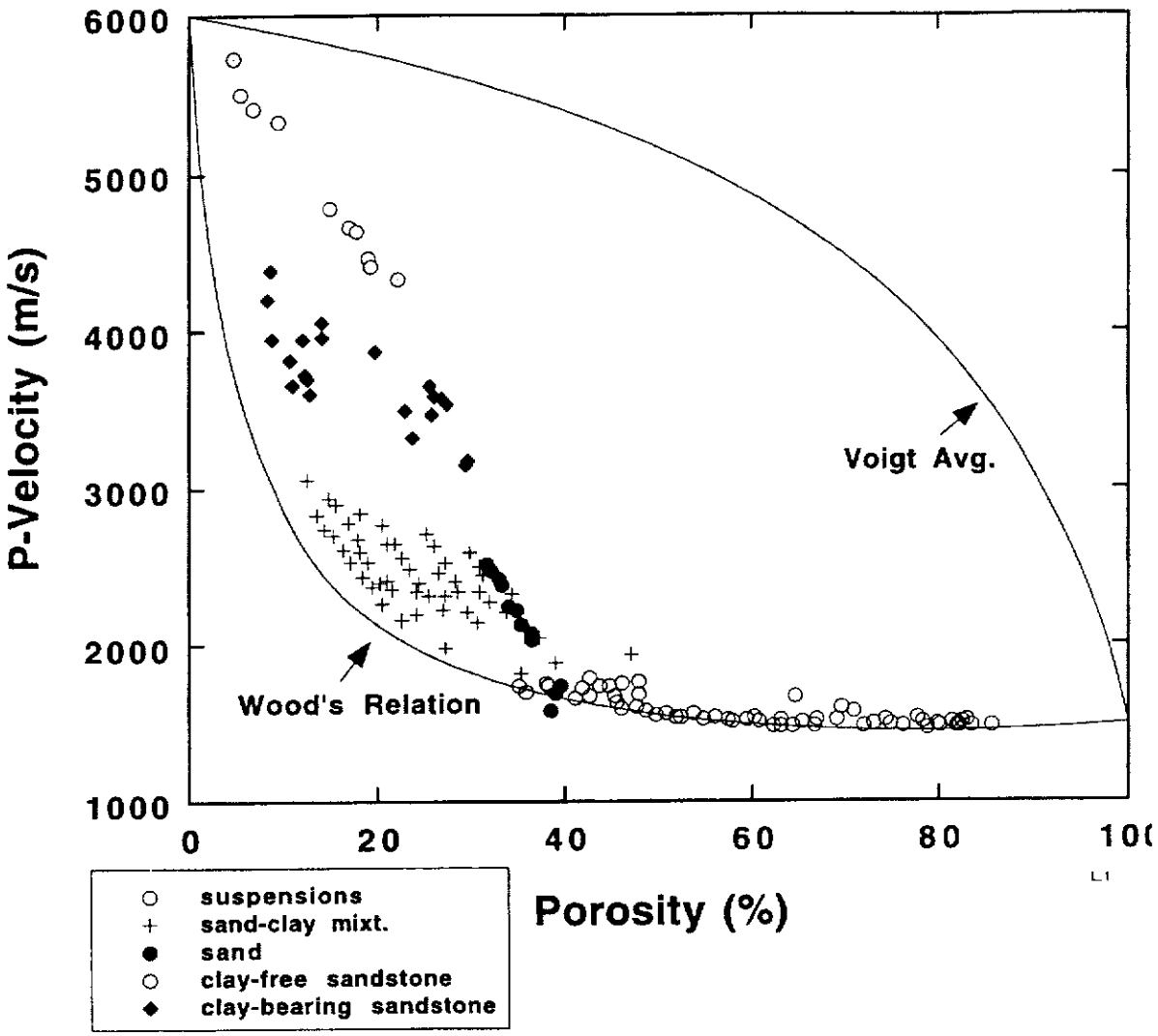

Figure 4.1: Velocity – porosity relationship in clastic sediments compared with the Voigt and Reuss bounds (Woods Relations describes the Reuss bound in terms of velocity). Note that the points fall closer to the Reuss bound, which perfectly describes grains in suspension. (after Marion, 1990).

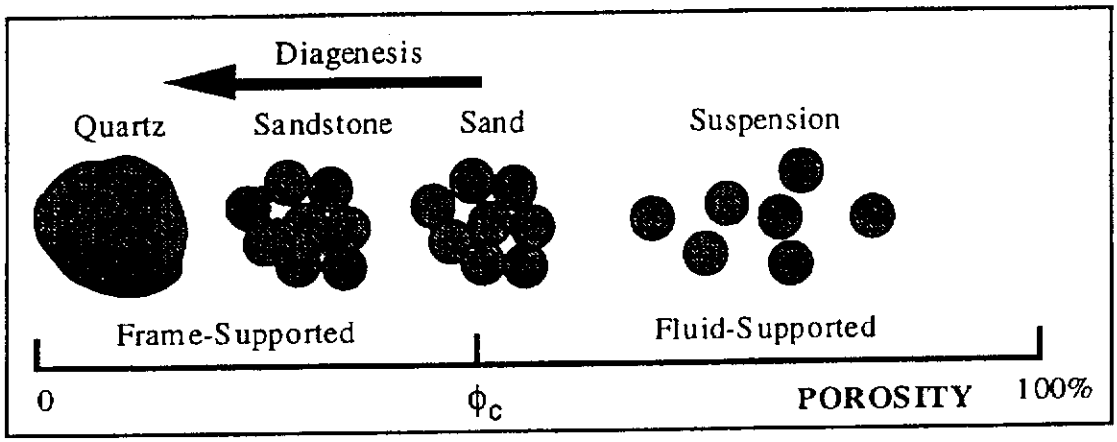

Figure 4.2: Schematic diagram of the transition between grains in suspension and grains in contact at critical porosity (after Nur *et al*, 1998).

4.5 Assigning Values to Elastic Constants

For a complete acoustic description of a sediment, P- and S-wave velocities and the waves' attenuations are required (Bell and Shirley, 1980). Unfortunately, there is a lack of shear wave data in the literature due to the difficulty of generating and detecting such waves in a highly attenuating medium.

The effective elastic moduli can be calculated from velocity measurements by rearranging Gassman's equations into the form

$$K = \rho\left(V_p^2 - \frac{4}{3}V_s^2\right) , \tag{4.13}$$

and

$$\mu = \rho V_s^2 \ . \tag{4.14}$$

However, this requires V_s to be known, which is rarely the case. One of the few publications to cite V_s data was by Blangy *et al.* (1993). They were able to make reasonable estimates of μ from measurements of dry sand, but were unable to adequately explain the measurements of saturated sand. The conclusion was that further work is required to understand V_s data in unconsolidated sands, especially at low pressures.

Without V_s, values for μ must be guessed, and would usually be adjusted to fit the observations. Examples of μ values used for saturated sand range from zero (Wyllie *et al.*, 1956; Purnell, 1986) to $2.0 * 10^{12}$ Pa (Han, 1994). Shirley and Hampton (1978) concluded that realistic sediments have values of μ between 10^4 and 10^5 Pa. Shumway (1958) initially assumed $\mu = 0$, but found that the predicted velocities were lower than the observed, and so changed μ to $5.5 * 10^{10}$ Pa to match the observations. The value of μ also depends strongly on grain shape, which varies significantly between different sands. Angular grains have a higher μ than rounded grains (Domenico, 1977).

In terms of P-wave velocity only, the bulk modulus is defined as:

$$K = \frac{\rho V_p^2}{1+Q} \quad . \tag{4.15}$$

This means that, for materials of similar density and velocity, the bulk modulus is dependent on the quality factor Q, which is inherently difficult to quantify and is usually approximated (anywhere from 0 to 100 for unconsolidated sands). Therefore, this method of calculating K is subject to large errors.

4.6 Attenuation

Attenuation usually refers to intrinsic attenuation, which is the process by which seismic energy is converted to heat as a result of the inelasticity of rocks. Measurements of attenuation also include apparent attenuation, which may be present as a result of effects such as scattering (Jones, 1986). Intrinsic attenuation is commonly described by the quality factor Q.

Q is governed by grain shape, sorting and the fraction of clay-sized minerals. The effect of clay in unconsolidated sand is the opposite of its effect on consolidated rocks for low clay fractions. It appears to stiffen the contacts between the sand grains and subsequently increase the velocity. All theories struggle to predict Q. It is also one of the parameters most sensitive parameters affected by saturation, especially at low pressure (Jones *et al.*, 1997). There are several ways to define Q, one of which is in terms of the attenuation coefficient (α):

$$\frac{1}{Q} = \frac{\alpha.V}{8.686\pi.f} \quad , \tag{4.16}$$

where α is the attenuation in dBm^{-1} and f is the frequency.

The attenuation coefficient varies as a linear function of frequency. Q is determined from the slope of the line fitted to the natural log of the spectral ratio (Toksoz *et al.*, 1979). Attenuation (= 1/Q) is not a commonly used attribute because there are many incomplete and contradictory theories, and a lack of robust techniques to derive it from seismic or well data (Batzle *et al.*, 1996). Attenuation is frequently studied in the laboratory, but the effects seen at high frequency in the laboratory are not applicable to low frequency and, therefore, the results cannot be totally related to field attenuation mechanisms (Gist, 1994).

In rocks, the dominant mechanism of attenuation is the interaction between the fluid and the frame, rather than any intrinsic losses in the fluid or frame itself (Purnell, 1986). Attenuation has been linked to the degree of fluid saturation (Murphy, 1984), the permeability and clay content (Klimentos and McCann, 1990), the grain size, and the pore and crack geometry (Akbar *et al.*, 1993). Shatilo (1996) observed a strong correlation between attenuation and porosity (0.81), and with permeability (0.72), but was not able to separate the two factors.

Understanding the factors affecting attenuation in unconsolidated sands is much harder. Attenuation predicted by Biot theory is inadequate to explain most observations (Batzle *et al.*, 1996). Gardner *et al.* (1964) described attenuation in fluid-saturated rock as the sum of 'sloshing', from the mobility of fluid within the rock (or 'squirt flow'), and 'jostling' from friction between the grains in the framework, which is not a part of Biot theory. Figure 4.3 from Stoll (1977) shows that friction between the grains in unconsolidated sand is a major contributor to attenuation.

When clay particles are present in sandstone, attenuation is much higher than predicted by Biot theory, which was derived for smooth-walled glass beads. The addition of clay particles creates a network of microporosity within themselves that increases the surface area between frame and fluid. Klimentos and McCann (1988) argued that Biot theory can predict the increase in attenuation if this increase is allowed for. The increase in surface area was also acknowledged by Gist (1994), who attributed the

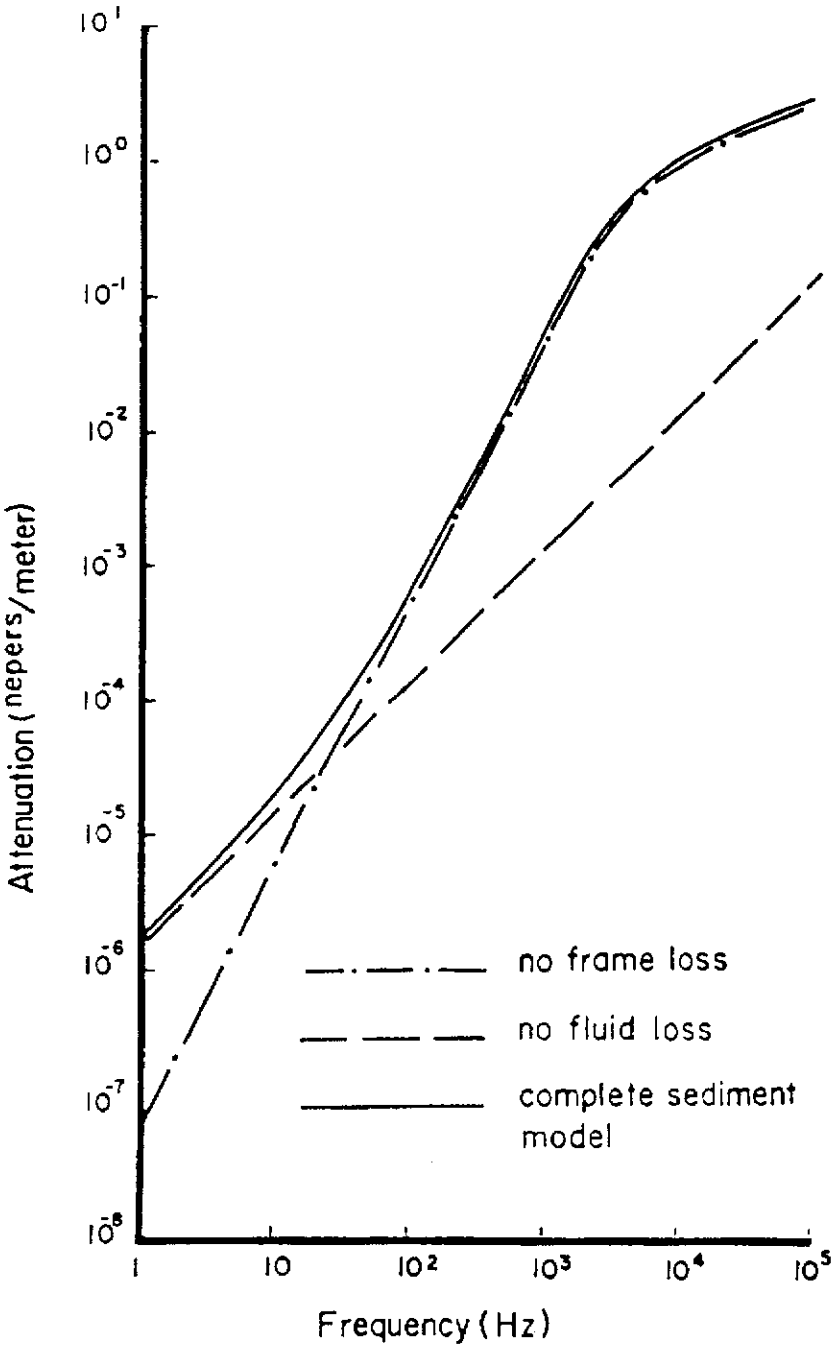

Figure 4.3: Mechanisms of attenuation in unconsolidated sands in terms of fluid related losses and friction between sands grains in the sediment frame. One neper equals approximately 9 dB (after Stoll, 1977).

increase in attenuation to differences in the pore-wall surface, which is much rougher with the presence of clay.

Until recently a common assumption was that Q was independent of frequency. Intergranular friction is usually considered frequency independent, although it is the hardest attenuation mechanism to constrain theoretically. When the sand grains are elongated or angular, anisotropy also has a significant affect on attenuation. Attenuation perpendicular to the pore orientation is greater than parallel to it (Akbar *et al.*, 1993), and the ratio increases with pore radius and saturation.

Green and Esquivel-Sirvent (1999) found that attenuation was highest at the transition between grains in suspension and in contact (ie. critical porosity) irrespective of the frequency. Attenuation is always highest at low effective pressures, which unfortunately constrains the maximum size of models possible for this thesis using ultrasonic transducers with limited energy output.

4.7 Velocity Dispersion

Dispersion is the variation of velocity with frequency, which broadens and distorts the shape of the waveform. It is difficult to separate the two observations of velocity dispersion and attenuation as the two are intimately related. Seismic waves are always attenuated as they travel through rocks and velocities almost always increase with frequency. The rate of change for both usually increases from dry to saturated conditions and both usually decrease with increasing effective pressures. These effects make comparisons between field and laboratory data difficult but can also be used to help understand the characteristics of the pore space and fluid. If the velocities of a rock are known at different frequencies then attenuation can be estimated and vice versa.

Upscaling refers to the use of high frequency measurements to determine effects at lower frequencies. This is necessary to relate measurements at different scales

increasing from laboratory measurements through sonic logs, crosswell tomography, VSPs and surface seismic. Seismic velocity depends not just on the rock and fluid properties, but also on the measurement scale relative to the geologic scale. While scaling is a problem for determining absolute values of velocities, fortunately for experiments such as those in this thesis, relative changes are still very relevent.

Many physical mechanisms have been proposed and modelled to explain velocity dispersion in rocks, such as scattering, viscous and inertial fluid effects, thermoelastic effects and phase changes. While the various dispersion mechanisms have distinct mathematical descriptions, most follow the same trend and can be described with a simplified approach by three parameters:

i) A low frequency limiting velocity (relaxed state),
ii) a high frequency limiting velocity (unrelaxed state), and
iii) a characteristic frequency range in which the velocity change is most rapid.

All models require details of the pore geometry to estimate the characteristic frequency, which are very difficult to constrain. Analysis of dispersion is limited by our ability to measure it accurately (Liu and Nur, 1996). The uncertainty of pore geometry, permeability and scale of heterogeneity, as well as the approximations involved in the theories, makes detailed analysis extremely difficult.

4.7.1 Fluid mechanisms

There are two dominant fluid mechanisms that affect velocity and attenuation in rocks, the Biot 'global flow' model, where the average relative motion of fluid and solid lead to dispersion and attenuation, and the Squirt or 'local flow' model (Dvorkin *et al.*, 1995), where grain-scale fluid motion has the same effect. In the Biot model, the fluid is forced to move with the solid by viscous friction and inertial coupling, sometimes referred to as 'dynamic poroelasticity'. In the squirt flow model, the fluid is squeezed out of thin compliant pores that are deformed by the passing wave into larger pores.

As with most velocity models, these two dispersion mechanisms are well suited for describing experimental data results, but they are not suited for *a priori* predictions about the behaviour of a porous rock. Endres and Knight (1997) concluded that the relative magnitude of each dispersion mechanism depends on the pore structures and fluids. In most cases the squirt flow will dominate, although if the pores are 'stiff' or the pore fluid modulus is low, the dispersion effects of squirt flow will be lower than the effects from the Biot mechanism. These two mechanisms have traditionally been modelled separately, with the Biot mechanism treated at the macroscopic level and squirt flow modelled at the individual pore scale. A unified model was proposed by Dvorkin and Nur (1993), which they called the Biot-squirt (BISQ) model.

A simplistic explanation of the difference between the high and low frequency limits in Biot's theory is that at low frequencies, the sediment frame and fluid are perfectly coupled and move together. At high frequencies, the frame moves too quickly for the fluid to keep up (ie. equilibrate) and so the apparent mass is less and hence the velocity is higher.

In the squirt flow model high frequencies have an elastic stiffening effect on the fluid in the smaller and more compliant pores or cracks (sometimes referred to as soft porosity). When a seismic wave passes through a rock it is compressed and increments of pore pressure are induced in the pore fluid. Diffusion refers to the time taken for the pore pressure to diffuse and equilibrate isothermally from the passing of the wave. At low frequencies there is time for the fluid to equilibrate within the period of the wave. At high frequencies there is less time for diffusion within the period of the wave so the fluid is effectively stiffer, which increases the velocity. The frequency dependent distribution of pore pressure leads to velocity dispersion and the tendency for the fluid to flow leads to attenuation (Mavko *et al.*, 1998). In unconsolidated sands, incomplete grain to grain contacts may allow a thin film to exist between grain surfaces. The squirt flow mechanism allows for the dissipation of energy as a passing seismic wave drives film out of the contact region and into the adjacent pore (Murphy *et al.*, 1986).

The out of phase motion between the fluid and frame in Biot's theory give rise to another wave known as the 'slow P-wave'. Biot predicted the slow wave in 1956, but it was not proven until it was measured for the first time in the laboratory by Plona (1980) using sintered glass beads. It has since been measured in unconsolidated saturated sand (eg. Chotiros, 1995) but is still poorly constrained. Klimentos and McCann (1988) observed the slow wave in artificial rocks but noted that it 'dissapeared' when clay was present, which they cited as the reason it is not observed in real rocks.

The frequency range that the squirt flow mechanism comes into play is narrow in idealized models of uniform grain and pore size. However, typical sands have a much more diverse microstructure, which Winkler (1985) cites as the reason for the mechanism being effective over several orders of magnitude in frequency in his results.

Attenuation tends to be highest over the frequency range where the increase in velocity is greatest. Attenuation peaks at a critical frequency, which can vary between sediments. Measurements from different samples in the laboratory at a set frequency may in effect be sampling different relative positions on the dispersion curve and be more indicative of a shift in critical frequency than a change in absolute attenuation.

The presence of heterogeneities can also cause dispersion where the drift in velocity with frequency has the opposite trend (negative dispersion) to attenuation related dispersion, which is known as 'fast path' effects (Mukerji *et al.*, 1995). This has been observed in comparisons between low frequency VSP measurements and higher frequency sonic logs by Boirel *et al.* (1997). They concluded that the longer travel path between source and receiver on the VSP relative to the sonic log, which only samples the rock at the well, allowed enough room for the waves to deviate around the slower patches and arrive quicker travelling a longer ray path. Winkler (1983) also observed negative dispersion in a range of dry sandstones, which decreased with increasing effective pressure. The same samples exhibited positive dispersion when saturated, which also decreased with increasing pressure until becoming slightly negative at very high pressures (40 MPa).

The low frequency behaviour of saturated rocks is often estimated using high frequency measurements of both dry and saturated samples plus the properties of the fluid (Figure 4.4, from Winkler, 1986). A key assumption of this technique is that dry velocities are independent of frequency. This is supported by experiment (eg. Peselnick and Outerbridge, 1961; Spencer, 1981) and does not violate theory as long as all dispersion is considered to be fluid related. The dry velocity is measured at high frequency and assumed to equal the low frequency velocity. The 'dry' state must include any chemical weakening of the frame caused by the pore fluids, (Winkler, 1985), such that the only difference between the dry and saturated behaviour is the pore fluid itself. These effects can be large at room pressures or if extreme drying procedures are used. The low frequency saturated velocity is derived using Gassman's relations and the known properties of the pore fluid. The fractional increase of the high frequency velocity relative to the low frequency velocity equals the amount of dispersion from intrinsic attenuation.

However, the assumption that all dispersion is fluid related is incorrect if scattering losses are significant which, as discussed in the following section, is likely to be the case with ultrasonic measurements.

4.7.2 Scattering

Brown and Seifert (1991) represented the approximate total apparent attenuation as the sum of the effective attenuation caused by scattering and the intrinsic attenuation from fluid effects. Measurable travel times of seismic events depend on the scale of the seismic wavelength relative to the geological feature size. In general, the velocity inferred from arrival times is slower when the wavelength is longer than the scale of the heterogeneity and faster when the wavelength is shorter (Mukerji *et al.*, 1995).

The ratio of seismic wavelength to grain size in unconsolidated sediments determines the amount of attenuation that will result from scattering. When the wavelength is much larger than the grain size or scale of heterogeneity, the medium is effectively

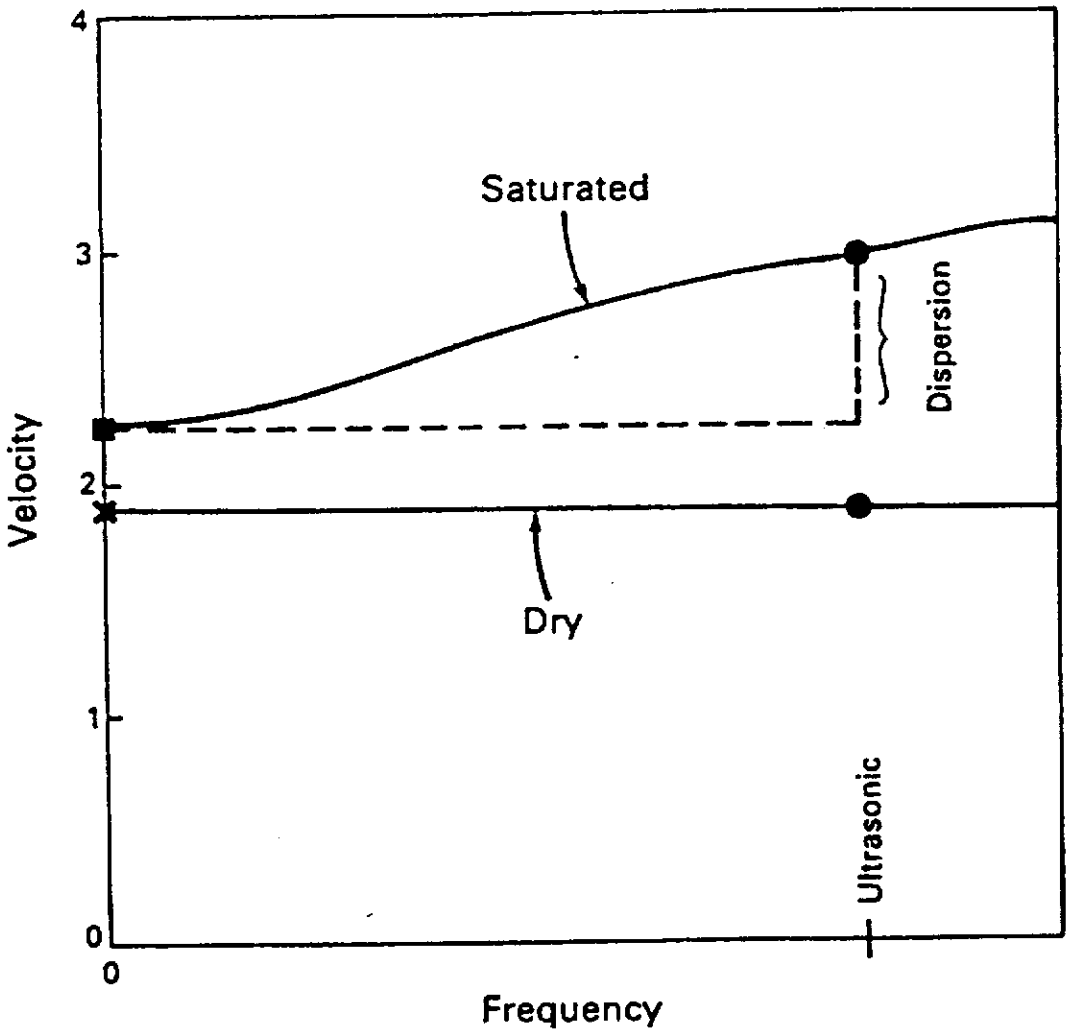

Figure 4.4: Schematic representation of velocity as a function of frequency, used to estimate velocity dispersion. Dots represent ultrasonic laboratory measurements. Cross represents extrapolated low-frequency dry velocity, which is assumed to equal the high frequency velocity. Square represents the low frequency saturated velocity that is estimated from the dry velocity using Gassman's relations (1951). Total velocity dispersion equals the fractional increase of the high frequency saturated velocity relative to the low frequency velocity (after Winkler, 1986).

homogeneous and scattering effects may be negligible. In this case, the behaviour can be modelled with effective medium theories such as the Voigt-Reuss or Hashin-Shtrikman bounds. At the opposite limit, when the wavelength is much smaller than the grain size, the medium may be treated as a piecewise homogeneous medium, which can be modelled with ray theory. Here, the total travel time equals the sum of the travel times through each component. This was demonstrated by Marion (1994) with measurements from stacked plastic and steel disks at various wavelength to thickness ratios (Figure 4.5).

When the wavelength (λ) is similar to the grain diameter (d) there are two scattering mechanisms that can contribute to attenuation, Mei scattering, where $\lambda \approx d$, and Rayleigh scattering, where $\lambda > d$ (Figure 4.6). In the Rayleigh scattering domain the velocity slightly decreases with increasing frequency, which is followed by a rapid increase in velocity owing to Mei scattering (Mavko *et al.*, 1998). It is usually assumed that the Rayleigh domain is appropriate for ultrasonic laboratory measurements because the wavelength is larger than the grain size. For the measurements in this thesis, the wavelength ($\approx$ 1.6 mm) is at least five times larger than the largest grain size used (300 μm). Prasad (1997) suggested that grain size alone does not account for all of the scattering in ultrasonic data, but that grain clusters of similar impedance can also act as scatterers.

4.8 Parameters that Influence Velocity

An attempt has been made here to separate the influence of each parameter of the individual sediment components. However, it should be remembered that every component is interlinked and this helps explain how similar observations in the literature can be attributed to different parameters. Much of the problem lies in alternate interpretations of the theory and the wide range of values assigned to each parameter. For example, it is well known that the P-wave velocity of saturated sand is somewhere around 1700 ms^{-1}. However, Stoll (1998), noted that..."it is easy to show

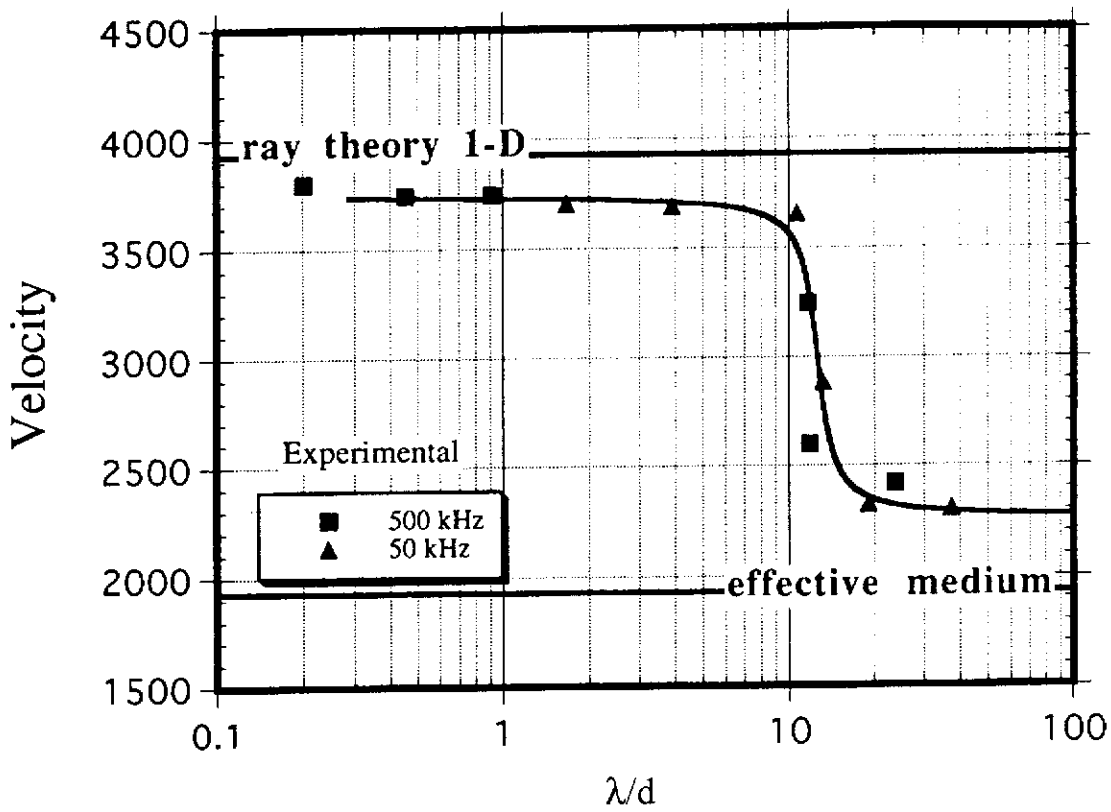

Figure 4.5: Laboratory measurements of velocity versus λ/d for normal incidence propagation through a stratified sample of plastic and steel layers at the transitions from short to long wavelength behaviour. A smooth curve has been drawn through the data points to indicate the trend. The velocities predicted from ray theory ($\lambda < d$) and effective medium theory ($\lambda >> d$) are also shown (after Marion *et al*, 1994).

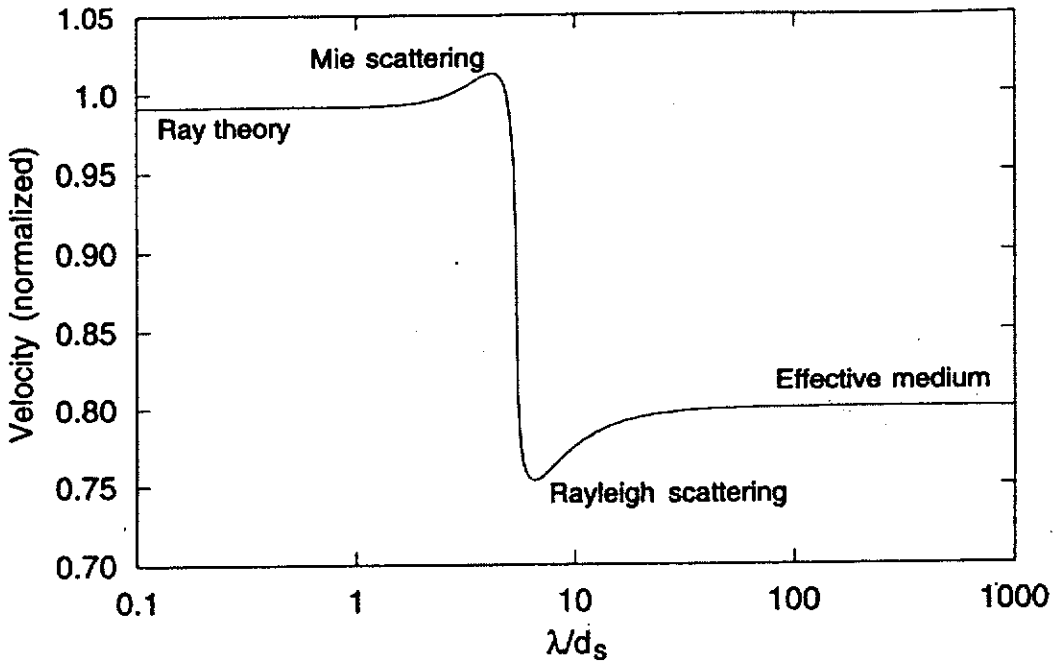

Figure 4.6: General scale dependence of velocity that is expected owing to scattering in heterogeneous media. At very long wavelengths ($\lambda >> d$) the velocity is close to the effective medium result. As the wavelength decreases (ie. frequency increases) Rayleigh scattering causes a slight decrease in velocity. This is usually followed by a rapid and much larger increase in velocity owing to Mie scattering ($\lambda \approx d$) (after Mavko, 1998).

that any number of different combinations of parameters will result in velocities in the region of 1700 ms^{-1}".

4.8.1 Porosity

Porosity is often claimed to be the most important parameter in terms of sediment velocity (e.g. Brandt, 1960; Talwani *et al.*, 1973). This may be true, but only in terms of what it implies with regards to other parameters such grain sorting, clay content and compaction. The porosity of a sand can be altered without much subsequent change in velocity. For example, in Talwani's experiments the porosity of coarse-grained sand was reduced by crushing the sample under large confining pressures, which increased the velocity markedly. When the pressure was released the porosity remained low, but the velocity returned back almost to the initial velocity at high porosity.

Porosity can vary as a consequence of a change in grain size, sorting, packing, clay content, confining pressure or cementation. It is not possible to measure the effect of a change in porosity while keeping all other factors constant because the porosity can only vary as a result of a change in one or more other factors. In a sense, porosity is not really a component of a sediment but rather the space remaining after all other solid components are put together, so it does not actually cause a change in velocity. For example, the porosity of sediments generally decreases with depth due to compaction from the overburden. In addition, the velocity of sediments generally increases with depth. Therefore, a correlation usually exists between porosity and velocity. However, to state that the change in porosity causes the velocity increase does not tell the whole story. The cause of the velocity increase can be a result of a number of factors and the relative influence of each factor depends on the conditions.

The important issue when considering the effect of porosity on velocity is the mechanism of the porosity change (Figure 4.7). An increase in confining pressure due to the overburden will stiffen the matrix and increase the velocity with little change in porosity. The overburden pressure may also increase the number of contacts between

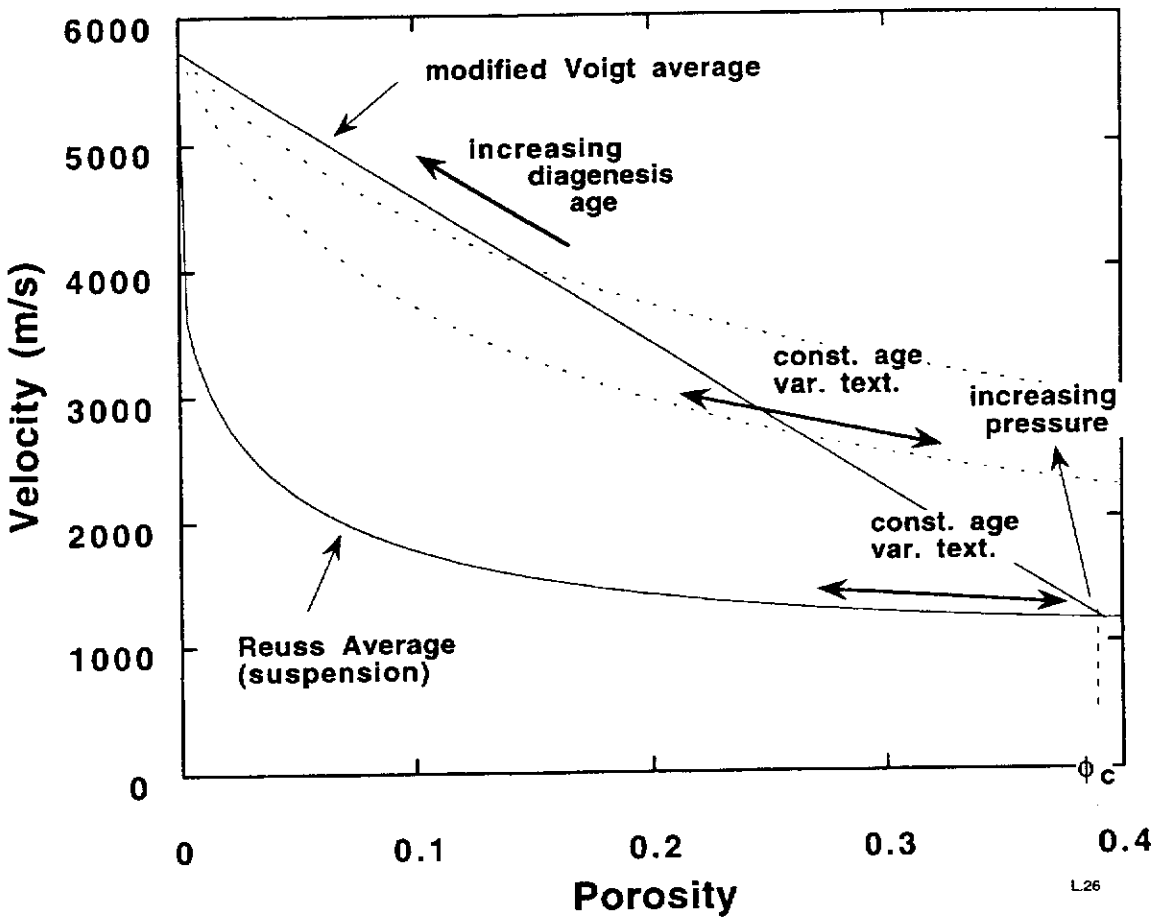

Figure 4.7: Generalized velocity – porosity relationship. The trend is for the sound velocity to increase with decreasing porosity but the relationship depends on the mechanism of the porosity reduction (after Mavko, 1998).

adjacent grains if they become rearranged or crushed into smaller grains, which will affect both the velocity and porosity. Depending on the conditions and the composition of the sediment and fluid, diagenesis may occur over time, which will cement the grains together and substantially increase the velocity and also reduce porosity. Sediments of similar age and grain shape, and under similar pressure conditions may have very similar velocities, but cover a range of porosities that are a result of variations in texture. Similarly, laboratory samples of sand, such as those used in this thesis, also have similar velocities, but cover a range of porosities that is mostly dependent on the grain sorting.

Comparing in-situ sands with laboratory samples is suspect because differences in consolidation can affect velocity more than porosity or clay content (Blangy *et al.*, 1993). Physically sampling a poorly consolidated or unconsolidated sand will change its properties. Many velocity models explain the possible effects of porosity by dividing it into soft pores and stiff pores. The soft pores dominate the influence on velocity and attenuation because they are most affected by changes in fluid type or pressure (Mavko and Jizba, 1991).

Blangy *et al.* (1993) found that for consolidated samples with fixed mineralogy and clay content, there appears to be a linear relationship between dry bulk modulus and porosity, but once again this relationship was not clear for unconsolidated samples. As is the case with many experiments with unconsolidated sand, they were unable to fit a function relating the moduli to porosity because of the large scatter in the data. It also wasn't possible to distinguish the effects of clay from porosity in their samples.

4.8.2 Permeability

Permeability (k) is a measure of the ease with which a fluid can pass through the pore spaces of a sediment. The flow rate (V) is linearly related to the pressure gradient dp/dt by the following equation, known as Darcy's law:

$$V = \frac{k}{\eta} * A * \frac{dp}{dl} \quad , \tag{4.17}$$

where k is the permeability of the medium, η is the viscosity of the fluid, and A is the cross sectional area. The unit of permeability is the Darcy although it is commonly expressed in millidarcys. In a water-saturated rock with a permeability of 1 Darcy, a pressure gradient of 1 bar/cm gives a flow rate of 1 cm/sec.

Permeability is strongly dependent on both the pore size and the tortuosity of the pores (Klimentos and McCann, 1988). There are many ways of estimating tortuosity, none of which is ideal. Even if an adequate estimate of tortuosity is achieved, integrating it into permeability equations involves other assumptions such as a constant pore radius. Clarke (1979) found that permeability is proportional to the square of the grain size for sands of constant porosity. The permeability of sands can be estimated with the Kozeny-Carman equation (Bear, 1972), but this involves assumptions on the specific surface area of the grains in a unit volume of solid. The Kozeny-Carman equation may be written as:

$$k = \frac{B.\phi^3}{\tau.S^2} \quad , \tag{4.18}$$

where B is a geometric factor, τ is the tortuosity and S is the specific pore surface area. The dependence on the cube of the porosity indicates a strong scale dependence, that is, one large pore will allow easier flow than many small pores of equal cross-sectional area. In multiphase fluids, the presence of one fluid may alter the effective permeability of a rock to another fluid, such that the effective permeabilities of the component fluids may not add up to the total permeability (Dullien, 1992).

The effects of permeability on seismic velocity are frequency dependent and extremely difficult to quantify. A decrease in permeability will shift the frequency range where dispersion is greatest to lower frequencies (Batzle *et al.*, 1997).

4.8.3 Mineralogy

Velocity tests on a variety of grain types ranging from quartz sands to crushed basalt (Talwani *et al.*, 1973), demonstrated that mineralogy plays only a minor role in the velocity of an unconsolidated sediment. The elastic properties are controlled by cementation and not at all sensitive to the actual modulus of the grains (Han, 1994). The mineralogy will largely determine the density of sediment, which is a major factor controlling the velocity of a consolidated rock, but is only minor factor for unconsolidated sands.

4.8.4 Grain Packing

To understand how a random arrangement of sands grains of varying grain sizes pack together, first consider the simplest case of one-component packing, that is, the packing of single size spherical particles. The results presented below are taken from a study by McGeary (1961), with spherical particles. Theoretical packing arrangements range from simple cubic, through orthorhombic, where a layer of grains sit in the cavities of the grains below in a 2-D sense, to 'double nested', where systematic nesting of spheres occurs in both axial and transverse directions (Figure 4.8). Theoretically, the closest possible packing is close packed or 'triple nesting', either face centred cubic (FCC) or hexagonal close-packed (HCP). However, such close packing cannot occur mechanically because the vertical force causes the elevated spheres to move downward to a position identical to the double nested case.

Cubic packing is unstable and does not occur experimentally. Orthorhombic packing has a calculated porosity of 39.5% while the double nested packing arrangement has a porosity of 30.2%. Experimentally measured packing densities, after vibration had been applied to settle the grains into the tightest achievable packing, average about 37.5% porosity. This suggests that only about one fifth of the possible double nesting actually takes place.

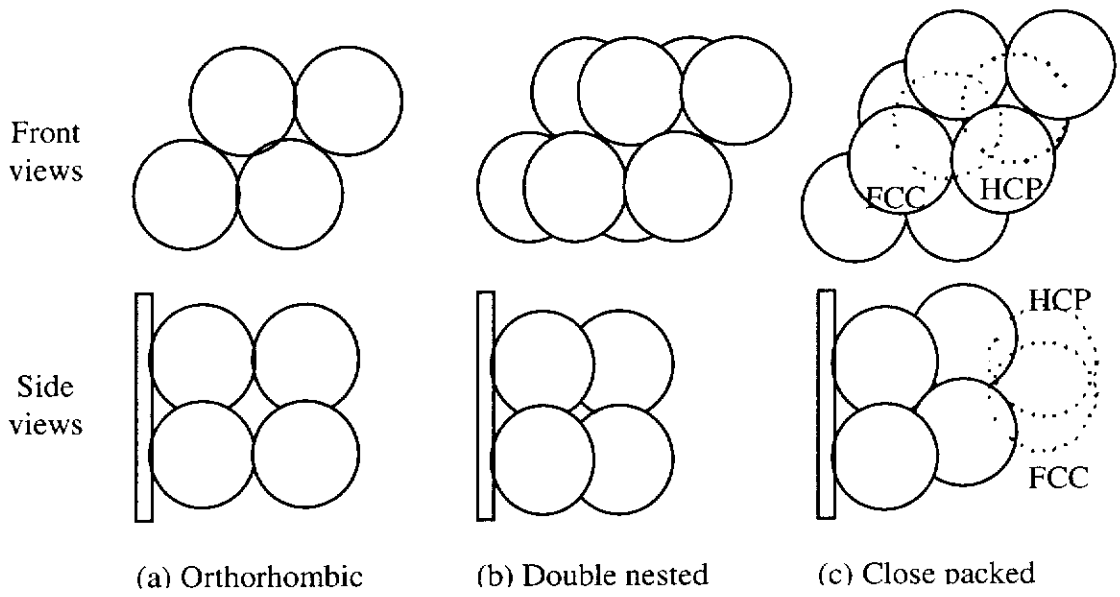

Figure 4.8: Possible arrangements for the packing of identical spherical grains (after McGeary, 1961).

The lowest porosity achieved by McGeary (1961) was 4.9% using four different grain sizes with diameter ratios of 1:7:38:316, but this is an unrealistic case for two reasons. Firstly, it involves four discrete grain sizes with no sizes in between and the exact proportions of each required to achieve minimum porosity, and secondly, a specific technique was required to achieve that packing. He found that when the grain sizes varied considerably, effective blending could not be achieved by simply applying vibration, and in fact this caused segregation. This last characteristic has since been observed by many others and will prove significant for this research.

In practice, the porosities of typical sediments range from 25 to 40%. Most laboratory studies involve porosities around 30% and nearly always involve vibrating the sands beforehand to achieve this. With typical sandy sediments, where there is a normal distribution of grain sizes over a certain range, porosity is mainly dependent on the degree of sorting and partly on the average grain size. The porosity of a very well-sorted sand is about 42% and the porosity of a poorly sorted sand, regardless of grain size, is about 30%. This relationship, along with associated permeabilities, is shown in Figure 4.9 from Sneider (1997).

4.8.5 Grain Shape

The number of intergranular contacts and the nature in which the grains interlock governs frame rigidity. Smaller grains in general tend to be more angular than larger grains and have more contacts (Hamilton, 1971). Domenico (1977) also noted that angular grains have a higher shear modulus than rounded grains. Therefore, grain shape may be an important factor when comparing results between sands of different grain size, although it is rarely mentioned in the literature.

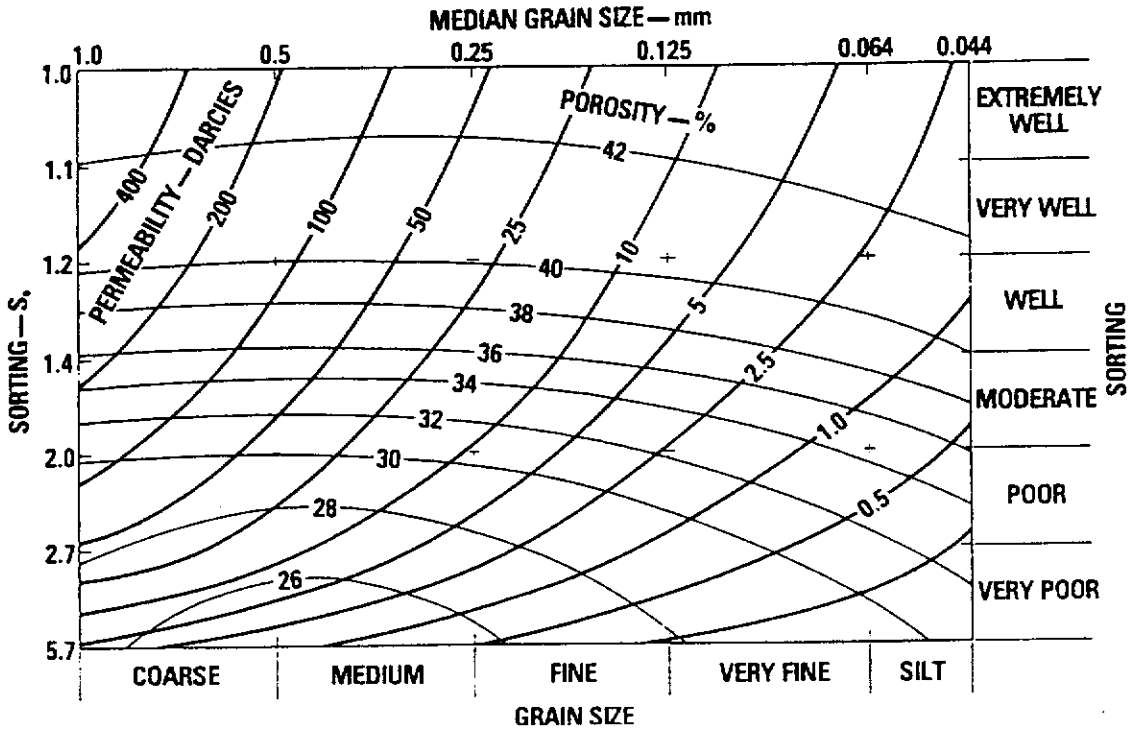

Figure 4.9: Porosity and permeability of mixed and saturated packed sand of different sizes and sortings (after Sneider, 1997).

4.8.6 Clay content

References to clay can mean either any clay-sized mineral, with a grain size less than 2 μm, or more specifically the range of hydrous aluminosilicate minerals, such as kaolin, illite and montmorillonite. In most cases the clay mineral is inferred and they have some special properties, particularly with regards to water adsorption, that makes their influence on both consolidated and unconsolidated sands significant. The expansion characteristics of clay play a significant role in the acoustic, petrophysical and mechanical properties of sedimentary rocks (Mese and Tutuncu, 1996).

When unconsolidated sand also contains clay particles, the result is a bimodal grain size distribution. The large ratio between the sand and clay grain sizes (in the order of 100:1) results in two different cases depending on the amount of clay present. When the percentage of clay is low, the packing can be considered close to ideal. That is, the small clay particles do not disturb the original packing of the larger sand grains and vice-versa. In this case, the sand grains are assumed to be load bearing and the clay minerals fill the pore space without disturbing the sand pack (Figure 4.10). This geometry is commonly referred to as 'dispersed clay in sand matrix'. The porosity of the mixture decreases linearly with increasing clay volume fraction to the point where the amount of clay equals the sand porosity (Marion *et al.*, 1992). McGeary (1961) showed that when the clay fraction becomes greater than the sand porosity, addition of clay expands the sand lattice. The sand grains become disconnected, the clay becomes a load-bearing component, and porosity increases linearly with increasing clay volume due to the replacement of sand grains by porous shaley material. However, this is assuming that there is no compaction.

While minimum porosity occurs when the clay volume equals the sand porosity, the amount of clay where this minimum is achieved is strongly dependent on the amount of compaction that takes place, especially over the first few atmospheres of pressure. Experiments by Marion *et al.* (1992) using clean Ottawa sand demonstrated a minimum

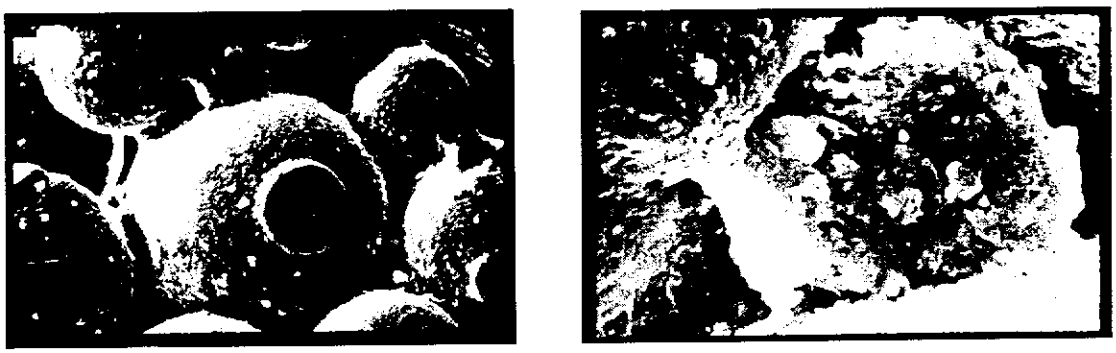

(a) (b)

Figure 4.10: (a) Electron microphotograph of glass-bead rock after partial saturation with kaolinite. Mean grain size of beads 250 μm. (b) Same rock with higher magnification. Note the clay filling the pore throats (after Klimentos and McCann, 1988).

porosity with an initial 20% by volume clay fraction at low pressure, but with 40% initial clay volume when subjected to high confining pressure.

Clay minerals, by virtue of their grain size, have a large specific surface area. Ions on the surface of the clay crystal are O^{2-} or $(OH)^{-}$, and so water is held to the surface as an adsorption layer by hydrogen bonds (Scott, 1980). The type of clay is significant as the volume of water in the adsorbed layer depends on the crystal structure (Katahara, 1996). One adsorbed layer of water makes up 20% of the mineral volume in smectite, but only 4% in illite.

When clays are in suspension, if the particles are close together they are attracted to each other by Van der Waals forces or molecular bonds (Scott, 1980). The strength of this attraction decreases inversely as the 5^{th} or 6^{th} power of interparticle distance, and so does not come into effect unless the adsorbed water layer is squeezed out by compaction. If the pore fluid is free to drain, compaction reduces the thickness of the adsorbed layers and causes contact between particles. If the confining pressure is removed and the fluid is free to return, some expansion takes place as the adsorbed layers return to their original thickness. However, particles that have been forced into contact do not return to their original position and, therefore, much of the volume change is irreversible. For this reason, the influence of clay on the velocity of sediments is strongly dependent on the burial history, which also makes comparisons between different studies difficult.

When clay is mixed with water it initially forms a suspension, which slowly becomes increasingly dense through the action of gravity and interparticle attraction (Shirley and Hampton, 1978). If left to stand for a week, the clay approaches a constant porosity of 75%. The sound velocity in this mixture is actually lower than water (Bell and Shirley, 1980), but this has little relevance to the influence of clay in sand.

Most research in this area deals with the effect of clay in loose sands at high pressures (greater than 10 MPa) to simulate reservoir conditions. Data published by Marion *et al.* (1992) show a fairly consistent increase in P-wave velocity for volumes of clay up to

the initial porosity of the sand. Up to this point, the clay simply fills in the pore spaces and effectively raises the bulk modulus of the pore fluid (K_w). This trend roughly follows that predicted by Gassman's relations (Gassman, 1951) if treating the clay as part of the pore fluid. For clay contents greater than the sand porosity, the clay particles become load-bearing members and the velocity actually decreases with increasing clay content. In this case, Gassman's relations fail to account for the trends observed. Marion also showed a fairly uniform trend of increasing velocity with pressure. However, these results were for pressures above 10 MPa. Clays are known to undergo significant compaction over the first few atmospheres of pressure, while the rate of compaction rapidly slows and becomes more linear at higher pressures. There is also considerable scatter in the observational data although a good fit with theory is claimed (Figure 4.11). For these reasons, for sands containing clay, it is not a simple matter of extrapolation of Marion's results to atmospheric pressure.

Clay provides a weak cementation, which increases μ considerably while actually decreasing the bulk modulus of the sediment frame (K_f) slightly (Han, 1994). The result can be an increase in S-wave velocity by as much as 100% and a smaller increase in P-wave velocity by around 20%. Thus, the ratio of V_p to V_s is reduced and, consequently, Poisson's ratio (σ) is much lower than in clean sands. Han also found that the amount of clay made a much bigger difference than the type of clay. Clay minerals are flat or 'platy' and therefore become preferentially aligned by compaction. The porosity will be crack-like and therefore increase the degree of anisotropy.

Batzle and Han (1997) found that flushing brine saturated sandstones with distilled water caused a decrease in permeability by two orders of magnitude which they attributed to swelling of clays in the pore spaces. This also had the effect of shifting the frequency range where velocity dispersion is greatest to lower frequencies. Measurements of the elastic properties of various solid clays by Wang *et al.* (1998) showed that the bulk and shear moduli appeared to increase with MgO content, although this does not necessarily have any bearing on the effect of different clays in saturated sand.

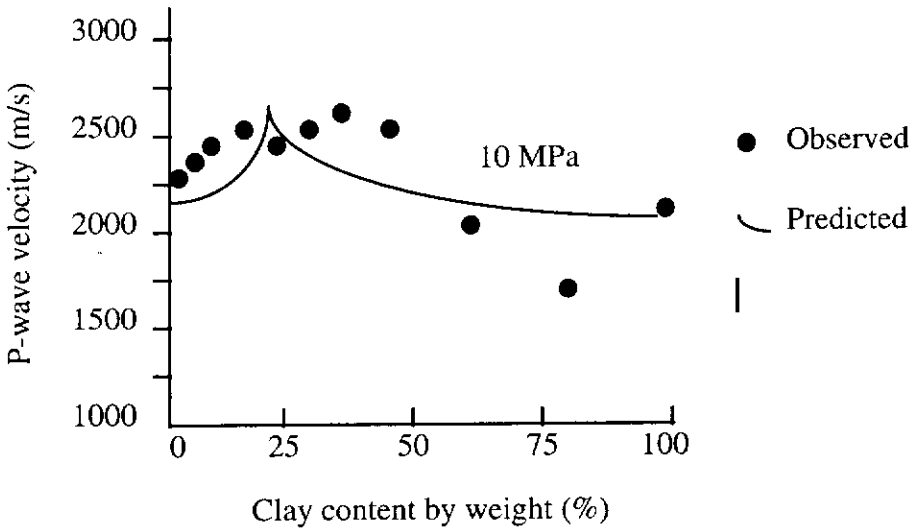

Figure 4.11: Comparison of predicted versus observed changes in P-wave velocities with increasing clay content at 10 MPa confining pressure (modified after Marion *et al.*, 1992).

Although this research deals purely with unconsolidated sands, it's worthwhile comparing these results against the effect that clay has on rocks. An increase in clay content decreases the sound velocity in sandstone (Kowallis *et al.*, 1984), which is the opposite to its effect on loose sand. In rocks, adding clay serves to decrease the shear modulus (μ), through the interactions between pore fluid and clay minerals which act to soften the rock matrix (Toksoz *et al.*, 1976). The effect of clay on loose sediments is the opposite in that it appears to stiffen the contacts between the sand grains (Han *et al.*, 1986). This is in agreement with data published by Blangy *et al.* (1993) where the velocity of both consolidated and unconsolidated sands with clay was greater than consolidated 'clean' sandstone, and less that unconsolidated clean sand, at reservoir pressures (30 MPa). Interestingly, Blangy *et al.* chose not to show any of his data recorded at atmospheric pressure but claimed similar effects. There was probably considerably more scatter in that data.

4.8.7 Pressure

All of the models in this thesis were run under room conditions. However, it is necessary to review the effects of pressure on the acoustic properties of sediments. This is because much of the existing research on saturated sands was performed under high pressures (to simulate reservoir conditions) although extrapolation of these results to atmospheric pressure is, in most cases, invalid.

Effective (or differential) pressure is the confining pressure minus the pore pressure. When the volume of water is greater than the pore volume of a sediment, as is the case with saturated sands, all of the pressure from the water above is on the pore fluid only, that is, the differential pressure is zero. A change in the P-wave velocity is proportional to the change in differential pressure only (Wyllie *et al.*, 1958). It is often written that the sound velocity in a sediment increases with pressure, but this statement implies increasing confining pressure which, in the case of laboratory studies, is externally applied, or in the field, is from the overlying sediments. When the pore pressure

remains constant, the increase in confining pressure equates to an increase in differential pressure, which causes the velocity change.

Brandt (1960) showed that the acoustic velocity in unconsolidated marine sediments is independent of the depth of overlying water. This is because the velocity is dependent on the effective pressure, which is zero regardless of water depth. In some cases, within a sedimentary sequence, the pore pressure may be increased by the swelling of clays. This in turn causes a decrease in the P-wave velocity because the increase in pore pressure leads to a decrease in differential pressure (Mese and Tucunco, 1996).

Domenico (1977) was able to achieve a good fit to his velocity observations based on the exponential equation

$$V = (A.P_d)^n \quad , \tag{4.19}$$

where V can be either P- or S-wave velocity, P_d is the differential pressure, and A and n are constants. For P-wave velocity in unconsolidated brine-saturated angular (Ottawa) sand he used values of A = 4500, and n = 0.55.

Talwani *et al.* (1973) found that the elastic moduli of unconsolidated sediments are not unique functions of pressure, but that they exhibit hysterisis. His experiments involved sands with an initial grain size around 700 μm. The P-wave velocities were repeatedly measured as the confining pressure was increased to 250 MPa. The pressure resulted in many of the sand grains being crushed, so that the end result was a range of grain sizes from powder up to 700 μm, which simultaneously resulted in an increase in velocity and a decrease in porosity. However, as the pressure was released, the velocity change was reversed while the porosity change was not (Figure 4.12). As mentioned before, this brings into question the influence on velocity that is often associated with porosity.

The cause of increasing velocity with differential pressure is perhaps best described by Stoll (1998)...'As the macroscopic confining stress increases, intergranular forces at grain contacts increase with an attendant increase in the size of the minute areas of

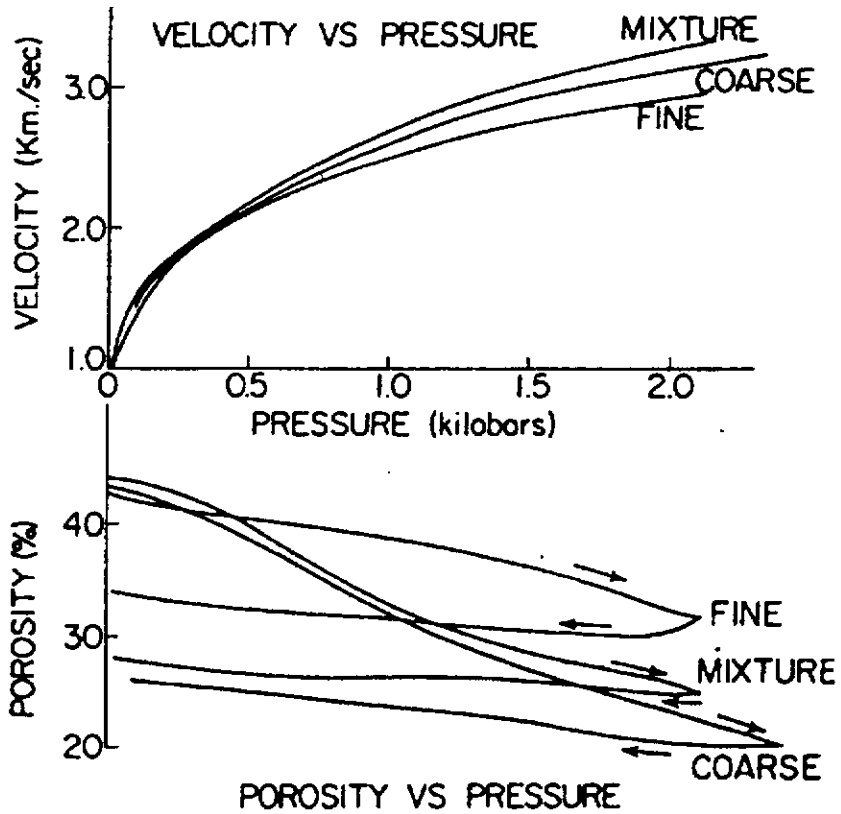

Figure 4.12: P-wave velocity and porosity change in three sands as confining pressure is increased and released. The velocity is independent of the pressure history, whereas porosity is not (after Talwani *et al.*, 1973).

contact. This changes both normal and tangential compliance at each contact, and hence the macroscopic bulk and shear moduli of the assemblage of particles has changed'.

When comparing results from in-situ studies with those made in a laboratory it is important to consider the influence of other effects. Domenico (1977) found that the increase in velocity with differential pressure was not as high in the laboratory as in-situ because of the lack of sedimentation (i.e., cementation) that takes place in the laboratory. It is impossible to adequately quantify the effects of cementation that occurs in-situ because physically sampling the loosely consolidated sediment changes its properties. Consolidated rocks can be similarly affected. The release in confining pressure or the process of drilling may create more cracks in the rock, which will increase the pressure dependence on velocity measured in the laboratory relative to its behaviour in-situ.

At high frequencies, fluids in thin cracks and soft pores act more like solids because they have less time to equilibrate, and this increases the sound velocity. High effective pressure tends to close thin cracks and soft pores, which increases the velocity at all frequencies. Therefore, higher effective pressure reduces frequency dependence.

The relationship of velocity change with increasing effective pressure has been established since the original contributions of Gassman, with subsequent modifications to allow for differences between typical sand grain contacts and the ideal case of spheres as used by Gassman. However, while most publications claim a good fit between observations and the modified theory, the data become remarkably scattered as the curve approaches zero differential pressure. This trend exists with regards to many other influences on sand velocity such as the porosity (Blangy *et al.*, 1993), the presence of clay (Marion and Nur, 1991), or changes in the elastic moduli (Gardner *et al.*, 1964; Hamilton, 1971). In fact, while there are multitudes of publications on pressure effects, it is very difficult to find an example where the 'best fit' curve to the observations has been extended to zero effective pressure. This is probably because it doesn't apply.

The only way to know the pressure dependence of wave velocities for a particular sediment or rock is to measure it. Rock physics can be used to describe and understand the seismic behaviour of a rock, but is still very limited in its ability to predict velocities.

4.8.8 Pore Pressure

Pore pressures in sediments may sometimes rise above the lithostatic pressure for a number of reasons. For example, a high rate of deposition may not allow enough time for pore pressures to equilibrate as the porosity is reduced by compaction. Other causes can be tectonic stresses, hydrocarbon generation or the de-watering of clays from de-hydration reactions. As mentioned previously, an increase in pore pressure results in a decrease in effective or differential pressure, which subsequently reduces the seismic velocity as cracks are opened and the frame is softened.

Christensen and Wang (1985) found that, to a first approximation, velocities are governed by the effective pressure (P_{eff}):

$$P_{eff} = P_c - \alpha P_p \ , \tag{4.20}$$

where P_c and P_p are confining and pore pressures respectively. The attenuation coefficient α is constant for a given rock and in most cases close to 1 for both P and S-wave velocities.

However, when gas is present the relationship is not as simple. An increase in pore pressure reduces the compressibility of gas, which increases the pore fluid bulk modulus and tends to raise the velocity (Mavko *et al.*, 1998). An ideal gas at 300 atmospheres pressure is 300 times less compressible than the same gas at room pressure. A change in pore pressure can also change the degree of saturation as gas moves in and out of solution.

4.8.9 Temperature

Del Grosso (1974) published an equation for the speed of sound in water as a function of pressure, temperature and salinity. This equation, termed NRL II, contains 19 terms to 12 significant figures (six of the terms go to zero for fresh water) and is accepted as a valid reference for underwater acoustics. Medwin (1975) published a simplified equation that is accurate to better than 1 ms^{-1} for realistic parameters:

$$V_w = 1449.2 + 4.6T - 0.065T^2 + 0.00029T^2 + (1.34 - 0.010T)(S - 35) + 0.016D \quad , \tag{4.21}$$

where T is the temperature in degrees Celsius, S is the salinity in parts-per-thousand and D is the depth in metres.

At room pressure, the P-wave velocity of water increases with temperature, reaching a maximum at about 80°C (Batzle and Wang, 1992). The velocity increase of loose saturated sands roughly follows that of water (Shumway, 1958), as the effects are dominated by the change in the bulk modulus of the pore fluid (K_f). The particular material used makes no difference, which is a consequence of the relative amplitudes of the moduli of the sedimentary components and the relative insensitivity of the sediment grains to changes in temperature (Bell and Shirley, 1980). S-wave velocities, and P- and S-wave attenuation are independent of temperature.

The water temperature in the tank used for the physical modelling experiments in this thesis fluctuates by up to two degrees daily. This is insignificant for any one survey as it has minimal effect on reflections but could be important for the time-lapse surveys described in Chapter Six. For this reason, it was considered necessary to establish experimentally the temperature dependence on velocity of the particular sands used in this thesis, the results of which will be presented in Chapter Five.

The sound velocity in sand is most sensitive to temperature when the pore fluid contains oil. As the temperature is increased, the compressibility of oil increases and the viscosity decreases (Wang *et al.*, 1990), and this both decreases the velocity and increases attenuation. In field situations other factors can be important, such as gas coming out of solution. The density and bulk modulus of gas is reduced substantially with increasing temperature at high pressures, but remains fairly stable at room pressures (Batzle and Wang, 1992). The role of pore fluids is discussed further in the next section.

4.8.10 Pore fluid

The pore fluid affects the pore space compressibility, which is a key parameter controlling seismic wave propagation. Increasing pore compressibility decreases the seismic velocity. It also enhances the sensitivity of velocity to changes in stress, pore pressure and saturation (Mavko and Mukerji, 1995). Seismic effects from changes in pore fluid provide the basis for time-lapse seismic monitoring of fluid flow. Besides the effect of the fluid on the bulk modulus of the sediment, chemical effects on the surface of the grains can also affect the velocity (Murphy, 1984).

When considering the acoustic properties of sediments, the relevant pore fluids for hydrocarbon exploration are water, brine, oil and gas. The majority of the models in this thesis use fresh water as the pore fluid, with gas and oil introduced in the time-lapse models. The effect of brine is also relevant as many rock physics publications use it as the pore fluid. The influence of gas is included in the following section as part of the effects of partial saturation.

The empirical dependence of gas, oil and brine properties on temperature, pressure and composition are described by the Batzle-Wang Formulae (Batzle and Wang, 1992). The Batzle-Wang bulk moduli are the adiabatic moduli, which they argue are more appropriate for seismic wave propagation than the isothermal moduli, which are measured in standard pressure-velocity-temperature (PVT) tests. The isothermal

moduli can be 20% lower than the adiabatic moduli for oil, and 50% lower for gas, although the difference for water or brine is negligible.

When several fluid phases are present, the common approach is to treat the fluid as a single-phase effective fluid with the bulk modulus described by the Reuss average. This is only valid when the fluids are mixed at the finest scales. When this is not the case, patchy saturation models are more appropriate.

The velocity in unconsolidated sands is strongly dependent on the stiffness of the grain to grain contacts, which can be affected by the presence of oil. The oil acts as viscous cement whose properties are frequency dependent (Leurer and Dvorkin, 1998). The viscosity of the pore fluid has a strong influence on the critical frequency. An increase in viscosity increases dispersion and shifts it to a lower frequency (Batzle *et al.*, 1996). This effect is predicted by squirt flow theory but the frequency shift is the opposite of the Biot loss mechanism. Both of these viscosity effects on attenuation need to be considered when analysing laboratory measurements over a narrow frequency range. Apparent attenuation changes from fluid effects may be misleading if there is a significant shift in the frequency range of dispersion.

The Biot loss mechanism is usually in the order of one or two percent and so is smaller than most of the effects seen. However, it is the only mechanism for which the dispersion bounds can be rigorously calculated from theory (Winkler, 1986). The Biot loss mechanism occurs when the viscous skin depth is approximately equal to the pore size. The frequency (ω) at which this occurs is given by (Johnson and Plona, 1982):

$$\omega = 2\eta / \left(\rho_f a^2 \right) , \tag{4.22}$$

where η is the fluid viscosity and ρ_f is the fluid density. This equation tells us that a fluid such as oil with viscosity two orders of magnitude higher than water will increase the Biot peak frequency by two orders of magnitude. A simple interpretation of the effect of increasing viscosity on high frequencies (when the fluid is unrelaxed)

suggested by Mavko and Jizba (1991) is that it is mechanically the same as increasing the confining pressure to close the 'soft' pores.

4.8.10.1 Oil

Oils are usually mixtures of a whole range of compounds, including gases. Crude oils are usually heavier and have a more complex composition (Batzle and Wang, 1992). The weight of an oil is usually described as an American Petroleum Institute oil gravity number, (API), defined in terms of its density (ρ_o) as:

$$API = \frac{141.5}{\rho_o} - 131.5 \ . \tag{4.23}$$

A heavy oil has an API number around five, with a light oil nearly 100. The difference in viscosity is several orders of magnitude, which has substantial effects on attenuation and velocity dispersion. The sound velocity in oil decreases rapidly with density (ie. increasing API). When oils contain dissolved gases, known as live oils, the density and viscosity are reduced. Because such strong effects are possible, analyses based on dead oils can be grossly incorrect (Batzle and Wang, 1992).

At room temperature and pressure, the specific gravity of oil can range from 0.5 to greater than 1, with most lying between 0.7 and 0.8. The velocity range is 1250 ms^{-1} to 1600 ms^{-1}. The density, viscosity and bulk modulus of oil increase with both molecular weight and pressure, but decreases with temperature. Figure 4.13 from Wang *et al.* (1990) shows that the velocity of oil decreases systematically with increasing API, regardless of temperature.

4.8.10.2 Brine

Brine is peculiar in that the bulk modulus reaches a maximum between 40°C and 80°C. It is able to absorb far less gas than oil can, and so the acoustic impedance contrast with

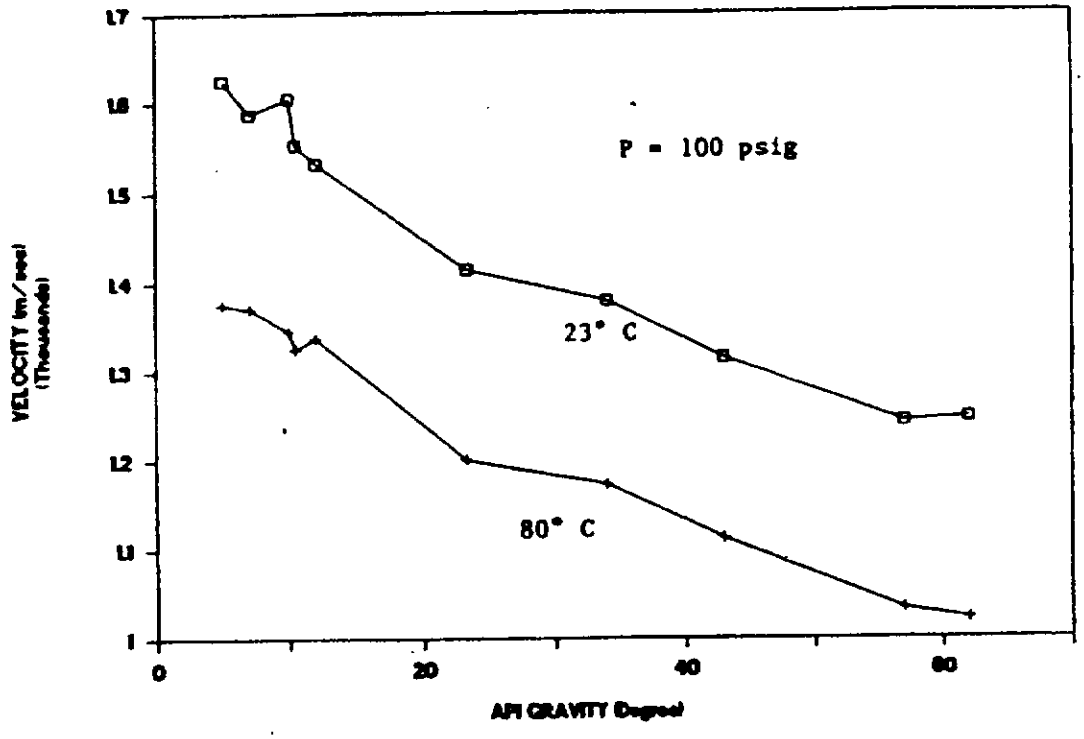

Figure 4.13: Acoustic velocities versus API oil gravity at 23° and 80° C and 100 psig (after Wang *et al*, 1990).

a live oil may be sufficient to produce a seismic bright spot (Clarke, 1992). The most likely case in which this direct hydrocarbon indicator occurs is with light oils in unconsolidated sand. The bulk modulus of brine increases with salinity. The viscosity decreases rapidly with increasing temperature but is little affected by pressure (Batzle and Wang, 1992).

4.8.11 Gas (partial saturation)

The following discussion on the effects of gas is provided in terms of partial saturation at atmospheric pressure, where the gas is air and assumed to have a negligible bulk modulus. However, different types of gas can make an appreciable difference, particularly at high pressures because the bulk modulus of gas increases linearly with pressure. In addition, saturation levels may change as gas goes into or out of solution depending on pressure conditions and fluid type. In most cases, the term saturation refers to the amount of air or gas in the pore fluid. However, when two fluids such as oil and water are mixed, the percentage of one fluid in the other may be expressed as relative saturation.

The presence of gas in unconsolidated sand has two contrasting effects. An increase in gas content means the bulk density will be reduced, and this means the velocity will be increased. The influence of density is linear and the magnitude of this effect ultimately depends on the porosity, up to a maximum velocity increase of around 12% (Brandt, 1960). An increase in gas content also reduces the bouyancy provided for the sand grains by the pore fluid, and so results in an increase in frame pressure, which also means an increase in velocity. However, the biggest effect from gas, and the most relevant for this research, is the large change in bulk modulus that occurs with just a fraction of one percent gas. At low pressures, the bulk modulus of water with a small amount of gas added decreases very quickly to near the bulk modulus of gas only (Figure 4.14, from Batzle and Wang, 1992). Stoll (1989) found that the bulk modulus of the pore fluid was reduced by an order of magnitude with a small amount of gas, from 2 GPa to 0.2 GPa. This change in bulk modulus happens rapidly over

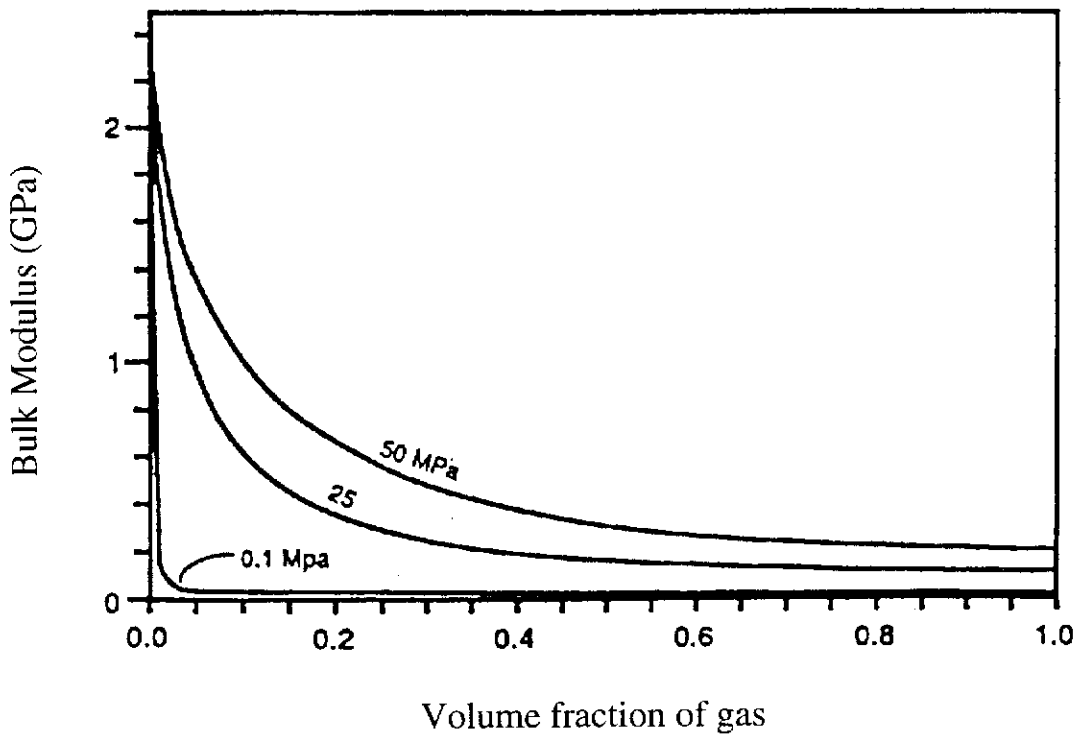

Figure 4.14: The calculated bulk modulus for mixtures of gas in brine. Note that at low pressure the bulk modulus drops almost to zero with just one percent by volume of gas (after Batzle and Wang, 1992).

the first few percent gas and then remains fairly constant up to 100%, so at greater gas percentages the effects of the density change begin to dominate. This results in a maximum velocity at 100% fluid saturation and a minimum velocity at 90% (Domenico, 1977). Domenico also found that with low gas percentages the distribution was uneven and tended to occupy the larger pores.

At low saturation levels, liquid exists as pendular rings around grain contacts (Palmer and Traviolia, 1980). The effect of the liquid film on the grain contacts may be contrasting. The grains may be effectively held together by the fluid, but the stiffness of the contact area itself may be reduced (Bacharach *et al.*, 1998). Attenuation is usually greater in partially saturated rock than in either the dry or the fully saturated case.

In sand, the difference between the dry and saturated case for the bulk and shear moduli is not certain. Adding water to a sand produces only a small change in the S-wave velocity, and so it seems reasonable to infer that there is very little change in interparticle compliance and hence the elastic moduli of the frame. At the same time, there is a large increase in the P-wave velocity because the voids are now filled with an incompressible fluid and hence the overall bulk modulus is much higher. These effects on velocity are predicted by Biot theory (in the general case), or by Gassman's relations if fluid motion relative to the frame is neglected (Stoll, 1998). However, disagreement between rock physicists seems to arise from alternate interpretations of Biot theory.

Stoll (1998) stated that there is very little change in the elastic moduli of the frame between the dry and saturated case, and that the velocity changes arise purely from the changes to the fluid moduli. Chotiros (1998) disagreed and argued that this assumption works well for porous materials with cemented frames but is not applicable to unconsolidated sands. While the values for dry and saturated sand are very similar at high differential pressures, at low pressure the frame moduli values differ substantially. Chotiros argued that a portion of the pore fluid becomes an integral part of the frame and helps transfer the compressional strain, which means that there is a large increase in the frame bulk modulus. Conversely, at low differential pressure, there is actually a decrease in the frame shear modulus, which Chotiros attributes to the capillary effect

having a tendency to maximize the contact area between fluid and grain. In order to gain access to all unexposed solid surfaces, the fluid tends to force the grains apart, giving a noticeable decrease in the shear modulus.

If Chotiros's (1998) interpretation is valid, then there are flow-on consequences for the value used for the bulk modulus of the sand grains. Most publications infer a grain bulk modulus that is equal to that of pure crystalline quartz. However, Chotiros used a 'measured' value for grain bulk modulus that is five times less than 'historical' values. Interestingly, his 'measured' values had 95% confidence limits that varied by a factor of three. In order to match his observations with predictions, the frame moduli were then adjusted to fit. To justify this in terms of Biot theory, Chotiros stated...'any part of the pore fluid that remains stationary relative to the frame and functions as an integral part of the frame must be counted as a component of the frame. Consequently, the operative grain and frame moduli are determined by the solid grains plus any part of the fluid that is held stationary relative to the frame'.

Rather than disputing the underlying (Biot) theory, the controversy lies in the definition of the boundary between frame and pore fluid. The elastic moduli of the sediment components are all interrelated in a complicated way, and they cannot be chosen independently if they are to represent a specific granular aggregate. It is impossible to say which idea is closer to the truth because in Biot's original theory, the bulk modulus of the grain was not even used directly.

4.8.12 Patchy saturation

Patchy saturation occurs when a sediment has pores that cover a range of aspect ratios. Pores with low aspect ratios such as thin cracks are less easily drained or flushed out by another fluid phase. Seismic velocities depend not only on the types of pore fluid and level of saturation, but also on the spatial scale of the distribution. The relationship of velocity to saturation is dependent on the relative scale of the saturation heterogeneity

to the seismic wavelength (Khaksar and Griffiths, 1999). When saturation is patchy, the effect on velocity will be spread out over a much larger range of saturations.

Saturation describes the relative volumes of different fluid phases on a macro scale. However, at grain scale, immiscible phases become discontinuously distributed and the average saturation level does not adequately describe the pore fluid. At low frequencies, the seismic wave sees small-scale variations in saturation as an average saturation level, which can be modelled with Gassman using a single 'effective fluid'. At high frequencies, saturation is effectively patchier relative to the wavelength. The waves see pores in isolated patches which may be either stiff (fluid filled) or soft (gas filled). The overall result is a higher effective velocity.

Figure 4.15, from Sengputa and Mavko (1998), shows the possible velocities for a mixture of oil and water in sandstone. An observed velocity of 2350 ms^{-1} could indicate that the oil saturation is anywhere from 99% for a homogeneous or fine scale distribution, to as low as 20% if the distribution is coarse scale or patchy.

While the observed acoustic behaviour of sediments can be explained in terms of the empirical relationships discussed in this section, it is not possible to predict the exact behaviour of the sands used in this research. To establish the optimum parameters and techniques for the design of the models in this thesis it was necessary to systematically measure the influence on velocity of a number of variations in sand texture and composition, which follows in the next Chapter. A summary of key parameters and their influence on the seismic velocity in unconsolidated sand is in the Appendix.

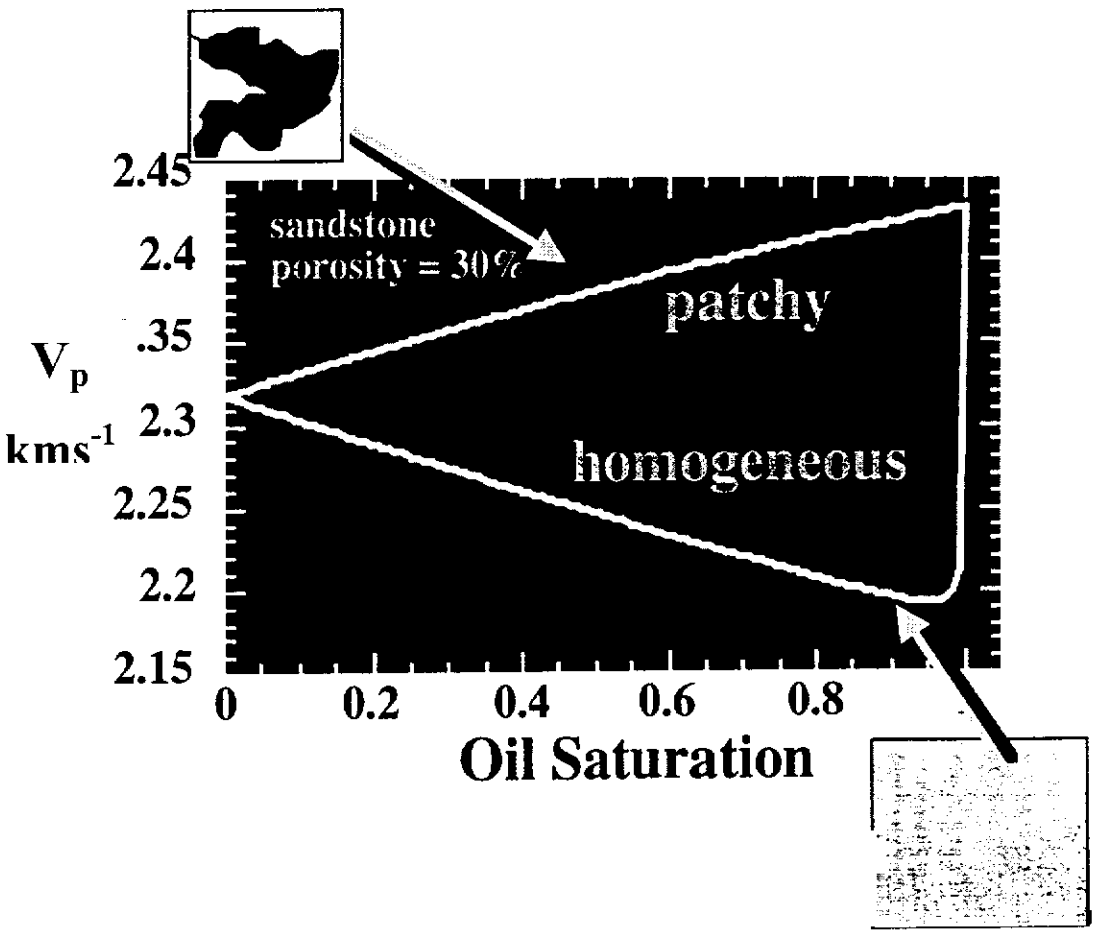

Figure 4.15: The velocity of a rock depends on the relative saturation and the scale of the fluid distribution relative to the seismic wavelength (after Sengupta and Mavko, 1998).

CHAPTER FIVE

ULTRASONIC MEASUREMENTS IN SAND

Considerable effort was spent on measuring the properties of a variety of quartz sands and, initially, mixtures of sand with other materials. This work was necessary to establish the best techniques to generate seismic reflections within sandbox models. Although there have been many studies on the acoustic properties of unconsolidated sands, they are in most cases a study of the effects of changing conditions on one particular sediment. The experiments presented in this Chapter were performed in an attempt to establish the effects of changing individual textural parameters. As will be seen, this is not entirely successful because the most significant factor affecting most of the experiments is the technique of preparing the samples for the experiments. It is physically impossible to prepare two samples in exactly the same way and the random variation that results can be greater than the variation caused by changing the particular parameter being investigated.

The most stable results are those using very well-sorted sands. These samples are least sensitive to 'human error'. This is because there is less variation possible in sorting and packing between samples. In addition, these samples have the largest porosity and permeability and so are easiest to saturate completely. This means that they exhibit the least variation with time and give by far the most repeatable results. The results reveal a number of trends that will prove in Chapter Six to be very important to the design of the sandbox models. However, experiments on recording reflections within sandbox models, which are presented in Section 5.8, reveal that the velocity results alone are of marginal value as a basis for establishing the necessary acoustic impedance contrasts within sandbox models.

Quartz sand is always the main granular material used for sandbox modelling, and is often the only material used. For this project, it was initially thought it would be necessary to test a range of other materials, which were required to provide a contrast in acoustic impedance with the sand. The choice of materials involved consideration of a number of factors such as availability, price, grain size and their previous use as modelling materials. Materials such as iron powder, garnet and illmenite sand, alumina, glass and glass bubbles were tested as they cover a range of grain sizes and densities. However, it soon became apparent that density plays a minor role in the acoustic behaviour of unconsolidated models. The contrast in calculated acoustic impedances is shown in section 5.8 to be only part of the reason why reflections are produced in these models. As such, this study quickly focussed on the properties of pure quartz sand. With the exception of clay, experiments with other minerals were not pursued past the preliminary stages of this research.

The standard sand used for all of these experiments is a moderately-sorted pure quartz sand, purchased in 20 kg bags from an industrial minerals processing plant. This sand has an average grain size of 200 μm and 95% of the grains are between 125 μm and 300 μm. There appears to be little variation in sorting and grain shape between bags purchased at different times. A photograph of the sand grains is shown in Figure 5.1, and the grain size distribution is shown in Figure 5.2. Most other variations of sand used here are sieved fractions of the standard sand. This was done both for convenience and to maintain as consistent grain shape as possible. The grains are sub-rounded although it appears that the smaller grains may be more angular than the larger grains, which is typical of all sediments. This almost certainly will have some effect on the acoustic properties, but it is not possible to quantify this from these experiments.

The range of experiments performed can be broadly divided into two groups. The first series of experiments presented are variations that affect the way the sample is saturated, such as the water temperature, the use of a vacuum chamber and underwater deposition. It is necessary to establish the effects of these variations before it is possible to conclude anything from the other results as they potentially have more influence on

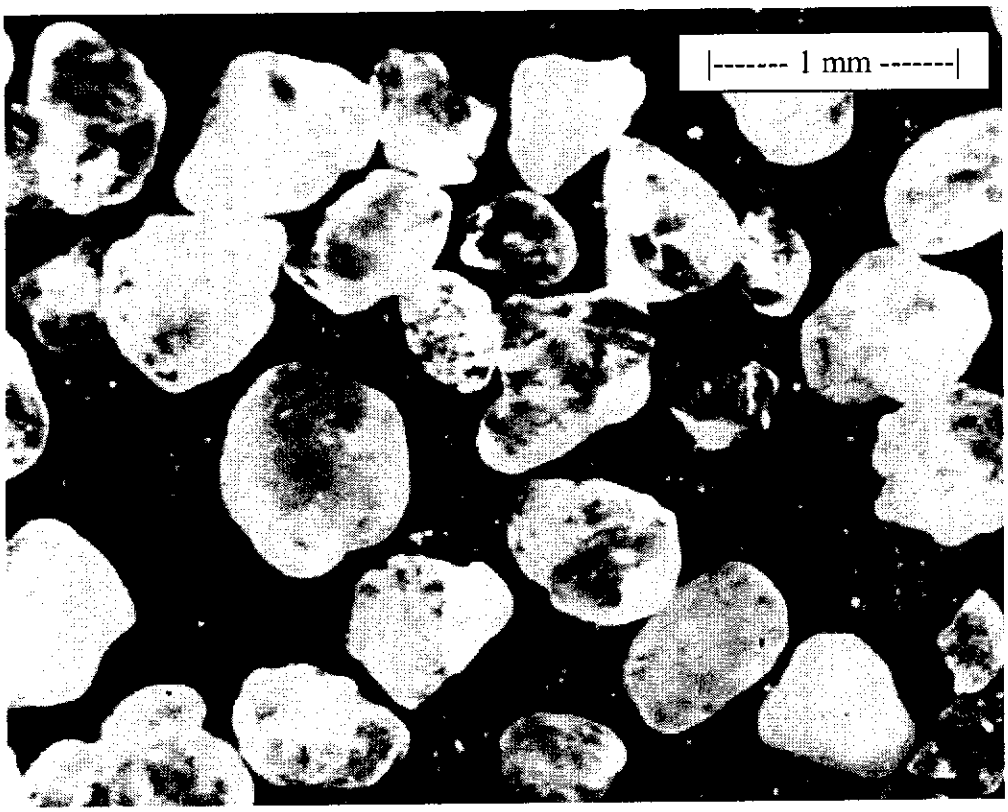

Figure 5.1: Photograph of the standard pure quartz sand used for this research, with average grain size 200 μm.

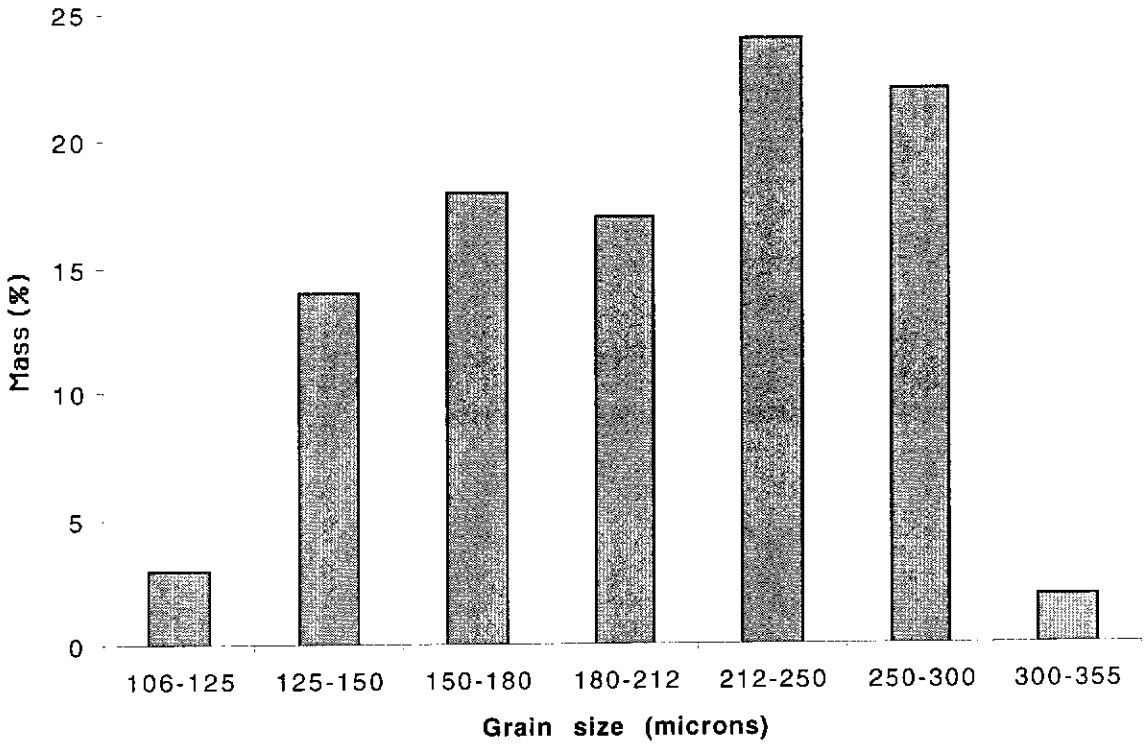

Figure 5.2: The grain size distribution of the standard sand used for many of the ultrasonic measurements determined from a sieving analysis. Other variations used are sieved fractions of this sand.

the results than any change in sand texture. The second series of experiments attempt to establish trends in the acoustic properties of sands that arise from systematic variations in an isolated parameter, such as grain size, packing or clay content. Some measures taken, such as the practice of applying vibration to compact the samples, can affect both the saturation and texture of the sample.

5.1 Porosity

Porosities were calculated from the dry and saturated masses of the samples in a container of known volume. The repeatability of these measurements suggests that the results are accurate to within around 1%. The biggest factor affecting the porosity was the handling technique.

The porosity of the standard sand used in this thesis averages 39% when simply poured into a container and saturated. The porosity of the same sand averages 37.7% when slowly sprinkled into the containers, which achieves a tighter packing configuration. Applying vibration to compact the dry samples brings the porosity in both cases to around 37%. The observed variation in porosity with handling technique is similar to, but slightly less than, measurements with similar sands by Krantz (1991) and Cobbold and Castro (1999). Only two of the eleven series of experiments presented in this Chapter showed any correlation between porosity and velocity.

5.2 Permeability

Permeability is difficult to measure, particularly for sediments containing silt and clay. There is still much uncertainty regarding the method of measurement and what the measurements mean, since results from different methods can differ by several orders of magnitude (Chotiros, 1995). An air permeameter (Figure 5.3) was used to measure the permeability of three sands used in this thesis, which were the standard sand and two

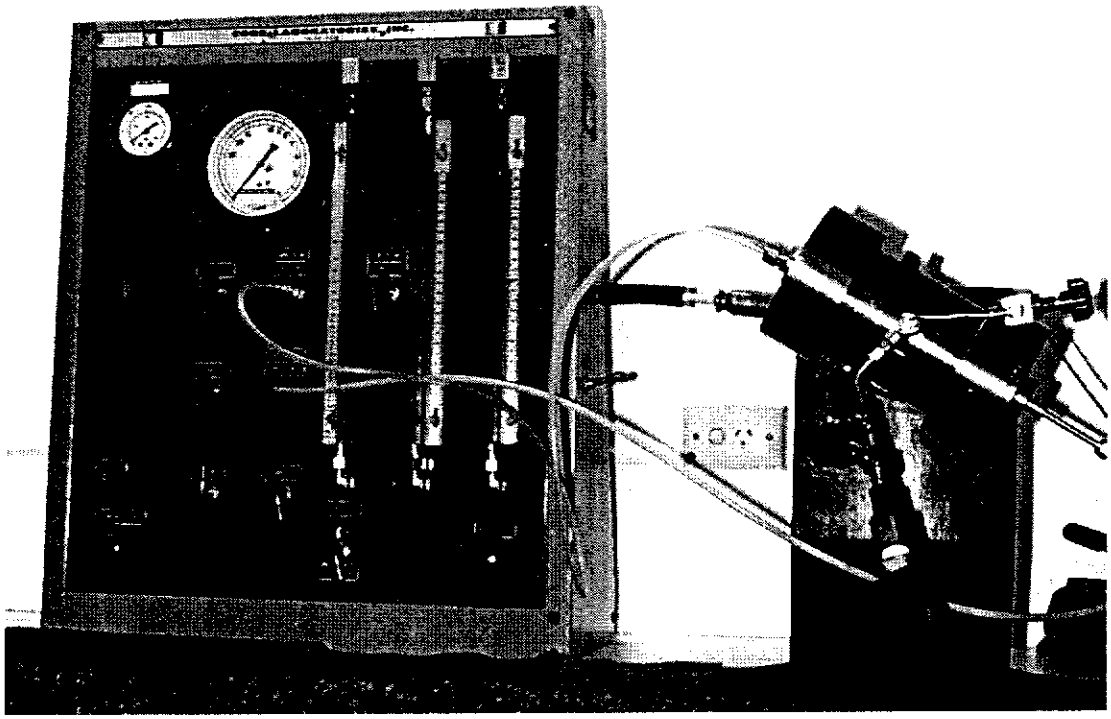

(a)

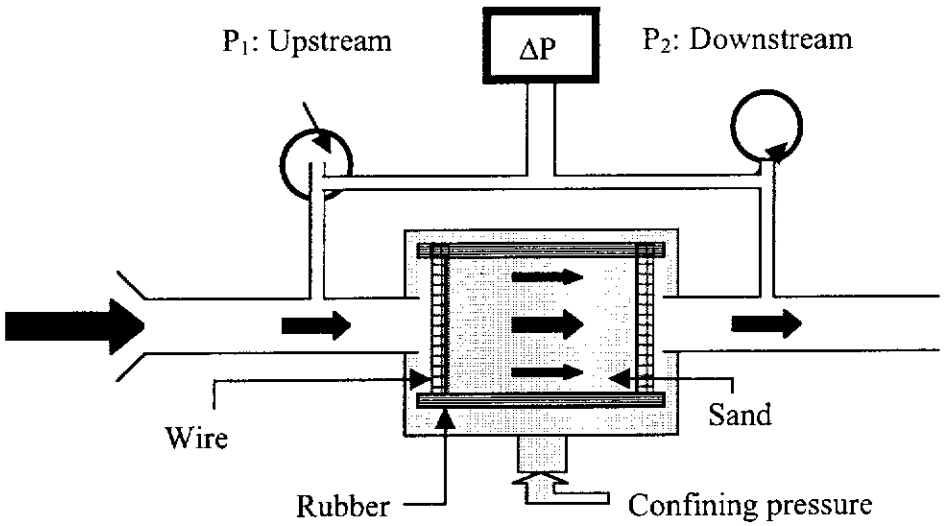

(b)

Figure 5.3: (a) Photograph and, (b) schematic diagram of the air permeameter used to measure the permeability of three unconsolidated sands. The flow rate of air and the pressure gradient across the sample are measured to calculate permeability from Darcy's Law.

very well-sorted sands with grain size ranges of 250 to 300 μm and 300 to 355 um. The well-sorted sands were chosen for the permeability measurements as they are important for the fluid flow models presented in Chapter Six.

The unconsolidated sand was placed in a rubber sleeve (boot) with wire mesh ends. The 50 μm wire mesh was manually clamped and sealed against the sides of the 38 mm diameter rubber sleeve. The mesh constrains the sand but has no measurable effect on the air flow. The length of the sand plugs were measured with vernier calipers and were at least 75 mm for each of the three sands measured. It was necessary to apply a small confining pressure of 100 psi to ensure no air flowed between the sleeve and sample. This would result in some compaction of the sand and probably reduce permeability readings slightly, but no corrections were made for this.

The permeability (K) was calculated from Darcy's law, rearranged from its form in equation 17 as follows,

$$K = \frac{V.\mu.L}{\Delta P.A} \quad . \tag{5.1}$$

V is the flow rate in cm^3s^{-1} and ΔP is the difference between the upstream (beginning) and the downstream (end) pressure, all of which are measured from analogue gauges on the air permeameter. L and A are the length and cross-sectional area of the sample respectively and μ is the viscosity of air in centipoise (0.018 cp).

The measured permeability of the standard sand was 9 darcy's. For very well-sorted sands with grain sizes ranges of 250 – 300 μm and 300 – 355 μm they were 14 darcy's and 18 darcy's respectively. These results are typical for clean, well-sorted sands (see Figure 4.9), but are much higher than most natural sediments, which are usually more compacted and contain some clay sized particles.

5.3 Velocity Measurements

Many of the velocity measurements taken for the wide range of material mixtures were the first experiments conducted for this research. This meant that much of the work was conducted before some of the problems were fully appreciated, such as the sensitivity to the handling technique and the importance of ensuring the samples were fully saturated.

Originally, velocities were calculated from measurements of the arrival times of an ultrasonic signal transmitted though the sand containers. However, it was necessary to use a container width of only 20 mm if a signal was to be successfully recorded through many of the samples. This resulted in very high measurement errors. There are two reasons this was necessary. Firstly, there is poor coupling of the energy between the flat, solid perspex container walls and the loose granular material. Secondly, strong reflections from the container walls reduced the amount of energy that was transmitted through the samples. The walls of the container also act to trap the air against the sides, which can be seen under close inspection and further complicates the acoustic transmission experiments. Of the samples with very high rates of attenuation, it is possible that the first detectable arrival used to calculate the velocity was actually from waves that travelled around the sand in the container walls. The effect of the container on the measured results was too great to allow any relevant trends on velocity or attenuation to be established. Once this was fully appreciated a better technique was devised, and is presented below.

5.4 Sample preparation

In the literature, methods of preparing samples for ultrasonic measurements vary considerably. The intentions are always to ensure that the samples are fully saturated although often little regard is given to the subsequent effects that different preparation techniques may have on the results. It will be demonstrated here that significant variations will occur in unconsolidated sand if this is not taken into consideration. An

example of the considerable effort that is sometimes necessary to achieve repeatable results was given by Bell and Shirley (1980). Their first step was to saturate the samples in deionized water. The samples were then boiled, left in a vacuum chamber for 24 hours, subjected to vibrations for several minutes and then left to stand overnight. Most published experiments involve one or more of these measures and are relevant to the design of the models in this thesis. The effects of these are investigated here.

5.4.1 Method

A container was designed by the author that allowed samples of precise lengths to be prepared but which would avoid the problems involved with transmitting the ultrasonic signal through the container walls. Figure 5.4 shows some of the containers used for the velocity measurements. The different length containers allowed amplitudes to be recorded over different length samples, and subsequently allowed the rate of attenuation to be estimated. However, most measurements were recorded in the 50 mm length containers, and were used for comparisons between different samples.

The effects from the container walls were avoided by positioning the transducers in direct contact with the sand. A base receiver transducer was built into a frame such that it protruded up from the frame by exactly the thickness of the sample container base. A hole was drilled through the bottom of each container that allowed the base transducer to be in contact with the sand. A sheet of thin 'cling wrap' plastic was glued on the inside face of each container base to hold the sand in place (Figure 5.5). Tests with an empty container showed that the cling wrap made no measurable difference to the recorded arrival times and only a slight difference to the amplitudes. The source transducer was set up directly over the base transducer and the separation between them could be precisely controlled with the physical modelling system's stepper motors. The source transducer was raised between measurements to allow each sample to be put in place and then lowered back into position such that it was in direct contact with the top surface of the sand (Figure 5.6). With each sample in position, zero offset

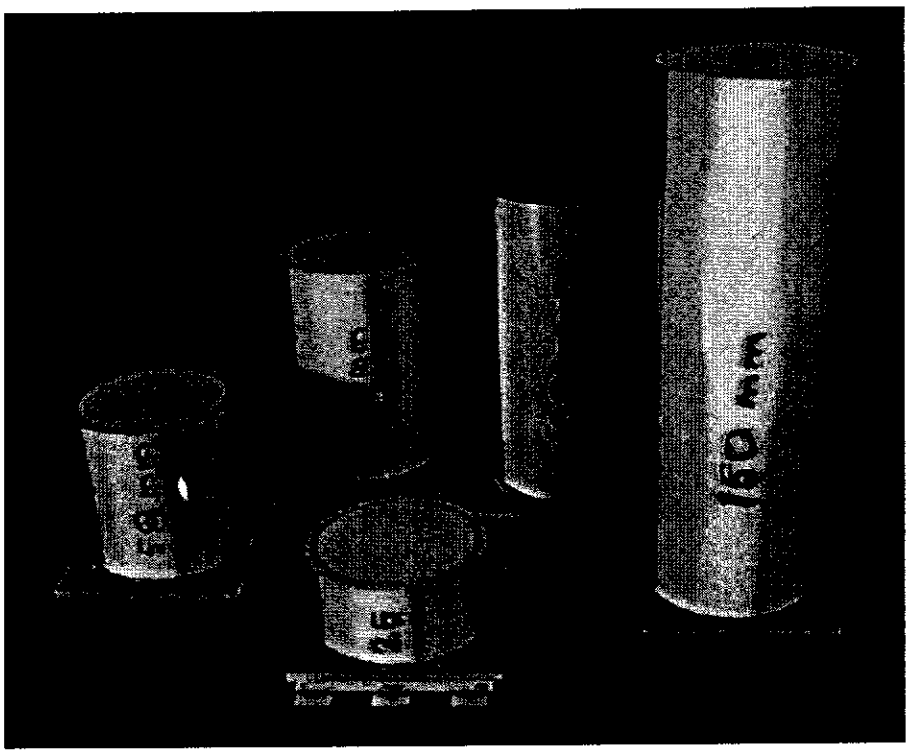

Figure 5.4: Photograph of some of the Perspex cylinders used for the ultrasonic measurements. Most of the velocity measurements were recorded with the 50 mm cylinders. The different sized cylinders were used to measure amplitudes at different sample lengths to estimate rates of attenuation.

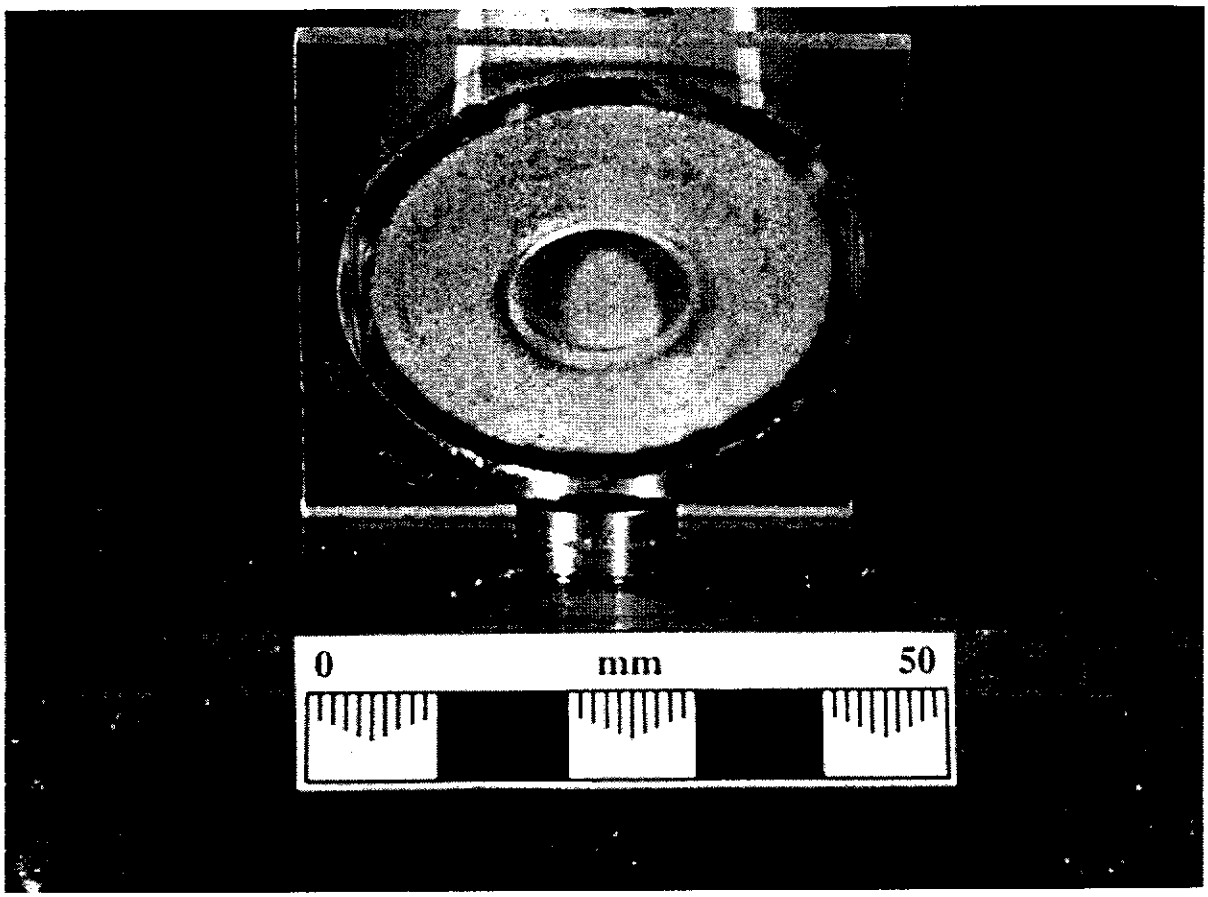

Figure 5.5: Photograph of the configuration used to allow the receiver transducer to be in contact with the base of the sand in the perspex cylinder. The sand is held in place by a sheet of cling wrap that is glued to the inside of the container. The transducer is raised from the base such that it is in direct contact with the cling wrap.

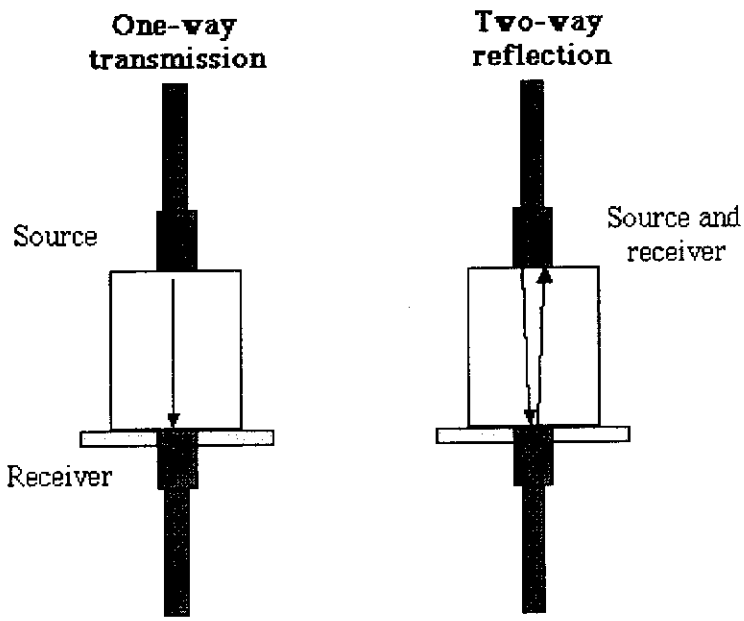

Figure 5.6: Schematic diagram of configuration used for the ultrasonic measurements. The source transducer is lowered into contact with the top surface of the sand after it is put into place. The source transducer can also be used as a receiver to record any reflections that may be generated within the models.

reflections were also recorded by repeating the measurements with the source transducer also acting as the receiver. This will be discussed further in Section 5.8. In cases where random variation between samples was very large, measurements were sometimes averaged over several samples to allow a reasonable trend to emerge.

5.4.2 Errors

Techniques of handling or preparing samples of unconsolidated sand for measurements are the biggest factors affecting results. However, there are also many other possible reasons why published results may differ from those presented here, some of which have been discussed in Chapter Four, and are summarised here:

1. The low total pressure (atmospheric) and zero effective pressure (confining pressure minus pore pressure) used in this thesis means that the rate of energy attenuation is extremely high. This requires that the length of the sample used must be kept small to allow the recording of a transmitted pulse from an ultrasonic transducer. This results in significant errors in velocity determination.
2. A fraction of a percent of gas has significant effects on velocity and attenuation. Domenico (1976) found that uneven microscopic distribution of gas was responsible for the discrepency between measured and computed velocities at high saturation. This affected many of the models in this thesis and was an important problem to solve before reliable results were attainable.
3. Velocities are often calculated from first arrival travel times and it is assumed that the ray path travelled is the shortest direct path, but this is not necessarily the case (Wyllie *et al.*, 1958). Waves travelling this direct path may in fact be slower than the waves travelling only within the fluid, or be attenuated by the constant transitions from fluid to grain to the point of being imperceptible. The fastest waves may be those that travel only in the skeletal frame, and follow a longer 'fast path' through sand grain contacts (Klimentos and McCann, 1988).
4. The sands used by different researchers may have similar average grain sizes but they are not the same samples. Subtle variations in sorting, grain shape and packing

make little difference to the porosity and density but have large effects on the acoustic response. This even applies to different samples of the same sand, which are often heterogeneous at grain-scale and can also give varying results depending on how they are handled.

5. For experiments involving clay, the type used can make a difference and the influence can change over time. Expansion characteristics of clay play a significant role in the acoustic properties in sedimentary rocks (Mese and Tutuncu, 1996).

6. The effects of velocity dispersion are not fully understood. In most cases with pulse measurements, the first arrival is assumed to be the dominant frequency or the highest frequency. However, Liu and Nur (1996) suggested that the first break is the lowest frequency.

7. The effect of temperature on saturated sands follows that of water. This can make a difference of around 80 ms^{-1} between 10° C and 30° C.

8. Vibration applied to loose sand packages makes a significant difference to the packing of the grains and can increase the velocity by up to 100 ms^{-1}.

9. Of the rare published results at or near room pressure conditions, such as those by Han (1994), the samples were first put through several cycles of high confining pressure to remove the effects of hysteresis. Han found that when the confining pressure was removed, porosities returned to close to the original value, but the velocities were irreversibly increased. Elliott and Wiley (1975) also found that pressure cycling was necessary before repeatable results were possible with Ottawa sand.

10. Wyllie *et al.* (1956) suggests that edge effects from the sample container are significant when the length of the sample is less than 1000 times the average grain size. This is the case here and with most published laboratory measurements

11. Different methods of picking arrival times yield different velocities. First arrival travel times will give the signal or energy velocity, while methods based on cross-correlation or picking an amplitude extremum will yield the group velocity, which can be up to 5% slower than the signal velocity at low pressure (Molyneux and Schmitt, 1997). An example will be given later that illustrates how different trends may emerge depending on the method used to pick travel times.

Measurement errors cited in other publications for loose sand velocities are in most cases estimated at 100 ms^{-1} or greater. For example, Marion *et al.* (1992) estimated errors greater than 100 ms^{-1}, Kowallis *et al.* (1984) cited errors of 200 ms^{-1}, and Chotiros (1995) suggested that errors may be as high as 300 ms^{-1}.

It is important to distinguish between errors caused by random variation between samples, which affects the repeatability of the results, and actual measurement errors, which can be very low if care is taken to calibrate the measurements. The recorded signal for the experiments reported in this thesis are digitally sampled every 0.1 μs. Arrival times can usually be picked to the nearest sample point, which equates to a velocity error of around 4 ms^{-1} for the 50 mm length samples used in most cases for these measurements. Although the absolute accuracy of the calculated velocity depends on assumptions about dispersion and the method used to calibrate the measurements, relative changes in velocity in any one series of measurements are precise to the nearest digital sample. Tests on removing and replacing the sand containers from the apparatus used for the measurements, showed that the arrival times for any particular sand sample were repeatable to within the nearest digital sample point.

Generally, measured velocities of clean sand were repeatable to within 50 ms^{-1} if great care was taken. Very well-sorted samples, which have high porosity and permeability, were much less sensitive to different handling techniques and were repeatable to within around 20 ms^{-1}. The low permeability samples containing significant amounts of clay-sized particles (>1%), produced unreliable results. It was difficult to get homogeneous mixing of the clay in the sand. This affected repeatability, and achieving full saturation was also difficult.

5.4.3 Velocity picking

The velocity of water is measured from the slope of the arrival time for a particular event with increasing distance between the transducers. It does not matter whether the first arrival or a later peak or trough is used for the velocity calculations in water,

because there is no dispersion. The precision of the transducer movements means that the water velocity measurements have very small errors (< 5 ms^{-1}).

The velocity that is derived for the measurements in sand depends on which arrival is used for the calculations. If the first detected arrival is used, the velocity calculated is the signal or energy velocity. If the arrival time of the amplitude extremum is used (which is usually the second peak for these experiments), the velocity derived is the group velocity. For most of the measurements in sand presented here, the second maximum peak is usually picked, rather than the onset of the first arrival. This is because the true first arrival is imperceptible with many of the samples due to the high rate of attenuation. Therefore, the first detected arrival on different samples will often represent a different position on the transmitted waveform. The signal and group velocities are often significantly different. Unless specified otherwise, the group velocity is implied for all of the measurements in this chapter.

5.4.4 Calibration

The data recorded by the physical modelling system is automatically scaled by a factor of 1:10 000 before it is analysed on the workstation. Therefore, the vertical time scale in all of the shot records shown is scaled one-way time in milliseconds. Two corrections are made to the picked arrival time before it is used to calculate the velocity (Figure 5.7). Firstly, there is a delay that results from the fact that the true location of the source is behind the face of the transducer, such that the first arrival time at zero distance is several μs. Secondly, allowance must be made for the particular arrival that is picked on the transmitted signal. Because a stronger, later arrival that is easily identified on all samples is usually picked, rather than the first arrival, the travel time for this later event at zero distance is estimated and subtracted from the measured travel time. This means that the choice of arrival for picking will affect the calculated velocity when dispersion is very high because there are relative shifts in travel times between the first and later arrivals.

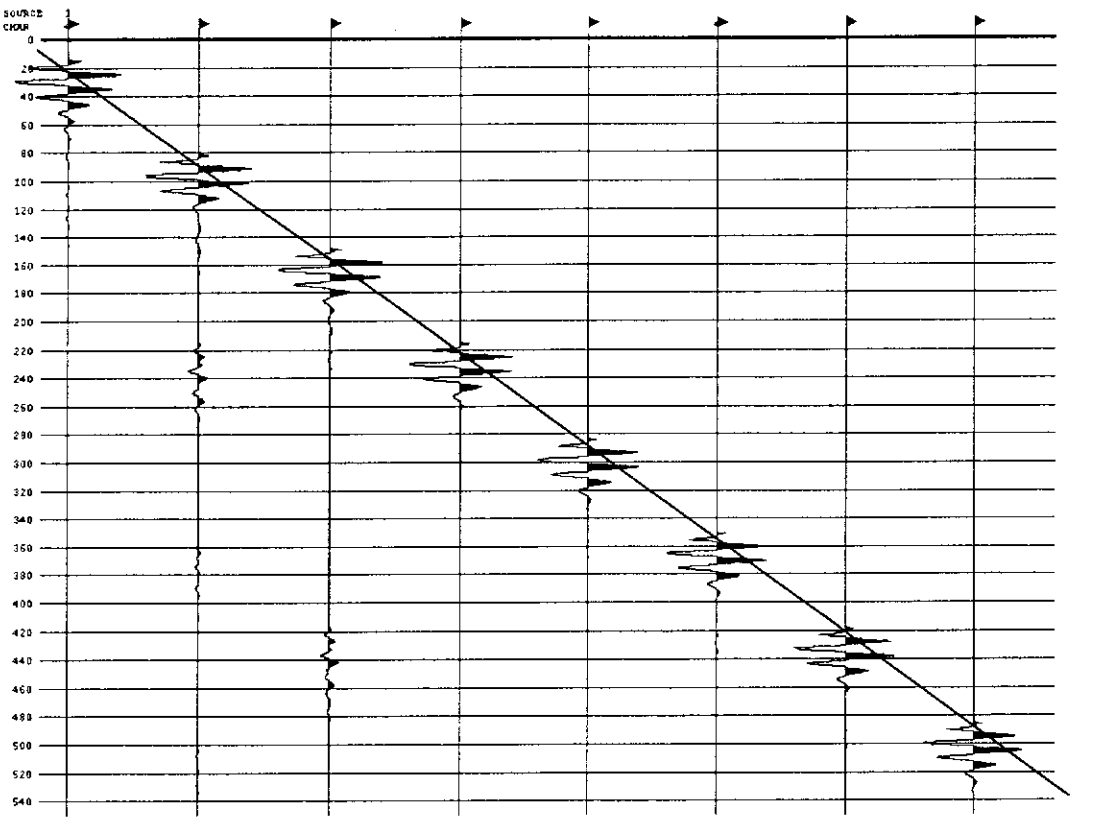

Figure 5.7: Ultrasonic signal recorded as the distance between the source and receiver transducers is increased in 10 mm increments. The vertical axis is scaled one-way time in milliseconds. The slope of the line is used to calculate the velocity of the water. The zero-distance intercept, which is drawn through the onset of the second peak in this example, is used to calibrate the arrival times measured in the sand samples.

5.4.5 Shear-wave measurements

Shear waves are very difficult to measure with piezoelectric transducers. This is due to poor coupling of the acoustic energy between the stiff transducer and the soft sediment (Shirley, 1978), plus the high rate of attenuation. Shear wave transducers also generate and receive a small component of P-waves, with better coupling to the sand. An attempt was made to record shear waves in some of the sands used in this thesis. It was found, however, that the P-wave arrivals dominated the recorded data and identifying the S-wave arrivals, if present, was too difficult. Unfortunately, without S-wave velocities the bulk and shear moduli cannot be determined accurately.

Piezoelectric bender elements are better suited to generating and measuring S-waves in unconsolidated sand. Shirley and Hampton (1978) measured S-wave velocities of 95 ms^{-1} in a water saturated beach sand, and around 200 ms^{-1} in a coarse sand. They estimated rates of attenuation around 30-40 dBm^{-1}. Hamilton (1971) published a collection of S-wave velocities from the literature that were recorded in unconsolidated sands with a variety of techniques. The values for broadly similar sands ranged from 50 ms^{-1} to almost 300 ms^{-1}.

5.5 Attenuation

Attenuation measurements were not given a high priority for the research reported here, for a number of reasons. The effects seen at high frequency in the laboratory are not applicable to low frequency and, therefore, the results cannot be used to conclude much about field attenuation mechanisms (Gist, 1994). It must be remembered that at ultrasonic frequencies we are observing a combination of intrinsic attenuation and scattering losses. There are also other extraneous losses involved with ultrasonic measurements of attenuation such as coupling losses and wedging effects (Toksoz and Johnston, 1981). Wedging effects can occur if the ends of the sample are not exactly parallel and losses due to phase variations over the surface of the transducer may result.

In addition, different methods of calculating attenuation can give results that vary by a factor of three or four (Chotiros, 1995). Nevertheless, estimates of attenuation were made for some of the sands used and are presented here.

One of the most straightforward methods of determining attenuation in the laboratory is to compare the recorded amplitudes at different transducer source/receiver intervals. A plot of amplitudes versus separation, with corrections for spreading loss, will yield the attenuation coefficient (α). Shirley and Hampton (1978) found this method to be flawed when working with unconsolidated sands because movement of the transducers disturbed the sediment enough to cause erroneous readings. They suggested that the sediment frame was fractured by the transducer motion, thus lowering the shear modulus of the material. Bell and Shirley (1980) used values obtained in water (where attenuation is negligible) to represent the geometric divergence of the energy from the source. The attenuation (α) in dBm^{-1} was then calculated using amplitudes recorded by two transducers at different separations with the following formula:

$$\alpha = \frac{1}{x_2 - x_1} * 20 \log\left[\frac{A(x_1)}{A(x_2)}\right], \tag{5.2}$$

where x_1 and x_2 are two different transducer distances ($x_2 > x_1$) with respective amplitudes $A(x_1)$ and $A(x_2)$.

Values obtained by Bell and Shirley (1980) for unconsolidated water-saturated sand at 700 kHz were 218 dB. Values obtained for saturated clay at 120 kHz were between 1 and 10 dBm^{-1}, much less than the estimated measurement error of 25 dBm^{-1}. An alternative method is to use one fixed receiver and to estimate the attenuation by comparing amplitudes against a standardised calibration media of known attenuation. This can introduce significant measurement errors from the unknown accuracy of transducer separation.

5.5.1 Method

The configuration used here to measure amplitudes cannot be used to measure values at different distances within a single sample. To estimate attenuation it was necessary to make up different length samples of the same sand. This introduced significant uncertainty as a result of random variation between samples. It was also difficult to measure the same event in several different length samples due to the high rate of energy absorption. This resulted in most estimates being based on just two end points, measured from 50 mm and 75 mm length samples.

A plot of amplitudes recorded in water versus transducer separation was used to calculate the correction needed to account for spreading losses from the ultrasonic source (which does not spread spherically like the energy from a point source does). This was then applied to the measured amplitudes in sand to estimate the relative change in amplitude with distance. As discussed in Chapter Three, the ultrasonic transducers emit a long mixed-phase signal that has several strong cycles of peaks and troughs. The relative amplitudes of each peak and trough were found to decay linearly with increasing transducer separation in water. However, an inspection of the changes in the waveform that occur when the signal is transmitted through sand showed that the relative change in amplitude varies considerably, depending on the event measured. This phenomenon combined with the natural variation between the two different length samples, meant that the values of attenuation calculated here were at best an indication of the true rate of attenuation. It was not considered realistic to attempt to measure amplitudes at different distances for every variation of sand tested, although amplitudes measured from the 50 mm samples could be compared to the standard sand to indicate relative attenuation.

Values for the quality factor Q were derived from the attenuation coefficient using equation 4.16. Estimates of α and Q for seven sands measured (including two samples of the standard sand) are given in Table 5.1, along with the measured velocities and porosities. Although the velocity and porosity of all of the sands, as shown in Table 5.1, are similar, there is a large range in values for α and Q. Measured values of Q in

Description of sand	Grain size (μm)	Velocity (ms^{-1})	Porosity (%)	α (dBm^{-1})	Q
Standard sand #1 Moderately sorted	100 – 350	1751	37.2	299	54
Standard sand #2 Moderately sorted	100 – 300	1727	38.0	347	46
Fine grained Well sorted	125 – 180	1692	41.8	169	95
Fine to medium grained Well sorted	180 – 212	1692	40.0	273	59
Medium grained Well sorted	212 – 250	1689	40.1	137	117
Medium grained Moderately sorted	100 – 400	1721	38.4	236	68
Fine & medium grained Bi-modal mixture	50 – 300	1701	38.7	512	31

Table 5.1: Measured physical properties of seven different sands.

the literature for saturated unconsolidated sand range from 2 to greater than 100 (Carmichael, 1989). The range in Q values derived for the seven sands shown in Table 5.1 is from 31 to 117, which is possibly more an indication of the difficulties in accurately determining Q than true differences between the sands.

5.6 Experiments – improving saturation

Several measures were implemented in an attempt to overcome problems with saturating the samples. Some of the effects of these steps are discussed here.

5.6.1 Saturation changes with time

When a sand sample is initially saturated with water, a small amount of air is trapped within the smaller pores. Velocities measured at this stage are not the true velocities of the saturated sand and the rate of attenuation is much higher than in the case of full saturation. If the sample is left in a tank of water for a number of days, the sound velocity of the sand increases by up to 100 ms^{-1}. Once this was discovered, samples were routinely left standing in water for a period of one week before measurements were taken. Some clear examples of this change over time are illustrated in the following sections. The problem arises from the imperfect method of saturating the sands. All porous media have a percentage of irreducible air saturation when saturated under Darcian flow conditions. As the air is expelled from the sand, it becomes disconnected and immobile when its content becomes less than some limiting value (Bacharach and Nur, 1998a).

The exact cause of the change in seismic response over time is not known. It could be a result of the air having enough time to slowly migrate upwards and outwards from the sand. It is possible that the air is absorbed into solution, although comparisons between distilled and non-distilled water did not reveal any measurable difference in behaviour. Another explanation is that initially the air may be present as many small bubbles in the

smallest pores of the sand, which over time coalesce into larger bubbles. In this case, the style of saturation would change from homogeneous to patchy, which would increase the seismic velocity even though the overall saturation level may not change.

The amount of time required for the samples to approach an asymptotic velocity varied between samples. Well-sorted sands with high porosities and permeabilites generally approach a maximum velocity after two or three days. Samples with lower permeability such as those containing clay were found to be still changing after sitting in water for one week.

5.6.2 Vibration while saturated

One trend that was expected and was clearly evident from the velocity tests was that applying vibration to the saturated sands increased the velocities. A typical sample would undergo a velocity increase of around 100 ms^{-1} if subjected to a few minutes of gentle vibration on a vibrating table. There are two reasons for this, firstly the agitation allows some of the tiny air bubbles to migrate their way up through the sand and escape, and secondly the grains are able to achieve tighter packing, which results in compaction and increases the rigidity of the frame.

Air can be observed breaking through the sand surface of fresh samples when vibration is applied, but this is not observed on samples that have been sitting in water for a number of days. This suggests that vibrating the samples is one way of reducing the amount of time that is necessary for the sand to reach full saturation and, subsequently, for the velocity to reach its maximum. However, consideration must be given to the effects that vibration has on the grain packing. Because of the bouyancy of the sand grains in water, applying vibration to saturated sand may not achieve packing densities as high as applying vibration before saturation.

5.6.3 Vacuum

A vacuum chamber is frequently mentioned in the literature as a means to extract all of the air from samples before measurements are taken. This is apparently effective when the sample is saturated while in the vacuum chamber. However, facilities to do this for this research were not available. Some tests were conducted to see if placing samples in a vacuum after saturation would reduce the amount of time necessary to record stable results. For the samples that were difficult to saturate, small air bubbles could be seen trapped against the container walls. It was found that the vacuum caused these small bubbles to coalesce into large pockets of air within the sand, which rendered the sample useless for acoustic measurements (Figure 5.8).

5.6.4 Saturating water temperature

It was found that much more efficient saturation could be achieved by saturating the sands with hot water and then allowing them to cool down to room temperature before the measurements were taken. Figure 5.9 shows how the velocity of the sand increases with the temperature of the water used to saturate the samples. A clear increase in velocity is evident at water temperatures above 50°C. The cause of the velocity increase is the improvement in saturation. The hot water has lower surface tension (zero at boiling point) which improves the wettability of the sand (ie. it lowers the irreducible air saturation). The higher temperature would possibly also expand any air that is left in the model so that it would be expelled from the sand more efficiently. Any air bubbles remaining after saturation would then shrink as the sand cools and possibly be absorbed into solution. Figure 5.9 also shows that after one week in water, the sound velocity in all samples increased to approximately the same value. The use of hot water effectively reduces the amount of time required for the velocity of the sand to stabilize, but does not change the ultimate velocity in the sand.

The use of hot water is more effective in the small samples used to record velocities than it is in larger models. In larger models, the water is cooled down by the sand

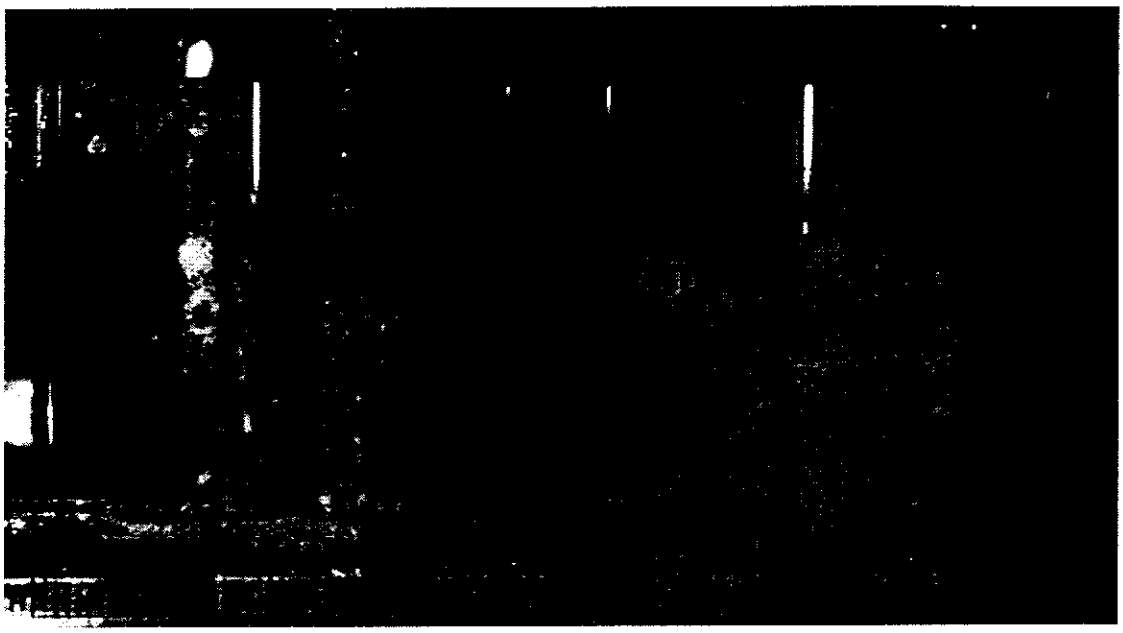

Figure 5.8: Photograph of two containers of saturated sand after 10 minutes in a vacuum chamber. Small air bubbles that were originally lining the inside walls have coalesced into one large air pocket that displaces the sand out of the container.

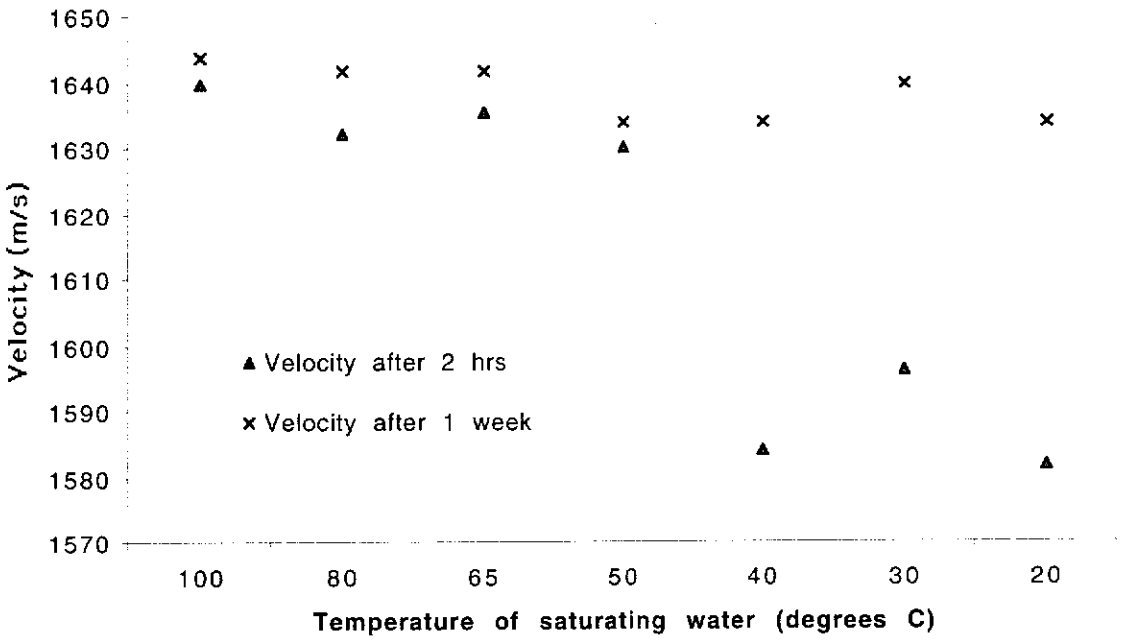

Figure 5.9: The sound velocity in sand at room temperature, relative to the temperature of the water used to saturate the sand. The sands saturated in cool water have low velocities initially, but after one week in water all sands reach a similar velocity.

grains, which are at room temperature, as it migrates through the models. Nevertheless, this method was found to be an effective way to reduce the turn around time of the experiments and was adopted as standard procedure.

5.6.5 Deposition under water

The possibility of building the models underwater was investigated to see if that approach would overcome the problems of fully saturating the sand. Figure 5.10 shows a series of six seismic shot gathers recorded using the same sample, prepared under water, over a period of one week. The first shot record was recorded immediately after the sand was deposited into the container full of water. At this stage the sand is very close to suspension and the porosity is around 43%. The results are very poor and estimating the velocity is impossible. The sand was then subjected to gentle vibrations for a few minutes to compact the sand. The second shot record shows that this enabled a signal to be detected and the velocity at this point was somewhere around 1300 ms^{-1}, which is 200 ms^{-1} slower than water. The vibration caused the surface of the sand to subside by about two millimeters and the porosity was subsequently reduced to around 41%. Extra sand was then added to bring the sand back to its original height of 50 mm, which resulted in the deteriorated signal shown in the third shot gather. The sample was then subjected to further vibration and left to stand for around six hours before the fourth shot gather was recorded. The velocity at this stage had risen to around 1470 ms^{-1}, still 30 ms^{-1} slower that the velocity of water. The fifth and sixth shot gathers show that the velocity stabilized at 1530 ms^{-1} after two days, faster than the velocity in water but 170 ms^{-1} slower than similar sands deposited while dry and then saturated. The amplitudes are slightly higher in the sixth shot gather, which was recorded after one week, although they remained very low relative to the amplitudes recorded in the sands that were deposited dry. The noise visible on the traces in Figure 5.10 is a result of the high scaling of the amplitudes that was necessary to see the transmitted signal.

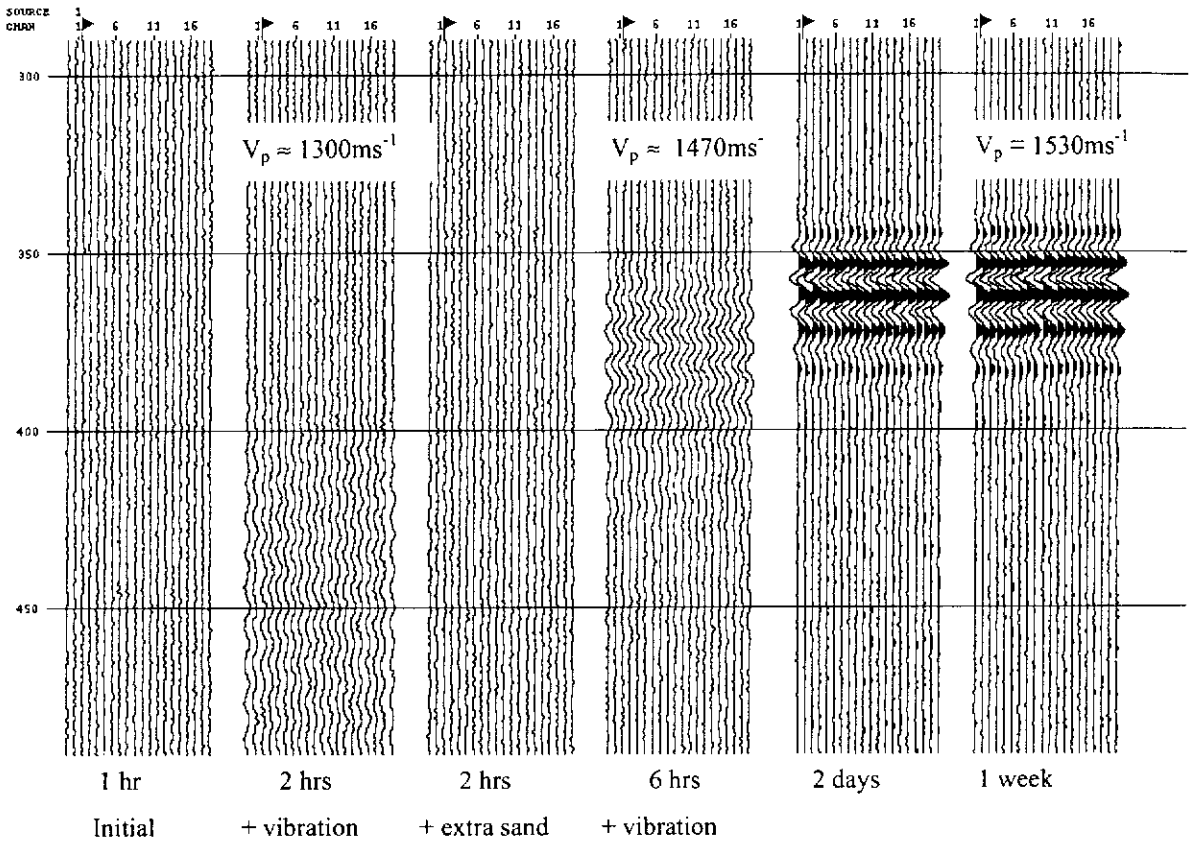

Figure 5.10: Six shot gathers that illustrate how the velocity and attenuation of sound through sand deposited underwater changes with time. The vertical axis is scaled one-way time in milliseconds. Initially no signal can be detected. Applying vibration and leaving the sand to stand in water improves the transmission until the velocity stabilizes after two days at 1530 ms^{-1}. The velocity and amplitude after 1 week are still much lower than those in sands that are deposited while dry and then saturated.

5.7 Experiments – changing parameters

5.7.1 Vibration while dry

Applying vibrations to the dry samples proved to be the single biggest factor affecting the acoustic properties. Vibration allows the grains to settle into a tighter packing configuration, which reduces the porosity and stiffens the sand matrix. This in turn increases the elastic moduli and subsequently the velocities in the sand. The magnitude of this velocity increase depends on several factors such as the initial grain sorting, the method of preparing the sample, and the magnitude and duration of the applied vibrations. This relationship was too complex to be quantified. The average increase in velocity that can be expected to result from applying vibration is around 50 ms^{-1} for clean sands and up to 100 ms^{-1} for sands with small clay fractions.

Recent studies of spheres settling under vibrations indicate that the approach to the steady-state porosity is logarithmic in time (Jaeger *et al.*, 1996). However, the trend for these experiments appeared to be that the porosity approached a minimum very quickly, while the velocity continued to increase slightly with further vibration. The role of grain shape in this process is critical and needs to be better understood.

The trend observed with the clean sands in general was that one or two sharp taps on the sample container by hand would achieve almost the same result as placing the samples on a vibrating table. Cobbold and Castro (1999) also found this to be true with their experiments on effective stress in well-sorted sands. This was routinely done for the majority of variations tested here as it produced more realistic and consistent results. If no vibration of any kind was applied, saturating the samples caused the surface to subside as the sand compacted. This then required more sand to be added to bring the height of the sample back to 50 mm. The only other alternative was to estimate how much the sample height had been reduced and then attempt to allow for it in the measurements, thus introducing large errors. The amount of subsidence that occurred

from vibration of the well-sorted sands was around 1mm in the 50 mm containers (ie. 2%) but was as high as 7 mm with samples that contained a significant amount of clay. It was found that if the containers were filled to overflowing and then tapped by hand before the sample height was levelled at 50 mm, then the sand would not subside appreciably when saturated, so that and extra sand was not required.

When models comprise two or more layers of sand with contrasting textures, applying vibration tends to smear the boundaries between them and so this is not an appropriate measure for many of the models in this thesis. If the duration or magnitude of the applied vibration is too high, grains of different sizes will separate into different regions of the container. This may at first appear to violate the principle that entropy must increase, which normally favours mixing, but in this case it is outweighed by dynamic effects (Jaeger *et al.*, 1996). Both segregation and convection will occur if the acceleration of the container is greater than the gravitational acceleration. In this case, the sand dilates and a convection roll continuously transports grains. In cylindrical or rectangular vessels, the flow is usually upward in the centre and downward in a thin stream down the sidewalls. It is thought that friction with the walls of the container contributes to this effect, and is a different situation from convection in fluids.

The mechanisms that cause segregation when sand is vibrated are still not completely understood, although experiments have shown a direct link with convection (Ehrichs *et al.*, 1995). Large particles become entrained in the upward convective flow but are unable to follow the smaller grains in the downward flow. This phenomenon was exploited when building models for this research, to create sand layers with transitional changes in grain size.

5.7.2 Deposition method

Cobbold and Castro (1999) found that poured sand has higher porosity than sieved or sprinkled sand. When sand is poured it does not achieve an efficient packing geometry. Acoustic measurements of these sands are subject to uncontrolled fluctuations and great

care is required to achieve repeatable results. As with all factors related to the preparation and handling of the samples, this affects the well-sorted sands less than the poorly sorted sands and much less than sands containing clay. Figure 5.11 shows a comparison of the velocities and relative amplitudes recorded from 12 samples of the standard sand, which were deposited in three different ways. The sand in the first four samples was poured into the containers, tapped lightly by hand and saturated. The sand for the second group of four samples was gently sprinkled on as one continuous motion from a large scoop of the same sand. The second group of sands has lower porosity, and higher velocity and peak amplitude than the sands that were poured into the containers. Applying vibration to the poured samples before saturation would bring the velocity in these sands up to that of the samples that were sprinkled.

The sand in the third group of four samples was also sprinkled into the containers, but in this case each container was filled from several small scoops to create subtle layers. This resulted in similar porosities and amplitudes as the second group but the sound velocity was slightly higher. The reason for this is the heterogeneous nature of the grain packing, which will be discussed in Section 5.8.

These results are from one of only two series of experiments that exhibited a trend of velocity dependence on porosity (Figure 5.12). They were the only results where a correlation was observed between porosity and group velocity.

5.7.3 Grain size

As previously mentioned, the results from the well-sorted sands are the most robust of all the sand variations tested. These sands are much less susceptible to random variations in packing and problems with achieving full saturation. This allows clear trends in behaviour to be established.

Figure 5.13 shows the transmission shot records from five different well-sorted sands with different grain sizes. These results clearly show a trend of changing velocity,

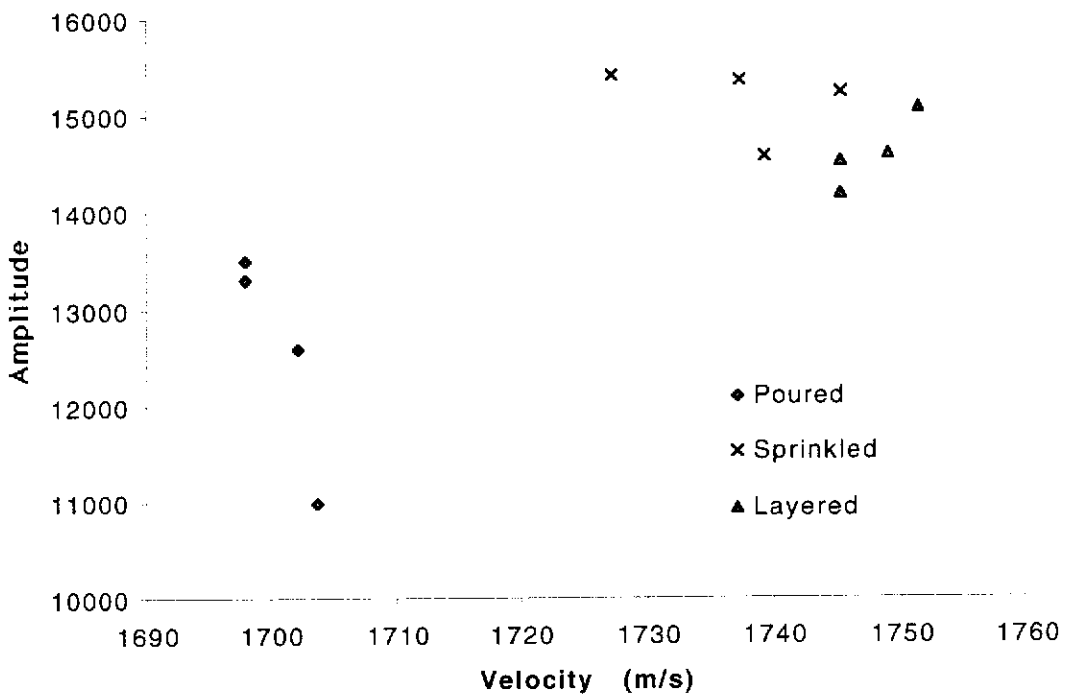

Figure 5.11: The variation in sound velocity and peak amplitudes in the standard sand depending on the technique of deposition. Poured sand has lower velocity and higher attenuation than the sprinkled sands due to less efficient grain packing.

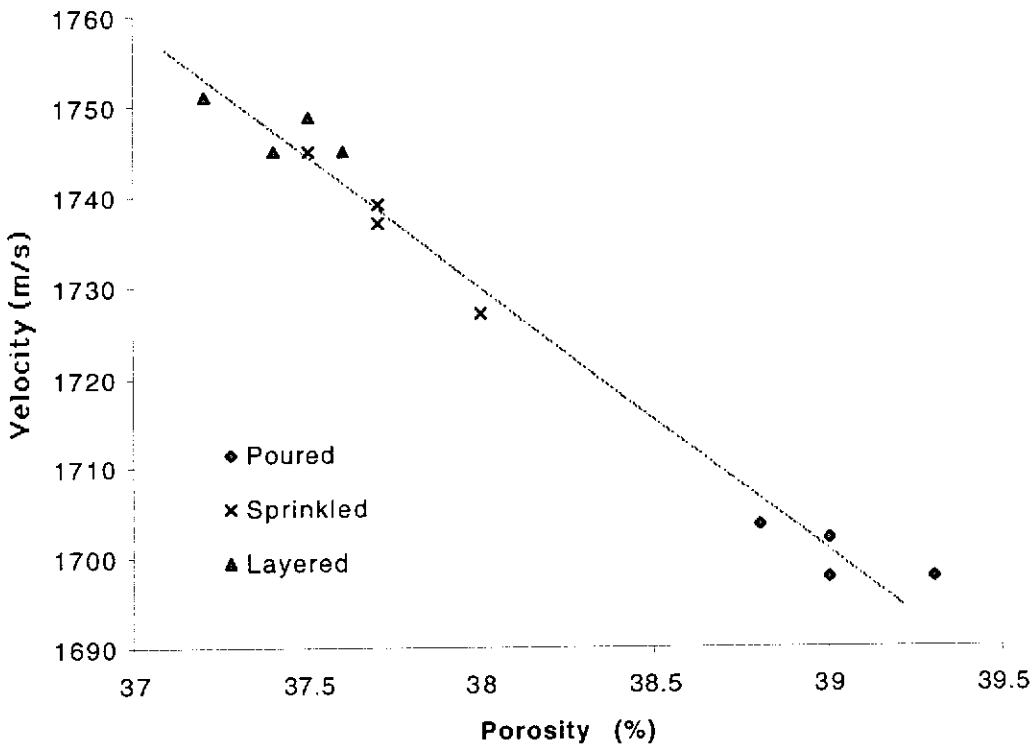

Figure 5.12: The velocity/porosity relationship for the standard sand. The porosity variation is purely a result of the grain packing, which is determined by the method of deposition.

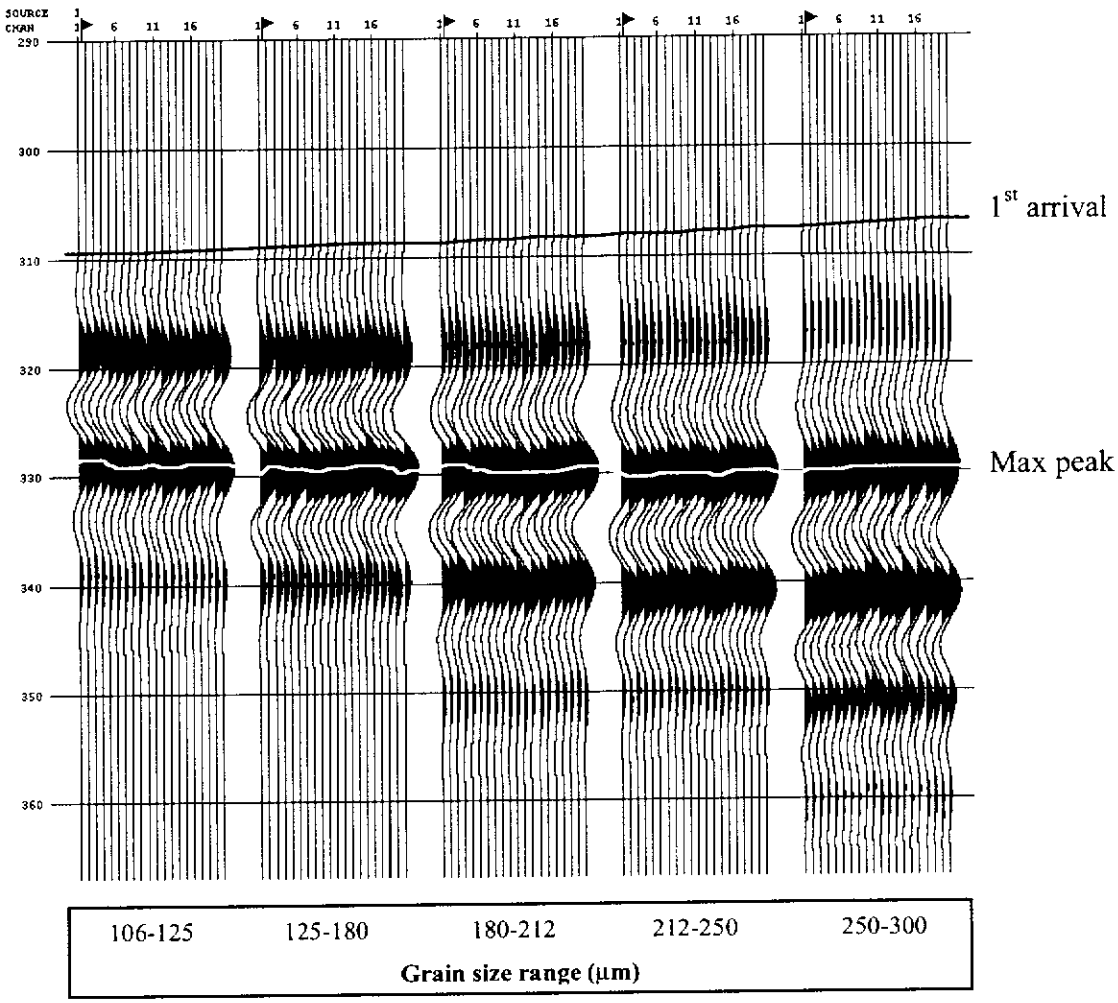

Figure 5.13: Shot records from five well sorted sands of different grain sizes. The vertical axis is scaled (1:10 000) one-way travel time in milliseconds. The travel times for the onset of the first arrivals is used to calculate the signal velocity, which increases with grain size. The travel times for the maximum amplitude peak is used to calculate the group velocity, which is constant regardless of grain size.

attenuation and dispersion with grain size. Two sets of samples were prepared for five different grain size ranges between 106 μm and 300 μm. The first set was prepared in the standard way where the sand was poured into the containers and tapped by hand to settle the sand into a stable packing arrangement. The second set of samples was subjected to one minute of gentle vibrations, which compacted the sand and reduced the porosity by an average of 2%. The figures shown below (Figures 5.14 to 5.18) include both the compacted and uncompacted results.

As previously mentioned, the measured velocities depend on which arrival is used for the calculations. If the first detected arrival is used, the velocity measured is the signal or energy velocity. If the arrival time of the amplitude extremum is used (in this case the second peak) the velocity derived is the group velocity. Unless specified otherwise, the group velocity is implied for all of the results shown in this thesis, because it is the only one that can be picked unambiguously from samples with different rates of attenuation. However, the smooth trend in the shot records from the well-sorted sands allows both the group and energy velocity to be measured accurately.

Figure 5.14 is a graph comparing the energy and group velocities from the well-sorted sands as a function of grain size, for both the vibrated and non-vibrated case. The energy velocity increases by around 20 ms^{-1} as the grain size is increased from between 106 μm and 125 μm to between 250 μm and 300 μm. However, the group velocity is constant for all of the grain sizes. Both group and energy velocities in the compacted sands are around 50 ms^{-1} faster than the respective velocity in the corresponding uncompacted sand.

It appears that the dominant dispersion mechanism is scattering, which causes negative dispersion (Winkler, 1986). That is, lower frequencies are faster than higher frequencies. A graph of the instantaneous frequencies of both the first arrival trough and the maximum amplitude peak relative to grain size is shown in Figure 5.15 and supports this observation. The first arrivals detected (which in this case are troughs) have lower instantaneous frequencies than the corresponding peaks arriving one and a half periods later, which suggests that the lower frequencies are arriving before the

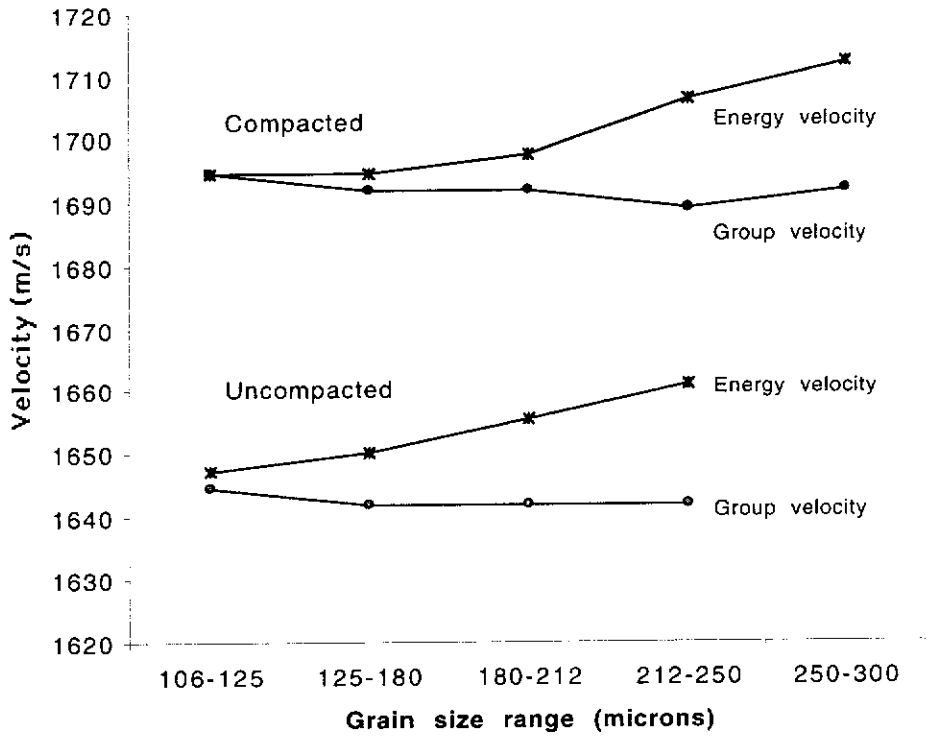

Figure 5.14: Comparison between energy and group velocities for different grain sizes of well sorted sand. The energy velocity is calculated from the first arrivals, while the group velocities are calculated from the arrival time of the maximum peak. The same trend is evident regardless of whether the sands were compacted with applied vibration or not.

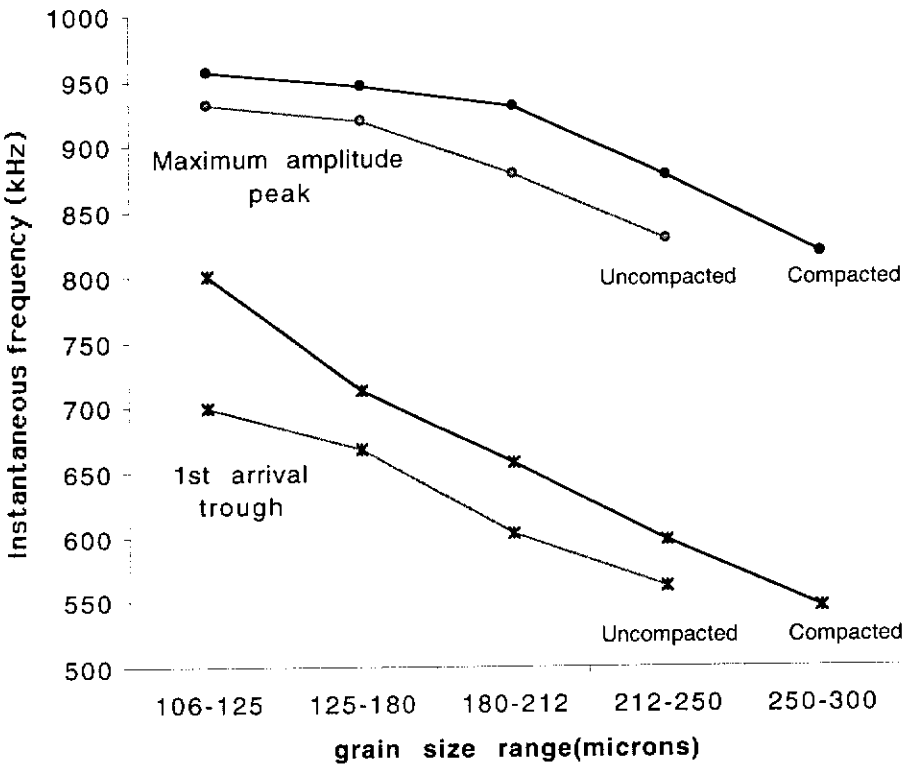

Figure 5.15: Instantaneous frequency of different arrivals relative to grain size in well sorted sand. The lower frequency of the first arrival indicates negative dispersion, which is probably a result of scattering. The same trend is evident for both the compacted and non-compacted cases.

higher frequencies. The trend for all arrivals is one of decreasing frequency with increasing grain size, supporting the conclusion that Rayleigh scattering is the main dispersion mechanism.

The Biot model of the fluid loss mechanism predicts that positive dispersion will occur at high frequencies and that the frequency where dispersion is greatest is dependent on the pore size. Therefore, smaller grains should shift the Biot mechanism to a higher frequency, which means that the dispersion observed at a fixed frequency should decrease with grain size. However, this probably plays only a minor role relative to frame losses and scattering.

Figure 5.14 showed that all velocities measured for the vibrated sands are higher than in the non-vibrated case. The applied vibration also reduces the porosity of all of the sands. However, contrasting trends emerge when the two velocity types are plotted against the measured porosities. The energy velocities, which are calculated from first arrivals, show a trend of increasing velocity with decreasing porosity (Figure 5.16a). These results and those for the different methods of deposition are the only results where a correlation of velocity with porosity was observed. However, contrasting with this trend are the corresponding group velocity measurements from the same sands (Figure 5.16b). In this case, the velocities appear to depend only on whether vibration was applied or not, regardless of grain size or porosity.

Figure 5.17 shows the relative change in the first trough, maximum (2^{nd}) peak and RMS amplitudes with increasing grain size for both the vibrated case (Figure 5.17a) and non-vibrated case (Figure 5.17b). The amplitudes in each case have been normalised about the smallest grain size sample to allow a visual comparison between relative changes with grain size. For the vibrated case, the first trough amplitudes decrease with increasing grain size, which is consistent with attenuation and dispersion from scattering losses increasing with grain size. However, the maximum peak and RMS amplitudes appear to increase with grain size at first, and then the peak amplitudes decrease for grain sizes larger than 200 μm, while the RMS amplitudes remain fairly

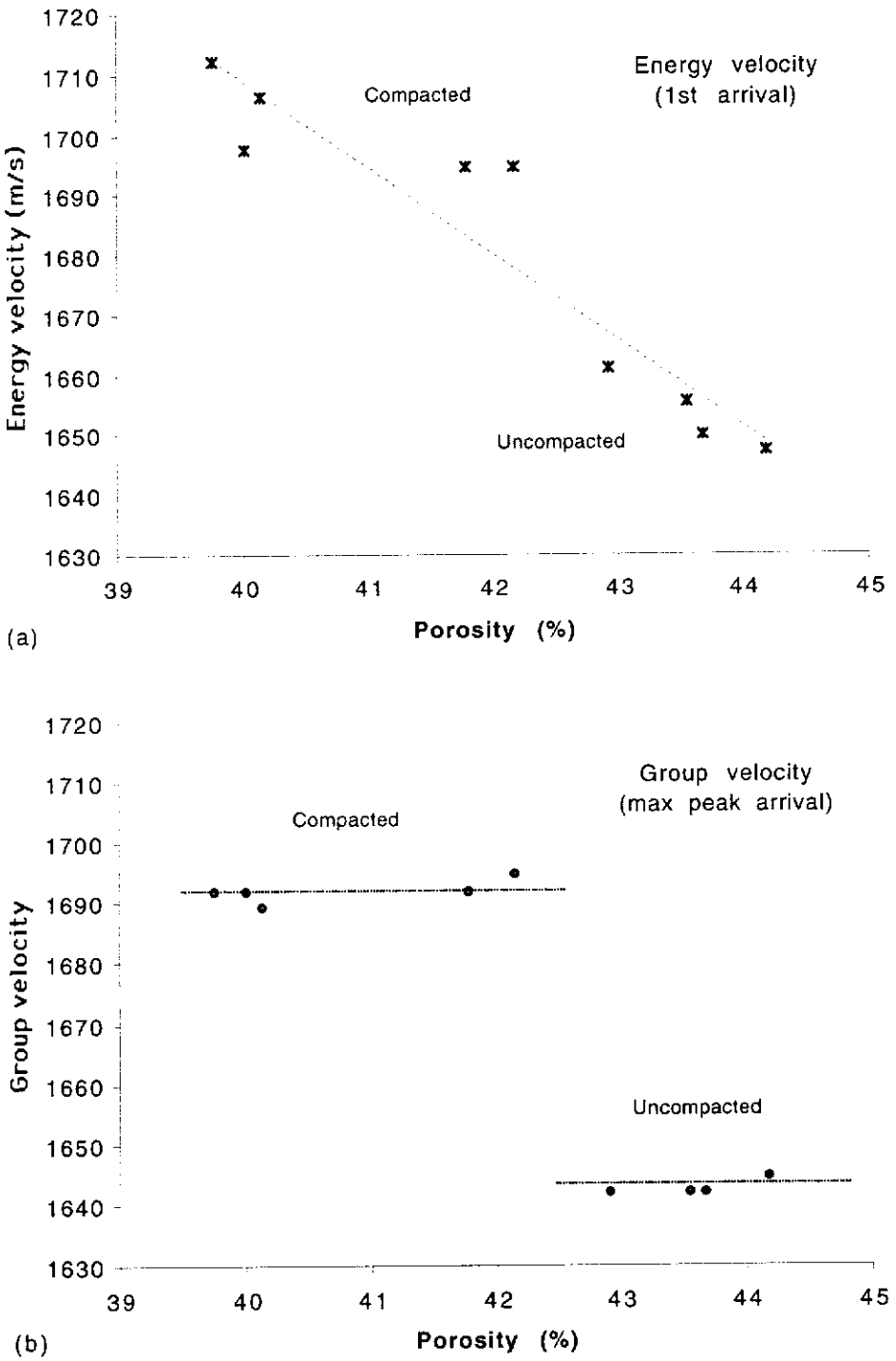

Figure 5.16: The relationship of (a) energy, and (b) group velocity to porosity for well sorted sands. For each cluster of measurements, the porosity decreases with grain size. The energy velocity appears to be influenced by the porosity and amount of compaction. The group velocity is increased by compaction, but appears insensitive to porosity.

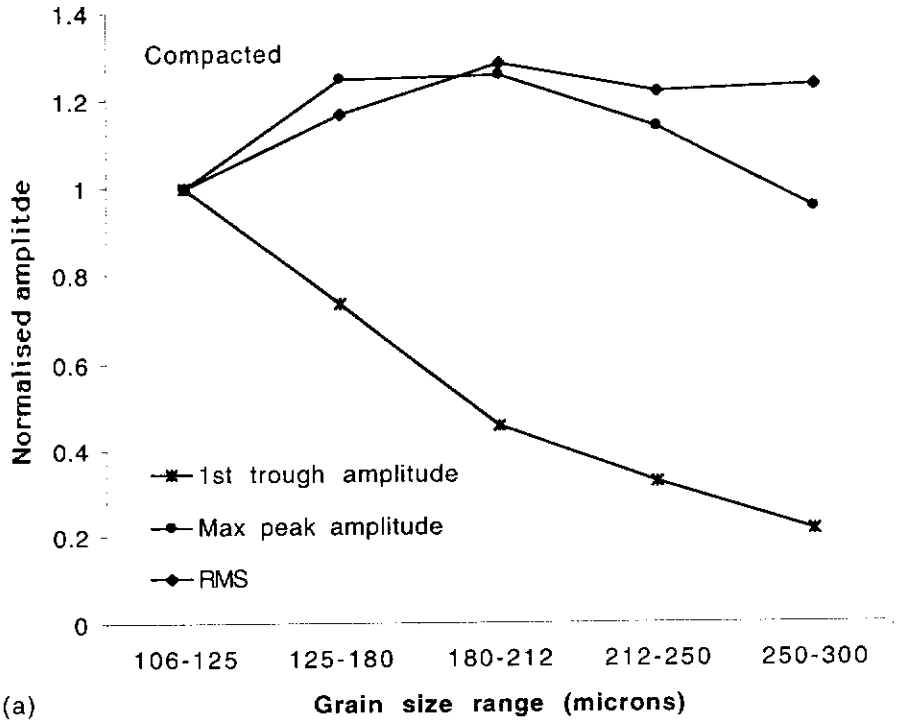

(a)

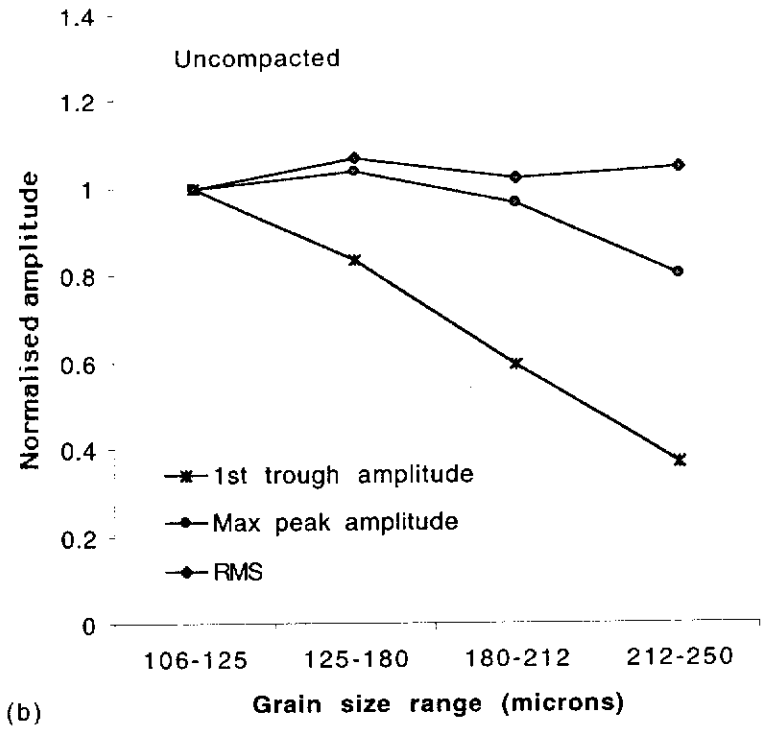

(b)

Figure 5.17: Normalised amplitudes as a function of grain size for (a) compacted, and (b) uncompacted well sorted sands. The amplitude of the first arrival trough decreases with increasing grain size, but the maximum amplitude peak and RMS amplitudes are less affected.

consistent. Similar results are observed in the non-vibrated sands, although there is less variation in all amplitude measurements with increasing grain size.

The amplitudes of the first arrival troughs are always higher in the vibrated case than in the non-vibrated case. However, it is interesting to note that both the RMS amplitudes and the maximum peak amplitudes for the smaller grained non-vibrated sands are in fact slightly higher than those for the corresponding vibrated sands. This is shown in Figure 5.18, where the amplitude values are plotted in their original (ie. non-normalised) form.

5.7.4 Temperature

Published data on the temperature dependence of sound velocity in sand by Bell and Shirley (1980) showed that the velocity increase in unconsolidated sand with increasing temperature roughly follows that of water (Figure 5.19). The relevance of these results to this research is in terms of the time-lapse experiments in Chapter Six. The temperature of the water in the tank used for these experiments was found to oscillate by up to 2°C daily depending on outside temperatures. As it was not possible to control the variations in water temperature, a method of allowing for any velocity changes in the sands was sought. This could then potentially be applied to the time-lapse data to allow better matching of data sets recorded at different temperatures.

A trend line fitted to the data from Bell and Shirley (1980) suggested that the velocity of sand increased as a constant ratio of the velocity in water with increasing temperature. However, as Figure 5.19 shows, the data points were scattered and this trend was not conclusive. It was decided that it would be necessary to establish the trend of the velocity dependence on temperature for the sand used in this research. A series of three experiments were run where the velocity of sound through water and in two different sands were monitored as a function of changing temperature. The two sands tested were the standard moderately-sorted sand and a well-sorted sand with grain sizes between 212 and 250 μm. A temperature probe (accurate to within 0.3°C) was used to

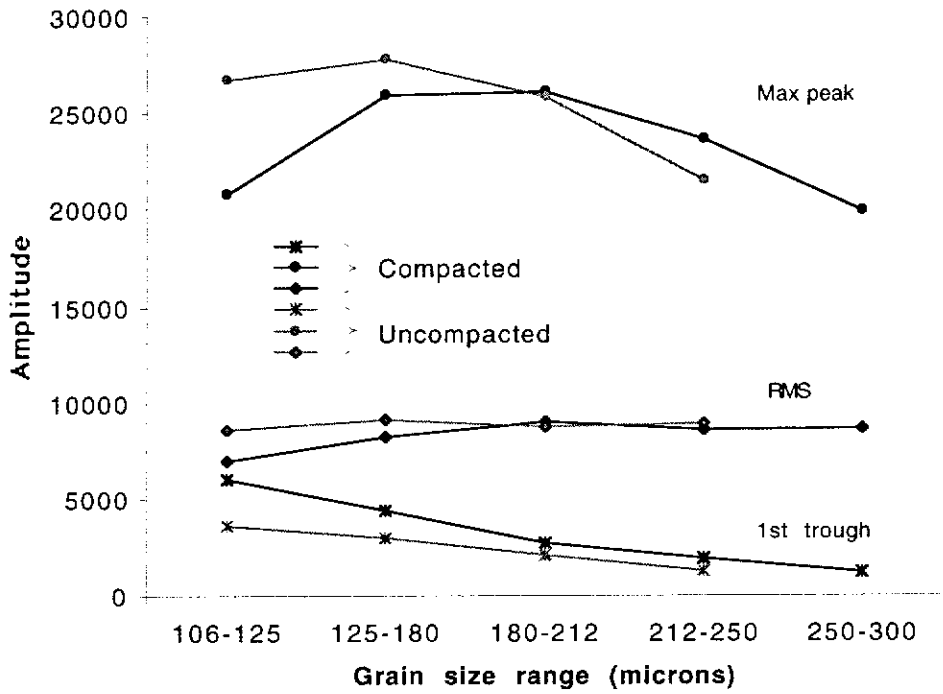

Figure 5.18: Relative amplitudes for compacted and uncompacted well sorted sands. The amplitude of the first arrival (trough) is higher for the compacted sands than for the uncompacted sands. However, the maximum peak and RMS amplitudes for the smaller grain sizes are higher for the uncompacted case.

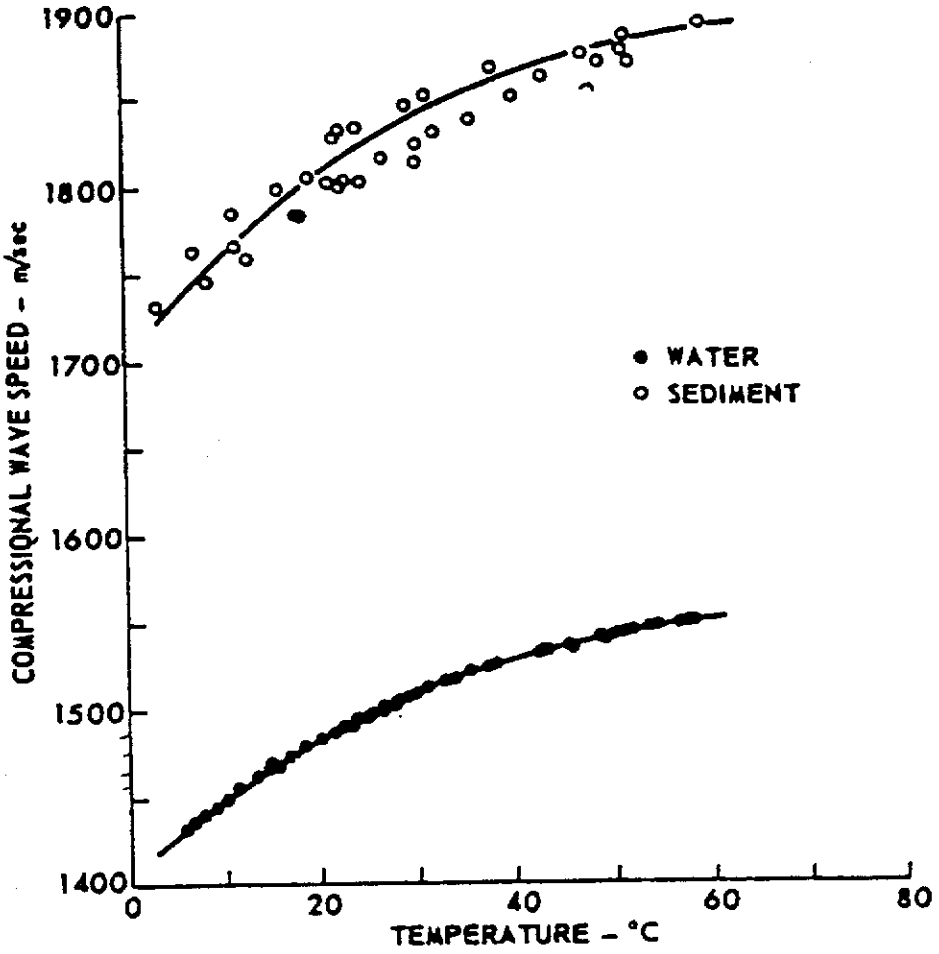

Figure 5.19: P-wave sound velocity through water and unconsolidated sand as a function of temperature at 700 kHz (after Bell and Shirley, 1980).

monitor temperature changes with time while the arrival times of a pulse transmitted between two transducers at a set distance were continuously recorded. The velocity changes in the water and in each of the two sands were recorded as separate experiments. For each experiment, the travel times were monitored for around one hour as the water temperature was reduced from room temperature to 4°C, by adding ice to the tank. A heater was then placed in the tank that heated the water to 33°C over the next 12 hours while monitoring continued. The heater was then removed to allow the water to return to room temperature, completing one experiment.

For each experiment, the same sample was used for measurements at all temperatures. This meant there was no random variation in behaviour that plagues most of the other measurements in this research and so the changes in travel time were smooth and consistent. Arrival times were accurately picked to the nearest digital sample in time, which corresponds to increments in velocity around 4 ms^{-1} and is effectively the maximum error. In fact, resampling of the data at smaller time increments would have allowed an even smoother trend in the measured velocities, but this was considered unnecessary.

The observed change in water velocity with temperature was consistent with the equation for sound velocity in water given by Medwin (1975), confirming that the method used to calibrate the velocity measurements is valid. The results from the two sands diverge slightly with increasing temperature (Figure 5.20). The sound velocity of the standard sand appears to follow the trend implied by Bell and Shirley (1980), whereby velocity increases as a ratio of the velocity in water (around 1.16 in this case). However, the velocity increase in the well-sorted sand is not as great and appears to remain constant relative to the water temperature. The trends for both sands are much less ambiguous than the scattered data from Bell and Shirley.

The temperature probe for the water measurements was placed directly alongside the transducers and it is assumed that this records the true temperature of the water. For the sand measurements, the probe was inserted into the sand container such that it recorded the temperature in the middle of the sample. Tests showed that the probe did not

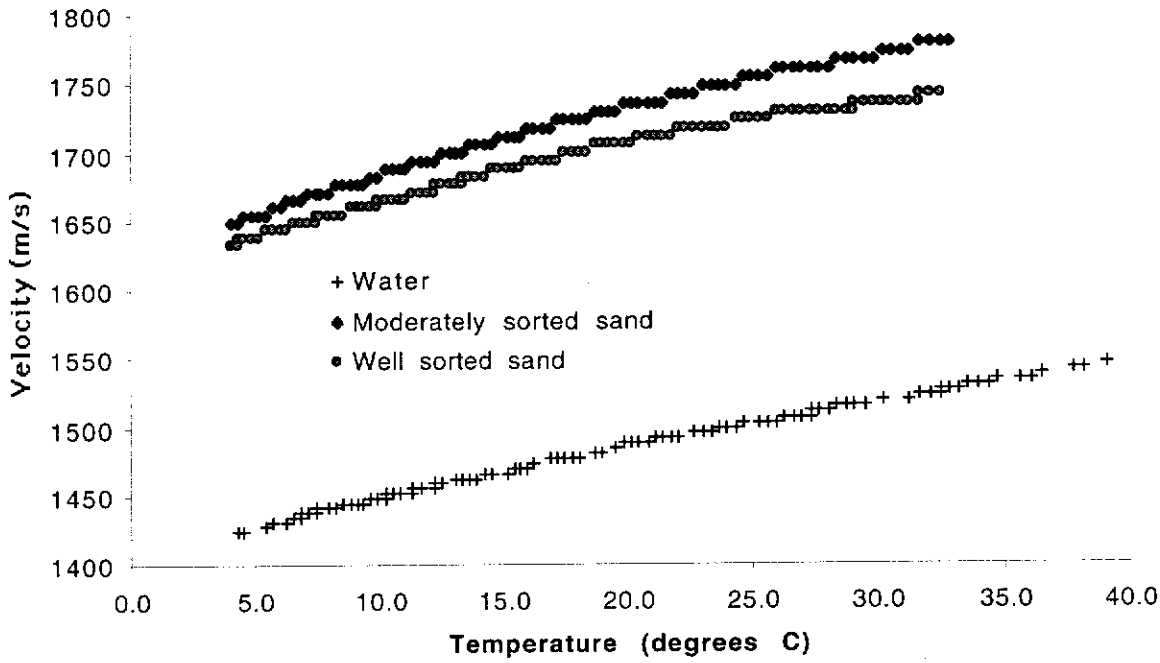

Figure 5.20: The velocity of sound in fresh water and in two sands as a function of temperature.

influence the arrival times. However, different temperatures were observed for the same velocity depending on whether the water was being heated or cooled. This suggested that a temperature gradient existed in the sand such that as the water was heated or cooled, the temperature change in the middle of the sand lagged slightly behind the water temperature. The average sand temperature determines the velocity, but the probe measures the temperature in the middle of the sand.

Comparisons between the velocity curves obtained for both increasing and decreasing sand temperatures showed that the difference between the average sand temperature and the temperature measured by the probe was around 1°C for most of the measurements. However, this was as high as 2.5°C when the temperature change was most rapid (Figure 5.21). This occurred when ice was first added to the water and to a lesser degree when the heater was first turned on in the cold water and off in the hot water. This is illustrated in Figure 5.22, which shows the change in both temperature and velocity with time. The velocities shown in Figure 5.20 are the measurements taken in sand while the water tank was being heated from 4°C to 33°C, which are least affected by this problem except at very low temperatures. No corrections have been made for the lag in the temperatures measured by the probe relative to the average temperature of the sand.

The velocities had returned to their original room temperature velocity when they were measured again one day later. This confirmed that the effect was a result of the temperature gradient in the sand as the water temperature was changed, rather than from hysteresis effects, whereby the properties of the sand are altered.

No change in dispersion was observed with changes in temperature. That is, there was no relative shift in travel time between adjacent peaks and troughs in the transmitted signal. Therefore, the calculated velocities were not dependent on the particular event that was picked for the travel time measurements. However, an increase in peak amplitudes with temperature of around 20% was observed in both sands between 4°C and 33°C, suggesting that attenuation decreases with increasing temperature.

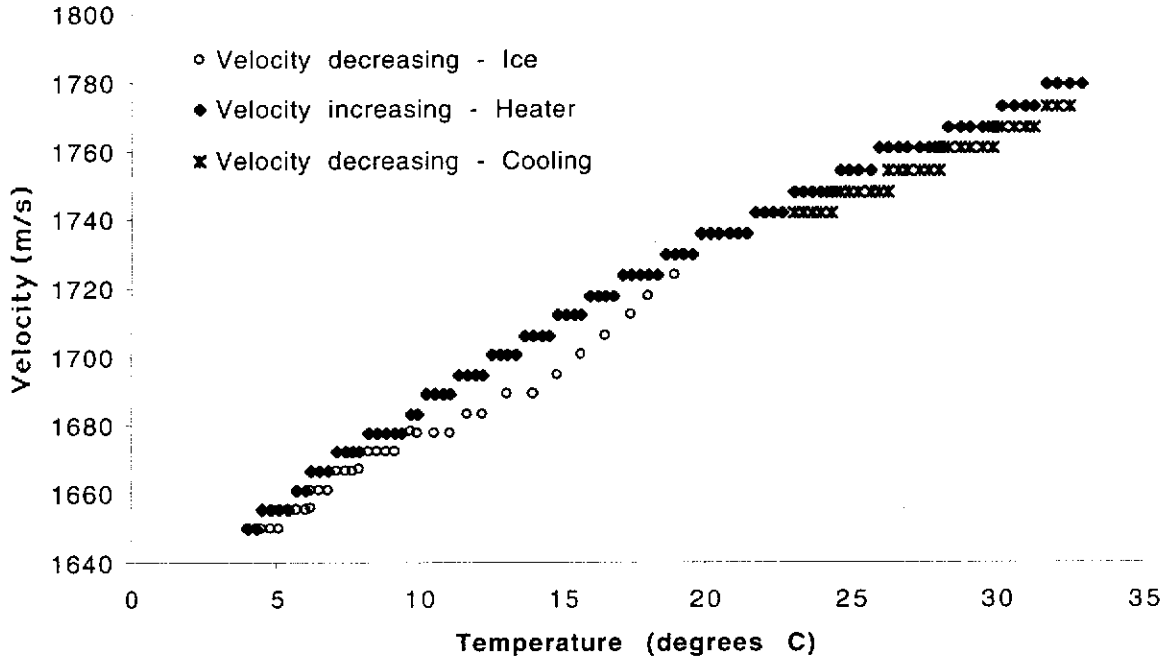

Figure 5.21: The discrepancy between the velocity measured as a function of increasing and decreasing temperature. The observed velocity changes as a function of the average sand temperature. The temperature was recorded from the middle of the sand, which may be slightly cooler or warmer than the average temperature depending on the whether the temperature is increasing or decreasing. The largest difference existed when the rate of temperature change was highest, which occurred when ice was added to the water tank.

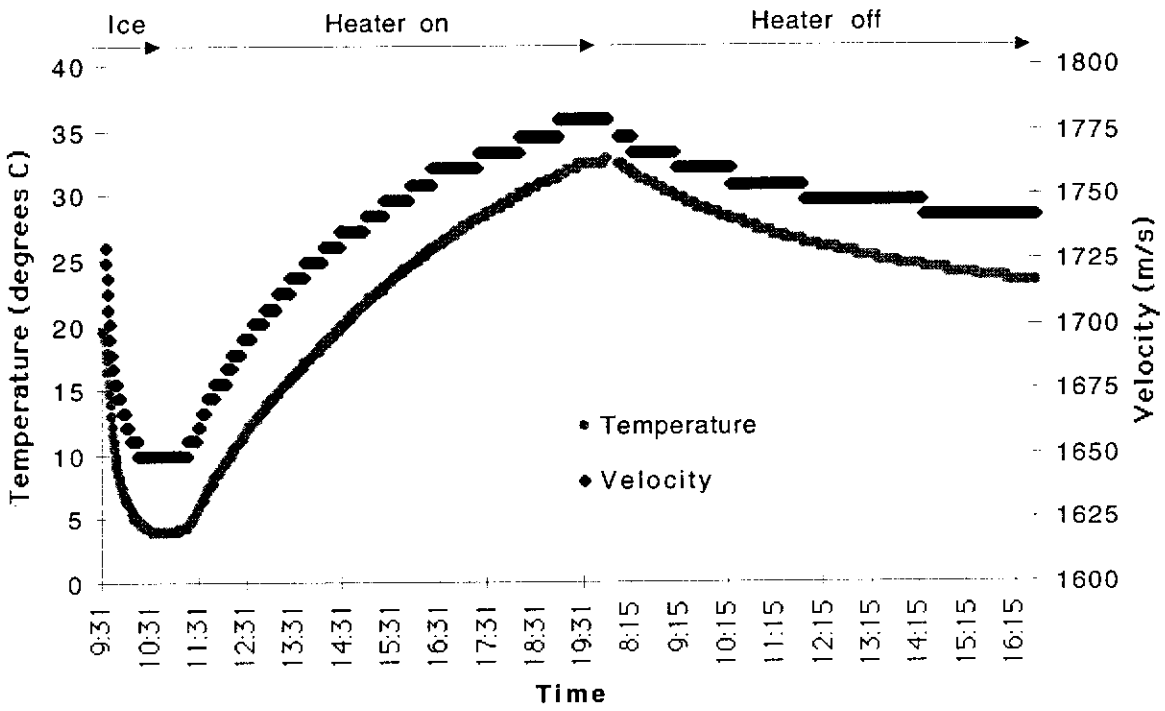

Figure 5.22: The change in water temperature and sound velocity in sand with time. The most rapid change occurred when ice was first added to the water tank and to a lesser degree when the heater was first turned on in the cold water, and off in the warm water.

5.7.5 Clay content

A small percentage of clay mixed with sand has a large effect on the physical properties of the sand. Various experiments were performed with samples containing weight percentages of clay between 1% to 50%. The clay used in these experiments was kaolin powder ($Al_2Si_2O_5(OH)_4$) which has a grain size of 1 to 4 μm. These mixtures were by far the most sensitive to random variations and consistently repeatable results were not possible. It was not possible to detect any ultrasonic arrivals from samples with more than 1wt% clay if steps were not taken to remove the air and compact the sample. When the percentage of clay was higher than 5%, the mixture had to be stirred to remove all of the air and it formed a slurry. The behaviour of clay in the laboratory at atmospheric pressure is too variable and completely unrepresentative of its behaviour under geological conditions. A small amount of overburden or confining pressure will dramatically change the acoustic and mechanical properties of clay. The behaviour of clay observed in some of the experimental reflection models in Section 5.8 suggests that just 100 mm of sand overburden will affect the acoustic properties of the sand and clay mixtures.

Velocity experiments conducted for this research at atmospheric pressure on sands with low clay fractions are lower than, but follow the trend of, results published by Marion *et al.* (1992), at 10 MPa confining pressure. The lower velocities measured here relative to those published by Marion, and elsewhere, are due to the lack of compaction and settling of the grains that is usually applied to give reliable results. The addition of clay increases the cohesion between the sand grains and consequently raises the acoustic velocity by increasing the frame's bulk and shear moduli. A sound velocity of around 1900 ms^{-1} was measured in a 10wt% mixture of clay in sand, and 2100 ms^{-1} was measured in a sand with 50wt% clay, but these results were unreliable. Similar samples measured under 10 MPa confining pressure (Marion *et al.*, 1992) had velocities around 2200 ms^{-1} for both 10wt% and 50wt% clay in sand.

It is estimated from the amount of compaction that occurs when the samples are vibrated and saturated that all of the sands containing clay had initial porosities of at least 45% when poured into the containers while dry, rising to around 55% for the sands with more than 10wt% clay. However, this reduced to between 40% and 43% after saturation of the sands with less than 5wt% clay. For the mixtures with more than 5wt% clay, it was not possible to estimate accurate porosities due to problems of saturating them.

An example of the sensitivity of physical properties of sand to clay content at atmospheric pressure and the large changes that occur with time is provided in Figure 5.23, which shows the shot records from a series of sands with clay fractions increasing from 0% to 0.9wt% clay in 0.1wt% increments. Velocity measurements were only possible from samples that contained less than 0.6wt% clay. The samples with more than 0.6wt% appeared to saturate fully when hot water was poured in, but it was not possible to detect a transmitted signal. The measurements were taken one hour after the samples were prepared (Figure 5.23a), and then repeated one day later (5.23b) and again after one week (5.23c). The change in velocity with time is shown in Figure 5.24. The trend of decreasing velocity with increasing clay content is an indication of the difficulty of fully saturating the samples. After one week, the velocities in the samples with less than 0.6wt% clay had increased and stabilized. The measurements for larger clay percentages are meaningless. The change in maximum peak amplitudes with time for the same sands is plotted in Figure 5.25, which illustrates the sensitivity of the laboratory measurements to small amounts of clay. The disjointed trends in the measurements reflects the difficulty in achieving homogeneous mixing of the clay in the sand, so that large variations are possible between different measurements from the same mixture.

It is likely that the sensitivity of the ultrasonic measurements to such minor amounts of clay would be substantially reduced under higher confining pressures. The measurements taken here are not representative of shaley sands under geological conditions. In the literature, there are clear trends that show an increase in velocity with clay content for similar mixtures under significant confining pressures. The problems

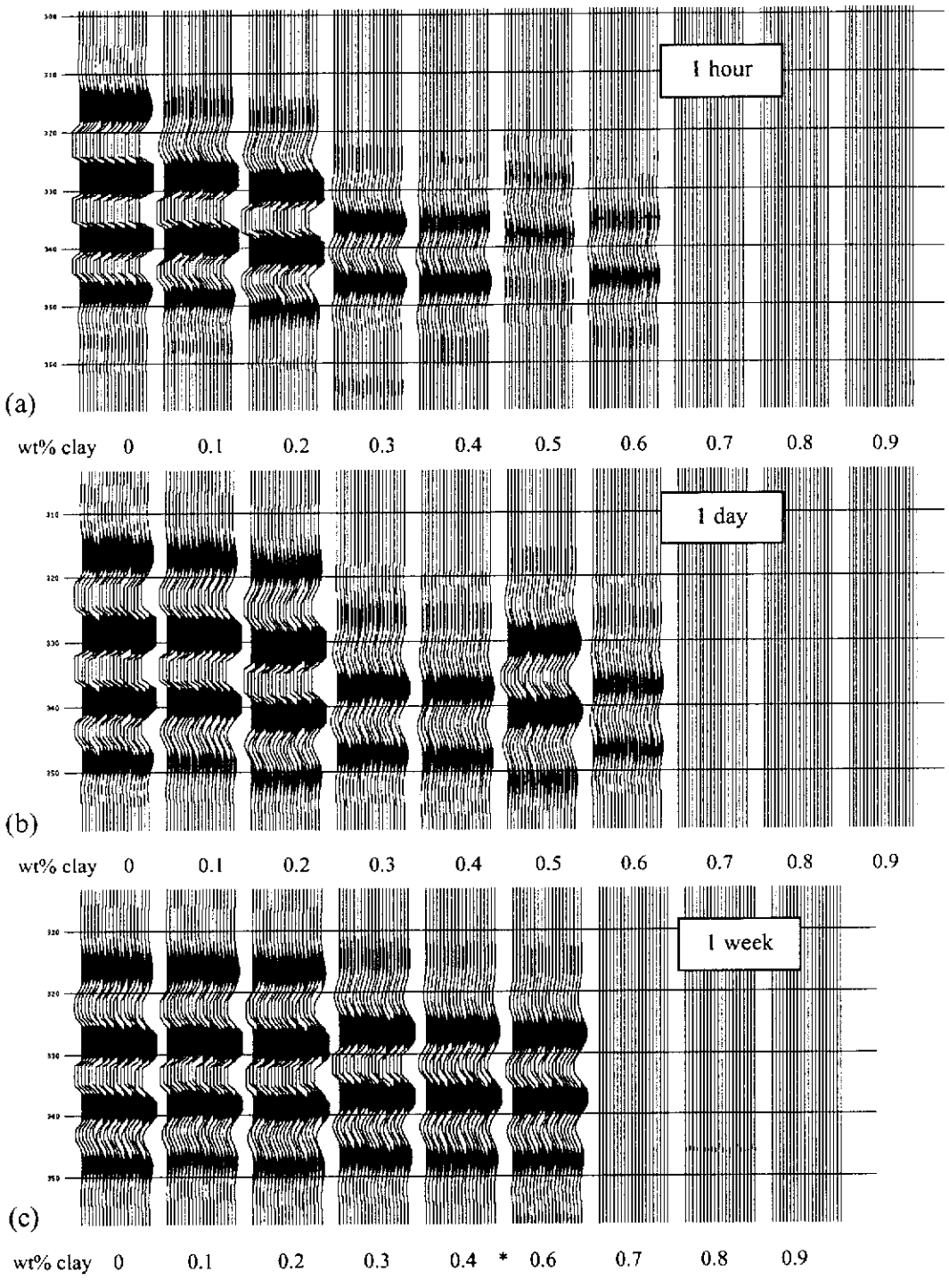

* No data was recorded for 0.5wt% sample after one week in water.

Figure 5.23: Shot records of the standard sand mixed with small percentages (<1%) of clay after (a) one hour, (b) one day, and (c) one week in water. The vertical axis is scaled one-way travel time in milliseconds. Data is very poor for clay fractions greater than 0.6wt% at room pressure due to difficulties in fully saturating the samples. Full saturation is not achieved unless steps are taken such as stirring the samples.

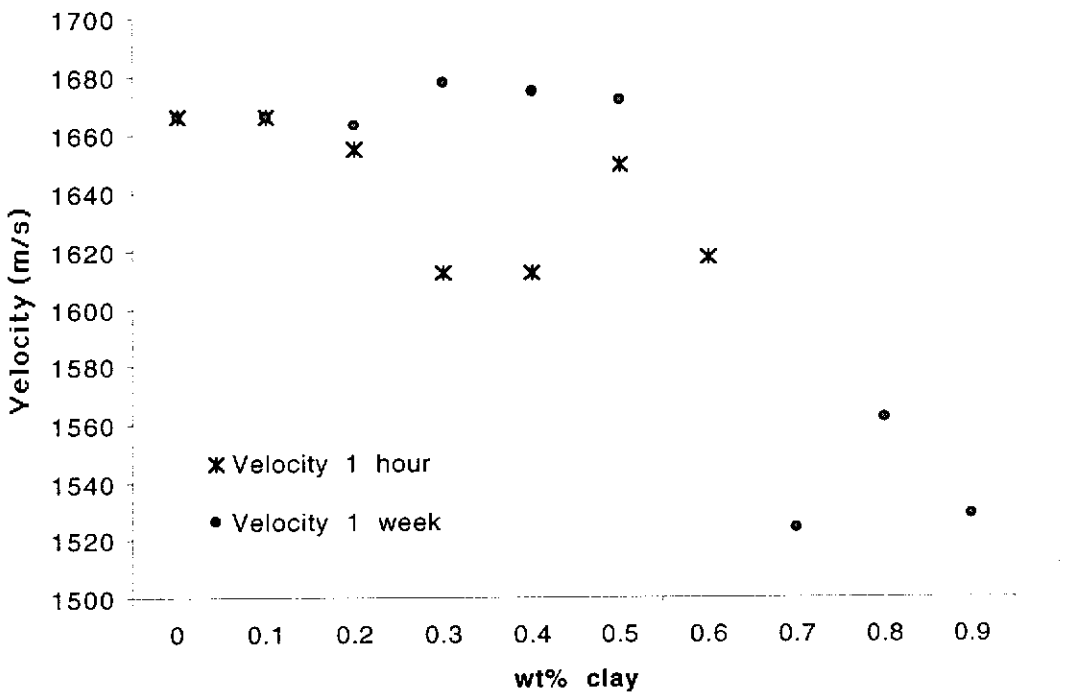

Figure 5.24: The sound velocity in sand and clay mixtures at room pressure after one hour and one week in water. The measurements are unreliable for percentages of clay greater than 0.6% due to difficulties with saturating the samples. After one week in water the trend is towards increasing velocity with clay content.

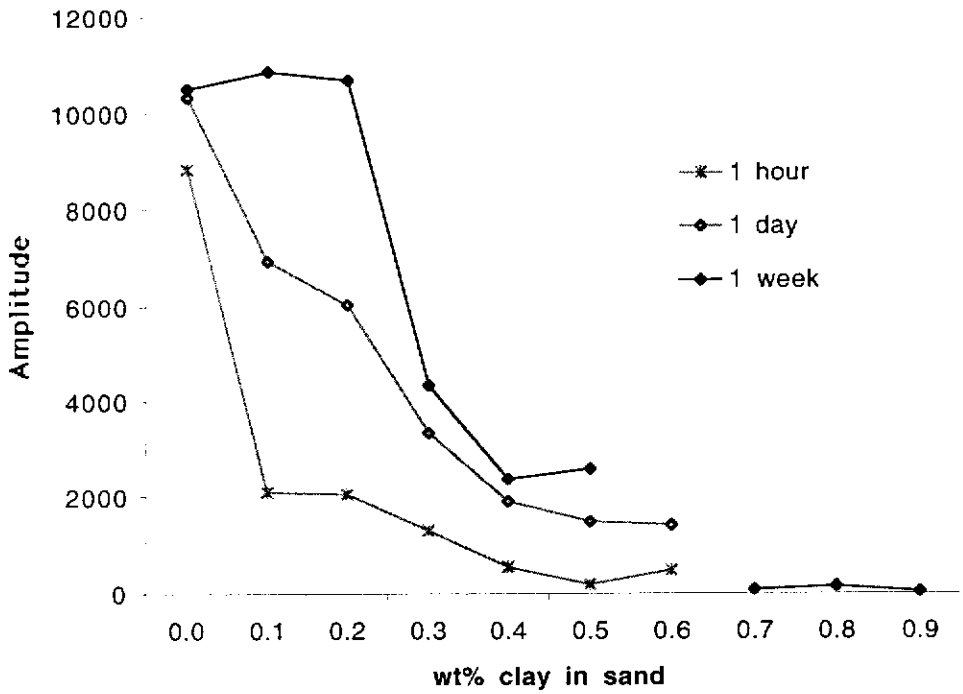

Figure 5.25: The change in peak amplitudes with time as a function of clay content.

encountered here with regards to the high rate of attenuation that prevents a signal being recorded for samples with high clay fractions, are not evident in the literature where the samples are put under pressure.

5.7.6 Pore fluids – kerosene

Some velocity measurements were made with different water and kerosene mixtures in well-sorted sand. These results are important for the time-lapse fluid flow models in Chapter Six. If the effect of different kerosene saturation levels on the velocity of saturated sand could be determined, then it would be possible to estimate relative kerosene saturation levels from changes in interval velocities within the fluid flow models. Kerosene was chosen due to its immiscibility with water, and its velocity and density contrast. Other oils were considered but kerosene was found to provide the largest acoustic impedance contrast with water and saturating the sands was easier due to its relatively low viscosity.

As shown in Figure 4.15, the effect on velocity of adding kerosene to the water-saturated sands depends on the scale at which the fluids are mixed, relative to the seismic wavelength. Homogeneous mixing at grain scale would result in acoustic properties dominated by the more compressible fluid (ie. kerosene). In this case, the velocity in the sand at 10% kerosene saturation would be close to the velocity at 100% kerosene velocity. If the mixing is patchy, the velocity will be closer to the linear-weighted average of the velocities in 100% water and 100% kerosene saturated sand.

Figure 5.26 shows the velocities measured in well-sorted (250-300 μm) sand for mixtures of kerosene and water. An approximate trend line assuming homogeneous mixing of the fluids is also indicated, along with the linear trend for patchy mixing. These results suggest that the patchy model is more appropriate for these kerosene and water mixtures. This was expected because it was not possible to saturate the sand uniformly with the mixtures of kerosene and water at grain scale. The patchy saturation model is also more appropriate for the fluid flow experiments in Chapter Six. The

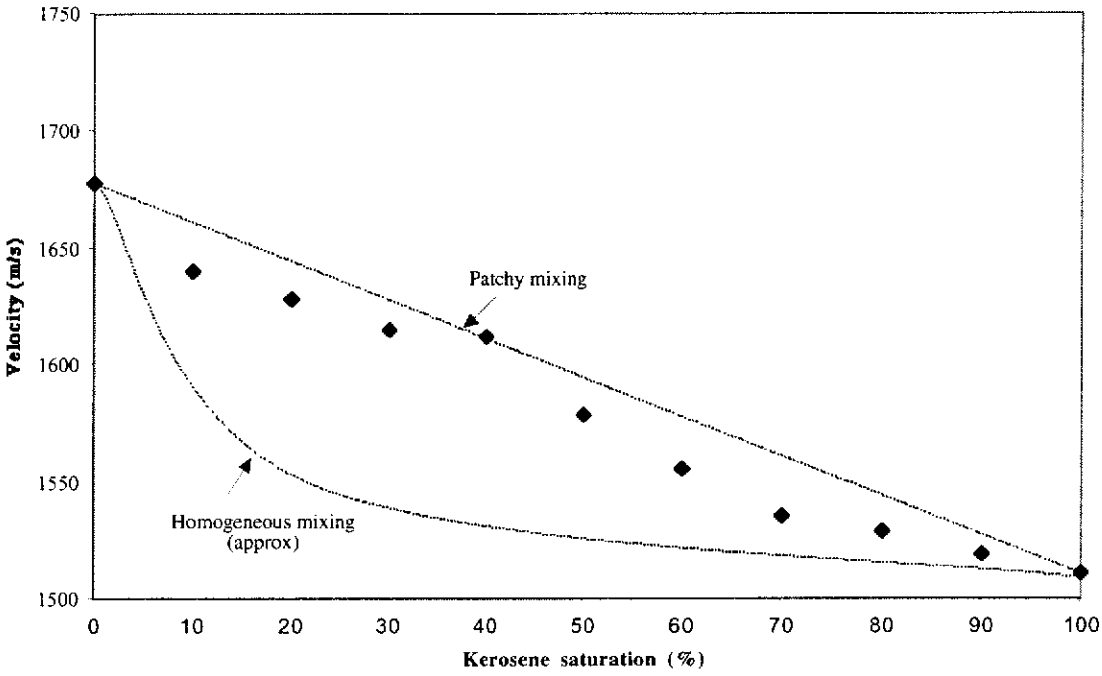

Figure 5.26: The measured velocity in sand as a function of water and kerosene saturation. Trend lines indicate the expected velocities depending on the scale at which the two immiscible fluids are mixed. If the fluids are mixed homogeneously at grain scale, the velocity will be strongly influenced by small amounts of the more compressible fluid (kerosene), as predicted by Biot-Gassman theory. If the fluid mix is coarse scale or patchy, the velocity will vary linearly with kerosene saturation. The measured velocity indicates that the patchy model is more appropriate for these mixtures.

results for two end members of 100% water and 100% kerosene saturation are accurate velocities. However, while the average kerosene saturation level in the sample was known in each case, the relative saturation directly in the path of the transmitted ultrasonic signal may be considerably different due to uneven mixing, contributing to the scatter in the data.

The next section progresses from the one-way transmission experiments presented so far, to two-way reflection experiments within layers of unconsolidated sand.

5.8 Reflections within sand

During this research, hundreds of models were built over several years in an attempt to establish the best technique of generating reflections within sandbox models. As with the velocity experiments, it became apparent that the technique of building the models was more significant than the materials used. Reflections were strongly influenced by such things as how the sand was sprinkled into the container, how the water was poured in, the amount of time between building the model and recording the seismic data, and the amount of care taken to ensure there was a smooth consistent layer interface. The application of vibration to settle the grain packing also proved to be significant.

Continuous refinements in the techniques of model building were made as the importance of each of the above factors became apparent. Unfortunately, this makes valid comparisons between different vintages of model data difficult. For example, in the early experiments it was thought that a mix of at least 10% clay in sand was required to ensure a reflection could be recorded at a depth of 20 mm in sand. However, after three years of refinement, a stronger reflection could be produced using only 1% clay. In fact, it will be shown that it is not necessary to use clay in the models at all. A series of examples are presented that illustrate the most important factors affecting the recording of reflections from within sandbox models.

5.8.1 Models

All of the examples shown below are simple 'layer cake' models comprising two or three horizontal sand layers. The sand was slowly sprinkled into the model container so that it would be well packed. The surface was manually graded flat by hand so that the interface with the overlying sand would be smooth and continuous. The overlying sand layer was then added, with special care taken not to disturb the smooth surface of the underlying mix, and was also graded to provide as flat a surface as possible for the seismic reflection experiments. The model containers were lightly tapped by hand to settle the grains slightly but were not subjected to vibration unless stated otherwise.

Initially, the models were saturated through a hose connected to the base of the model container to ensure that they were fully saturated from the bottom upwards. However, it was found that pouring water in from one end of the model was equally as effective as long as the flow rate was slow enough to allow the water to flow along the base of the model and then upwards. If the inflow of water was too rapid, the surface of the model would be flooded before all of the sand below was fully saturated, creating an air pocket which would often burst through the model. Saturating the models from one end was a quicker and more convenient method and did not adversely affect the results as long as care was taken.

All of the 2-D seismic profiles shown here are zero-offset data, which were acquired using the same transducer as both the source and receiver. The model data is scaled by a factor of 1:10 000 before it is loaded onto the workstation. The time scale of the seismic displays is, therefore, in milliseconds, scaled two-way travel time. The dimensions of the models are stated in true dimensions, with the scaled dimensions in brackets.

5.8.1.1 *Repeatability*

Producing the same response from two supposedly identical models is one of the greatest limitations with seismic imaging of sandbox models and has proven to be the most difficult to overcome. As with the velocity tests, quantifying the effects of variation in texture and clay content was not possible due to the difficulty in keeping all other factors constant, and, as such, there was a large range of values recorded for models built using the same parameters. It seems that unless the sands can be added consistently, which would require automation with precision down to grain scale, then a truly repeatable response will not be possible.

Random variations occur that are beyond the control of the model building process and results in different reflection amplitudes between models that are intended to be the same. Even when extreme care is taken to build two identical models, the average amplitudes for the same reflecting horizon can vary by a factor of two between the models. Relative reflection amplitudes between adjacent traces in any one seismic profile often vary by more than an order of magnitude, which highlights the difficulty in quantifying any difference between models where there is a deliberate change in parameters.

5.8.1.2 *Estimating Reflection Coefficients*

Predicting the reflection coefficient from the sound velocity and density measurements proved futile because, once a reasonable method of building the models was established, the reflections were invariably stronger than predicted. The examples shown below illustrate that the reflection from the interface between two sands depends not only on the acoustic impedance of each sand layer, but more significantly on the way the two sands combine at the interface. The strongest reflections are recorded from models with the largest contrast in grain sizes between layers, rather than the largest contrast in acoustic impedance.

The observed reflection coefficients were estimated by comparing the amplitudes from the model surface reflection (ie. the water-bottom) relative to the layer interface reflection. The reflection coefficient predicted for the water bottom from the acoustic impedance formula (see equation 2.1) is around 0.3. Stoll (1977) suggested that at ultrasonic frequencies, some of the incident P-wave energy will be converted to the 'slow P-wave' and essentially be lost at the interface. This would reduce the reflection coefficient to around 0.28, or even as low as 0.2 if the sand has a small amount of gas in the pore water.

All of the figures shown are unprocessed seismic records that have not had any gain applied. The reflection coefficients stated for each model were estimated from the recorded reflected amplitudes and are, therefore, conservative estimates. To correctly estimate the reflection coefficient from the relative amplitudes of the water bottom and layer interface, gain should be applied to compensate for the attenuation of energy in the top sand layer. Some attempt was made to do this whereby gain was applied to the data in the form of Q compensation. The value of Q is nominated beforehand and applied over the interval of the sand layers. It was found that the results obtained from this varied enormously depending on the Q value chosen. The true value of Q will vary for each model and it was not possible to estimate this accurately enough to trust these results.

The following examples are only a small subset of all of the reflection experiments performed. The majority of these experiments were recorded before the model building techniques were adequately refined and so the results are erratic and can be misleading. The estimates of the reflection coefficients are intended only to show that the reflections cannot be solely a result of the acoustic impedance contrast between the sand layers. They cannot be used for predictive purposes because the results are much more dependent on how the models are constructed than on the composition.

5.8.2 Reflections from Changes in Clay Content

Of all the early experiments with different materials, only mixtures of clay with sand produced consistent reflections at the interface with a layer of clean sand. Attempts were made to establish the dependence of the reflection strength on mixture proportions. As with the velocity tests, clay fractions above about 5% also caused a reduction in permeability that made it difficult to properly saturate the sand, which in turn made it impossible to conclude whether the increased acoustic impedance contrast was from the added clay or the presence of air. A trend of increasing reflection amplitude with percentage clay was evident for clay fractions less than 5wt%. However, difficulties with saturation and the change with time of the models made reliable results impossible with clay.

Katahara (1996) noted the large variation in previous clay studies and attributed it, in part, to the fact that samples change over time (in the laboratory) and with diagenesis (in-situ). The properties of sand and clay composites depend not only on the clay properties, but on the size, shape and alignment of the particles and pores. Such textural variables differ from one sample to another and in any given sample will evolve with compaction and diagenesis.

Figure 5.27 is an example of a seismic survey from a model where reflections have been recorded from the top and bottom interfaces of a sand and clay layer within a sand model. The model comprises a 15 mm thick layer of the standard clean sand (150 m scaled) overlying a 10 mm (100 m) thick layer of a mixture of 3wt% clay in the standard sand. The interval times between the top and base reflections of each layer can be used to calculate the velocity of each layer. The top standard sand layer has a velocity of 1700 ms^{-1}, which was expected from the transmission velocity tests. However, the velocity in the sand and clay layer was expected to be between 1700 ms^{-1} and 1800 ms^{-1}, but is actually 1900 ms^{-1}. The measurement error is higher in this case than in the velocity test because the layer was only 10 mm thick, but other similar models also showed consistently higher than expected velocities in sand and clay layers. There are two possible reasons for this. Firstly, the sand and clay layer is compacted

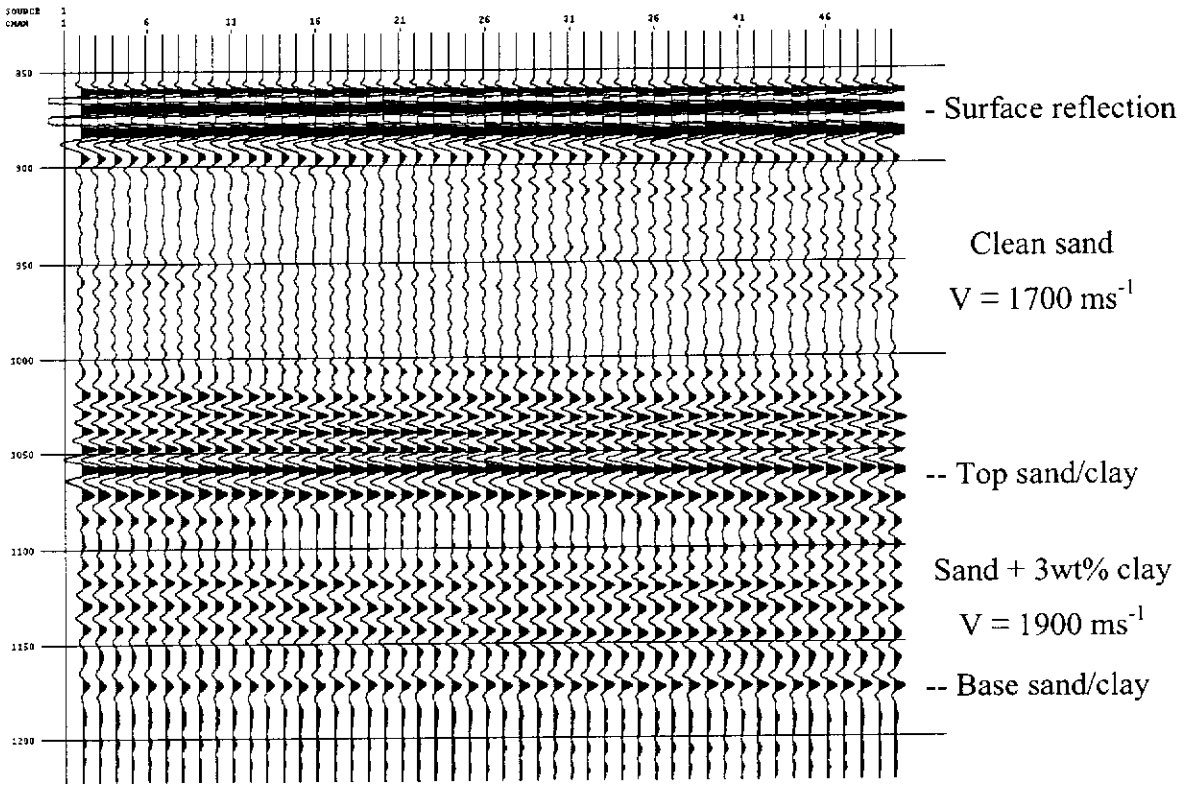

Figure 5.27: Zero-offset seismic section of a three-layer sand model. The middle layer is a mixture of sand and 3wt% clay and had a thickness of 10 mm (100 m scaled). The interval velocity calculated from the top and bottom reflections of the clay horizon was 1900 ms^{-1}, which is significantly higher than that for similar mixtures measured in the velocity experiments. The increase was attributed in part to compaction from the sand overburden and from a slight increase in confining pressure. This increase in velocity was only observed in layers that contain clay.

slightly when it is saturated, as was observed in the velocity tests, such that the true thickness of the layer was slightly less than 10 mm, leading to an artificially high velocity. Secondly, the mass of the sand overburden applies a small but significant confining pressure that results in stiffer grain contacts and higher elastic moduli.

5.8.3 Reflections from Changes in Grain Size and Distribution

As the method of generating reflections within the sand models was refined, the apparent reflection strength increased. The percentage of clay mixed with the sand was continually reduced to lower the acoustic impedance contrasts within the models. This was done to reduce the amount of energy that was reflected and hence allow more energy to be transmitted through the interface to the next horizon boundary. The goal was to refine the models to the point where as many layers as possible could be imaged with the limited transducer energy available. This process continued until eventually, it was discovered that reflections could be produced without any clay in the sand at all.

Clay had been used in the initial models because the velocity measurements indicated that only a very small acoustic impedance contrast would be possible if only clean sands were used. However, it became apparent that strong reflections were possible with little or no contrast in the acoustic impedance between two layers of clean sand (Sherlock, 1998). The possible mechanisms for these reflections were investigated and are presented below.

5.8.3.1 Grain Size Variations

Figure 5.28 shows two examples of reflections recorded within two-layer sand models where the only contrast between the layers is the grain size. Both models comprised two well-sorted sands with grain size ranges of 106 to 125 μm and 180 – 212 μm and the top layers were 20 mm (200 m) thick. The model shown in Figure 5.28a has the fine grain sand overlying the medium grain sand, while the model in Figure 5.28b has the fine grain sand as the lower layer. As both sands were well sorted, the porosities

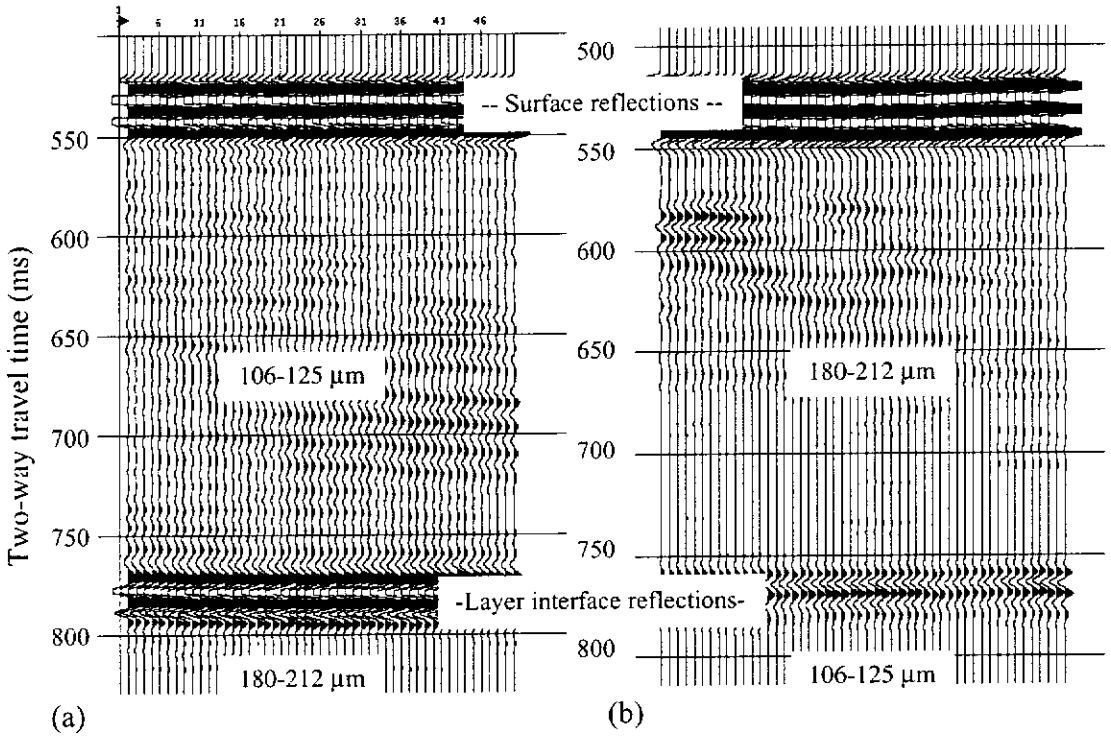

Figure 5.28: Seismic reflections from two-layer sand models with well-sorted sands of contrasting grain sizes. (a) Very fine grained sand (106-125 µm) overlying medium grained sand (180-212 µm). (b) Medium grained sand overlying very fine-grained sand. Note that a stronger reflection results when the finer grained sand is on top.

were very similar. Measurements of porosity taken as part of the velocity tests indicated that the fine grain sand may have slightly lower porosity, which means that it would have slightly higher saturated density. The velocities in each of the sands were assumed to be equal. If the reflection from the layer interface was purely a result of the contrast in acoustic impedance, the reflection coefficient in both cases would be expected to be around 0.01. However, the reflections in both models were clearly much stronger. The observed reflection coefficient for the model with the fine grain sand on top was at least 0.2 and for the model with the fine sand on the bottom it was around 0.1. Similar results have also been recorded from many other models with different combinations of grain size contrasts.

It is suggested here that the reflections are not a result of the contrast in acoustic impedance between the sands, but rather a consequence of the combination of the two sands at the layer interface. While the porosity of each sand layer was around 40%, the porosity along the interface between the sands may be much lower depending on the grain size combination. Clarke (1979) showed that bi-modal mixtures of two different grain sizes can have porosities as low as 12% if the relative grain sizes and proportions of each are ideal. In this case the porosity is more likely to be around 20% to 30% as the contrast in grain sizes is relatively small and they are presumably mixed in equal proportions at the interface. Although the porosity change does not directly cause the reflection, it is suggested that the subsequent effect on the rigidity of the grain packing at the interface does.

The strongest reflections are produced from the models comprising the greatest contrast in grain sizes. However, as shown in Figure 5.28, there is also a significant difference depending on which sand is on top. When the finer grained sand is overlying the coarser grained sand (Figure 5.28a), the reflections are usually stronger than when the situation is reversed. The smaller grains appear to fall into the cavities between the larger grains, which makes the packing much tighter at the interface. However, when the sequence of these two layers is reversed (Figure 5.28b), the resulting reflection amplitudes are lower. It is suggested that this is because the larger grains can only sit on top of the fine-grained surface, as they are too large to fit into the cavities of the

smaller grains. Instead of the combination of grains causing a reduction in porosity, the result may be the opposite.

Theory suggests that if the two layers are reversed, the impedance contrast is also reversed and the reflection produced should have the same amplitude but opposite polarity. However, both of the models in Figure 5.28 have the same polarity of reflections. In fact, nearly all of the sand models in this thesis have reflections with the same polarity, as a result of a positive acoustic impedance contrast at the interface. This is because it is physically impossible to deposit the large grains onto the surface of the fine grains such that the porosity is actually higher than in either of the two layers. Attempts to do this resulted in weak reflections that were not coherent across the entire seismic section and were difficult to identify. The top sand in the model shown in Figure 5.28 (b) was sprinkled onto the surface of the fine grain sand carefully from around 50 mm above the surface. It is suggested that the falling grains tend to bury themselves slightly into the surface of the fine grains, resulting in an interface with lower porosity and tighter packing. The amount of care taken to sprinkle the top layer onto the surface of the lower sand has a remarkable influence on the result. This extreme sensitivity means that these experiments are particularly difficult to repeat.

5.8.3.2 Grain Packing Variations

Unless all of the grains within a layer of sand are of equal size, there will be a certain degree of uneven grain distribution. Nearly all sands, including those used for this research, comprise a range of grain sizes but the sand is still assumed to be fundamentally homogeneous, which implies a uniform distribution of all grain sizes throughout the package. The surface of the sand layers in these models is manually graded as a means of removing excess sand from the pile and to produce a flat horizontal boundary with the next overlying sand. It was discovered that physically grading the flat horizon alters the way in which the grains are packed at that surface. While this process removes the excess sand, some of the smallest grains will fall into cavities on the surface and be left behind, so that the end result is a surface where the

grain packing and porosity will be significantly different from that in the rest of the sand package.

The existence of these changes in packing will have an effect on the reflections produced from layer interfaces and this can be demonstrated with a two-layer model where the same sand is used for both layers (Figure 5.29). The seismic data recorded over this model show a clear reflection where the sand was graded flat at a depth of 20 mm (200 m scaled). The predicted reflection coefficient for this interface is zero, which means there should not be a reflection because there is no contrast between the two sand layers. However, the observed reflection coefficient is at least 0.1. Without a contrast in acoustic impedance, the observed reflection can only be a result of the effect that grading the horizon has on the interface. Unfortunately, this means that all of the reflections recorded from models that were built in this manner must have been influenced by this phenomenon. Therefore, the reflection amplitudes observed for these models give little indication of the true contrast between the different sands used. However, it does indicate how significant even the most subtle of changes can be to the acoustic properties of unconsolidated sands. It also gives some insight into possible mechanisms for seismic stratigraphic reflections, which are internal reflections recorded from within lithological units and are possibly controlled by changes in grain size and distribution.

5.8.3.3 Grain Sorting Variations

As mentioned above, any one layer of sand in the model is assumed to be fundamentally homogeneous, which implies that the different grain sizes within the sand are evenly distributed. In sedimentary sequences this is not the case, and it is demonstrated here that it is not the case with sandbox models either.

In nature, the average grain size of a sedimentary unit and the range of grain sizes deposited depend mainly on the energy within the particular depositional environment. In fluvial systems, grains are sorted such that the larger pebbles and boulders come to

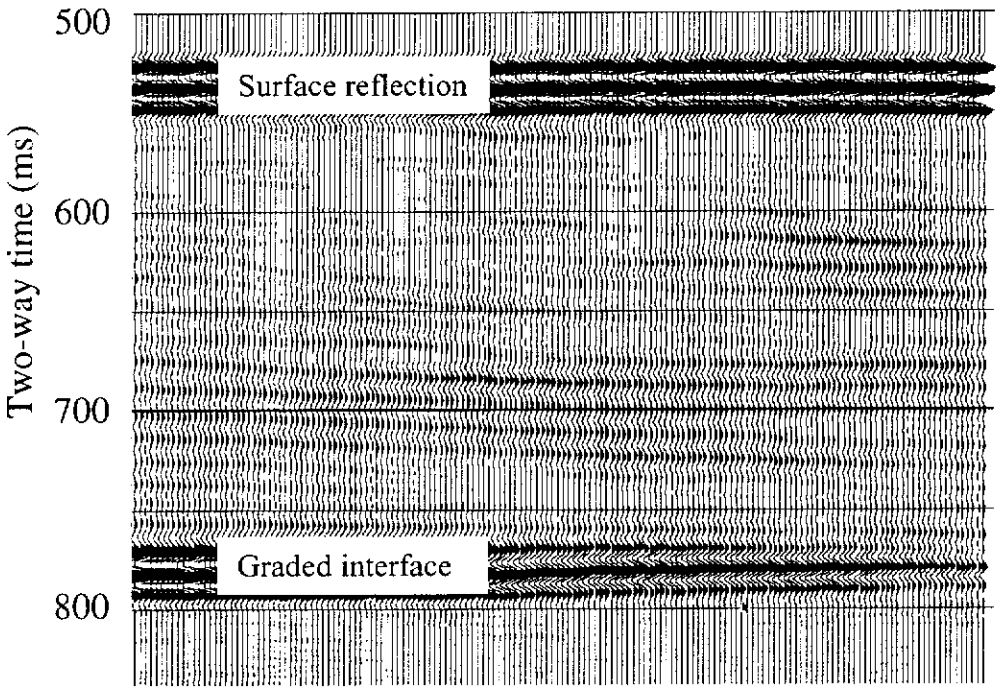

Figure 5.29: Seismic section showing a reflection recorded from the interface between two layers of the same moderately-sorted sand. The reflection is produced by the change in grain packing that results from grading the horizon.

rest early upstream, whereas the finer grained sands are carried further downstream by the flowing water. This process continues into the marine environment, where the sediments are progressively sorted into finer grains until eventually the finest silt-sized grains come to rest in quiet, deep marine conditions. The degree of sorting that occurs within any sequence depends firstly on the initial range of grain sizes within the environment, and secondly on the amount of time and energy within the system that allows the different size fractions to be separated. Other cyclic variations such as sea level changes or seasonal effects can, for example, result in a fining-upwards sequence being repeated. The end result is stratigraphic changes that take place within a lithological unit that may otherwise be considered homogeneous on a larger scale.

It was found that the environment of deposition is also significant when building sandbox models. Low amplitude reflections within what was intended to be homogeneous sand units within the models were initially viewed as noise. However, this noise is actually a result of similar natural variations in grain sorting that occur as the sand is sprinkled into the model containers. The presence of these low-amplitude 'stratigraphic' reflections can be influenced by the initial sorting of the sand and also by the method of 'deposition'.

To prove this observation, results from two models are shown in Figure 5.30 where the top sands for both models have the same average grain size (200 μm) and were sprinkled into the container in the same manner. However, the two sands vary in the degree of sorting of the grains. The first model (Figure 5.30a) uses the standard moderately-sorted sand. The sand in the second model (Figure 5.30b) has been sieved so that the grain size range was 180 – 212 μm. The corresponding seismic sections show that the well-sorted sand generates less noise. There is less natural variation in sorting for this layer because there is a much narrower range of grain sizes to begin with. The standard sand model generates much more noise and this is due to the natural segregation of the grains as they are sprinkled into the container.

The amount of segregation that occurs with poorly sorted sand in the models depends on the initial volume of sand taken with each scoop, and also the rate that it is sprinkled

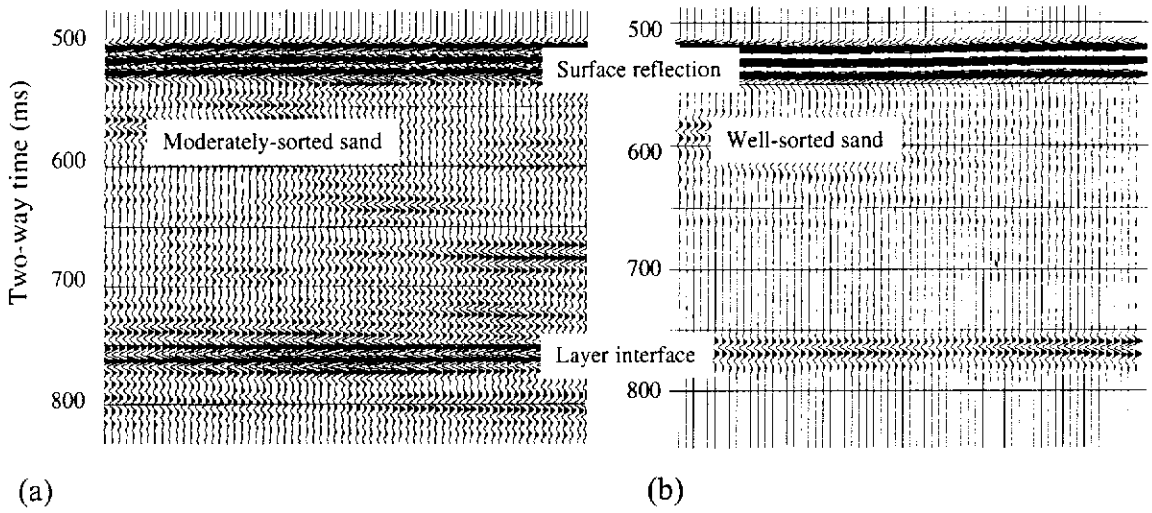

Figure 5.30: Comparison of noise generated within sand layers due to grain size distribution. (a) Moderately sorted sand is heterogeneous and generates low amplitude reflections within the layer. (b) Well sorted sand with the same average grain size (200 μm) generates less noise because less segregation of different grain sizes is possible.

in, which is a similar mechanism to natural deposition. If a scoop of sand is poured into the container, there is no time for the grains to segregate into different sizes. However, if the sand is sprinkled in carefully by shaking the scoop of sand over a significant length of time then there is a much larger degree of sorting. This can actually be seen with the naked eye where the larger grains tend to fall in first, leaving behind a larger fraction of the smaller grains to fall in last. This effectively creates a fining upwards sequence that subsequently manifests itself in the resulting seismic image as 'stratigraphic' reflections. This indicates potential to image much more subtle details from sandbox models than just the gross structure that was originally sought, and a model is presented in the next chapter which takes advantage of this.

The degree and scale of heterogeneity within the sand depends largely on how the sands are deposited. As discussed in Section 5.7, this also has an effect on the velocity and rate of attenuation in the sand (see Figure 5.11). The velocity of the sand is higher when the sands are sprinkled in slowly because the grain packing is tighter. However, the velocity in the sands that were sprinkled in as one continuous scoop of sand (referred to here as 'sprinkled') have slightly lower sound velocities than the sands that were deposited in several small scoops (referred to as 'layered'). The slightly higher velocity in the layered sands suggests that the grains are packed tighter than in the sprinkled case. If this is so, then the rate of attenuation in the layered sands should intuitively be lower because these sands are able to transmit the seismic energy more efficiently. However, the relative amplitudes shown in Figure 5.11 indicate that this is not the case. It is suggested here that the layered sands do in fact have a lower rate of intrinsic attenuation, but the layering that results from the segregation of grains also causes some of the energy to be reflected, which in turn reduces the amount of energy being transmitted. This would then explain the lower amplitudes that were recorded in the layered sands in the velocity experiments, because they were measuring the transmitted energy.

Six shot records are shown in Figure 5.31 to support this conclusion. The shot records were recorded from the same samples that were used in Figure 5.11 to measure the velocities and amplitudes. However, in this case the records are from the two-way

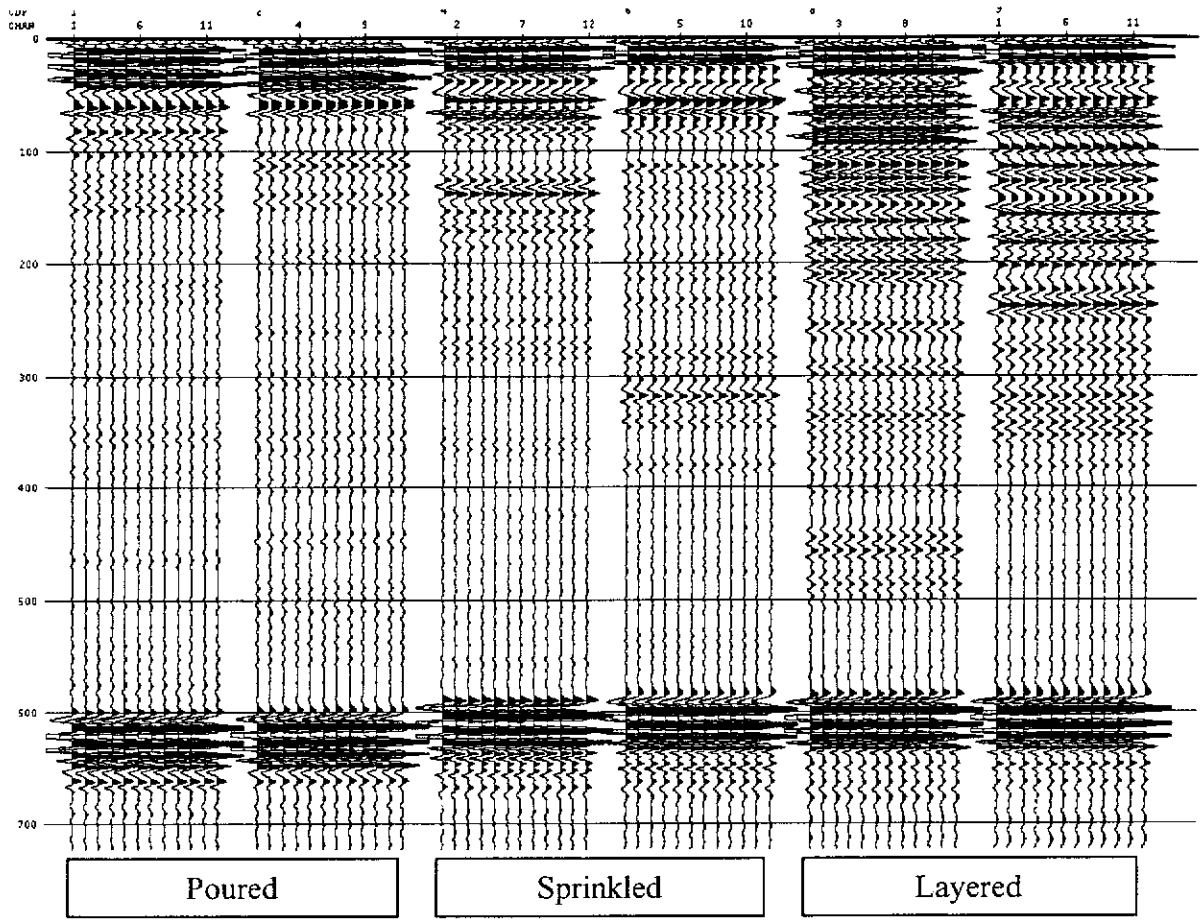

Figure 5.31: Six two-way reflection records that correspond to the one-way transmission data plotted in Figure 5.11. The layered sands are sprinkled into the containers in several small scoops that create heterogeneous grain sorting. The velocities in both the sprinkled and layered sands are faster than in the poured sand, but the layered sands produce stronger reflections.

reflection measurements, rather than the one-way transmission records that were used for the measurements in Figure 5.11. The arrival times for the reflections from the end of the samples are lower (ie. the velocities are higher) for the sprinkled and layered sands than for the poured sands, which supports the velocity measurements from the transmission records. However, while the arrival times for the sprinkled and layered sands are similar, the records from the layered sands have more internal reflections. These reflections are a result of the layering that was induced by the method of deposition and effectively reduce the amount of energy that is transmitted through the samples.

The effects of these small-scale heterogeneities do not appear in other studies of velocity and attenuation within sand, as they are invariably experiments involving acoustic transmission, not reflection as is the case here. The heterogeneities exist within any one sample and, therefore, any effect on velocity and attenuation on the one-way records are averaged over the length of the sample. Calculations of the elastic parameters from such measurements do not indicate how the properties may vary within the sample and cannot allow for the loss of energy through internal reflections. The two-way reflection records in Figure 5.31 demonstrate that small-scale variations in packing and sorting can influence the measured acoustic properties, particularly with ultrasonic laboratory measurements.

5.8.4 Techniques to Improve Reflection Quality

The same techniques of improving the data quality that were tested in the velocity measurements were also tried on the reflection models. The most significant findings are presented here.

5.8.4.1 Vibration

Heterogeneity of the grain packing results in inconsistent reflection characteristics and has been a major stumbling block in applying seismic modelling methods to sand

models. In the velocity measurements, applying vibrations to the models was shown to have the biggest influence on the properties of the sand. A number of similar models were subjected to varying degrees of vibration to see if there was a relationship between the time spent on the vibrating table to settle the packing of the grains and the resulting reflections recorded in the models. Once again, the large variation between models made it difficult to demonstrate a clear trend. However, the effect appeared to be that up to one minute on a vibrating table produced tighter packing and stronger reflections. Some compaction of the sand is visible over the first few seconds as the thickness of the sand is slightly reduced but the reflections appear to continually improve slightly with further vibration. For vibration times greater than one minute, there was a decrease in the resulting reflection strength but there was no further compaction observed.

The initial improvement in the reflections coincides with a decrease in the 'stratigraphic' reflections present within the overlying sand, which is probably a result of more uniform packing throughout the layer. The improvement in the reflection from the layer boundary may be a result of more efficient energy transmission through the top layer, rather than being from any changes that take place at the actual interface.

For the models that were subjected to vibration times greater than one minute, the changes in reflection amplitudes are most likely to be a result of the sands from each layer mixing together. This causes the interface to become more diffuse as the grains are rearranged. The amount of time on the vibrating table that this takes obviously depends on the amplitude of the applied vibrations. Using a layer of sand with a different colour in a transparent perspex container allows this to be seen with the naked eye. The first few seconds of vibration results in a noticeable compaction of the whole sand column. Further vibration appears to have no effect until, after a while, the interface between the coloured sand layer and the white sand becomes less well defined. Eventually the change in colour becomes very gradual and the position of the original layer boundary cannot be seen.

The initial improvement in energy transmission that comes with applied vibrations is important when progressing to models where several layer reflections are desired. However, smooth and consistent layer boundaries are even more vital. A similar method to that used for the velocity experiments was adopted, where the model containers were tapped lightly by hand but were not placed on the vibrating table. This improves the consistency of the results but does not degrade the horizon and 'stratigraphic' reflections from within the models.

5.8.4.2 Time

When the models are saturated with cold water they do not, at least initially, reach full saturation. This effect was noted in the velocity experiments but is better illustrated in the following reflection experiment. Seismic lines were recorded over the same two-layer model every day for one week. Figure 5.32 shows the difference in the reflections recorded after one hour and after seven days. The comparison clearly shows that the extra time in the water tank results in an outstanding improvement in signal-to-noise ratio (SNR).

This effect occurs with all models whether the reflections are produced from changes in clay content or from changes in grain size alone, although further long term measurements are needed to fully establish the changes that occur with time. Some models were kept in the water tank for periods of up to two months but it was not feasible to keep many models for long periods because the physical modelling system was in continuous use for a range of research projects. The observed improvement in the reflections that were recorded from the mixed sand and clay layers appears to stabilize after several weeks. However, the reflections from some of the models comprising only grain size contrasts appeared to deteriorate after two months. This was not observed in all of the long term models and further work is needed to explain the observations.

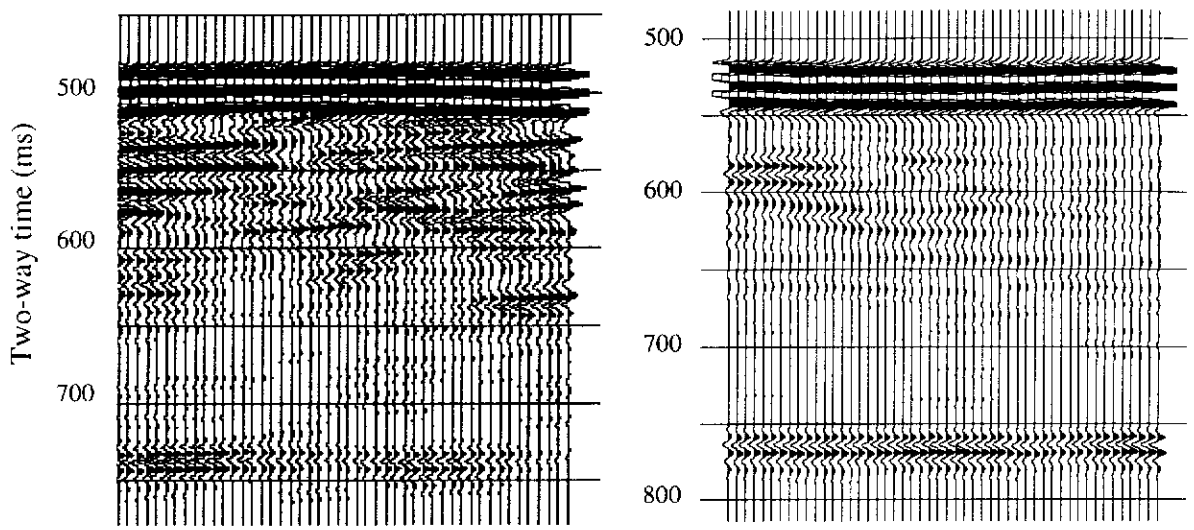

Figure 5.32: Comparison of seismic section recorded over the same two-layer sand model at different times. (a) After one hour the sand is not fully saturated and most of the energy is attenuated near the surface of the model. (b) After one week there is much less noise in the near surface and the reflection from the layer interface is more uniform and continuous.

5.8.4.3 *Hot Water*

Experiments were performed where the sand was saturated with boiling water to see if it would improve the results in the same way that it did for the velocity measurements. Figure 5.33 shows a simple comparison where normal tap water was used to saturate one model, while boiling water was used to saturate another. The models were then placed in the same cold water tank and left to stand for a three hours so that the hot water model would cool to the temperature of its surroundings. The results show a remarkable improvement in the reflections that were produced from the model where boiling water was used. Repeating the seismic surveys one week later showed that the reflection quality of the model saturated in cold water had caught up with the boiling water model, to the point that they were as similar as could be expected if they were saturated identically in the first place. Boiling water was adopted as standard procedure to saturate the models because it reduced the turn around time of the models.

Another important benefit of using boiling water to saturate the models is that it is more able to penetrate the less permeable sands because the viscosity and surface tension are reduced. This is particularly useful if the models comprise significant amounts of clay.

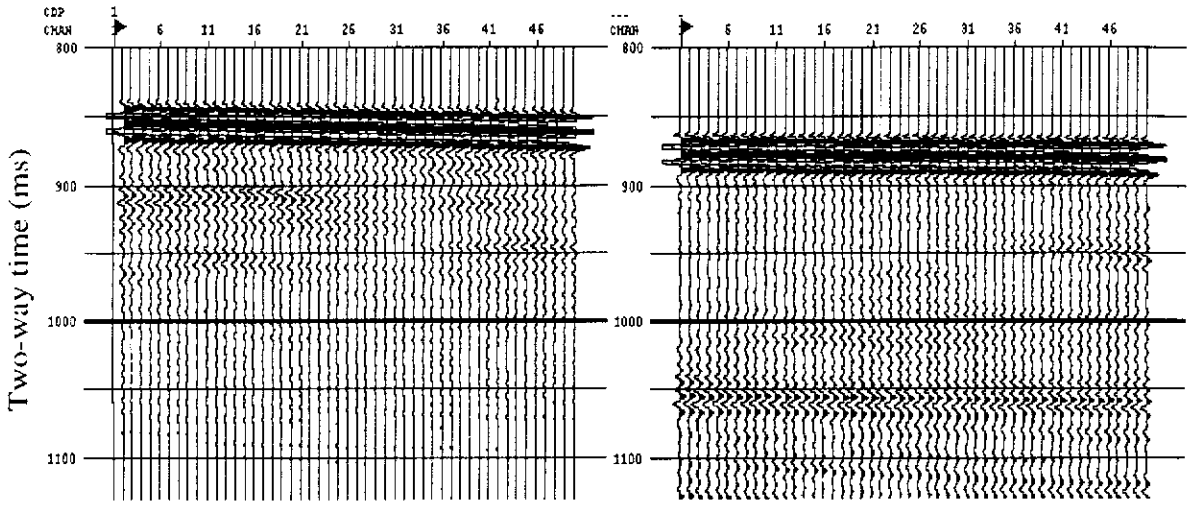

(a) Cold water (b) Hot water

Figure 5.33: Comparison of the reflections recorded over similar models three hours after saturation with (a) tap water at room temperature, and (b) boiling water. The hot water is more efficient at saturating the model. The difference in reflection arrival times is due to slightly different model dimensions.

CHAPTER SIX

MODELS

Once the techniques of recording a seismic reflection within a sandbox model were adequately developed, the next stage was to extend this to recording several reflections within multi-layer models and reflections from models comprising dipping layers. This Chapter discusses the development of the science towards the seismic imaging of more geologically realistic models.

6.1 Multiple Layer Models

Limitations on the energy output of the transducers and the high rate of attenuation make imaging multiple layers difficult. Various combinations of sands with contrasts in clay content or grain sizes were tested in an attempt to achieve the best balance of reflected energy and transmitted energy, thereby allowing as many layers to be imaged as possible. Every reflection event reduces the amount of energy transmitted, and so a balance is required between a reflection coefficient that is high enough to detect the horizon, but is as low as possible to allow as much energy as possible through to the underlying layer.

Progressive refinements in the various techniques discussed in previous chapters mean that reflections can now be recorded from much more subtle acoustic impedance contrasts than was possible in the early experiments. This means that there is effectively more energy available to record a greater number of deeper reflections. Figure 6.1 shows a profile recorded over a four-layer model. The depth to the first layer boundary is 20 mm (200 m scaled) and each subsequent horizon interval is progressively smaller to ensure that any peg-leg multiples, if present, are not misidentified as primary reflections. This four-layer model is the most successful to

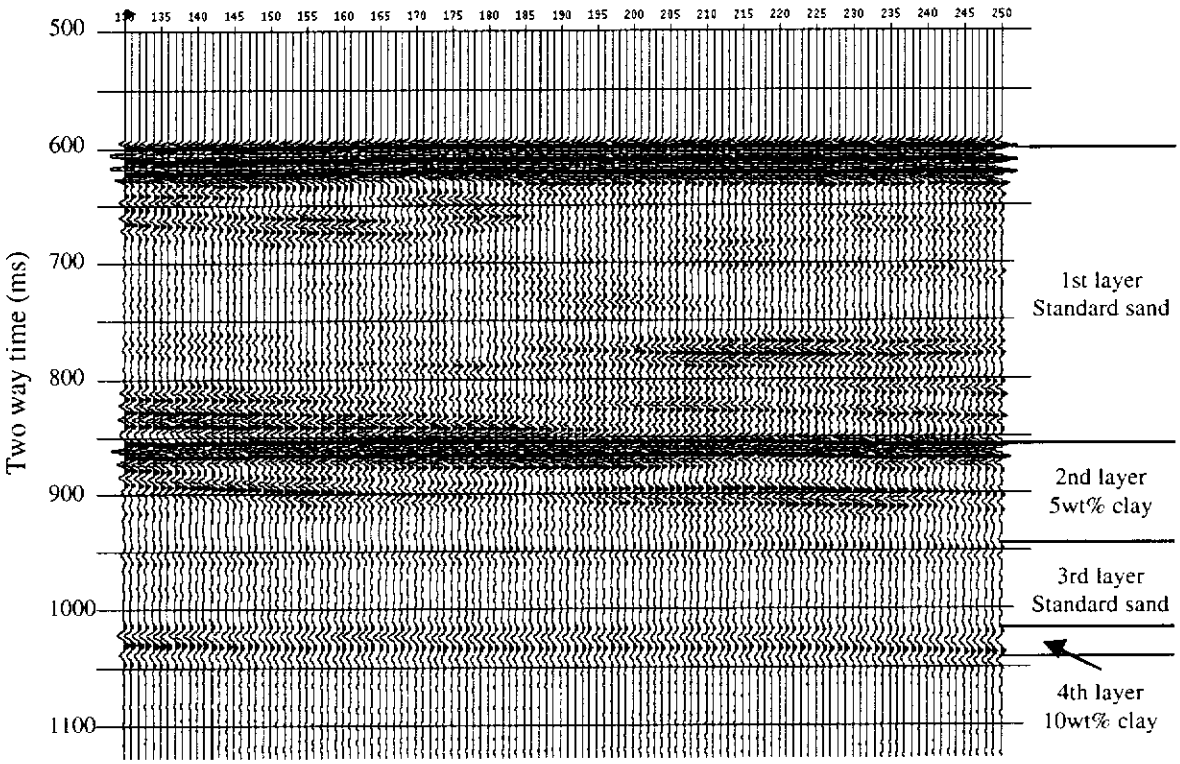

Figure 6.1: Seismic section of a sandbox model with four layer reflections. Tuning effects make it difficult to resolve the top and base of the fourth layer, which is only 2 mm (20 m) thick.

date in terms of the number of clearly imaged layers achieved. The deepest layer is just 2 mm (20 m) thick. The top and base reflections from this layer, at around 1020 ms and 1045 ms, are difficult to resolve due to interference between the two, known as 'tuning' effects. This is effectively the limit of vertical resolution.

6.2 Unconformity Models

Experiments with models comprising dipping layers had shown that dips of at least 10 degrees could be successfully imaged with zero-offset data acquisition. Various models were built comprising a sand layer with one horizontal and one dipping surface so that they form a wedge that pinches out within the model. These models were designed to introduce some geological complexity and show how a dipping reflection might affect the ability to image other reflections below it. They also illustrate the effects of tuning from the middle layer as it pinches out better than the previous multi-layer model shown in Figure 6.1.

Two configurations are shown below. The first model began with two thick horizontal layers. An 'angular unconformity' was then built in by grading away some of the model at an angle of 4°, cutting across the two layers so that the upper layer formed a wedge. A third layer of sand was then deposited on top of the unconformity so that the sand wedge pinched out below the unconformity. A schematic diagram of this model and the corresponding seismic image are shown in Figure 6.2. The second model began with just one horizontal layer, which was also graded at 4° to produce an angular unconformity similar to the first model. Two more horizontal layers of sand were then carefully poured onto the unconformity so that, this time, the middle layer pinched out above the unconformity. This model and its seismic image are shown in Figure 6.3.

The seismic data from both of these models clearly image the unconformities and pinch-outs. In addition they also show the stratigraphic nature of the sands onlapping the unconformity. Again this is a consequence of the way in which the sands are sorted

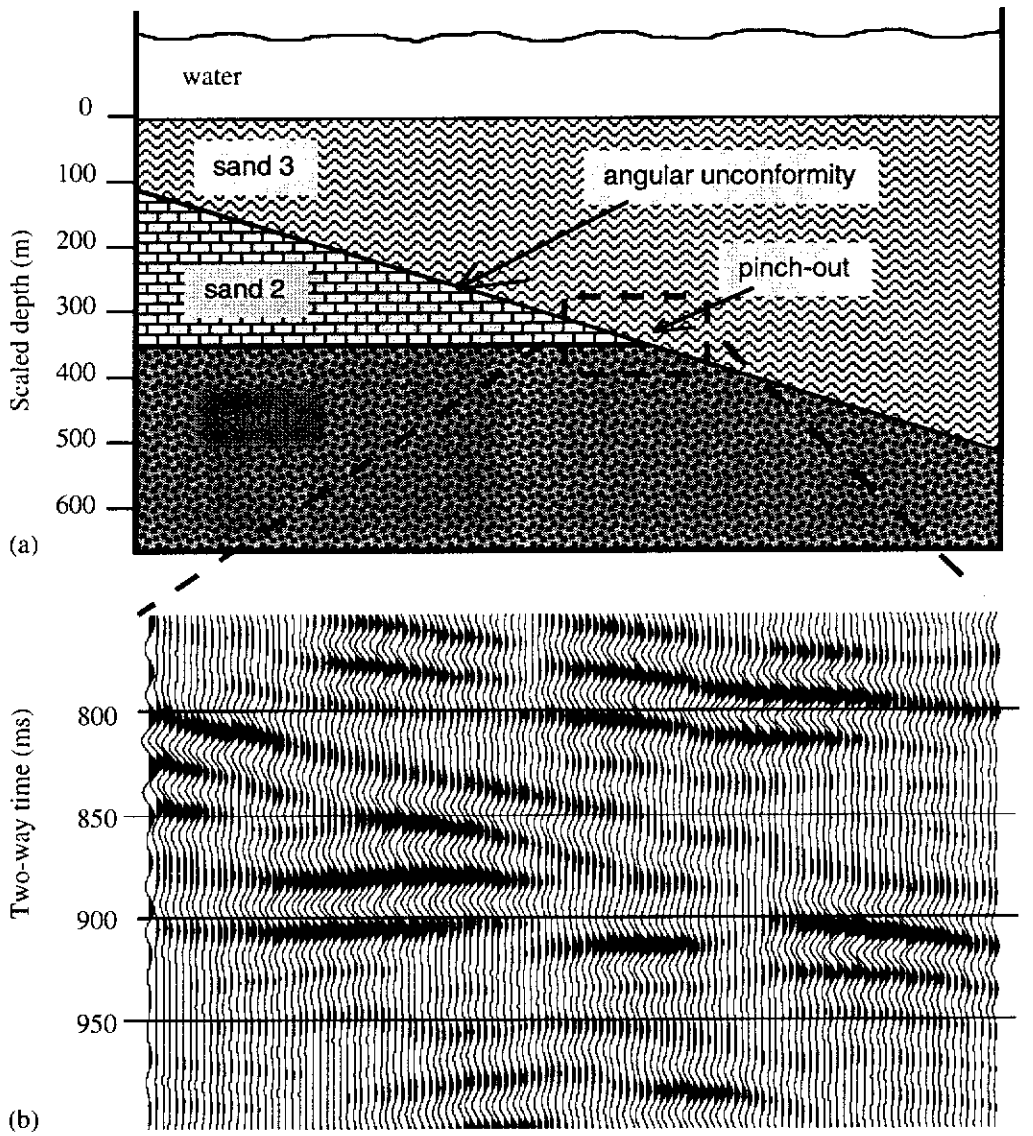

Figure 6.2: (a) Schematic diagram of sandbox model with an unconformity cutting across two layers to form a pinch-out. (b) Seismic section recorded over the pinch-out area of the model. Note the tuning effects as the middle layer thins below the limit of resolution.

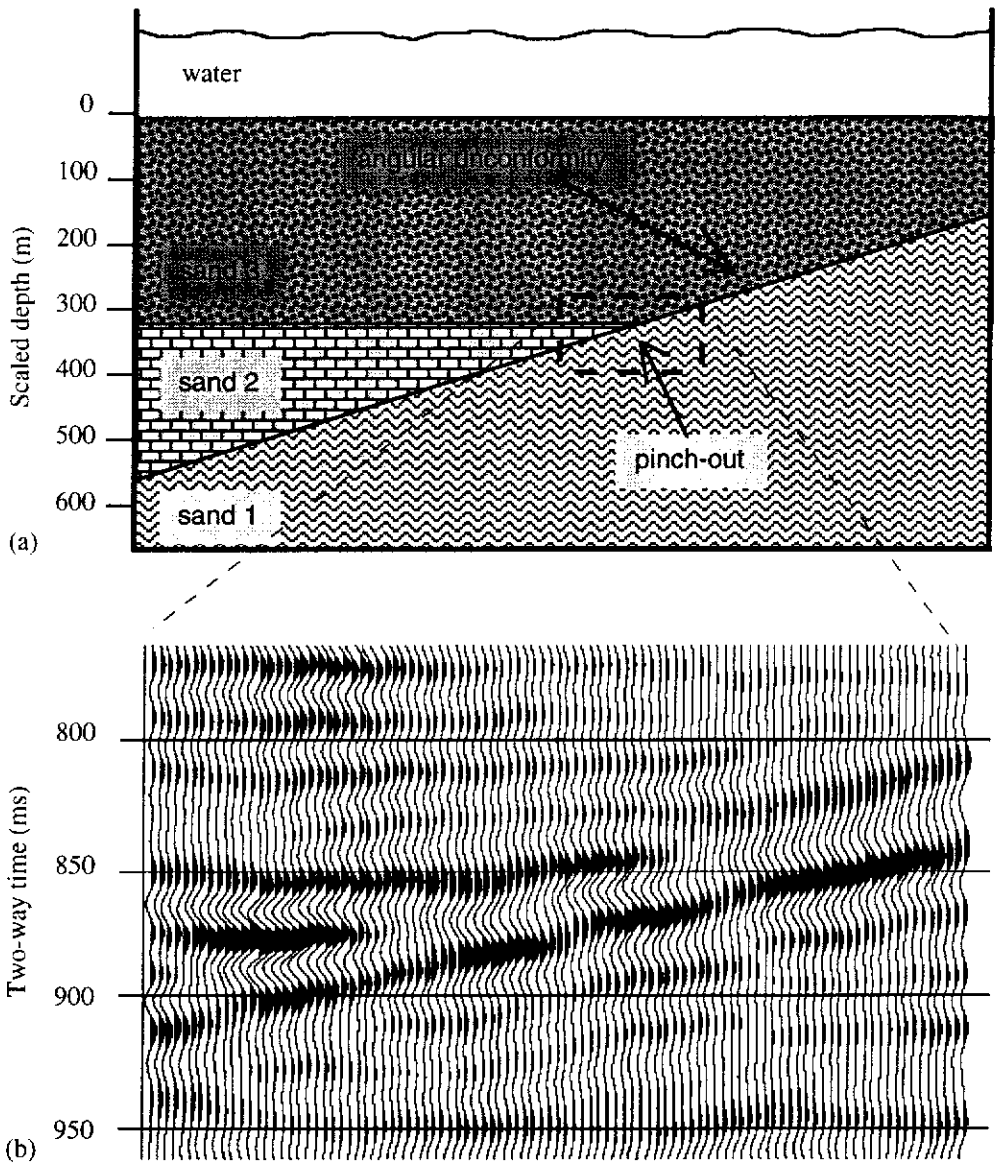

Figure 6.3: (a) Schematic diagram of sandbox model with two layers overlying an unconformity. (b) Seismic section recorded over the pinch-out area of the model.

as they are deposited. This illustrates the tremendous potential for using seismic to help interpret sandbox model structures.

6.3 Stratigraphic Models

As discussed in Chapter Five, seismic reflections can be produced within sandbox models from changes in grain size alone. These changes in grain size can be built into a model by sieving the sands into the desired grain-size distributions before depositing them into the model. Figure 5.29 showed that changes in packing induced by grading the horizons in the model are significant enough to produce a reflection. These reflections are analagous to stratigraphic reflections as there is no actual change in lithology, rather just a change in grain distribution. Similar reflections can be produced from models where the changes in grain packing are even more subtle. Figure 5.31 showed that the method of depositing the sand into the models can induce stratigraphic style reflections from changes in grain distribution within a sand layer that is homogeneous on a larger scale.

A model was designed to exploit this effect of natural sorting, to generate a coherent horizon reflection that could be mapped in three dimensions within a layer of the standard sand. A 3-D zero-offset survey was recorded over this model and the stratigraphic horizon was interpreted on the workstation. Figure 6.4 shows a 2-D line taken from the 3-D survey recorded over this model and the stratigraphic reflection has been interpreted (in white). This reflection is within a 10 mm (100 m scaled) thick layer of the standard sand. The top and base reflections from this layer are a result of contrasts in grain sizes between the layers and can be identified easily as strong flat reflections at around 780 ms and 960 ms (scaled two-way travel time). The stratigraphic reflection within the layer is purely a result of the grain distribution within the middle sand layer and unlike most of the other models in this thesis, cannot be attributed in any way to artificial processes such as manually grading the horizon into the model. This layer was deposited as two separate scoops of the standard sand and

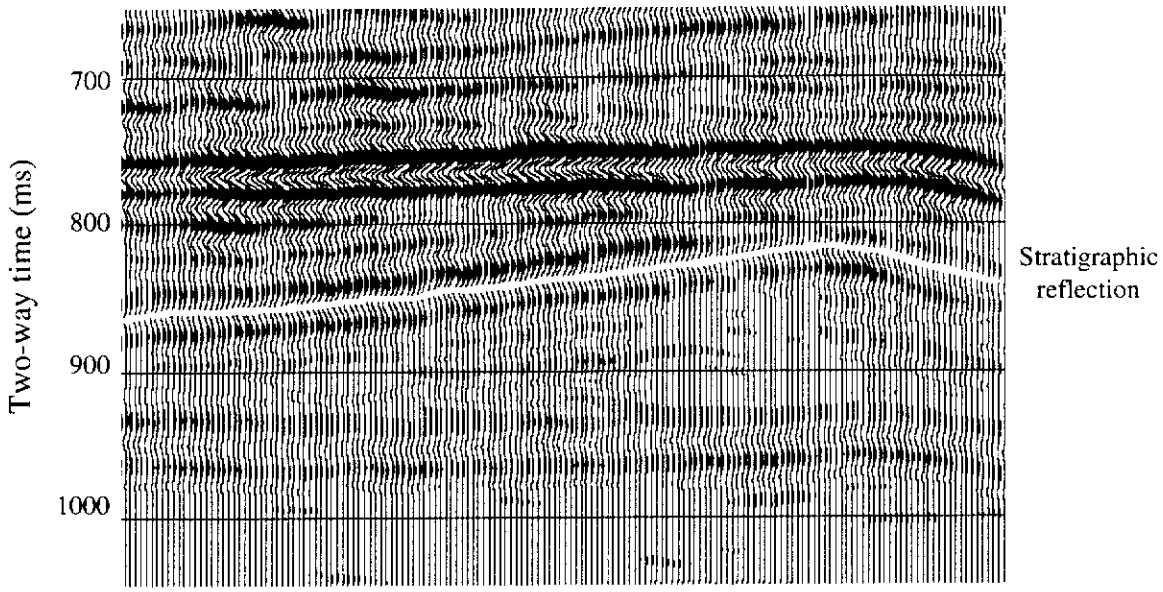

Figure 6.4: Seismic section of a sandbox model showing a stratigraphic type reflection that is produced by natural sorting of the grains as they are deposited in the model.

each scoop was sprinkled in slowly to induce two natural fining upwards sequences within the layer.

Figure 6.5 shows the 3-D interpretation of this model. The upper and lower flat horizons are the reflections from contrasts in grain sizes. The middle horizon is the stratigraphic reflection. This horizon represents the top surface of the first scoop of sand that was slowly sprinkled into the model.

6.4 Rift Models

The aim of the next model was to introduce some characteristics of conventional sandbox models to the reflection experiments, that is, to actively deform a model, while remaining as structurally simple as possible. In this way, the effects on the resultant seismic image may be analyzed without the ambiguity that exists in complex geological profiles. Figure 6.6 shows the apparatus used to produce a simple rift graben. The model has dimensions of 200 mm^2 (2 km^2) and a depth of 60 mm (600 m) and was designed to represent a thin shale horizon within a massive sandstone. A single 2 mm (20 m) thick 'shale' horizon, comprising a mix of 5wt% clay in sand, was deposited at a depth of 20 mm (200 m) in an otherwise pure sand model. A plastic sheet underlies half of the sand in the container and is attached to a moveable end-wall. As the wall was slowly extended by hand, a rift developed in the middle of the model, which was continuously infilled to simulate syn-rift sediments and to prevent the structure collapsing.

6.4.1 Zero-Offset 3-D Seismic Survey

A zero-offset 3-D seismic survey was recorded over this rift model. Figure 6.7 shows the 3-D interpretation of the middle 'shale' surface and the normal faults. The image clearly defines a rift graben bounded by normal faults. The position of these faults varies laterally along the strike of the graben, which is also seen on time slices of the

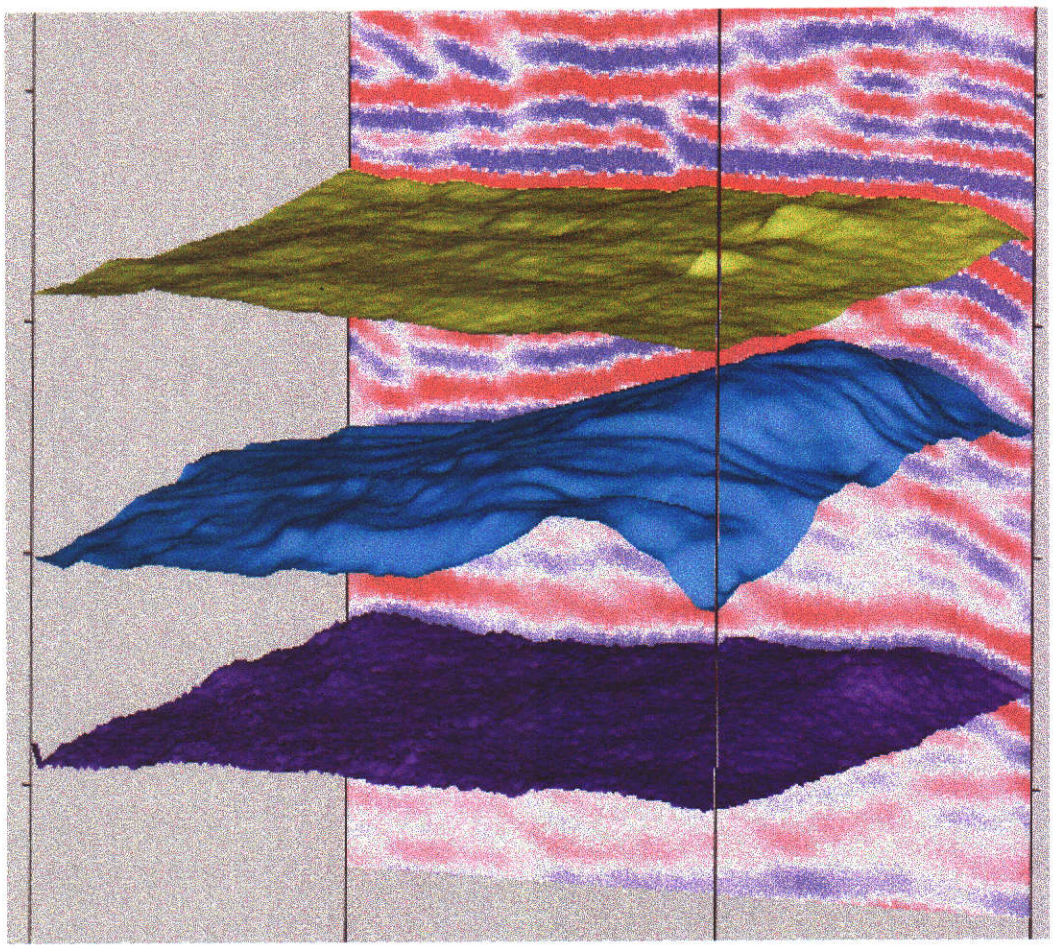

Figure 6.5: 3-D interpretation of the three reflecting horizons shown in Figure 6.4. The reflections from the upper and lower horizons are generated from a contrast in grain sizes between layers. The middle reflection is a result of natural sorting of the sand grains as they are deposited in the model.

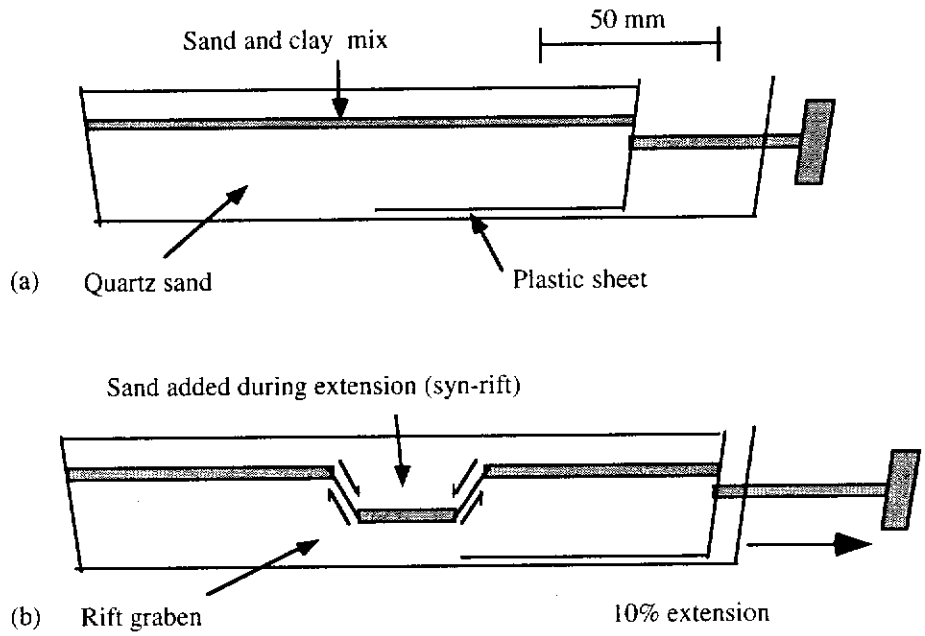

Figure 6.6: Schematic diagram of the apparatus used to generate a simple rift structure within a sandbox model. As the right end-wall is extended, extra sand is added to the graben as it forms, simulating syn-rift sedimentation and preventing the structure from collapsing.

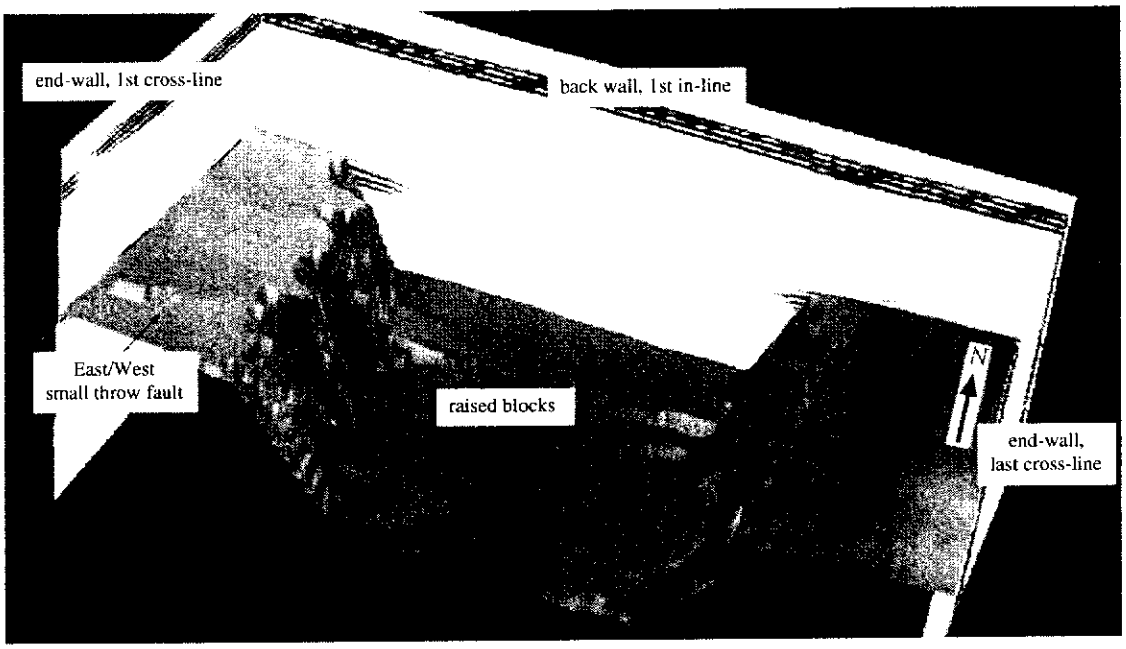

Figure 6.7: 3-D interpretation of the top of the 'shale' horizon in the rift model. Subtle features such as the raised blocks in the graben and the small-throw fault to the West were not apparent in the manually cut sections of the model.

model. Two small raised blocks are visible on the base of the graben which trend orthogonally to the strike of the rift, along with a small displacement fault which can be seen on the upper reflecting horizon to the west (north was chosen arbitrarily and is marked on the figure).

After the 3-D survey was recorded, the model was manually sectioned with a knife so that the model could also be interpreted in the same manner as conventional sandbox models. Sections from the model clearly reveal the gross form of the faults, but are unable to resolve the finer details of the model that are evident in the 3-D seismic image. The seismic image reveals features such as the degree of lateral variation along the strike of the fault, the small east-west fault on the horst block, and the two small raised blocks in the graben. Interpretation of this model with only conventional sectioning methods would mean that subtle details such as these would remain undetected.

6.4.2 Variable Offset 2-D Seismic Survey

A method of recording variable offset surveys was developed where the transducers are rotated with increasing offset such that they are always directed at the same CMP. This was demonstrated in Chapter Three with a model that comprised only a single horizontal layer reflection (see Figure 3.15). The same technique was applied to a rift model similar to the one above to test if this method is superior to zero-offset acquisition in terms of imaging geological structure. The model was built and deformed in the same manner as the example above but in this case the middle layer is a 10 mm (100 m) thick layer of very fine grained sand (63-90 μm) and does not contain any clay. The transducers were rotated such that they were focussed at a depth of 20 mm (200 m), which is the depth to the top of the very fine grained layer. As such, the reflection from the top of this layer should stack most effectively, with reflections above and below this depth being slightly out of focus. However, as shown in Chapter Three, these reflections should still stack fairly well, as the angle of incidence does not vary greatly for other reflections within the model.

Figure 6.8 shows a photograph and zero-offset seismic section from the second rift model. The photograph is of a section that was cut near the edge of the model and does not coincide exactly with the seismic sections. The section that corresponds directly with the seismic sections collapsed before a photograph could be taken. However, the photograph is representative of the gross form of the graben that is bounded by normal faults. The step on the left fault in the photograph is more pronounced than in the middle of the model where the seismic data were recorded. The zero-offset seismic data resolves the upper and lower boundaries of the fine grained layer very well where they are close to horizontal. However, the same boundaries are not resolved very well within the graben and the faults are very difficult to interpret.

The stacked variable offset seismic section that corresponds exactly to the zero-offset section in Figure 6.8 is shown in Figure 6.9a. The reflections from the layer boundaries within the graben have improved and a reflection from the original model surface that has moved down the faults as part of the graben is also evident. This reflection is also present in the zero-offset section but is difficult to interpret. The stacking of data recorded at different offsets has resulted in substantial diffractions from the faulted edges of the layers, which occurs with field data but is much less of a problem with zero-offset data recorded with directional transducers (see section 3.1.3). These diffractions can be collapsed with migration, which was applied post-stack to the variable-offset section and the result is shown in Figure 6.9b.

6.4.3 Images from Progressive Stages of Deformation

Deformation of conventional sandbox models is almost invariably performed while the models are dry, but another possibility of recording seismic at several stages of deformation would be to deform the model underwater. The response of analogue sandbox models is the same when deformed underwater, as long as the rate of deformation is slow enough such that the viscosity of the water does not influence the way sand grains are rearranged (B. Vendeville pers. comm. 1997). The rate of

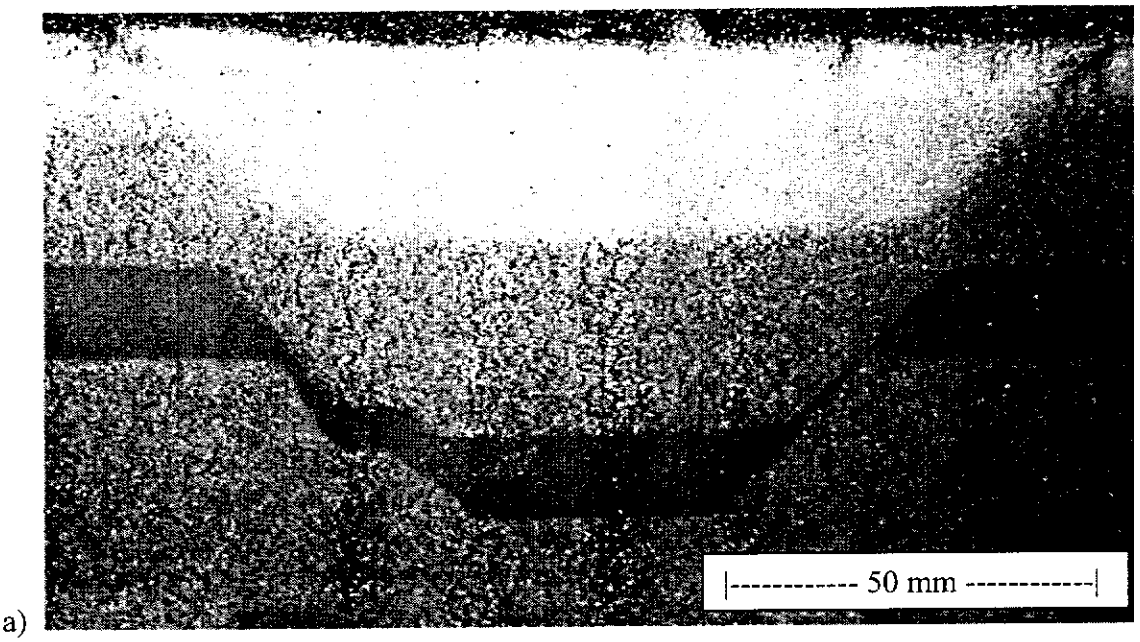

a)

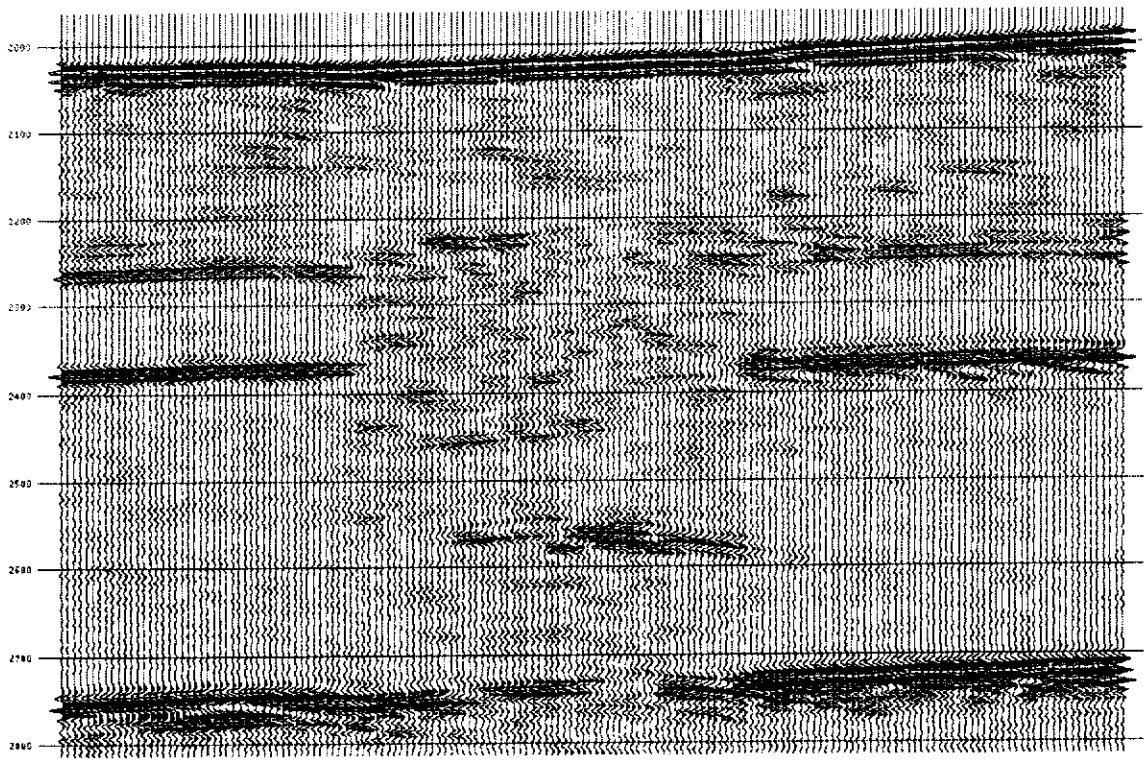

b)

Figure 6.8: (a) Photograph of a cross-section cut through a sandbox rift model. The middle layer is very fine-grained sand (63-90 μm). (b) Zero-offset seismic section from the same model shown in (a). The section in the photograph is not from the same line as the seismic section but illustrates the gross form of the graben.

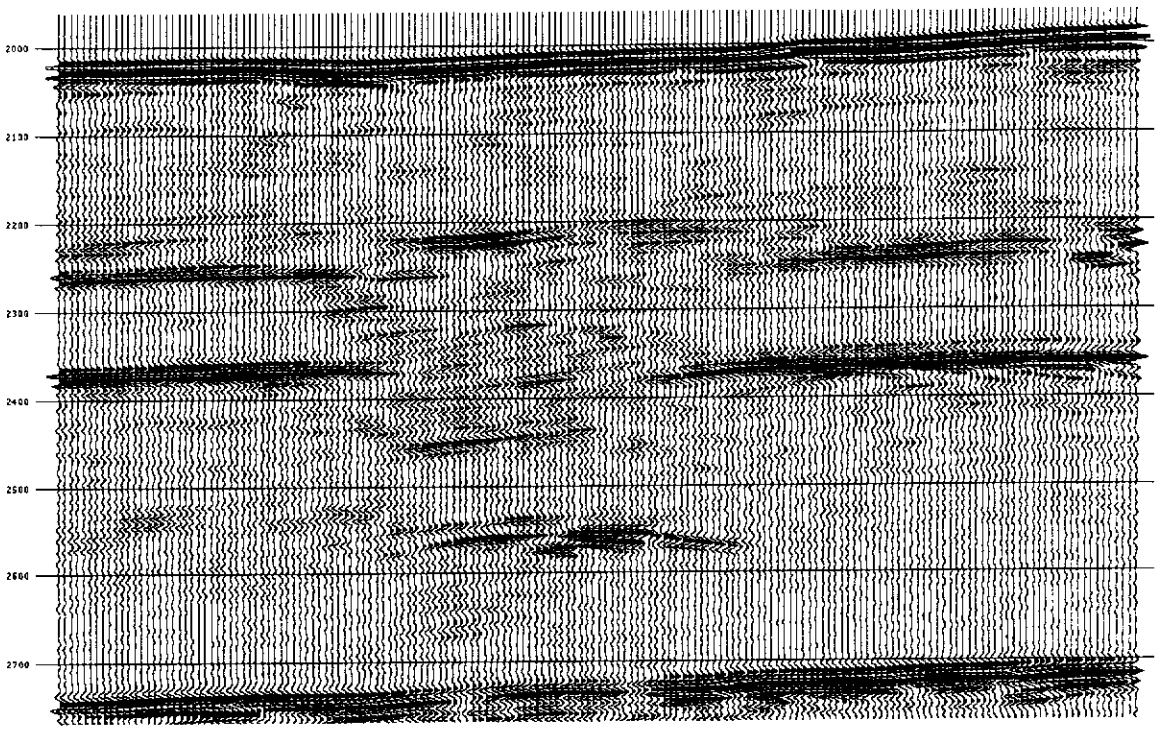

(a)

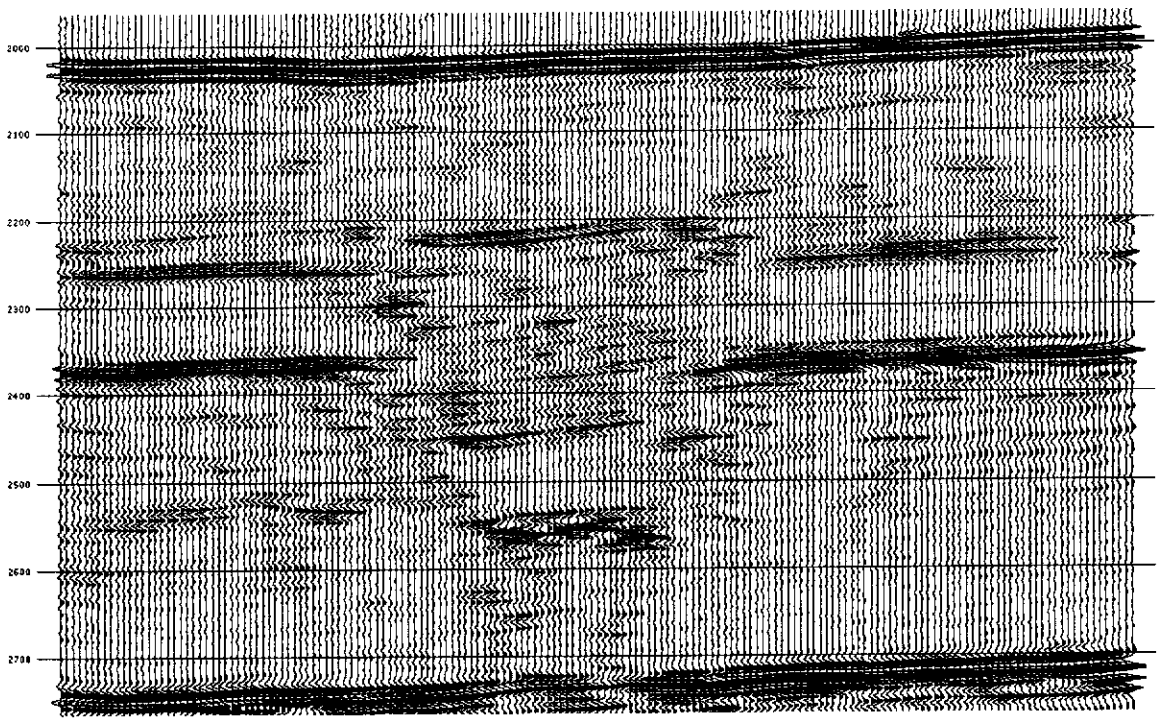

(b)

Figure 6.9: (a) Stacked variable-offset seismic section corresponding to the zero-offset section in Figure 6.8. (b) The same section shown in (a) after post-stack migration.

deformation can be controlled with stepper motors similar to the ones used to control the data acquisition.

Seismic data recorded over sandbox models at different stages of deformation would allow further insight to be gained from these models in terms of how faults are initiated, and how the rates of movement are transferred between related faults as the system develops. This is one of the potential benefits claimed for CT scanning of sandbox models and is, in a sense, time-lapse seismic on a geological time scale. To be able to follow the evolution of the structures would help considerably when the final structures prove very difficult to interpret. Images from stages of less complexity would indicate which faults are the most active at different stages, and would also ensure that some useful data were recorded, even if the final stages prove to be beyond the limit of resolution.

Further work is required to allow more complex faulting in sandbox models to be resolved. The main problem is that faulting rearranges the packing of the sand grains, which changes the seismic response. Further development of complex sandbox models would probably require the use of different materials that have genuine acoustic impedance contrasts, rather than rely on reflections caused by changes in grain packing at the interface alone. An example of where this might be immediately applicable would be salt diapir models such as those by Ge *et al* (1998).

6.5 Reservoir Models

The use of unconsolidated sand in seismic physical models allows different fluids to be incorporated for the first time. This also introduced the potential to develop the models for time-lapse experiments for fluid flow monitoring. The following examples illustrate the path of development towards this end.

6.5.1 Fluid-Only Traps

The aim of the following set of experiments was to test whether it is possible to image different fluid contacts and/or gas-fluid contacts within the seismic physical modelling environment. A simple apparatus was firstly built to trap gas and fluids under an anticlinal structure in a water tank, without the complications that come with using sand (Figure 6.10). The model was made from a partial sphere cut out of a vinyl ball, which was glued to a 150 mm diameter PVC pipe suspended in the water tank. In this case, a single transducer was placed under the trap rather than over the top of the model. This was done mainly for convenience, as it was easier to build the apparatus without having to worry about it getting in the way of the transducers. It was also felt that these models may have some relevance to reservoir monitoring via in-reservoir placement of geophones or hydrophones.

Four different situations were modelled, with the schematic diagrams and resulting seismic sections for each shown in Figures 6.11, which are:

1. Water only (Figure 6.11a): Results showed that only the edges of the anticline were imaged, which were reflections from the PVC pipe that was glued to the vinyl ball, and a small reflection from the top of the anticline which was possibly a small air bubble trapped under the ball. The rubber ball itself appeared to be acoustically transparent. However, a zero-offset section with recorded with directional transducers may not detect reflections due to ray path considerations.
2. Oil on water (Figure 6.11b): A small amount of oil was injected under the trap which floated on the surface of the water. This oil-water contact (OWC) was clearly imaged.
3. Air on oil on water (Figure 6.11c): Some air was then injected under the trap and results showed that both the air-oil contact (GOC for gas-oil contact) and the OWC were successfully imaged.
4. Oil filled to spill point (Figure 6.11d): More oil was added until it flowed out from under the trap and floated to the surface of the water tank. Again, both the GOC and OWC were well imaged.

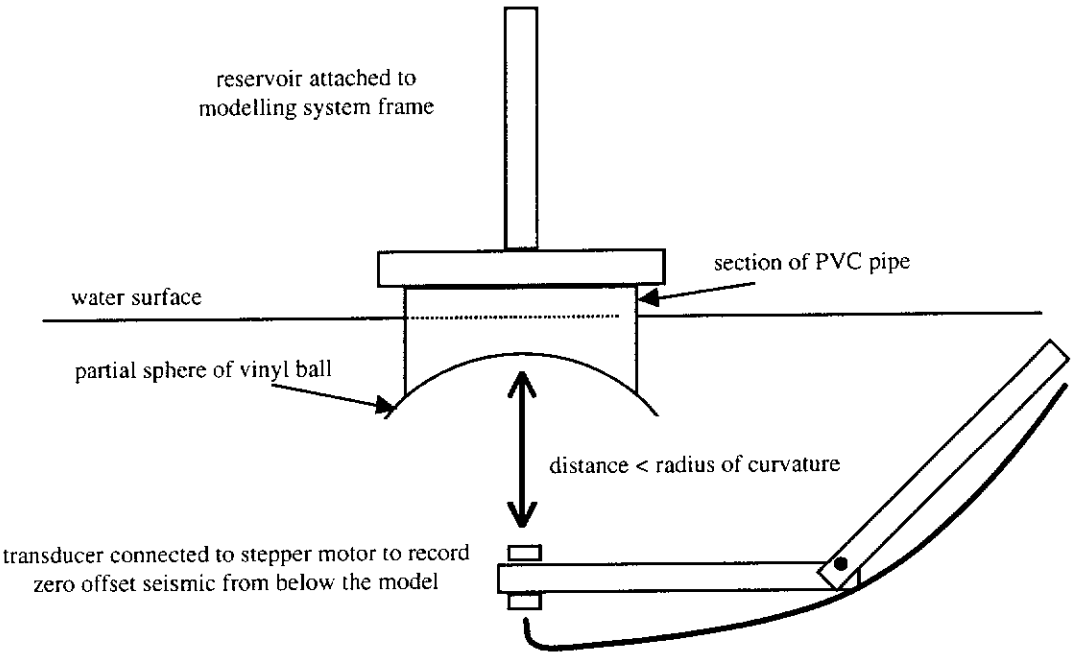

Figure 6.10: Schematic diagram of the apparatus used for the fluid models. The transducer is moved under the model to record reflections from the fluid and gas contacts under the anticline.

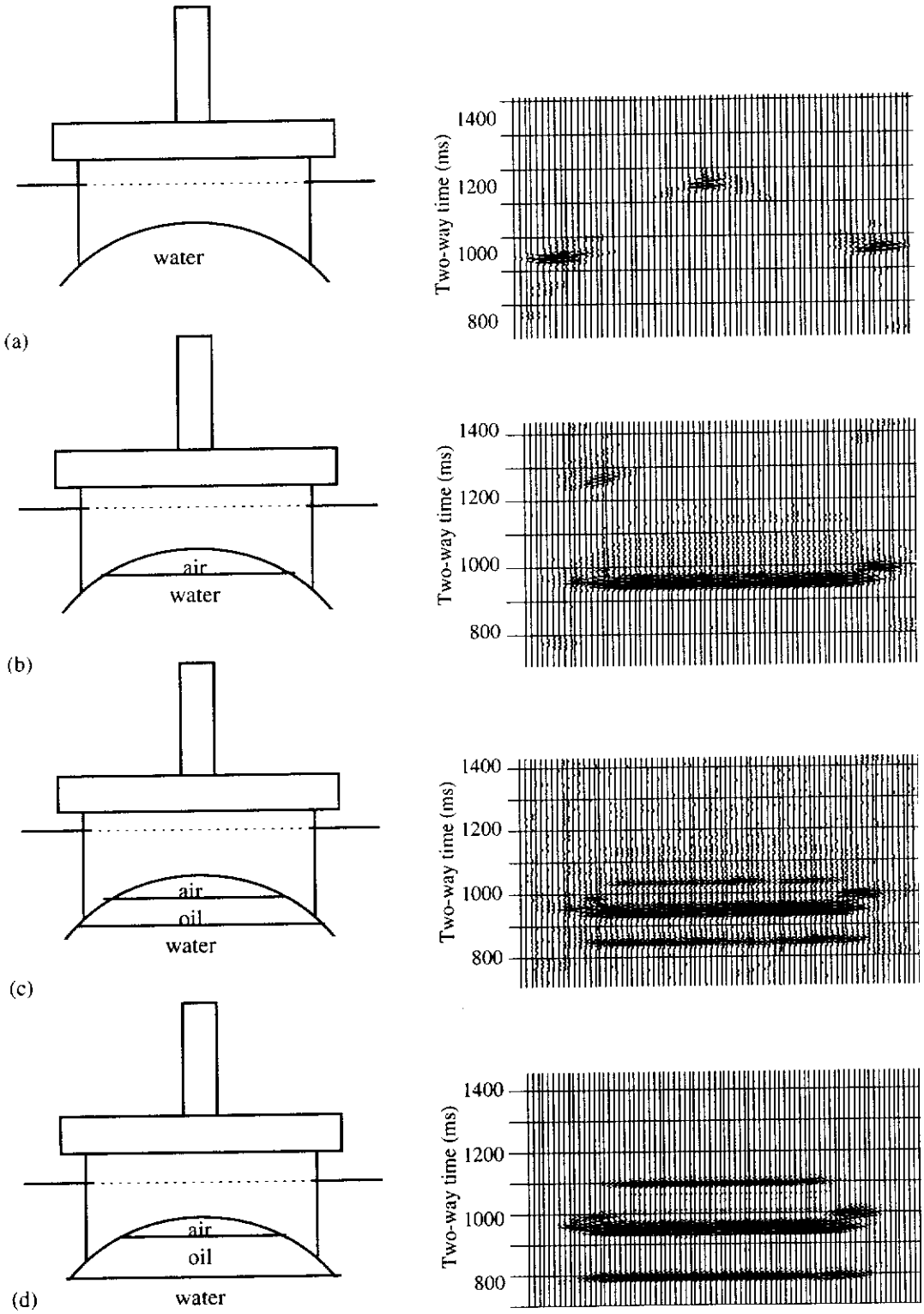

Figure 6.11: Four configurations of the fluid model and corresponding (inverted) seismic sections. (a) Water only. (b) Air injected under trap. (c) Oil added. (d) Oil filled to spill point.

6.5.2 Sand Traps

The successful imaging of the fluid and gas contacts in the previous example paved the way towards incorporating similar contacts within sandbox models. One of the problems first encountered when mixing clay with sand was its effect on reducing the permeability of the sand. This made it difficult to remove all of the air from the model when it was saturated and placed in a tank of water to simulate marine conditions. An antiformal 'gas trap' model was built to take advantage of this fact by using a clay and sand mix as a thin impermeable layer or 'shale' cap-rock overlying a sand anticline. As the model was saturated from the bottom upwards, a pocket of air was trapped under the anticline. The model and a 2-D seismic section recorded over it is shown in Figure 6.12. The seismic data shows a reflection from both the 'shale' layer and a reflection produced at the air/water contact. Interestingly, another seismic section recorded over the same model one month later revealed that this air-water contact was no longer present, which indicates that the 'shale' layer must have only been semi-permeable and that the air had slowly escaped from the model over time. This shows that potential now exists to develop these models further in terms of understanding the seismic effects of gas and fluid changes within a hydrocarbon reservoir over time.

6.6 Time-Lapse 3-D Models

The successful recording of seismic reflections within unconsolidated sands presents an opportunity to expand the role of physical modelling into the realms of the time-lapse 3-D (TL3-D) seismic method (Sherlock and Evans, 1999). This comes at a time when workers are predicting the demise of physical modelling due to the continual improvements in numerical modelling, even though numerical modelling is still very limited in its application to 3-D issues. In fact, in many ways, physical and numerical modelling are complementary rather than competing methods of reservoir simulation.

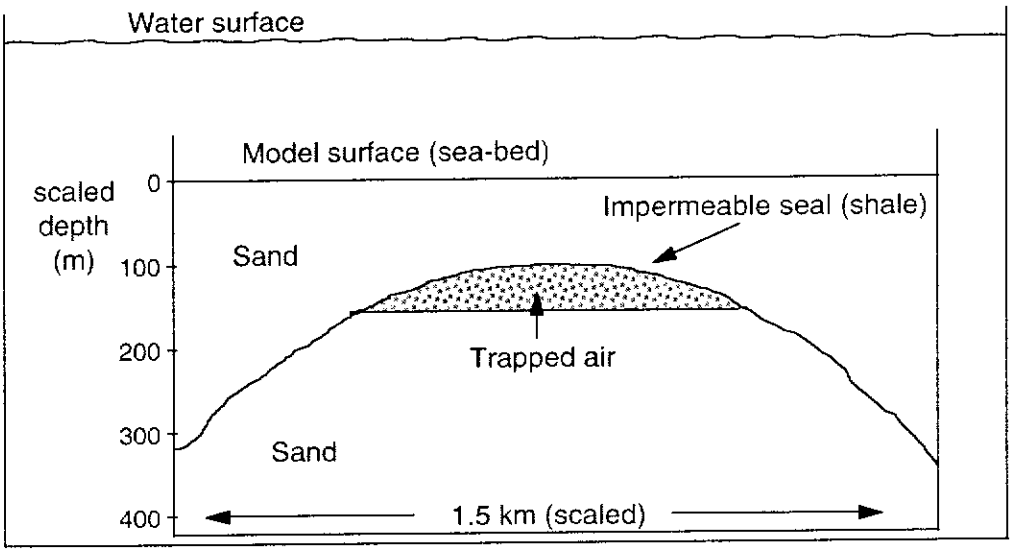

(a)

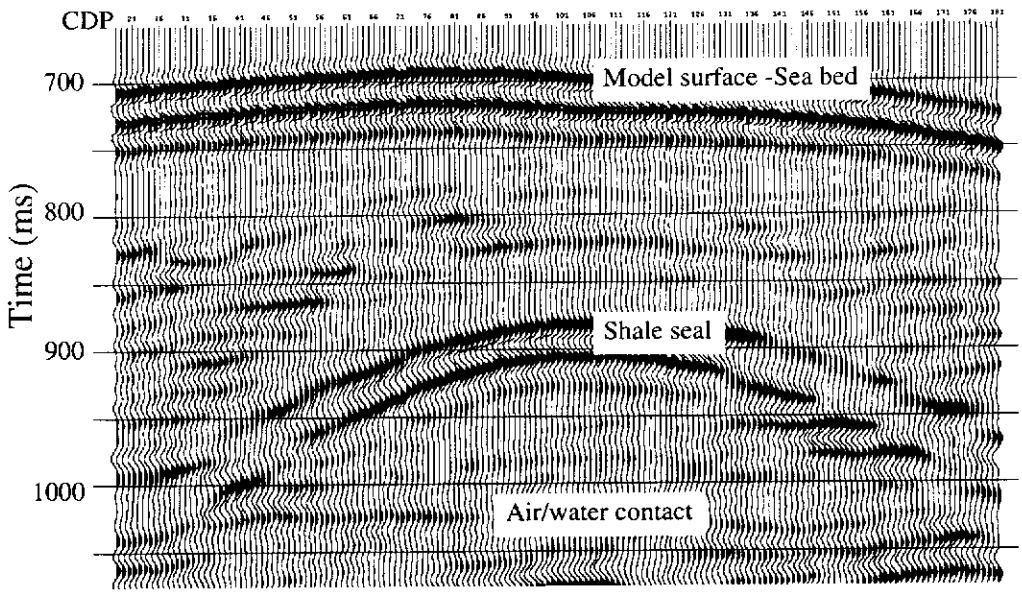

(b)

Figure 6.12: (a) Schematic diagram of sandbox gas-trap model. (b) Seismic section recorded over gas trap model showing a flat spot at the air water contact.

The computer-controlled physical modelling system allows superior acquisition repeatability to that possible in the field. Hence, most of the problems that plague field studies can be bypassed such that any anomalies seen on the difference sections can be directly attributed to changes that have occurred within the model. This makes it an ideal environment to study the time variant aspects of reservoirs that occur with hydrocarbon production. The development of 4-D seismic physical models will also provide a number of other advantages, which are:

1. The absence of complications from seasonal or climate factors.
2. Rapid data turn around in a matter of days, rather than having to revisit an area years later.
3. Potential to control the variations in fluid movement that occur within the model and compare the seismic interpretations against the known changes.
4. The ability to deliberately change acquisition parameters to test the effect on the resultant seismic difference volumes.

The most favourable reservoir conditions for a successful time-lapse study in the field are shallow, poorly consolidated reservoirs that undergo large changes in fluid saturation with production. These conditions allow for the greatest changes in seismic response and subsequently the best possible signal-to-noise ratio in the resulting difference sections. This is precisely the situation found in analogue sandbox models, providing an ideal starting point for physical time-lapse studies in the laboratory. As the technology progresses, models comprising more subtle changes can be developed.

Seismic physical modelling can also be tailored to reproduce problems encountered in the field when attempting to repeat a 3-D survey (Sherlock *et al.*, 2000). For example, it would be a simple matter to simulate undershooting a production platform that may not have been present when the first survey was recorded, to deliberately offset sail lines to simulate changes in streamer feathering, or change the temperature of the water to simulate a seasonal variation. The data recorded would then be ideal for testing the effectiveness of various matching filters and comparing them against the perfectly repeated data that could also be recorded over the same model. The size of the data

volumes recorded can also be tailored to minimise the memory requirements and increase computer speed. It is also possible to record as many surveys as desired over any one model to produce a series of difference volumes, which is another benefit of seismic physical modelling not afforded in the field.

6.6.1 Acquisition Repeatability

One of the biggest potential benefits of time-lapse physical modelling is avoiding the need for crossequalization of the two (or multiple) data sets. This removes any possibility that anomalies in difference volumes may be a consequence of the acquisition footprints or data processing and drastically reduces the cost and turn around time for TL3-D data. This is only possible, however, if the residual noise on the seismic physical modelling difference data is low relative to the changes in seismic response from fluid movement. Therefore, prior to the commencement of the TL3-D experiments, an initial feasibility study was required to test the repeatability inherent in the physical modelling acquisition system.

Tests of the modelling system repeatability were conducted by acquiring multiple 2-D seismic lines over a sandbox model without any changes to the model between surveys. Because the reflections in each seismic section should perfectly cancel on the 2-D difference section, any remaining amplitude on the difference section would be considered as residual noise. The relative amplitudes of the difference survey to the primary survey provide a measure of the repeatability, which can be expressed either as a percentage of the primary amplitudes, or as attenuation (in decibels).

The results of the first 'zero difference' test, comprising the differencing of two single fold, zero-offset 2-D sections recorded one after the other, showed that the average amplitude of the residual noise on the difference section was around 20 % of the primary survey (or 14dB down). While this is a very good result for unprocessed data, it is well below the repeatability achieved in successful TL3-D field case studies using crossequalization (eg. Altan *et al.*, 1999). The residual noise is almost entirely a result

of the imperfect cancellation of the signal, rather than being from ambient noise. The ambient noise on the primary seismic sections is very low and is mostly coherent. That is, it was reduced by almost 10 dB in the difference sections.

The first example of a time-lapse sandbox model was a pilot study built before any further refinements were made to the method of acquisition, and this was adequate to establish that such models were feasible. However, after this model, further tests were conducted to optimise the acquisition repeatability of the physical modelling system. These tests are presented below before the first time-lapse model is introduced.

6.6.1.1 Positioning

As discussed in Chapter Three, transducer movement in the physical modelling system is controlled by stepper motors. A test was conducted to determine the repeatability of the positioning of the transducers for multiple surveys. A laser pointer was mounted in the transducer bracket and a 3-D survey comprising 25 000 shot locations at 1 mm shot intervals (10 m scaled) was performed as a test for any cumulative error in the stepper motor positioning. After the survey was completed, the motors returned the pointer to the location of the first shot point and this was used to measure any change in position. Any error in positioning was imperceptible to the naked eye and must be less than 1 mm, which in scaled terms amounts to a maximum cumulative positioning error of 10 m in 250 km. This error is negligible relative to industry surveying standards and is unlikely to contribute significantly to the residual noise on the difference sections, given that the source has a diameter of 12 mm.

6.6.1.2 Acquisition Parameters

A number of acquisition tests were conducted to determine the optimum system settings to maximise repeatability. As before, the method used was to record two surveys over the same model without any changes. Comparisons between primary and difference

amplitudes were made with both the large model surface reflection and the ambient noise. Parameters tested were:

1. Number of shots per station (vertical summing): This improves the source signature repeatability at a cost of increased recording time and potential loss of some high frequency content.

2. Energy output: This is a compromise between high source energy, which is required for the production of reflections in highly attenuating sand, and source signature repeatability, which deteriorates at high energy levels due to distortion.

3. Damping: A damping resistor can be used to reduce the reverberation from the piezoelectric crystal at a cost of reduced energy output.

4. Dynamic range of A/D converter: This is a compromise between the resolution of the lower amplitude reflections and the amount of 'clipping' that occurs with the high amplitude reflections, such as that from the model surface.

6.6.1.3 Vertical summing

A series of repeated zero-offset seismic lines were recorded over a physical model to test the source signature repeatability of the physical modelling system. Each primary survey comprised 30 stations at 1 mm (10 m scaled) intervals and varied in the number of shots fired and summed at each location. This was done for both the maximum energy output setting (level 4) and at a reduced energy setting (level 3). The surveys were then repeated and subtracted from the corresponding primary surveys. The remaining amplitudes on the difference sections, or 'residual noise', were purely a result of imperfect cancellation between the primary and secondary surveys because no changes occurred in the model. The reduction in amplitudes from primary to difference survey was used to quantify the level of repeatability, and could be expressed as attenuation (in decibels) or as a percentage of the primary amplitudes.

Table 6.1 presents a summary of the average RMS amplitudes for both ambient noise and model surface reflection for the series of repeated 'zero difference' 2-D seismic lines. Vertical summing increases the amplitudes of both the noise and the surface reflection from the model with no change to the signal-to-noise ratio (SNR). However, summing does result in a large improvement in the difference section, with residual noise improving from 11 dB for a single shot per station, to almost 29 dB for 100 shots per station. Figure 6.13 shows the relationship of residual noise as a percentage of primary reflection amplitude relative to the number of shots summed. The improvement in source repeatability with vertical summing is approximately proportional to, but slightly less than, the square root of the number of shots summed per station. This is consistent with the principle that the SNR improves as the square root of fold.

It was now possible to choose the required level of source signature repeatability keeping in mind the extra time and memory required to shoot each survey, as this can be prohibitive with large 3-D surveys.

6.6.1.4 Energy Output

From Table 6.1 it is apparent that there is a reduction in residual noise with the lower energy output setting. The signal strength is set via an external trigger box, having energy levels of 14 to 94 μjoules, adjustable in four steps. Up to this point, all of the models in this thesis were recorded with the energy output set to maximum due to the high rate of attenuation in the unconsolidated sand. It appears that the maximum power setting causes some distortion of the output signal, deteriorating the repeatability. Experiments were conducted to test the repeatability as a function of source energy.

Table 6.2 shows the results from 'zero difference' sections recorded at different energy levels. The surface reflection amplitudes for energy levels 3 and 4 are very similar, as are the amplitudes for levels 1 and 2. The improvement in the attenuation of the reflection from differencing, however, appears to improve linearly with reduced power. The data for energy levels 1 to 3 were recorded on a separate day to the data for level 4.

Energy setting	4	4	4	3	3	3	3
Number of shots per station	1	5	20	1	5	20	100
Noise before differencing	262	577	1140	253	562	1120	464
Reflection before differencing	24200	53300	106000	23600	51700	103000	226000
RMS signal-to-noise	**92**	**92**	**93**	**93**	**92**	**92**	**488**
Noise before differencing	262	577	1140	253	562	1120	464
Noise after differencing	27.8	28.6	33.5	26.8	26.9	27.9	101
Percentage of original	**10.6**	**5.0**	**2.9**	**10.6**	**4.8**	**2.5**	**21.8**
Noise attenuation (dB)	**19.4**	**25.9**	**30.6**	**19.4**	**20.9**	**31.9**	**12.1**
Reflection before differencing	24200	53300	106000	23600	51700	103000	226000
Reflection after differencing	6730	6910	7310	6130	4350	5580	7910
Percentage of original	**27.8**	**13.0**	**6.9**	**25.9**	**8.4**	**5.4**	**3.5**
Reflection attenuation (dB)	**11.1**	**17.7**	**23.1**	**11.7**	**21.4**	**25.3**	**28.8**

Table 6.1: Amplitudes of reflections and noise on seismic physical modelling before and after differencing sections as a function of number of shots summed per station. Vertical summing improves the repeatability of the seismic data resulting in lower residual amplitudes on difference sections.

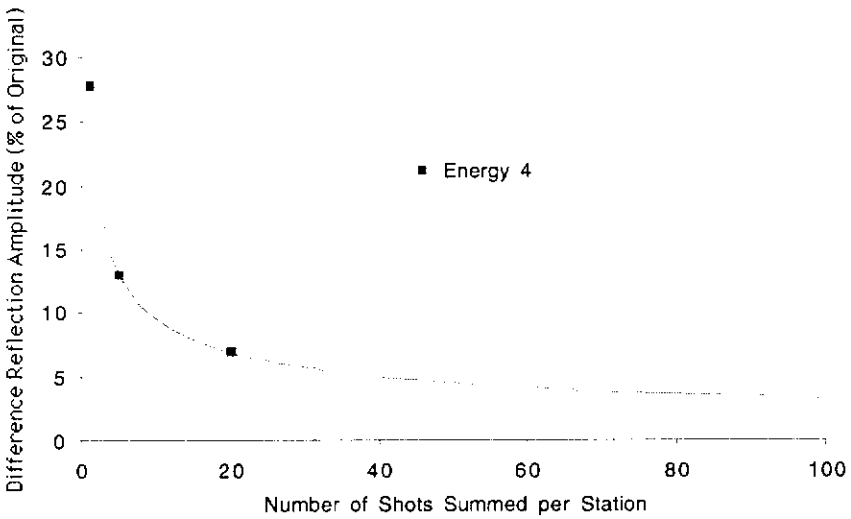

(a)

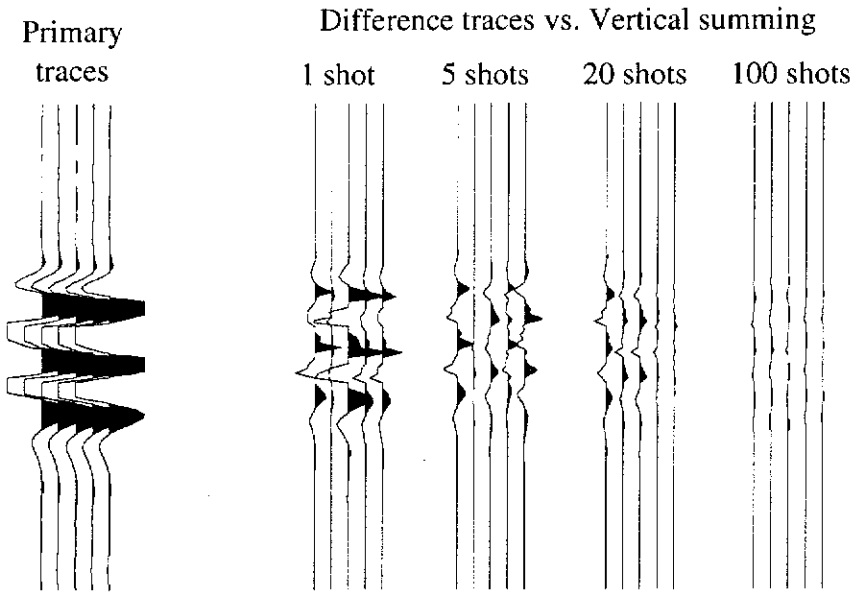

(b)

Figure 6.13: (a) Attenuation of reflection amplitudes on seismic difference sections as a function of number of shots summed per station. The line of best fit is a least squares power curve. (b) The seismic traces used to calculate the graph in (a). The traces show the reflection amplitudes from the difference sections as a function of number of shots summed per station relative to the primary reflection.

Energy setting	4	3	2	1
Number of shots per station	1	1	1	1
Noise before differencing	262	44.9	39.4	39.1
Reflection before differencing	24200	23100	14600	14500
RMS signal-to-noise	**92**	**516**	**371**	**371**
Noise before differencing	262	44.9	39.4	39.1
Noise after differencing	27.8	34.5	33.5	31.6
Percentage of original	**10.6**	**76.8**	**85.1**	**80.6**
Noise attenuation (dB)	**19.4**	**2.3**	**1.2**	**1.9**
Reflection before differencing	24200	23100	14600	14500
Reflection after differencing	6730	5600	3310	3021
Percentage of original	**27.8**	**24.2**	**22.6**	**20.8**
Reflection attenuation (dB)	**11.1**	**12.2**	**12.8**	**13.6**

Table 6.2: Attenuation of residual noise on difference sections as a function of transducer energy output. Noise levels are much greater for the maximum energy setting. However, the noise is coherent and cancels effectively in the seismic difference sections. The maximum energy setting is preferred for the unconsolidated sand models due to the high rate of attenuation.

The ambient noise in these three records is lower than in all other data sets and is anomalous. This is perhaps a result of a change in external interference between the two days (two weeks apart) that most of these tests were done. This noise is not greatly attenuated in the difference section and is, therefore, random. The ambient noise in most of the other seismic sections recorded for the parameter tests is much higher, but is attenuated by the differencing and must therefore be coherent.

The choice of energy setting ultimately depends on the requirements for the survey. The lower energy settings are inadequate for the time-lapse sand models in this thesis, but a reduction in energy to level 3 provides a worthwhile improvement in source repeatability without compromising the resulting seismic images.

6.6.1.5 Damping and Dynamic Range

A damping resistor on the pulser unit can be used to attenuate the reverberations of the source wavelet, although at considerable expense in terms of energy output. The voltage range of the oscilloscope and A/D converter can also be set to optimise the resolution of the digitally sampled signal. This range is usually set such that the highest reflection amplitudes from the model surface are clipped. This is done to improve the digital sampling of the subsurface reflections within the models, as these are generally much lower in amplitude than the surface reflection. However, it was thought that the clipping of the surface reflection may result in imperfect subtraction of the traces between time-lapse surveys.

A series of tests were then performed to quantify the effects of different damping and dynamic range settings on the acquisition repeatability. Table 6.3 shows a summary of the results. There is minor improvement in the differencing results with the damping resistor set to 5 (half) compared with no damping. However, this also reduces the primary amplitudes and SNR by around 40%, and so is not a valid option. Doubling the setting of the A/D converter (from 3V to 6V, peak to peak) effectively halves the reflection amplitudes, although not quite that for the high amplitude surface reflection. This is because the surface reflection is clipped at the lower setting but the full

	Single shot per station			20 shots per station	
	Standard	+ damping	+inc. range	Standard	+ both
Energy setting	4	4	4	3	3
Damping resistor setting	0	5	0	0	5
Dynamic range of recording system	P-P 3V	P-P 3V	P-P 6V	P-P 3V	P-P 6V
Number of shots per station	1	1	1	20	20
Noise before differencing	262	251	269	1130	1210
Reflection before differencing	24200	15700	15000	103000	24800
RMS signal-to-noise	**92**	**63**	**56**	**92**	**20**
Noise before differencing	262	251	269	1130	1210
Noise after differencing	27.8	26.7	18.7	27.9	16.0
Percentage of original	**10.6**	**10.7**	**6.9**	**2.5**	**1.3**
Noise attenuation (dB)	**19.4**	**19.3**	**23.1**	**31.9**	**37.6**
Surface reflection before differencing	24200	15700	15000	103000	24800
Surface reflection after differencing	6730	3480	3830	5580	1260
Percentage of original	**27.8**	**22.1**	**25.6**	**5.4**	**5.1**
Reflection attenuation (dB)	**11.1**	**13.0**	**11.7**	**25.3**	**25.9**

Table 6.3: Attenuation of residual noise as a function of source damping setting and dynamic range of A/D converter. Increased damping and dynamic range results in a minor improvement in differencing but reduces the reflection amplitudes. Furthermore, the improvement is lost when the data is vertically summed.

waveform is sampled at the higher setting. However, the ambient noise level remains roughly constant regardless of dynamic range, which means the slight improvement in differencing at higher settings comes at the expense of a reduced SNR and reduced resolution of the subtle low amplitude reflections in the models.

Table 6.3 also shows that the improvement from damping and increased dynamic range on the difference sections is less evident on data that has been vertically summed, and the reduction in SNR is much worse. It was decided that the best compromise was to stay with the original settings of no damping and a dynamic range of 3V.

6.6.2 Data Processing

Although this research does not deal with data processing issues or attempt crossequalization to match time-lapse data sets, there are two simple steps that can be used to improve the matching of two 'identical' physical model seismic lines, without altering the waveform or relative amplitudes. These processes are 'data resampling' at finer intervals and 'trace mixing'. A bulk static shift of one or two samples was sometimes necessary to match up the surface reflections in two-way travel time before differencing. This was attributed to slight changes in water temperature (less than 1°C) between time-lapse surveys. The bulk static shift is an effective but crude method of aligning such events. Larger variations in water temperature would require the data on one survey to be 'stretched' or squeezed' to adjust for the velocity changes between surveys.

6.6.2.1 Resampling

The sample rate of the physical modelling data was 0.1 μs (1 ms scaled). Resampling to finer intervals of 0.5 and 0.25 ms (scaled) did not change the recorded amplitudes of the ambient noise or surface reflection, but did improve the matching between data sets slightly (Table 6.4).

Energy setting	4	4	4
Number of shots per station	1	1	1
Sample rate	1ms	0.5ms	0.25ms
Noise before differencing	262	262	262
Reflection before differencing	24200	24200	24300
RMS signal-to -noise	**92.5**	**92.6**	**92.9**
Noise before differencing	262	262	262
Noise after differencing	27.8	26.0	25.8
Percentage of original	**10.6**	**9.9**	**9.8**
Noise attenuation (dB)	**19.4**	**20.0**	**20.1**
Reflection before differencing	24200	24200	24300
Reflection after differencing	6730	6550	6520
Percentage of original	**27.8**	**27.1**	**26.8**
Reflection attenuation (dB)	**11.1**	**11.3**	**11.4**

Table 6.4: Attenuation of residual noise as a result of digitally resampling the data at finer intervals.

6.6.2.2 *Trace Mixing*

Trace mixing is often used in industry as a means of smoothing the amplitudes across a seismic section, thereby removing random spikes and reducing noise levels. It involves, in this case, calculating the median amplitude of one trace with one or more adjacent traces on either side. Table 6.5 shows the improvement possible by applying a five trace median mix to the data before and after the data are merged, prior to differencing. Trace mixing the data after the two surveys have been merged smooths any differences in amplitude or misalignment of events between two surveys and, therefore, improves the attenuation of the reflections in the difference sections. However, this could also reduce any anomalies in difference sections from fluid flow because it is mixing "before" and "after" data and, therefore, is clearly inappropriate.

Trace mixing before the data sets are merged also improves the differencing results, and is effectively a similar process to vertical stacking for the surface reflection. This is because the adjacent traces should not vary significantly, assuming that the surface is horizontal and laterally invariant. However, it also has the effect of 'smearing' the data and reducing the horizontal resolution. It was decided that this was an unnecessary compromise, given the level of repeatability possible without trace mixing.

6.6.3 Time-Lapse 3-D Reservoir Models

Visual experiments of oil migration in water saturated sand have been investigated in one-dimension through vertical glass columns (Dembicki and Anderson, 1989; Catalan *et al.*, 1992), and in two-dimensions (Thomas and Clouse, 1995), which also utilized ultrasonic transmission times to help identify the oil pathways. The idea for the following models was similar in concept to the above examples. However, it used the two-way reflection method developed here, rather than the one-way transmission method of the above examples, which can only identify changes in velocity. In this way, it was extended to the three-dimensional case to map changes in saturation in

Energy setting	4	4	4	4
Number of shots per station	1	1	1	1
Median trace mixing (5 traces)	none	pre-merge	post-merge	pre- and post
Noise before differencing	262	261	259	258
Reflection before differencing	24200	24200	23500	23500
RMS signal-to -noise	**92.5**	**92.7**	**90.8**	**91.1**
Noise before differencing	262	261	259	258
Noise after differencing	27.8	17.0	9.4	11.1
Percentage of original	**10.6**	**6.5**	**3.6**	**4.3**
Noise attenuation (dB)	**19.4**	**23.6**	**28.7**	**27.2**
Reflection before differencing	24200	24200	23500	23500
Reflection after differencing	6730	4440	2100	1790
Percentage of original	27.8	18.3	8.9	7.6
Reflection attenuation (dB)	**11.1**	**14.7**	**20.9**	**22.3**

Table 6.5: Attenuation of residual noise with trace mixing applied before and after the two data sets are merged, prior to differencing.

different layers using interval velocities, rather than being restricted to the single layer case in the above examples.

Once developed, this technique could be extended to monitor models of true hydrocarbon recovery processes such as the models of water flooding by Rapoport (1958) and steam injection by Kimber and Farouq Ali (1991), which have also been restricted to 2-D.

6.6.4 Example 1 – Pilot Study

The example shown in Figure 6.14 (a) and (b) is from one of the first attempts to record time-lapse 3-D seismic data from a sandbox model, which was built before all of the parameter tests presented in the previous section were performed. This model was similar to the one used to record the seismic data shown in Figure 6.12, but in this case a syringe filled with air was mounted under the model container so that air could be injected into the model between surveys. As the air was injected it migrated up through the sand to create a gas chimney. Figure 6.14 (a) is a view of the pre-injection 3-D zero-offset seismic volume. The low amplitudes in the data have been rendered translucent to allow a visualisation of the data volume. Figure 6.14 (b) is the corresponding image of the 3-D difference survey, which was produced by subtracting traces of the post-injection survey from the corresponding traces of the pre-injection survey.

The images shown in Figures 6.14 are physical model data that have had no processing applied other than a gain function to compensate for the rapid absorption of energy that occurs in unconsolidated sand. Without crossequalization, differencing of the pre- and post-injection survey results in amplitudes other than near the injection site equal to around 20% of the primary surveys. These amplitudes are mostly a result of noise and can be seen to increase with time as the signal-to-noise ratio deteriorates. The high amplitudes seen in the middle of the volume in Figure 6.14 (b) are a direct result of the

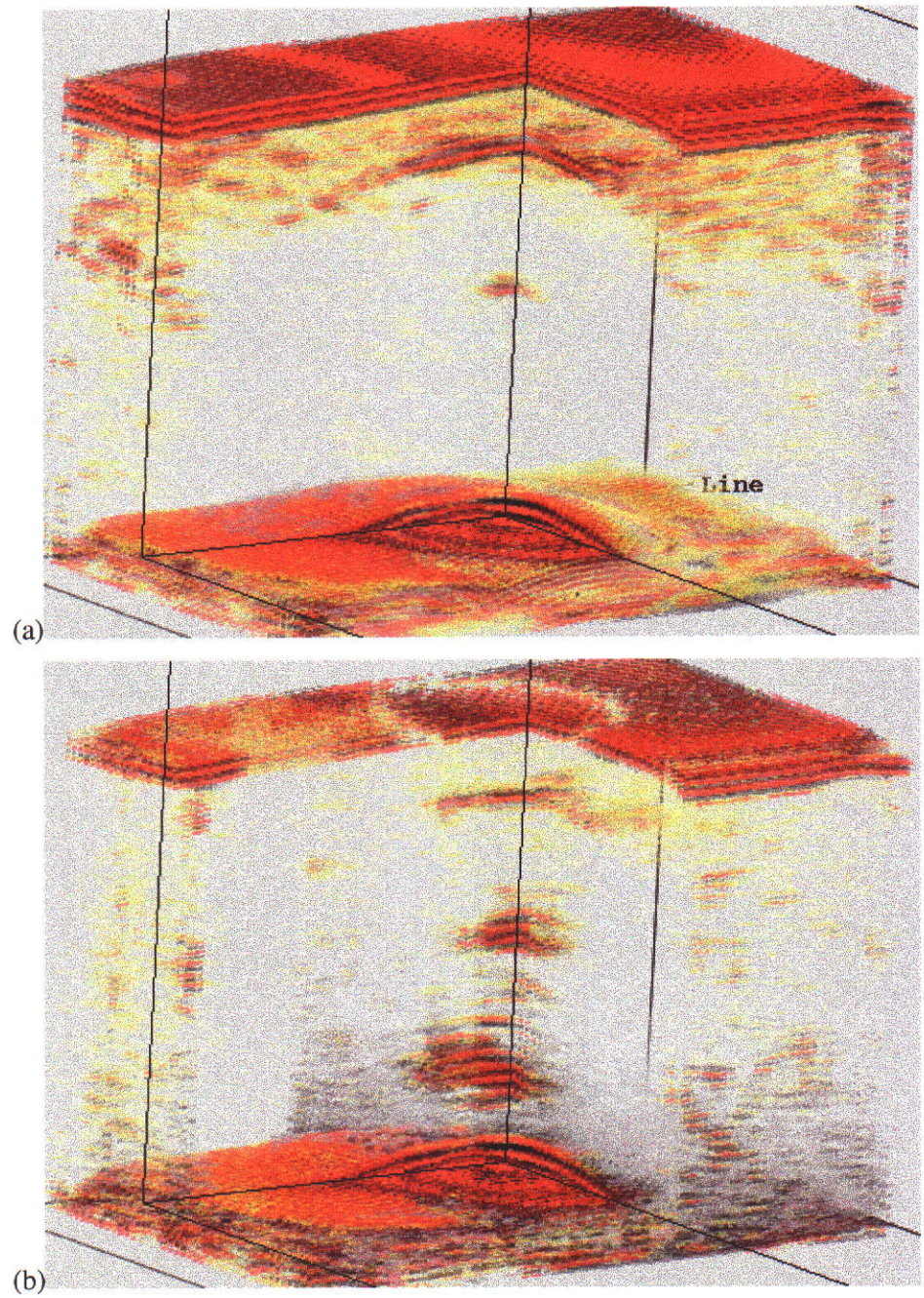

Figure 6.14: (a) 3-D visualisation of seismic data volume prior to injection of air. The low amplitudes are translucent to allow a view into the volume. (b) 3-D visualisation of the difference volume, produced by subtracting the 3-D data recorded after air injection from the pre-injection data. The high amplitudes in the middle of the difference volume is the 'gas chimney' created by the injected air.

air being injected from underneath the model and migrating up through the sand to form a gas chimney.

The injection of air caused the model surface to bulge upwards. This caused the surface reflections on the pre- and post-injection surveys to misalign in time. The effects of this on the difference volume can be seen in Figure 6.14 (b), where the amplitudes of the surface reflection are still high due to imperfect cancellation when the second volume was subtracted from the first. In addition, a 'ring' appears on the surface reflection that illustrates how the model has bulged directly over the gas zone.

6.6.5 Example 2 – Kerosene Flow Model

An improved model was designed with a 10 mm (100 m scaled) deep acrylic top layer to prevent a change in model dimensions from occurring with fluid injection, as shown in Figure 6.15 (a) and (b). The scaled dimensions of the model were 1.5 km x 0.8 km x 1.0 km. The top solid layer overlies two layers of unconsolidated sand. The lower sand layer was 50 mm (500 m) thick at the thickest end and dips downwards at an angle of 10 degrees. The lower sand was very well sorted with grain sizes between 200 μm and 250 μm. It had a porosity of 39% and the permeability was around 14 Darcies. The upper sand was the standard moderately sorted sand with an average grain size of 200 μm, 37% porosity and permeability around 9 Darcies. The dipping interface between the two sands was a semi-permeable boundary that may influence the fluid migration pathway. This interface produced a weak reflection from the small contrast between the two sands. The two reflections from the water/acrylic and acrylic/top sand interfaces, plus the reflection from the base of the model, were much stronger.

The model was saturated with boiling water through a pipe at one end of the model. Tests indicated that full saturation was achieved close to the inlet pipe, but not initially at the opposite end of the model where the water had by then been cooled by the room temperature sand grains. Further flushing of the model with boiling water was able to overcome this problem.

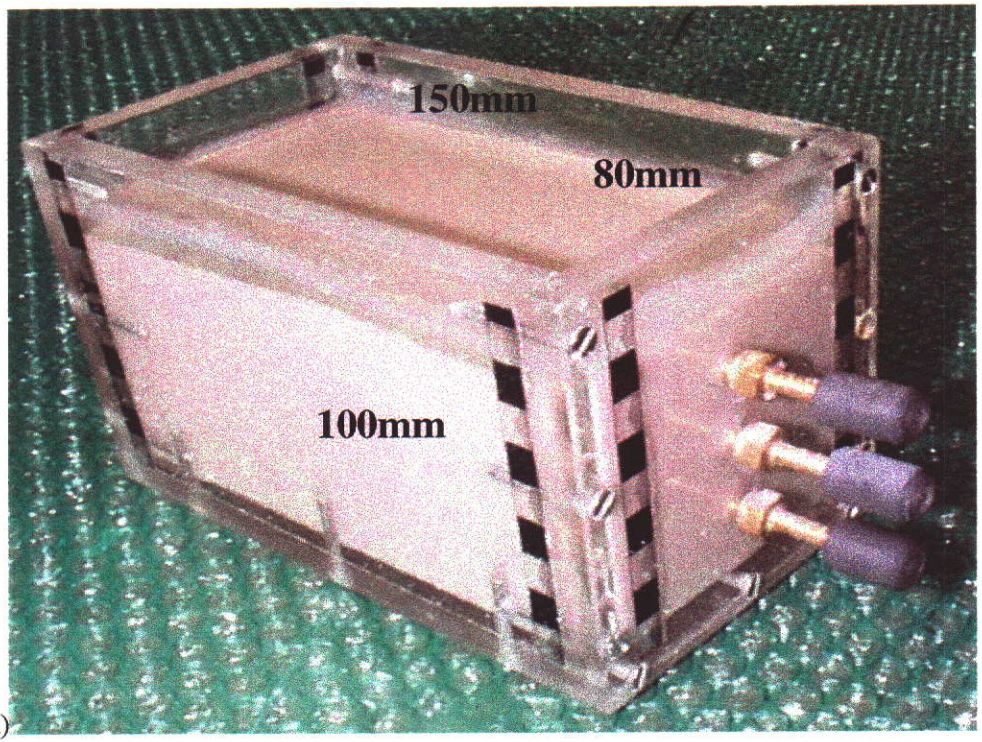

(a)

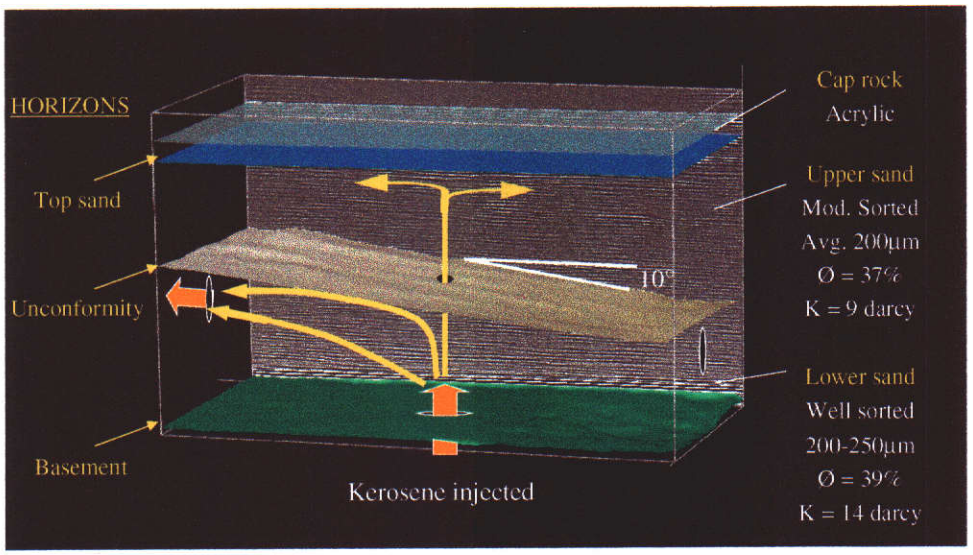

(b)

Figure 6.15: (a) Photograph of fluid flow model used for time-lapse physical modelling experiments. (b) Schematic diagram illustrating the possible fluid flow paths of kerosene within the water-saturated sands.

A series of zero-offset 3-D surveys were recorded during a systematic program of kerosene injections through the base of the model. The surveys comprised 70 in-lines with 140 traces per line and 1 mm (10 m) trace spacing (bins). Five shots were fired at each trace location and vertically summed. An outflow pipe was opened at the up-dip end of the model, just below the unconformity between the two sand layers, to allow the displaced water to escape.

Kerosene was chosen for the injections because of its relatively large density and velocity contrast with water (see Chapter 5.7.6). It was initially presumed that the kerosene would migrate along one of three possible pathways within the sand, which are indicated with yellow arrows in Figure 6.15 (b). The capillary force from the kerosene-water interfacial tension opposes the bouyancy of the kerosene (Berg, 1975). For migration to occur, the bouyancy must be greater than the capillary force. If this was the case, the kerosene may migrate vertically until becoming trapped below the acrylic cap rock. The second possibility was that the kerosene may migrate vertically within the lower sand and then migrate up-dip towards the outflow pipe below the unconformity. Although the top sand had only slightly lower porosity than the lower sand, the permeability was significantly lower and may provide a sufficient barrier to restrict the kerosene to the lower sand. The third possibility considered was that the flow of the displaced water would drive the kerosene directly to the outflow pipe.

Figure 6.16 shows the middle 2-D seismic line taken from the baseline 3-D survey recorded prior to the kerosene injections. The strong reflections at 1700 ms (scaled two-way time) and 1760 ms are from the top acrylic and top sand interfaces, respectively. The strong basement reflection is at 2550 ms.

Kerosene was injected through the centre of the base of the model over several days. The injections were done manually in several stages at a rate of around 5 mL per hour. After 30 mL of kerosene had been injected, which equalled around 15% of the pore volume, kerosene was observed exiting the outflow pipe at the up-dip end of the model. A second 3-D monitor survey was then recorded with identical acquisition parameters. Figure 6.17 (a) shows the lower half of the baseline seismic section that is shown in

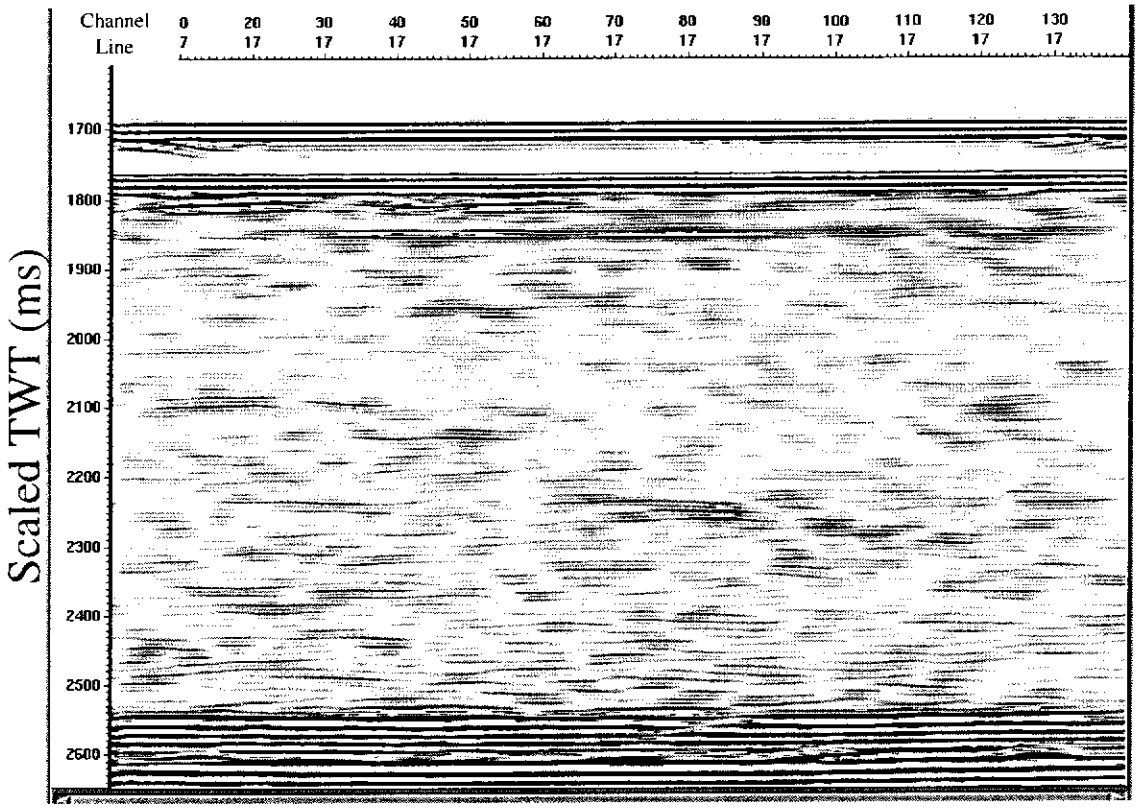

Figure 6.16: 2-D seismic line taken from the baseline 3-D survey over the kerosene fluid flow model prior to injection of kerosene. The strong reflections between 1700 ms and 1800 ms (scaled two-way travel time) are from the water/acrylic and acrylic/sand interfaces. The basement reflection is at 2550 ms.

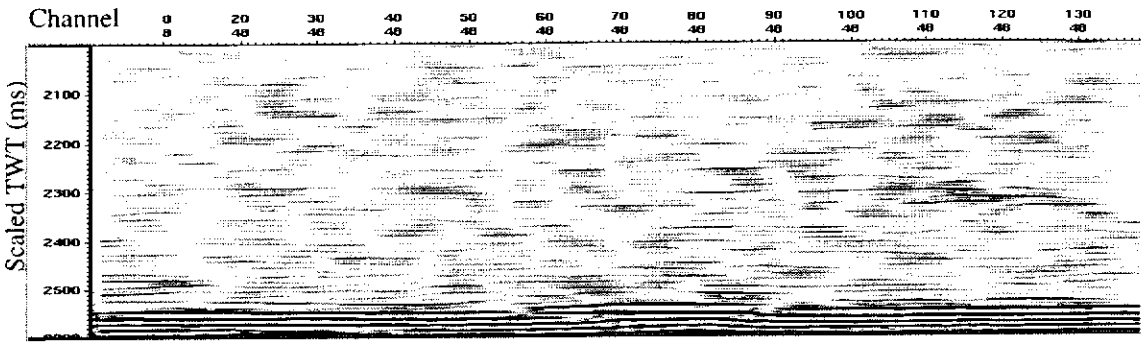

(a) Baseline seismic section.

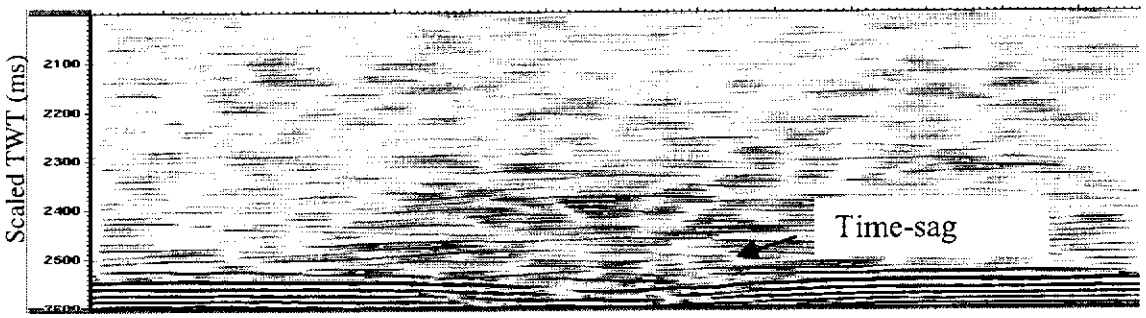

(b) Seismic section after 30 ml kerosene injection.

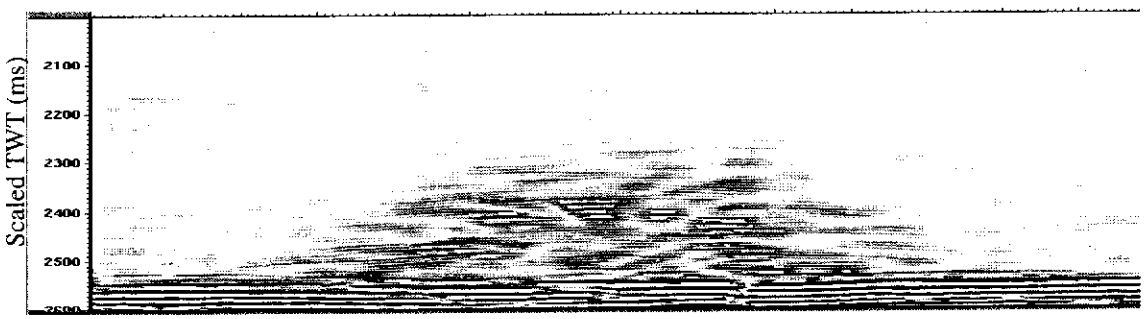

(c) Difference section (30 ml kerosene minus baseline).

Figure 6.17: (a) Lower half of the baseline 2-D seismic section shown in Figure 6.16. (b) Corresponding seismic section recorded after 30 ml of kerosene had been injected. At this point, the kerosene had reached the outflow pipe, up-dip from the injection site. (c) The difference section produced by subtracting (a) from (b). The kerosene appears to be remaining close to the injection site even though breakthrough has already occurred up-dip.

Figure 6.16. The corresponding section from the second monitor survey, recorded after the kerosene injections, is shown in Figure 6.17 (b). This section has higher amplitudes above the basement reflection from the kerosene around the injection site in the middle of the section. The arrival time of the basement reflection is increased around this area, a phenomenon known as 'push-down' or 'time-sag'. This is a result of a decrease in sound velocity within the regions where kerosene has replaced water in the sand pores.

The difference section produced by subtracting the baseline seismic survey from the monitor survey is shown in Figure 6.17 (c). The residual RMS amplitudes of the surface reflection in this difference section are around 20% of the baseline survey amplitudes. This result was poorer than expected from the repeatability tests and this was interpreted as a result of water temperature changes between surveys. The acquisition tests presented in Chapter 6.6.1 were from repeated 2-D seismic lines where no temperature changes could have occurred. However, the 3-D surveys were recorded on separate days and temperature changes of up to 1°C may have occurred, resulting in the reflection events misaligning in time on subsequent surveys.

The difference section clearly shows where the kerosene has displaced the water within the sand. The kerosene appears to remain close to the injection site, which suggested that the volume of kerosene remained below the minimum required to initiate migration. However, it is known from visual observations that some kerosene has already reached the outflow pipe up-dip from the injection site. It is not possible to tell how the kerosene may have migrated to the outflow pipe from the seismic sections alone.

Following the recording of the monitor survey, the up-dip outflow pipe was plugged and another pipe was opened at the down-dip end of the model, below the unconformity. More kerosene was then injected and breakthrough at the down-dip pipe was observed when the total volume of injected kerosene reached 55 ml. A second monitor survey was then recorded. Figure 6.18 (a) shows the 2-D seismic section that corresponds with the baseline survey shown in Figure 6.16. The time-sag of the basement reflection has increased in accordance with the extra volume of kerosene in

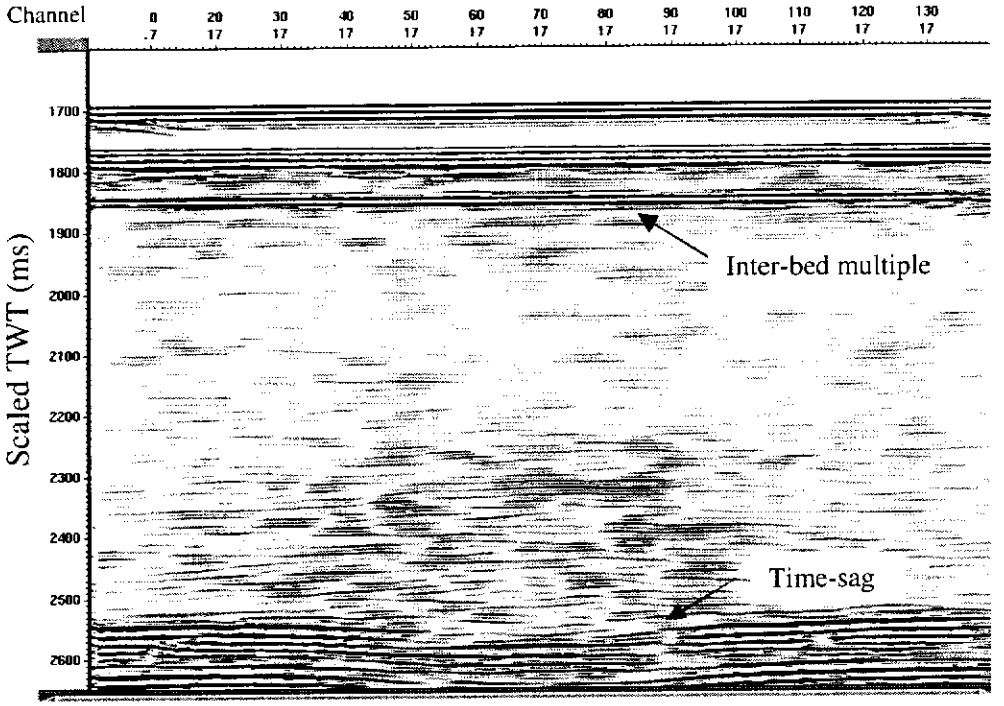

(a) 2-D seismic section after 55 ml kerosene injection.

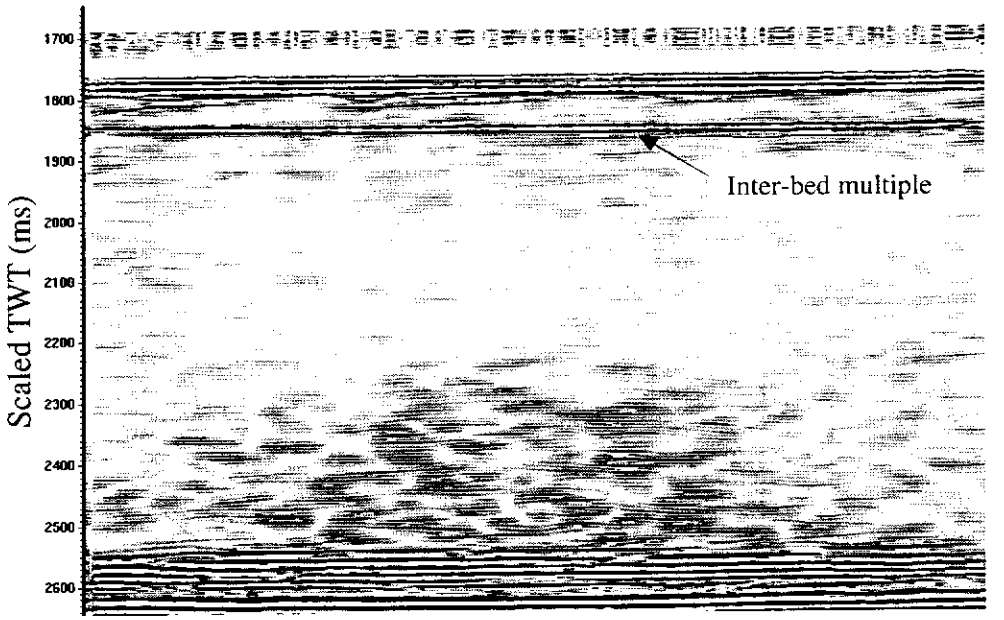

(b) Difference section (55 ml kerosene minus baseline section).

Figure 6.18: (a) 2-D seismic line corresponding with the baseline section shown in Figure 6.16, recorded after 55 ml of kerosene had been injected. At this point kerosene had reached the outflow pipe down-dip from the injection site. (b) The difference section produced by subtracting the baseline section from the 55 ml kerosene section. Note the interbed multiple resulting from the stronger impedance contrast at the acrylic/top sand interface.

the lower sand. However, in addition, an inter-bed multiple is now clearly visible below the top sand reflection, which is also visible on the difference section shown in Figure 6.18 (b). This multiple is visible to a lesser extent in both of the earlier seismic surveys and is a result of the strong impedance contrasts at the water/acrylic and acrylic/top sand interfaces. However, this multiple is much stronger in the final monitor survey, indicating that the impedance contrast at the acrylic/top-sand interface must have increased. This means that the kerosene must have also migrated to the top of the model.

To understand how the kerosene flowed to each of the outflow pipes it is necessary to look at maps of the basement time-horizon for each survey, which are shown in Figure 6.19. A small depression (ie. increased travel time) is observed on the baseline survey around the injection site. This probably was a result of a small amount of kerosene that leaked into the model prior to the injections. The basement horizon map from the seismic survey recorded after breakthrough observed up-dip shows that most of the kerosene has remained around the injection site, and that some kerosene has migrated to the left side of the model, beyond the coverage of the 3-D seismic survey. The kerosene has established a preferential flow pathway along the contact between the sand, the acrylic base and walls of the model. This contact is the most permeable pathway in the model. Similar edge effects have been observed visually in the 2-D fluid flow models by Catalan *et al.* (1992), and Thomas and Clouse (1995). This is a major limitation and is unavoidable in 2-D models. However, this could be easily avoided in future 3-D models by locating the injection site internally within the model, away from the edges. The basement time horizon map from the second monitor survey, after breakthrough was observed down-dip, shows that most of the kerosene has flowed around the walls of the model. It is possible that the flow path was influenced by the relatively rapid rate of injection, and a different result may have occurred with a slower injection rate.

Figure 6.19 (b) shows the kerosene saturation within the lower sand as a percentage of the pore volume. This was calculated from the interval velocity within the lower sand assuming a linear change in velocity with saturation. This assumption is based on the

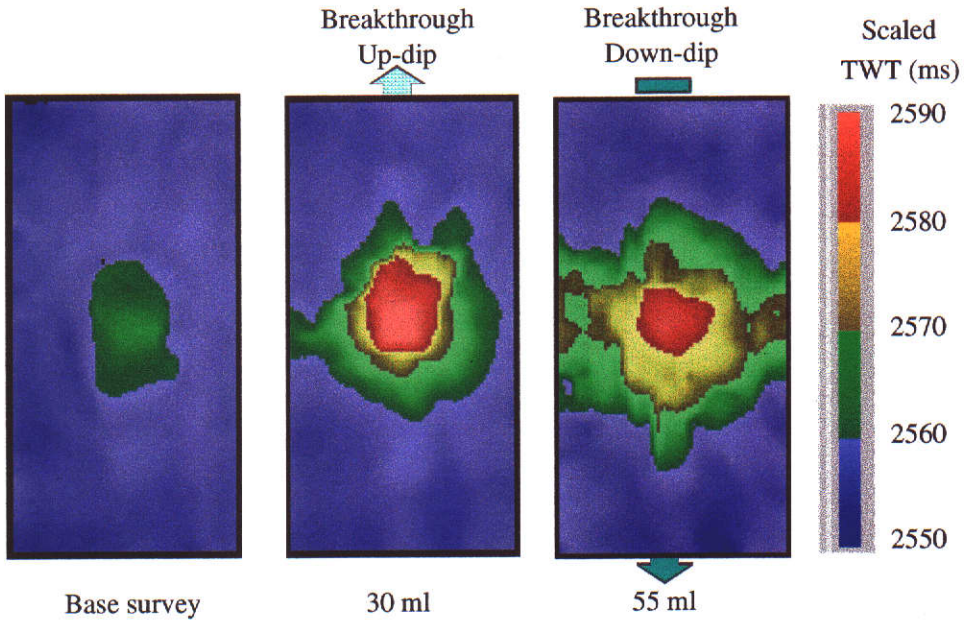

(a) Basement time horizons.

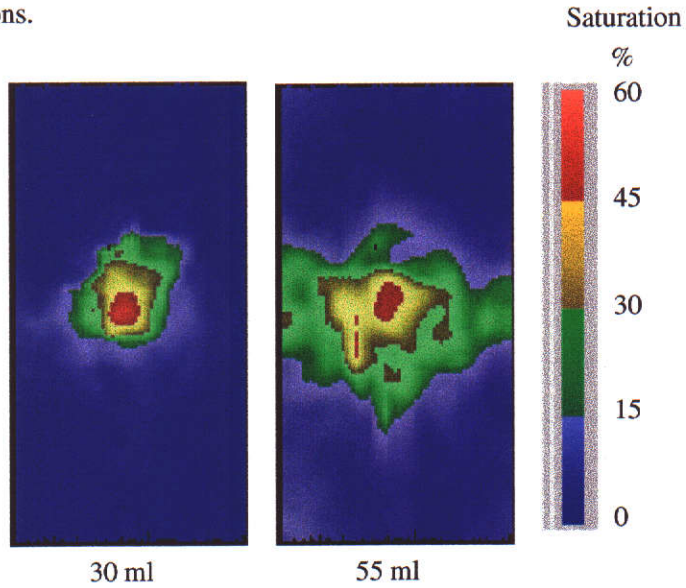

(b) Kerosene saturation in lower sand.

Figure 6.19: (a) Maps of basement reflection time horizons showing the time-sag that results from the kerosene replacing water in the lower sand. (b) The kerosene saturation in the lower sand expressed as a percentage of the pore volume.

'patchy' mixing model discussed in Chapter 5.7.6, whereby the kerosene and water distribution is heterogeneous within the pores at the ultrasonic wavelength scale.

The flow of kerosene into the upper sand, beneath the acrylic cap, is best shown with maps of the average amplitudes of the upper sand, shown in Figure 6.20 (a). The average amplitudes in the base survey are variable over the area of the survey, which indicates that the coupling between the acrylic cap and top sand is uneven. There was little change in these amplitudes after 30 ml of kerosene had been injected, but a large change after the injection of 55 ml. The flow of kerosene through the top sand is best seen on the difference maps (Figure 6.20b), which removes the influence of the uneven amplitudes from the base survey. After 30 ml of kerosene had been injected, a small amount of kerosene flooded into the top sand from along the left wall of the model up-dip from the injection site. This continued to occur even after the up-dip pipe was plugged and the down-dip pipe was opened. An interesting feature of the difference maps is the lineations in the amplitudes. These are a result of the 'acquisition footprint', which highlights areas where the repeatability is uneven.

6.6.6 Example 3 – Air Flow Model

In the last example, the configuration used was the same as the kerosene model except for two changes. Firstly, larger grains were used for the lower sand (250-300 μm instead of 200-250 μm). This was done to increase the permeability of the lower sand, which would hopefully help avoid the tendency for flow to occur around the model walls. Secondly, air was injected instead of kerosene, which increased bouyancy in water and lowered viscosity. A 2-D seismic section taken from the baseline survey over this model is shown in Figure 6.21. The larger grain size in the lower sand has resulted in significantly more scatter of the ultrasonic signal, resulting in considerable noise within the lower sand.

In this model, breakthrough was observed up-dip after only 6ml of air had been injected. This represented less than 3% of the pore volume of the lower sand. Figure

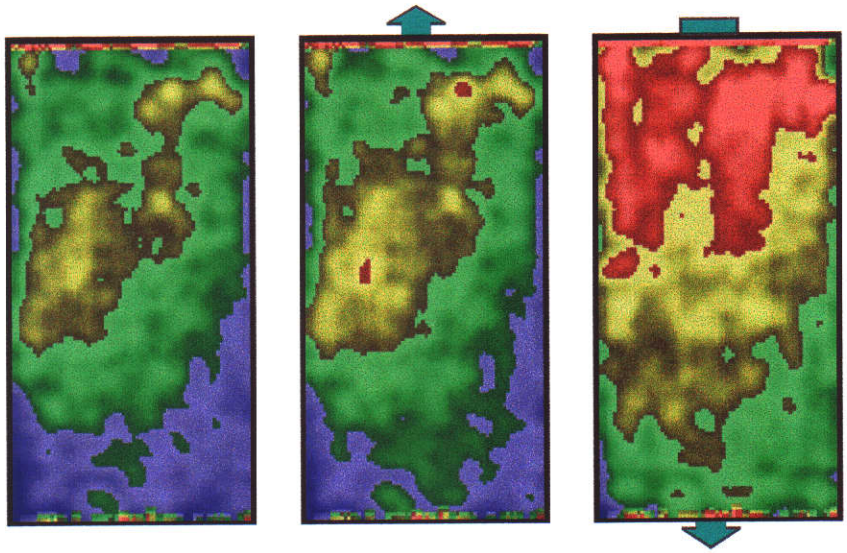

Base survey 30 ml 55 ml

(a) Average absolute amplitudes, Upper sand.

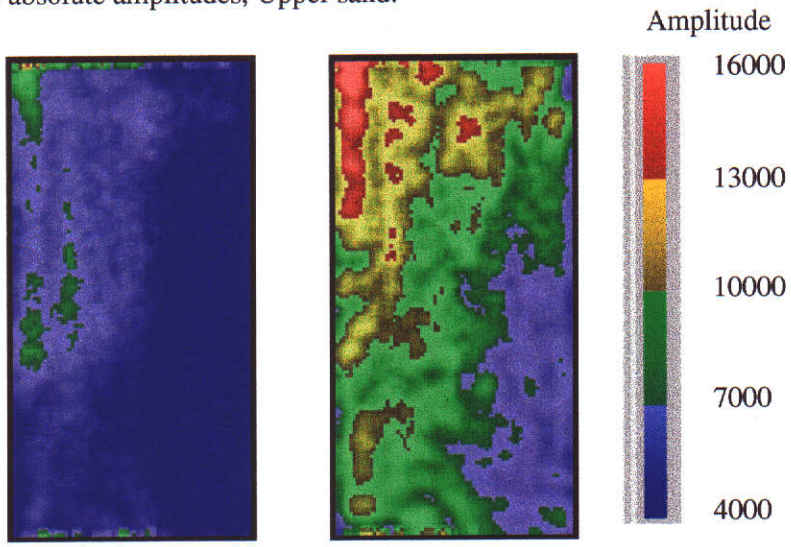

30 ml - base 55 ml - base

(b) Difference amplitudes, Upper sand.

Figure 6.20: (a) Maps of average absolute amplitudes in the upper sand as kerosene is injected into the lower sand. (b) Difference maps showing the change in average amplitude within the top sand as kerosene is injected. Note that the kerosene floods into the upper sand from the left side, up-dip from the injection site. This continues to occur even when the up-dip outflow pipe is plugged and the down-dip pipe is opened.

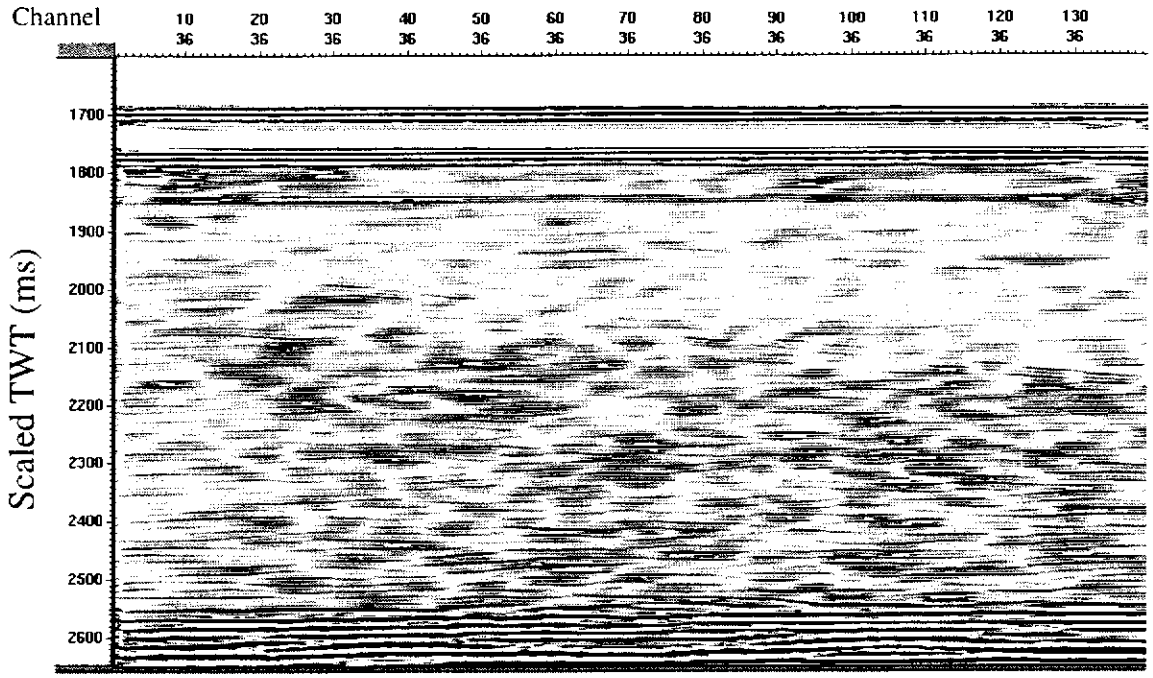

Figure 6.21: 2-D seismic line taken from the baseline survey of the air injection model prior to injection. Note the higher levels of noise from scattering in the lower sand due to the larger grain size (250 – 300 μm).

6.22 shows the lower half of the 2-D seismic section from Figure 6.21, along with the corresponding section from the monitor survey recorded after breakthrough up-dip, and the associated difference section. The difference section shows that the air migrated into the sand, rather than remaining close to the injection site as was the case in the kerosene example. The higher levels of noise from scattering within the lower sand have cancelled in the difference section, confirming that they are coherent reflections from scattering rather than random noise. The residual amplitudes of the surface reflection in this case are 26% of the amplitudes on the baseline survey, or 11.6 dB down.

Figure 6.23 shows the 3-D visualizations of the two data volumes recorded for the baseline and 6 ml injected air surveys. The unconformity between the upper and lower sands has been interpreted and is shown as a semi-opaque horizon. The data volume recorded after 6 ml air had been injected shows that only a small amount of air had reached the outflow pipe up-dip when breakthrough occurred. Most of the air had migrated sub-vertically and towards the outflow pipe up-dip. However, it appears that some of the air also migrated towards the down dip end of the model. This has been interpreted as being a result of a leaking pipe at the down-dip end of the model that was considered to have been sealed at the time.

The small amount of air that was observed breaking through after only 6 ml of air had been injected was possibly already present within the model before the injection program was initiated. It was concluded that this may have occurred when the model was set up before the baseline survey was recorded. Injection of air continued and very small amounts of air were observed breaking through the outflow pipe until the total volume had reached 14 ml, at which point it began to flow as a continuous stream. The up-dip pipe was then plugged and the down-dip pipe was opened. When the total volume of injected air had reached 44 ml, breakthrough was observed at the down-dip pipe.

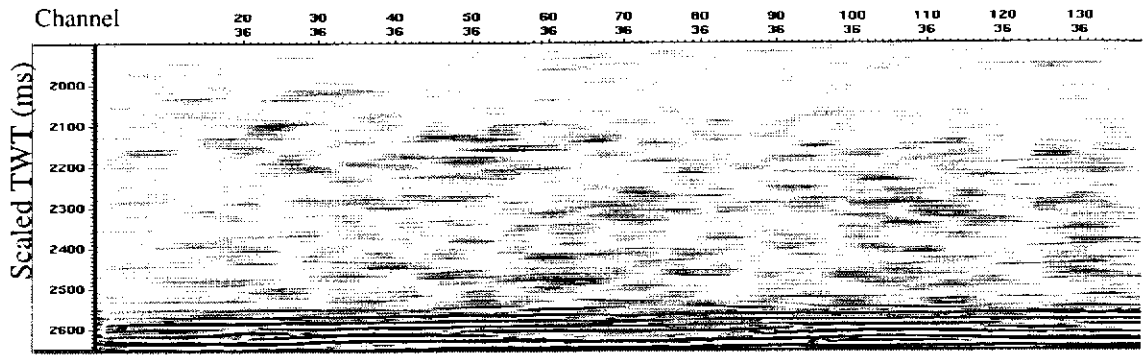

(a) Baseline seismic section.

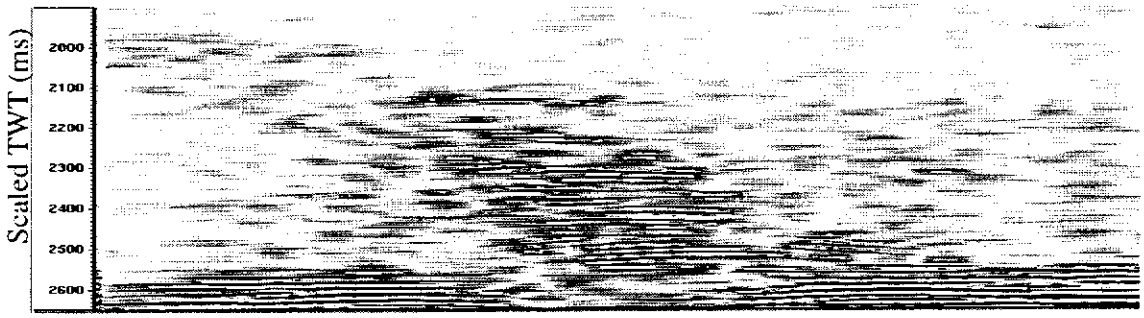

(b) Seismic section after 6 ml air injection.

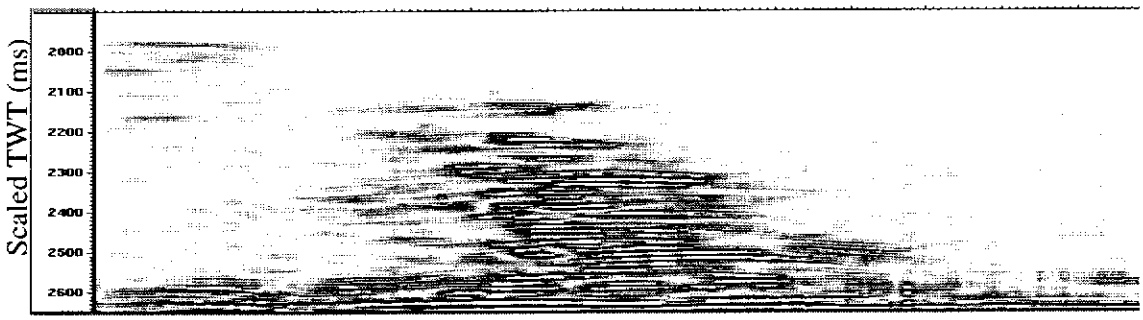

(c) Difference section (6 ml air minus baseline).

Figure 6.22: (a) Lower half of 2-D seismic section from baseline survey shown in Figure 6.21. (b) Corresponding seismic section recorded after 6 ml of air had been injected. At this point, the air had reached the outflow pipe up-dip from the injection site. (c) The difference section produced by subtracting (a) from (b). The air has migrated up through the sand and been swept across to the left by the fluid flow.

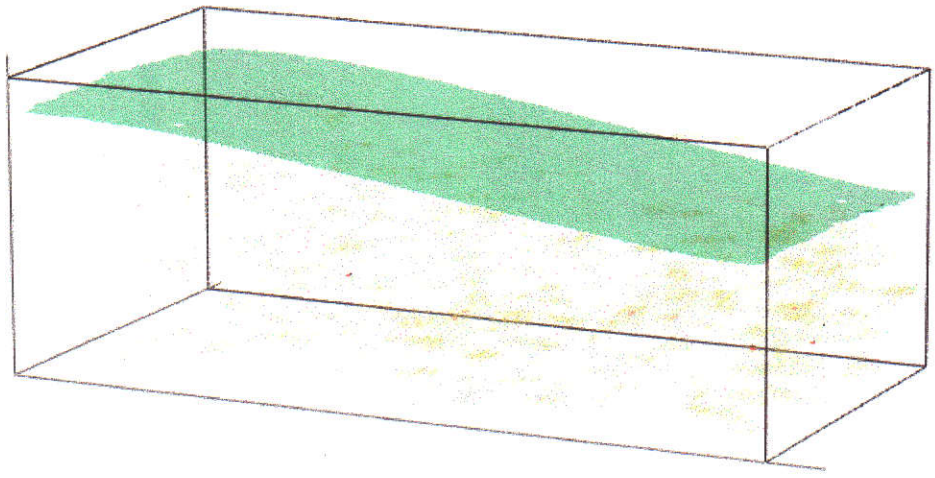

(a) Baseline survey prior to air injection. Outflow pipe open up-dip.

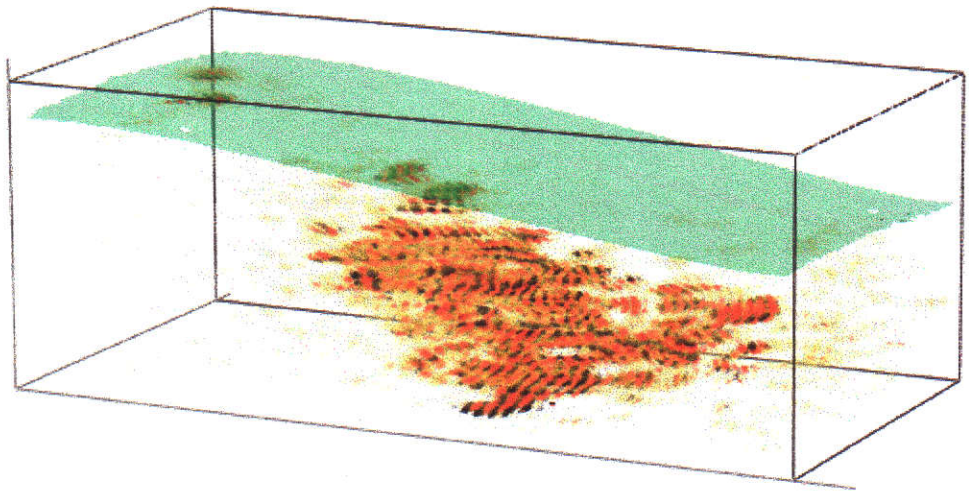

(b) After 6 ml of air has been injected. Breakthrough up-dip.

Figure 6.23: (a) 3-D visualization of seismic data volume from baseline seismic survey. The low amplitudes have been rendered translucent and the unconformity has been interpreted in green. No air has been injected at this stage. The low amplitude reflections are a result of scattering from the sand grains. (b) Corresponding image of the data volume recorded after 6 ml of air has been injected. At this point, air was observed breaking through the outflow pipe up-dip.

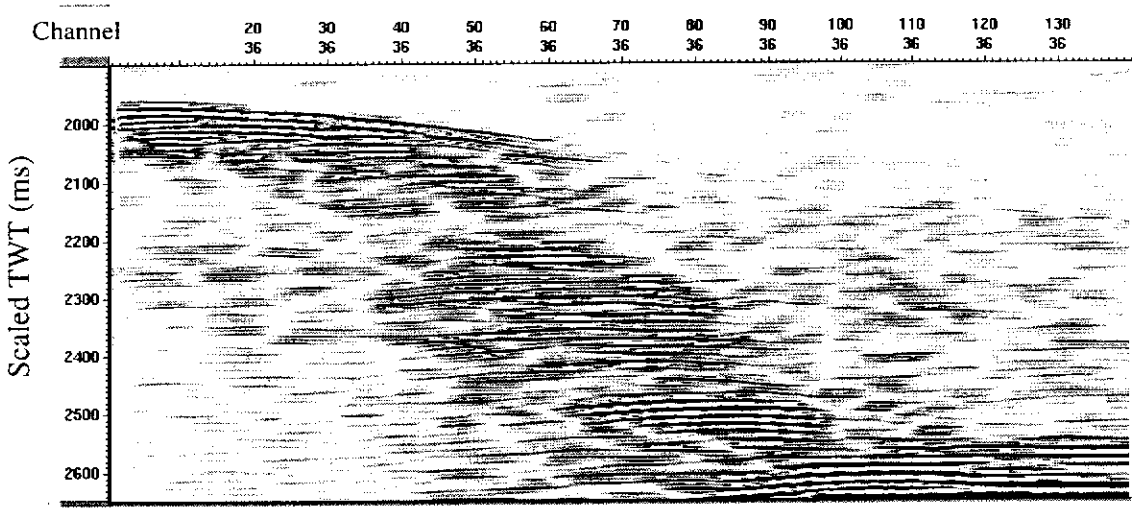

(a) Seismic section after 14 ml air injection. Outflow up-dip.

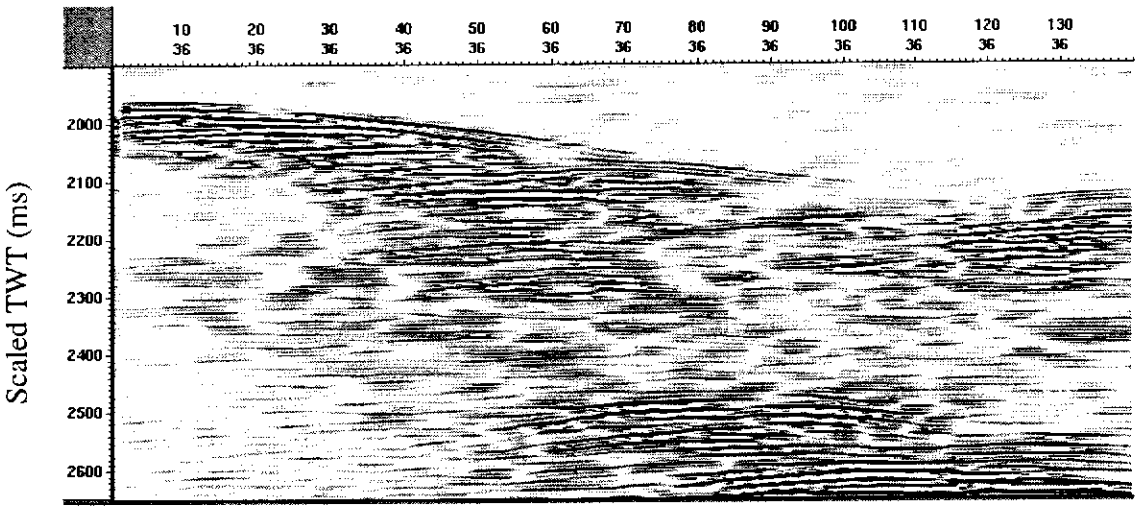

(b) Seismic section after 44 ml air injection. Outflow down-dip.

Figure 6.24: (a) 2-D seismic section after 14 ml of air had been injected. Note how the air has been trapped below the unconformity between the upper and lower sand layers. The outflow pipe up-dip was plugged after this survey and the down-dip pipe was opened. (b) Corresponding seismic section after 44 ml of air had been injected. At this point, the air had reached the outflow pipe down-dip.

Figure 6.24 (a) and (b) shows the corresponding 2-D seismic sections recorded after 14 ml and 44 ml of air had been injected, respectively. The flow of air was sub-vertical until it came into contact with the unconformity. The higher capillary pressure in the upper sand was sufficient to confine the air to the lower sand such that it was then forced to flow up-dip towards the outflow pipe. Once the up-dip pipe was plugged and the down-dip pipe opened, the air appears to have flowed down-dip while remaining trapped below the unconformity. The 3-D visualization of these two data sets (Figure 6.25) indicates that some air continued to collect up-dip of the injection site, while some migrated towards the down-dip pipe once it encountered the unconformity.

The injection of air into the lower sand has increased the rate of attenuation to the point that the basement reflection could no longer be detected. This prevented the possibility of mapping the saturation within the lower sand from the change in interval velocity. However, maps of the average absolute amplitudes within the lower sand are useful for showing how the air has migrated through the sand, as shown in Figure 6.26. These maps show that as the air migrated towards the outflow pipes, initially up-dip, and then down-dip, it also flowed preferentially to the right side of the model. This indicated that the lower sand had higher permeability on the right side of the model than on the left.

When the baseline seismic survey was subtracted from the final survey recorded after 44 ml air had been injected, the residual RMS amplitudes of the surface reflection were equal to 72% of the primary amplitudes. Investigation of the data sets after they were merged together, but before they were subtracted, revealed that the alignment of the events was progressively worse towards the down-dip end of the model, reaching a maximum of 5 ms, or approximately one third of the wavelength. This suggested that the down-dip end of the model had dropped by around 0.3 mm (3m scaled) before the last survey was recorded, which probably occurred during the process of physically opening the down-dip pipe. Once this was discovered, residual statics corrections were applied to the merged data sets and the differencing was performed again. This resulted in a decrease in residual amplitudes on the difference section to only 8% of the primary baseline amplitudes, or 21.8 dB down (Figure 6.27).

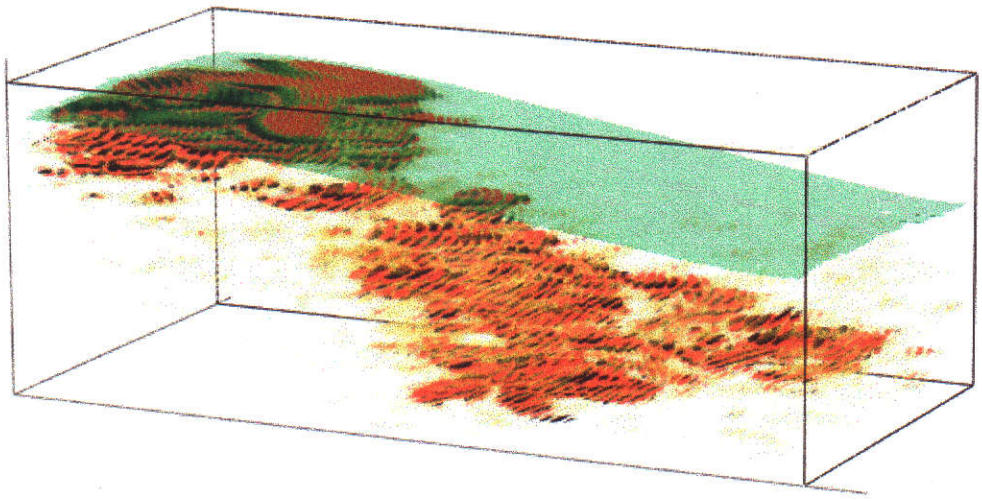

(a) After 14 ml of air had been injected. Air flowed up-dip.

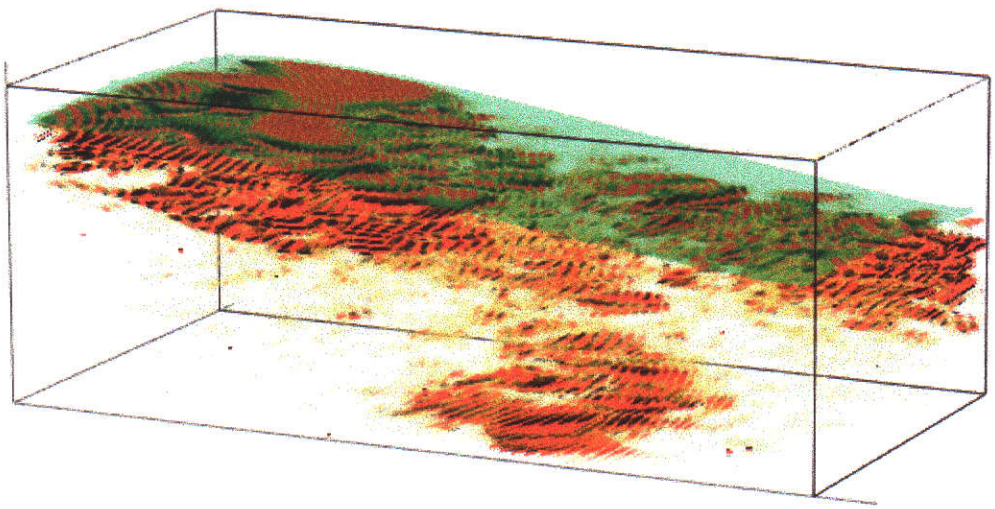

(b) After 44 ml of air has been injected. Up-dip outflow pipe was sealed and down-dip pipe opened. Breakthrough occurred down-dip.

Figure 6.25: (a) 3-D visualization of seismic data volume after 14 ml of air was injected. The low amplitudes have been rendered translucent to allow the flow path of air to be seen. The air has migrated up-dip and is trapped below the unconformity shown in green. (b) Corresponding image of the data volume recorded after 44 ml of air was injected. The up-dip outflow pipe was plugged after 14 ml of air had been injected and the down-dip pipe was opened. The air then flowed down-dip but remained below the unconformity.

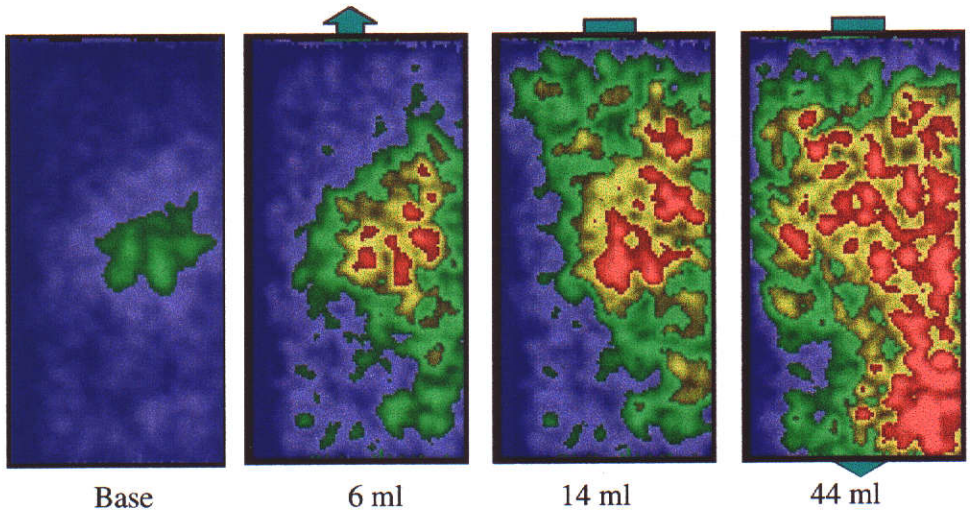

(a) Average absolute amplitudes, Lower sand.

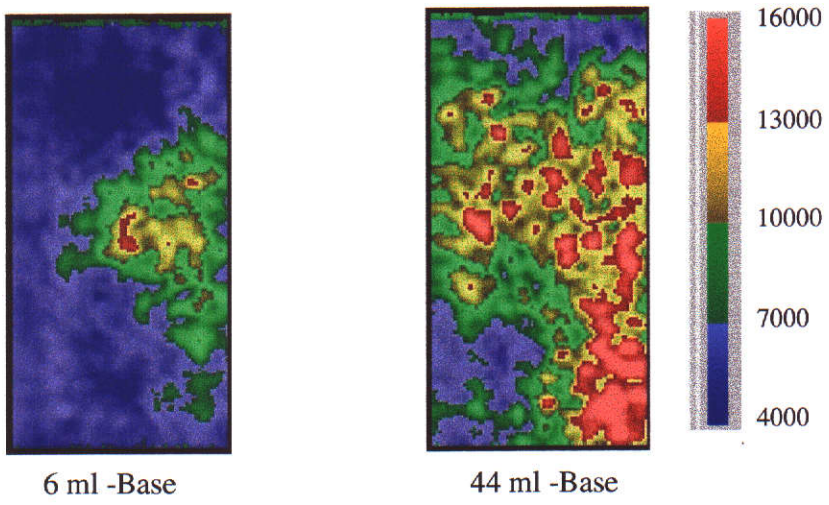

(b) Difference amplitudes, Lower sand.

Figure 6.26: (a) Maps of average absolute amplitudes in the lower sand as air is injected from below. (b) Difference maps showing the change in average amplitudes within the lower sand as air is injected. Note that as the air moves towards the outflow pipes it also moves to the right side of the model indicating that the sand is more permeable on the right side.

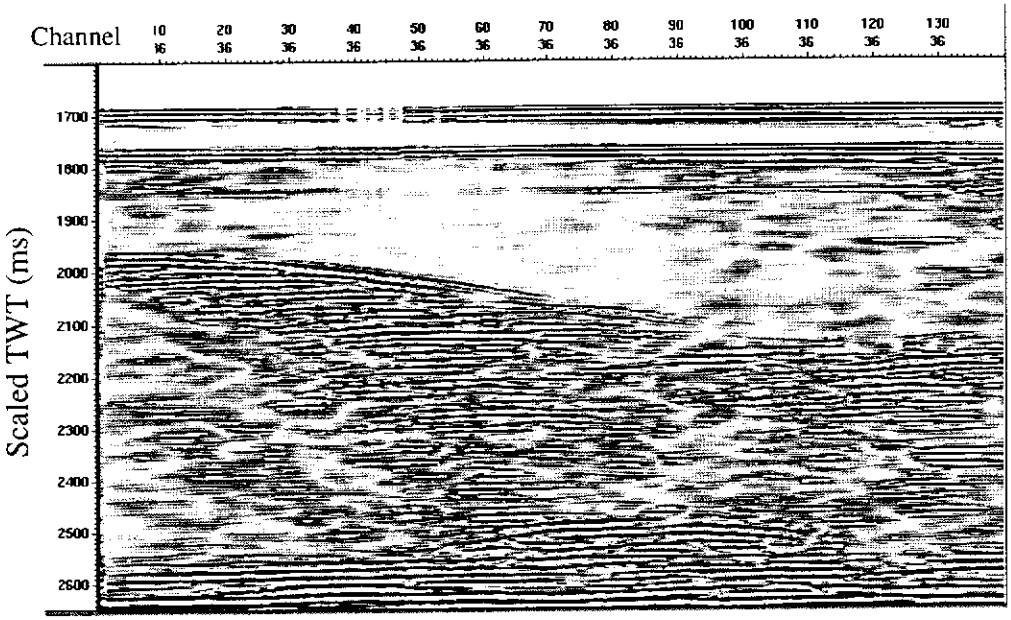

(a) 2-D difference section (44 ml air - base) - unprocessed data.

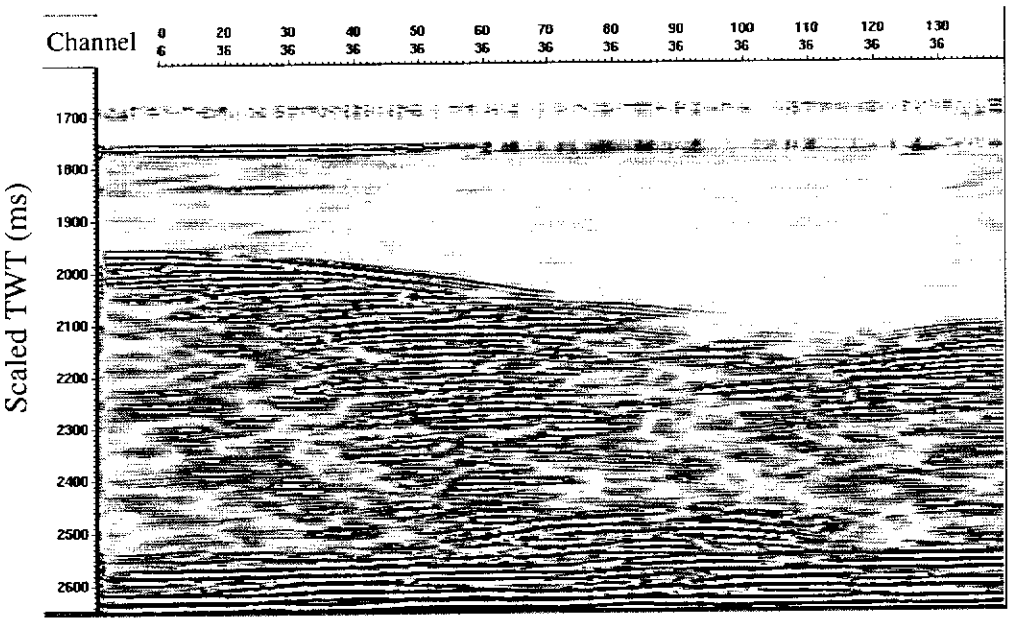

(b) 2-D difference section (44 ml air - base) after statics correction.

Figure 6.27: (a) 2-D difference section produced by subtracting the baseline section from the section recorded after 44 ml of air had been injected. The result is very poor, with residual amplitudes equal to 72% of the amplitudes on the baseline section. This is due to poor alignment of events as a result of the model being moved between surveys. (b) The corresponding difference section after residual statics corrections have been applied to correctly align the events. The residual amplitudes have been reduced to 8%.

6.7 Discussion

The seismic physical models developed for this thesis present an opportunity to complement the time-lapse research potential of numerical models. Numerical modelling, using rock physics and reservoir simulation, can help estimate the magnitude of reservoir changes, but repeatability and interpretability can only be determined by analysing multiple seismic surveys (Eastwood *et al.*, 1999). The expense and long turn-around times associated with field time-lapse case studies effectively limits the rate of advance of this burgeoning technology. However, seismic physical models can be used to generate multiple seismic surveys quickly and cheaply, and can be tailored to suit a particular problem for analysis.

Numerical modelling can systematically test changes to individual parameters but they are still very simplified for 3-D simulation. In addition, they require initial parameters to be specified first, which are based on assumptions on the physical properties. A numerical simulation is only as good as the parameters that are chosen for input, which must describe the reservoir in quantitative form and are subject to prejudice from the person(s) providing the input (Van De Graaff and Ealey, 1989). Unlike the physical models presented here, numerical modelling of fluid flow for reservoir simulation does not give an accurate prediction or image of the flow. Physical models provide real data that do not rely on assumptions. Once a model has been built, it is a simple matter to record a suite of 3-D surveys with different parameters and at a number of different time intervals. Subtle effects such as stratigraphic reflections are at this stage too complex for numerical modelling, particularly in poorly consolidated sands at low effective pressures where our ability to predict the behaviour of seismic waves is still lacking. Small-scale permeability heterogeneity such as cross-bedding should be taken into account to predict hydrocarbon recovery efficiency. This cannot be assessed from petrophysical studies of core measurements but must be determined through careful modelling studies (Kortekaas, 1983).

The changes in the physical properties from fluid movements within the time-lapse models presented in this thesis are much greater than would typically be encountered in the field. The level of repeatability that has been demonstrated with the models in this thesis means that more subtle and realistic models can now be considered. Ultimately, the role of unconsolidated sand in future seismic physical models is probably best served as one or two layers within a consolidated model to provide a more realistic reservoir analogue. This would also overcome the problems with attenuation that restricts the size of the models and the number of layers that can be imaged.

6.7.1 Consolidated models

Consolidated sands have higher seismic velocities than unconsolidated sands and are less sensitive to changes from fluid flow. In addition, they are able to support transmission of shear waves and so would provide a more realistic simulation of a typical reservoir environment. The development of techniques to use consolidated sands for seismic physical models would allow a number of other advances to be considered, such as applying confining and pore pressure to the models, and recording three-component seismic data. The improved signal transmission through consolidated sand would also permit lower energy settings for the transducers, which would reduce the resonant or 'ringy' nature of the output wavelet.

Preliminary experiments with cemented sand layers by Palmer (1999) suggest that modelling with cemented sands is promising, but much more work is required to establish the optimum mixtures and methods of building and saturating such layers. The use of consolidated sands in physical models would alleviate the need for the solid acrylic top layer that was used for the time-lapse models, which would also reduce the problems with inter-bed multiples.

The use of consolidated sands would permit the use of shear-wave transducers on the model surface to simulate recording with ocean-bottom surveys (OBS). OBS is used to record multi-component data, which can sometimes provide a much clearer image of a

reservoir than is possible from P-wave data alone. An example is the OBS data recorded over the Alba Field in the North Sea (MacLeod *et al.*, 1999). The recording of S-wave data would also allow improved analysis of changes in rock properties as a result of fluid movement, and would possibly allow reflections to be recorded below areas of high gas content.

The use of consolidated sands in seismic physical models would also allow anisotropic layers to be studied. It has been demonstrated that cemented sands will be anisotropic at atmospheric pressure if subjected to high confining pressures while solidifying in the laboratory (Thompson, 1998).

6.7.2 AVO models

Amplitude variations with offset (AVO) are another phenomenon that could be investigated with time-lapse models. AVO has been shown to work in principle with solid physical models (Tadepalli, 1995), and this could easily be extended to porous media to investigate the AVO effects due to fluid flow. The AVO modelling of Tadepalli's dealt purely with amplitudes of a single reflection from an interface. Hence, his work was not adversely affected by the problems of travel-time and waveform changes with offset that were demonstrated in Chapter 3. The variable offset acquisition method developed during this research overcomes these problems and would allow similar AVO research to be extended to more geologically realistic, multi-layer models. This is probably the most logical progression in developing these modelling techniques further because, in most cases, the effects from changes in fluids within a reservoir on seismic data are greatest at far offsets.

A common approach with field time-lapse data is to sort the data into near-offset and far-offset stacks. With physical modelling, it would be a simple matter to record near- and far-offset data without the need to record data from all offsets, thus saving significant time with the data acquisition. The recording of multi-offset data with separate source and receiver transducers also allows use of the inverse waveform that

was demonstrated in Chapter 3. This would then reduce the problems associated with the 'ringy' wavelet that is present in most of the data presented in this thesis.

AVO or multi-component data, where P- and S-wave impedances are derived, can theoretically be used to separate the effects of changes in pressure from saturation because S-waves are relatively insensitive to changes in saturation. This has been demonstrated with a synthetic example (Tura and Lumley, 1999), but it is less successful with real data (Landro, 1999). A physical model of such a situation would be very useful to prove that the method is viable.

6.7.3 Stress

The use of unconsolidated sand layers within an otherwise solid model would allow mechanisms of confining stress and pore-pressure to be implemented. Confining pressures have been applied to physical models previously in the form of a thick metal pressure plate that contained several fixed transducers (Savic, 1995). However, this was limited to a fixed acquisition configuration with low spatial resolution. It should be possible to apply small confining pressures to a solid physical model containing one or more poorly consolidated sand layers, but still enable free movement of transducers above the model. While the applied pressure would have to be well below those encountered in most reservoirs, they would most likely be high enough to result in more consistent and predictable acoustic properties, which in turn would allow better control over the models and more relevant results. The greatest changes to the acoustic properties of sediments with increasing pressure occur near atmospheric pressure. Confining pressures as low as several atmospheres are enough to allow relevant data to be recorded (Bacharach *et al.*, 1998). Results from such models can then be extrapolated to higher pressure without the large uncertainties associated with room pressure experiments such as those in this thesis.

Further studies on the low-pressure effects on the acoustic properties of sand would be worthwhile. An understanding of this is relevant to near surface problems with field

seismic data such as static corrections (Bacharach and Nur, 1998b). The cause of velocity increases with depth in the near surface is often attributed to transitional changes in saturation near the water table, but they may be more a factor of the increasing overburden. The role of fluids at low pressure needs further investigation as the effects possibly cancel to some degree where the fluid film stiffens the grain contacts by holding them together with surface tension, but the stiffness of the contact area itself may be reduced.

6.7.4 Fluid flow scaling

To get truly representative fluid flow behaviour in physical models, more care is required to adhere to correct scaling criteria for simulating fluid flow. These issues have not been addressed in this thesis. Scaling laws for modelling petroleum reservoirs were established by Geertsma *et al* (1956). To adhere to these scaling laws requires careful consideration of the relationship between porosity, permeability, fluid viscosity and density. Control over the rate of fluid injection or extraction requires a degree of precision that could only be achieved with automation. That is, computer-controlled stepper motors similar to those that are used for the seismic data acquisition would need to be used to control the rate of fluid injection.

An alternative to injection or extraction of fluids from the time-lapse models would be to develop ways to generate or dissolve gas within the models. A possible mechanism of generating changes in saturation within physical models would be to find a liquid that has a bubble point (ie. when gas is released out of solution) around room temperature, such that gas could be generated with a temperature change. Alternatively, it may be possible to generate gas within a physical model similar to experiments by Cobbold and Castro (1999), where carbon dioxide was generated by internal combustion of powdered charcoal and potassium chlorate.

6.7.5 Calibration of saturation changes

Quantitative analysis of the changes in saturation that occur within the physical models requires that an alternative method of determining the saturation levels be developed. This would then allow the changes in saturation to be calibrated to the seismic data. Possible techniques for doing this need to be investigated, which may include techniques such as CT scans, magnetic resonance imaging (MRI), electrical or chemical methods.

6.7.6 Scaling

The use of smaller grains in sandbox models would potentially overcome the scale restrictions imposed by the geological feature size-to-wavelength ratio and produce a more realistic seismic analogue of sedimentary environments. While it is not feasible to exactly reproduce the grain size-to wavelength ratio encountered in the field, a reduction in grain size by a factor of three (ie. a maximum grain size of 100 μm) would shift the models away from the Rayleigh scattering domain (see Section 4.7.2). In this case, velocity dispersion effects would still be significant, but it would then only be a result of 'squirt flow' effects, which are fairly well understood and could be accounted for when up-scaling the data. Measurements of the acoustic properties of these sands should be repeated using several different frequency transducers, which would then allow the velocity dispersion effects to be quantified. It is important to note that the relative changes in sound velocity from changes in pore fluid would be approximately constant regardless of frequency. Therefore, scaling limitations are much less of a problem for time-lapse seismic models.

6.7.7 Transducers

The transducers used in this thesis were not specifically designed for seismic physical modelling, and are particularly unsuitable for application to unconsolidated materials.

That is, they are not suitable for the amount of energy attenuation that occurs, which imposes considerable restrictions on the number of layers that can be imaged and the range of offsets that can be acquired. There are four areas of improvement in transducer characteristics would assist in advancing this technology further. These are a smaller physical size, higher energy output, a broader bandwidth (to give a less resonant signal), and an omni-directional waveform over a wide range of angles. Many of these requirements are mutually exclusive unless a new technology can be applied to generating simulated seismic signals for physical modelling.

CHAPTER SEVEN

CONCLUSIONS AND RECOMMENDATIONS

7.1 Conclusions

Analogue sandbox modelling has been providing an insight into the evolution of complex geological structures for many years. Seismic physical modelling has been used for the testing of numerical processing algorithms, and to evaluate interpretations of field seismic sections with scaled representations of geological formations. For this project, I set about developing methods to combine these two independent modelling techniques for the first time.

Prior to this project, seismic physical modelling had, of necessity, employed solid models of pre-determined geometries, the consensus being that the energy absorption and signal scatter characteristics of unconsolidated materials were too severe to allow their use in seismic models. Solid models were required to enable efficient wave propagation, and accurate control of all variables, but they are at least an order of magnitude more expensive and take much longer to build than a typical sandbox model. The subsequent images from solid models also lack the natural characteristics of field data, which restricts their value as a scientific tool. The techniques I have developed here have made large in-roads towards making sandbox models a viable alternative to solid seismic models.

The key to success in this project was the ability to overcome the problems of seismic wave propagation through unconsolidated materials. With all of the limitations discussed above, it is not suprising that seismic physical modelling has not ventured into the realms of analogue sandbox modelling before now. However, while previous attempts have concluded that they are unsuitable for use in seismic models, the examples I have presented in this thesis clearly demonstrate that they are.

I performed a comprehensive series of laboratory experiments to establish the factors that affect the acoustic properties of unconsolidated sands at atmospheric pressure. My results demonstrated the significance of a number of factors that are rarely considered in rock physics studies. These include not only the effects from changes in grain size and texture, but also particularly the influence that different methods of sample preparation can have on the final results. The significance of these factors, while not as great under the high confining pressures of most rock physics studies, is critical to the acoustic properties of sand at atmospheric pressure and such results have not previously been documented.

The laboratory experiments I performed showed that the single biggest limitation to modelling with sand is the difficulty in controlling the grain packing. I showed how the grain packing is influenced by the method of deposition, grain sorting and vibration, and I demonstrated the changes in seismic response that occur with variations to each of these parameters. I also showed that the method of saturating the sands is extremely significant. The temperature of the water used to saturate the models controls the surface tension and therefore influences the 'wettability' of the sand. The use of a vacuum chamber or vibrating table also affects the saturation level reached, and has a profound effect on the seismic response.

My results from the acoustic experiments were used to guide the design of physical models whereby contrasts in acoustic impedance were incorporated into models comprising unconsolidated sand. The ability to introduce such contrasts within these models allowed seismic images of them to be recorded for the first time. New methodologies can now be developed for imaging and interpreting complex structures, and allow a whole new regime of physical models to be considered. This new technology offers the potential to revitalize the seismic physical modelling industry at a time when many are predicting its demise and replacement with numerical modelling.

When modelling sedimentary sequences, the most important characteristics that should be preserved to scale are the rheological properties of the sediments. Sandbox models

have been shown to have the most representative scaled physical properties of natural sedimentary rocks. The systematic determination of the factors affecting seismic wave propagation through unconsolidated sands allowed me to devise a series of steps to reduce the rate of energy attenuation and increase the signal-to-noise ratio of the recorded data, thereby allowing two- and three-dimensional images of sandbox models to be produced.

When building unconsolidated seismic physical models, it is very important to apply the sand as gently and consistently as possible. The sand layers need to be homogeneous and the layer contacts as sharp as possible. Great care must be taken when saturating the model prior to recording the seismic surveys, to ensure that full saturation is achieved while the subtle structures remain undisturbed. For models comprising only simple structures, zero-offset recording will produce a reasonable image provided the transducer has been thoughtfully positioned with respect to both the depth in water and to the model, so that water column multiples arrive after the important primary reflections.

Models comprising more complex structures can now be imaged with data acquisition techniques developed here. Innovations such as the use of customized waveforms to control transducer outputs, combined with a new technique that I developed to systematically rotate the transducers to optimize energy available from each offset, have overcome many of the limitations previously associated with seismic physical modelling.

The advantages of being able to record seismic images from sandbox models do not only apply to the physical modelling aspects, but also expand the existing benefits of sandbox modelling. Analogue sandbox models are powerful tools, but are limited in the extent of information that can be gained from them by restrictions in section spacings and orientations. The ability to record 3-D images of such models increases their potential for helping understand complex geology. Sandbox models have been used to compare the structures produced with those interpreted on field seismic data, but now, direct comparisons of field seismic data with data from these models should be possible.

This technology, although still in its infancy, is already applicable to all forms of sandbox models to improve existing exploration and production seismic interpretations, and it also allows new styles of models to be considered. The rapid improvement in the quality of images that I have produced over the time span of this project indicates that there is still tremendous potential to improve these results further. Sandbox models offer great potential as a new physical modelling medium, to complement current physical modelling methods. This work provides a new level of technology that has applications to the petroleum industry and in the structural and tectonic interpretation of deep crustal seismic data.

However, the single biggest advantage that can be taken from this research is the ability to perform time-lapse experiments for fluid flow monitoring in the laboratory. The techniques I have developed to successfully model with porous media allows fluids to be incorporated into seismic physical models for the first time. The controlled laboratory environment, and the ability to consistently repeat 3-D data acquisition, allows time-lapse experiments to be performed without the need for costly and time consuming crossequalization of the data and subsequently avoids any pitfalls that may be associated with the process.

The opportunity now exists to combine the precision and much of the flexibility associated with numerical modelling with the true seismic response that comes from recording real data from models that undergo real changes representative of reservoir environments. This also avoids the expense and extensive computer time associated with numerically modelling in 3-D and allows rapid data turn around in a matter of days. The techniques I have developed here provide a new research tool that can be applied to study the seismic response of reservoir analogues as they change with time, or to compare the results of crossequalization methods with the 'correct' answers from models where the changes are known.

7.2 Recommendations

It is recommended that the next phase of development for seismic physical modelling should be to incorporate methods of cementing the sands. As discussed in Chapter Six, preliminary experiments suggest that modelling with cemented sands is promising, but much more work is required to establish the optimum mixtures and methods of building and saturating such layers. The use of consolidated sands in physical models would permit the use of shear-wave transducers on the model surface to simulate recording with ocean-bottom systems (OBS). The recording of S-wave data would allow improved analysis of changes in rock properties as a result of fluid movements, and would possibly allow reflections to be recorded below areas of high gas content. The use of consolidated sands in seismic physical models would also allow anisotropic layers to be incorporated.

Amplitude variations with offset (AVO) are another phenomenon that could be investigated with time-lapse models. AVO has been shown to work in principle with solid physical models and could easily be extended to porous media to investigate the AVO effects due to fluid flow. The variable offset acquisition method I developed during this research overcomes the problems of travel-time and waveform changes with offset that were demonstrated in Chapter Three. This is probably the most logical progression in developing these modelling techniques further because, in most cases, the effects from changes in fluids within a reservoir on seismic data are greatest at far offsets.

The use of unconsolidated sand layers within an otherwise solid model would allow mechanisms of applying confining stress and pore-pressure to be implemented. AVO or multi-component data can theoretically be used to separate the effects of changes in pressure from saturation because S-waves are relatively insensitive to changes in saturation. A physical model incorporating changes in pressure and saturation could be built to test these methods, which have previously been successful with synthetic data but much less so with field data.

The use of smaller grains in sandbox models are required to address the scale restrictions imposed by the geological feature size-to-wavelength ratio and produce a more realistic seismic analogue of sedimentary environments. While it is not feasible to exactly reproduce the grain size-to wavelength ratio encountered in the field, a reduction in grain size by a factor of three (ie. a maximum grain size of 100 μm) would shift the models away from the Rayleigh scattering domain. In this case, velocity dispersion effects would still be significant, but could be accounted for when up-scaling the data. Measurements of the acoustic properties of these sands should be repeated using several different frequency transducers, which would then allow the velocity dispersion effects to be quantified. Scaling limitations are much less of a problem for time-lapse seismic models because relative changes in sound velocity from changes in pore fluid would be approximately constant regardless of frequency.

To simulate truly representative fluid flow behaviour in physical models, more care is required to adhere to correct scaling criteria for simulating fluid flow. This requires consideration of the relationship between porosity, permeability, fluid viscosity and density. Adequate control over the rate of fluid injection requires that a method of automation be developed.

Quantitative analysis of the changes in saturation that occur within the physical models requires that an alternative method of determining the saturation levels be developed. This would then allow the changes in saturation to be calibrated to the seismic data. Possible techniques for doing this need to be investigated, which may include techniques such as CT scans, magnetic resonance imaging (MRI), electrical or chemical methods.

The seismic imaging techniques I have developed could be adapted for the interpretation of underwater turbidite models and used to better understand the structure and mechanisms of their formation. Turbidites contain a large proportion of the world's hydrocarbons but their complex architecture is seldom resolvable in seismic data and is a major drilling risk. Laboratory models are used to understand turbidite depositional

processes because they cannot be observed directly in nature. Building models underwater is also a more realistic analogue of marine deposition, although the lack of compaction would be the biggest limitation for recording seismic images of multi-layer turbidites. However, it would be an ideal technique for mapping the bathymetry of such models, and it should be possible to image at least one interface with an underlying turbidite flow, or to record multiple seismic images after successive turbidite flows. This would be a major advancement on current techniques, which at this stage rely solely on visual observations.

REFERENCES

Akbar, N., Dvorkin, J. and Nur, A., 1993, Relating P-wave attenuation to permeability: Geophysics, **58,** 1, 20-29.

Alexander, J., 1993, A discussion on the use of analogues for reservoir geology, *in* Ashton, M., Ed., Advances in Reservoir Geology: Geological Society Special Publications, 175-194.

Alexander, J. and Morris, S., 1994, Observations on experimental, nonchannelized, high-concentration turbidity currents and variations in deposits around obstacles: Journal of Sedimentary Research, **A64,** 4, 899-909.

Altan, S., Zhu, X., Walker, C., Dillon, G. and Brzostowski, M., 1999, Schiehallion - A 3D time lapse processing case history: 61st EAGE Conference and Technical Exhibition, EAGE, Expanded Abstracts, Paper 1-34.

Anderson, R. N., Gueren, G., He, W., Boulanger, A. and Mello, U., 1998, 4-D seismic reservoir simulation in a South Timbalier 295 turbidite reservoir: The Leading Edge, **17,** 10, 1416-1418.

Aritman, C. H., 1997, Repeatability study, - a step in the right direction: Ann. Internat. Mtg., Soc. Expl. Geophys., Expanded Abstracts, 96-99.

Ass'ad, J. M., Kusky, T. M., McDonald, J. A. and Tatham, R. K., 1992a, Implications of scale model seismic in the detection of natural fractures and microcracks: Journal of Seismic Exploration, **1,** 61-76.

Ass'ad, J. M., Tatham, R. H. and McDonald, J. A., 1992b, A physical model study of microcrack-induced anisotropy: Geophysics, **57,** 2, 1562-1570.

Bacharach, R. and Nur, A., 1997, Seismic detection of viscous contaminant using shallow seismic reflection: Stanford Rock Physics & Borehole Geophysics Project, Annual Report, Paper C5.

Bacharach, R. and Nur, A., 1998a, High-resolution shallow-seismic experiments in sand, Part I: Water table, fluid flow, and saturation: Geophysics, **63,** 4, 1225-1233.

Bacharach, R. and Nur, A., 1998b, Same wavelength GPR and ultra shallow seismic reflection on a river point bar: Sand stratigraphy and water table complexity: 67th Ann. Internat. Mtg., Soc. Expl. Geophys., Expanded Abstracts, 840-843.

Bacharach, R., Dvorkin, J. and Nur, A., 1998, High-resolution shallow-seismic experiments in sand, Part II: Velocities in shallow unconsolidated sand: Geophysics, **63,** 4, 1234-1240.

Batzle, M. and Wang, Z., 1992, Seismic properties of pore fluids: Geophysics, **57,** 11, 1396-1408.

Batzle, M., Christiansen, R. and Han, D., 1998, Reservoir recovery processes and geophysics: The Leading Edge, **17,** 10, 1444-1447.

Batzle, M., Han, D. and Castagna, J., 1996, Attenuation and velocity dispersion at seismic frequencies: 66th Ann. Mtg., Soc. Expl. Geophys., Expanded Abstracts, 1687-1690.

Batzle, M., Han, D. and Castangna, J., 1997, Seismic frequency measurement of velocity and attenuation: 67th Ann. Mtg., Soc. Expl. Geophys., Expanded Abstracts, 2030-2033.

Bear, J., 1972, Dynamics of fluids in porous media: American Elsevier Publishing Company.

Bell, D. W. and Shirley, D. J., 1980, Temperature variation of the acoustical properties of laboratory sediments: Journal of the Acoustical Society of America, **68,** 227-231.

Berg, R. R., 1975, Capillary Pressures in Stratigraphic Traps: American Association of Petroleum Geologists Bulletin, **59,** 939-956.

Biondi, B., Mavko, G., Mukerji, T., Ricket, J., Lumley, D., Deutsch, C., Gundeso, R. and Thiele, M., 1998, Reservoir monitoring: A multidisciplinary feasibility study: The Leading Edge, **17,** 10, 1404-1414.

Biot, M., 1956a, Theory of propagation of elastic waves in a fluid saturated porous solid; I-Low frequency range: Journal of the Acoustical Society of America, **28,** 168-178.

Biot, M., 1956b, Theory of propagation of elastic waves in a fluid saturated porous solid; II-High frequency range: Journal of the Acoustical Society of America, **28,** 179-191.

Biot, M. A., Willis, D. G., 1957, The elastic coefficients of the theory of consolidation: Journal of Applied Mechanics, **24,** 594-601.

Blangy, J. P., Strandenes, S., Moos, D. and Nur, A., 1993, Ultrasonic velocities in sands-revisited: Geophysics, **58,** 3, 344-356.

Blonk, B., Calvert, R. W., Koster, J. K. and van der Zee, G., 1999, Assessing the feasability of 4D-seismic reservoir monitoring: Journal of Petroleum Technology, **51,** 6, 32-33.

Boirel, S., Mukerji, T. and Mavko, G., 1997, Determination and quantification of the phenomena responsible for the drift between log and seismic measurements: Stanford Rock Physics & Borehole Geophysics Project, Annual Report, Paper E3.

Boschetti, F., Dentith, M. D. and List, R. D., 1996, A fractal-based algorithm for detecting first arrivals on seismic traces: Geophysics, **61, 4**, 1095-1102.

Boyle, F. A. and Chotiros, N. P., 1992, Experimental detection of a slow acoustic wave in sediment at shallow grazing angles: Journal of the Acoustical Society of America, **91,** 5, 2615-2619.

Brandt, H., 1960, Factors affecting compressional wave velocity in unconsolidated marine sand sediments: The Journal of the Acoustical Society of America, **32,** 2, 171-179.

Bridge, J. S. and Leeder, M. R., 1979, A simulation model of alluvial stratigraphy: Sedimentology, **26,** 617-644.

Brillouin, L., 1960, Wave propagation and group velocity: Academic Press.

Brown, A. R., 1996, Interpretation of three-dimensional seismic data: American Association of Petroleum Geologists.

Brown, R. J., Lawton, D. C. and Cheadle, S. P., 1991, Scaled physical modelling of anisotropic wave propagation: multioffset profiles over an orthorhombic medium: Geophysical Journal International, **107,** 693-702.

Bryerlee, J., 1978, Friction of rocks: Pure and Applied Geophysics, **116,** 615-626.

Buchanan, P. G. and McClay, K. R., 1991, Sandbox experiments of inverted listric and planar fault systems: Tectonophysics, **188,** 97-115.

Butler, D., Jarvis, K. and Knight, R., 1997, The use of bender elements to measure elastic wave velocities in unconsolidated materials: 67th Ann. Internat. Mtg., Soc. Expl. Geophys., Expanded Abstracts, 1016-1018.

Carcione, J. M., 1998, Viscoelastic effective rheologies for modelling wave propagation in porous media: Geophysical Prospecting, **46,** 249-270.

Carmichael, R. S., 1989, Practical handbook of physical properties of rocks and minerals: CRC Press.

Castagna, J. P. and Backus, M. M., Eds., 1993, Offset-dependent reflectivity - theory and practice of AVO analysis: *in* Investigations in Geophysics, Society of Exploration Geophysicsts.

Christiansen, R. and Batzle, M., 1998, Seismic signature of recovery processes: 67th Ann. Internat. Mtg., Soc. Expl. Geophys., Expanded Abstracts, 1060-1063.

Catalan, L., Xiaowen, F., Chatzis, I. and Dullien, F. A. L., 1992, An experimental study of secondary oil migration: AAPG Bulletin, **76,** 5, 638-650.

Chotiros, N. P., 1995, Biot model of sound propagation in water saturated sand: Journal of the Acoustical Society of America, **97,** 199-214.

Chotiros, N. P., 1998, Response to: "Comments on 'Biot model of sound propagation in water-saturated sand'": The Journal of the Acoustical Society of America, **103,** 5, 2726-2729.

Christensen, N. I. and Wang, H. F., 1985, The influence of pore pressure and confining pressure on dynamic elastic properties of Berea sandstone: Geophysics, **50,** 2, 207-213.

Clarke, R. H., 1979, Reservoir properties of conglomerates and conglomeratic sandstones: AAPG Bulletin, **63,** 5, 799-809.

Clarke, V. A., 1992, The effect of oil under in-situ conditions on the seismic properties of rocks: Geophysics, **57,** 7, 894-901.

Clay, C. S. and McNiel, H., 1955, An amplitude study on a seismic model: Geophysics, **20,** 4, 766-773.

Cloos, H., 1928, Experimente zur inneren tektonik: Centralblatt fur Mineralogie, **Abt,** B, 609-621.

Clowes, R. M., 1994, LITHOPROBE - Geoscience probing of inner space leads to new developments for mining exploration: Bull. C.I.M., **87,** 36-48.

Cobbold, P. R. and Castro, L., 1999, Fluid pressure and effective stress in sandbox models: Tectonophysics, **301,** 1-19.

Cobbold, P. R., Cosgrove, J. W. and Summers, J. M., 1971, Development of internal structures in deformed anisotropic rocks: Tectonophysics, **12,** 23-53.

Cockshell, C. D., O'Brien, G. W., McGee, A., Lovibond, R., Perincek, D. and Higgins, R. I., 1995, Western Otway Crayfish Group Troughs: APEA Journal, 385-404.

Colletta, B., Letouzey, J., Pinendo, R., Ballard, J. F. and Bale, P., 1991, Computerized X-ray tomography analysis of sandbox models: Examples of thin-skinned thrust systems: Geology, **19,** 1063-1067.

Davis, S., 1997, The expression of low-throw complex faults in surface seismic data: B.Sc. Hons. thesis, Curtin University of Technology.

Davy, P. and Cobbold, P. R., 1991, Experiments on shortening of a 4-layer model of the continental lithosphere: Tectonophysics, **188,** 1-25.

Del Grosso, V. A., 1974, New equation for the speed of sound in natural waters (with comparisons to other equations): Journal of the Acoustical Society of America, **56,** 4, 1084-1091.

Dellinger, J. and Vernik, L., 1992, Do core sample measurements record group of phase velocity: 62nd Ann. Internat. Mtg., Soc. Expl. Geophys., Expanded Abstracts, 662-665.

Dellinger, J. and Vernik, L., 1994, Do traveltimes in pulse-transmission experiments yield anisotropic group or phase velocities: Geophysics, **59,** 11, 1774-1779.

Dembicki, H. J. and Anderson, M. J., 1989, Secondary migration of oil: Experiments supporting efficient movement of seperate, bouyant oil phase along limited conduits: AAPG Bulletin, **73,** 8, 1018-1021.

Desrues, J., Chambon, R., Mokni, M. and Mazerolle, F., 1996, Void ratio evolution inside shear bands in triaxial sand specimens studied by computed tomography: Geotechnique, **46,** 3, 529-546.

Digranes, P., Stronen, L. K., Solheim, O. A. and Landro, M., 1999, 4D Seismic at the Gullfaks field - mapping the remaining oil: 61st EAGE Conference and Technical Exhibition, EAGE, Expanded Abstracts, Paper 5-17.

Domenico, S. N., 1976, Effect of brine-gas mixture on velocity in an unconsolidated sand reservoir: Geophysics, **41,** 5, 882-894.

Domenico, S. N., 1977, Elastic properties of unconsolidated porous sand reseroirs: Geophysics, **42,** 7, 1339-1368.

Donato, R. J., 1960a, Experimental investigation on the properties of Stonely waves: Geophysics, **3,** 441-443.

Donato, R. J., 1960b, Seismic model experiments on the shape and amplitude of the refracted wave: Geophysical Journal, **3,** 270-271.

Dooley, T. and McClay, K., 1997, Analog Modeling of Pull-Apart Basins: AAPG Bulletin, **81,** 11, 1804-1825.

Dula, W. F., 1991, Geometric models of listric normal faults and rollover folds: AAPG Bulletin, **75,** 1609-1625.

Dullien, F. A. L., 1992, Porous Media: Fluid Transport and Pore Structure: Academic Press.

Dvorkin, J. and Nur, A., 1993, Dynamic poroelasticity: A unified model with the squirt and the Biot mechanisms: Geophysics, **58,** 4, 524-533.

Dvorkin, J. and Nur, A., 1996, Elasticity of high-porosity sandstones: Theory for two North Sea data sets: Geophysics, **61,** 5, 1363-1370.

Dvorkin, J., Mavko, G. and Nur, A., 1995, Squirt flow in fully saturated rocks: Geophysics, **60,** 1, 97-107.

Dyer, B. C., Barkved, O., Jones, R. H., Folstad, P. G. and Rodriquez, S., 1999, Microseismic monitoring of the Valhall reservoir: 61st EAGE Conference and Technical Exhibition, EAGE, Expanded Abstracts, Paper 5-21.

East, R. J. R., Worthington, M. H. and Goulty, N. R., 1988, Convolutional back-projection imaging of physical models with crosshole seismic data: Geophysical Prospecting, **36,** 2, 139-148.

Eastwood, J., Johnston, D. H., Shyeh, J., Huang, X., Craft, K., Vauthrin, R. and Workman, R., 1999, Time-lapse-seismic processing and analysis: Journal of Petroleum Technology, **51,** 6, 28-30.

Eastwood, J., Johnston, D., Hwang, X., Craft, K. and Workman, R., 1998, Processing for robust time-lapse seismic analysis: Gulf of Mexico example, Lena Field: 68th Ann. Internat. Mtg., Soc. Expl. Geophys., Expanded Abstracts, 20-23.

Eastwood, J., Lebel, P., Dilay, A. and Blakeslee, S., 1994, Seismic monitoring of steam-based recovery of bitumen: The Leading Edge, **13,** 4, 242-251.

Ebrom, D. A. and McDonald, J. A., 1992, Sideswipe in a 3-D, 3-C model survey: The Leading Edge, **11,** 11, 45-49.

Ebrom, D. A. and Sheriff, R. E., 1992, Anisotropy and reservoir development, *in* Sheriff, R. E., Ed., Reservoir Geophysics: Society of Exploration Geophysics, 355-361.

Edwards, D. A., Leeder, M. R., Best, J. L. and Pantin, H. M., 1994, On experimental reflected density currents and the interpretation of certain turbidites: Sedimentology, **41,** 437-461.

Ehrichs, E. E., Jaeger, H. M., Karczmar, G. S., Knight, J. B., Kuperman, V. Y. and Nagel, S. R., 1995, Granular convection observed by magnetic resonance imaging: Science, **267,** 1632-1634.

Eiken, O., Waldemar, P., Schonewille, M., Haugen, G. U. and Duijndam, A., 1999, A proven concept for acquiring highly repeatable towed streamer seismic data: 61st EAGE Conference and Technical Exhibition, EAGE, Expanded Abstracts, Paper 1-40.

Elliott, S. E. and Wiley, B. F., 1975, Compressional velocities of partially saturated, unconsolidated sands: Geophysics, **40,** 6, 949-954.

Emmons, R., 1969, Strike-slip rupture patterns in sand models: Tectonophysics, **7,** 171-187.

Endres, A. L. and Knight, R. J., 1997, Incorporating pore geometry and fluid pressure communication into modeling the elastic behavior of porous rocks: Geophysics, **62,** 1, 106-117.

Evans, B. J., 1997, A handbook for seismic data acquisition in exploration: Society of Exploration Geophysicists.

Evans, B. J., Oke, B. F., Urosevic, M. and Chakraborty, K., 1995, A comparison of physical model with field data over Oliver Field, Vulcan Graben: APEA Journal, **35,** 1, 26-43.

Farouq Ali, S. M., Rojas, G., Zhu, T. and Dyer, S., 1991, Scaled model studies of carbon dioxide floods: SPE Reservoir Engineering, Paper 18751, May 1991, 273-283.

Forel, D. and Gardner, G. H. F., 1988, A three-dimensional perspective on two-dimensional dip moveout: Geophysics, **53,** 5, 604-610.

French, W. S., 1974, Two-dimensional and three-dimensional migration of model-experiment reflection profiles: Geophysics, **39,** 265-277.

Gapais, D., Fiquet, G. and Cobbold, P., 1991, Slip system domains 3. New insights in fault kinematics from plane strain sandbox experiments: Tectonophysics, **188,** 143-157.

Gardener, G. H. F., Wyllie, M. R. J. and Droschak, D. M., 1964, Effects of pressure and fluid saturation on the attenuation of elastic waves in sands: Journal of Petroleum Technology, **26,** 2, 189-198.

Gartrell, A. P., 1993, Sandbox analogue models of transfer zone formation above stepped listric detatchment faults: B.Sc. Hons. thesis, University of Western Australia.

Gartrell, A. P., 1997, Evolution of rift basins and low-angle detachments in multilayer analog models: Geology, **25,** 7, 615-618.

Gassman, F., 1951, Elastic waves through a packing of spheres: Geophysics, **16,** 673-685.

Ge, H. and Jackson, M. P. A., 1998, Physical modeling of structures formed by salt withdrawals: Implications for deformation caused by salt dissolution: AAPG Bulletin, **82,** 2, 228-250.

Ge, H., Jackson, M. P. A. and Vendeville, B. C., 1997, Kinematics and dynamics of salt tectonics driven by progradation: AAPG Bulletin, **81,** 3, 398-423.

Geertsma, J., Croes, G. A. and Schwarz, N., 1956, Theory of dimensionally scaled models of petroleum reservoirs: Petroleum Transactions, American Institute of Mining, Metallurgical , and Petroleum Engineers, **207,** 118-127.

Gist, G. A., 1994, Fluid effects on velocity and attenuation in sandstones: Journal of the Acoustical Society of America, **96,** 2, 1158-1173.

Green, D. H. and Esquivel-Sirvent, R., 1999, Acoustic behaviour at the fluid/solid transition of kaolinite suspension: Geophysics, **64,** 1, 88-92.

Guerin, W. H. G., Anderson, R. and Mello, U. T., 1998, Time-dependent reservoir characterization of the LF sand in the South Eugene Island 330 Field, Gulf of Mexico: The Leading Edge, **17,** 10, 1434-1438.

Guglielmo, G. J., Jackson, M. P. A. and Vendeville, B., 1997, Three-Dimensional Visualization of Salt Walls and Associated Fault Systems: AAPG Bulletin, **81,** 1, 46-61.

Gullaksen, E. M., Rekdal, T., Widmaier, M. and Strandenes, S., 1999, Evaluation of changes in acquisition for time lapse surveys based on modelling: 61st EAGE Conference and Technical Exhibition, EAGE, Expanded Abstracts, Paper 1-39.

Hamilton, E. L., 1971, Elastic properties of marine sediments: Journal of Geophysical Research, **76,** 2, 579-604.

Han, D., 1994, Weak cementation effect on velocities of sands: 64th Ann. Internat. Mtg., Soc. Expl. Geophys., Expanded Abstracts, 1069-1072.

Han, D., Nur, A. and Morgan, D., 1986, Effects of porosity and clay content on wave velocities in sandstones: Geophysics, **51,** 11, 2093-2107.

Hanmer, S., Corrigan, D. and Ganas, A., 1996, Orientation of nucleating faults in anisotropic media: insights from three-dimensional deformation experiments: Tectonophysics, **267,** 275-290.

Harris, L. B. and Cobbold, P. R., 1985, Development of conjugate shear bands during bulk simple shearing: Journal of Structural Geology, **7,** 37-44.

Harris, L. B., Higgins, R. I., Dentith, M. C. and Middleton, M. F., 1994, Transtensional analogue modelling applied to the Perth Basin, Western Australia: *The Sedimentary Basins of Western Australia*: Proceedings Petroleum Exploration Society Australia, Expanded Abstracts, 801-809.

Hashin, Z. and Shtrikman, S., 1963, A variational approach to the elastic behavior of multiphase materials: J. Mech. Phys. Solids, **11,** 127-140.

Hempton, M. and Neher, K., 1986, Experimental fracture, strain and subsidence patterns over en echelon strike-slip faults: Implications for the structural evolution of pull-apart basins: Journal of Structural Geology, **8,** 597-605.

Hickey, C. J. and Sabatier, J. M., 1997, Choosing Biot parameters for modeling water-saturated sand: Journal of the Acoustical Society of America, **102,** 3, 1480-1484.

Higgins, R. I. and Harris, L. B., 1997, The effect of cover composition on extensional faulting above re-activated basement faults: results from analogue modelling: Journal of Structural Geology, **19,** 89-98.

Hirsche, K., 1998, Time-lapse seismic monitoring of a SE Asian Field - a case history: 68th Ann. Internat. Mtg., Soc. Expl. Geophys., Expanded Abstracts, 24-26.

Horsefield, W. T., 1977, An experimental approach to basement controlled faulting: Geologie en Mijnbouw, **56,** 363-370.

Hounsfield, G. N., 1973, Computerized transverse axial scanning (tomography): British Journal of Radiology, **46,** 1016-1022.

Hsu, C.-J. and Schoenberg, M., 1990, Characterization of anisotropic elastic wave behavior in media with parallel fractures: 60th Ann. Internat. Mtg., Soc. Expl. Geophys., Expanded Abstracts, 1410-1412.

Hughes, S. R., Alexander, J. and Druitt, T. H., 1995, Anisotropic grain fabric: volcanic and laboratory analogues for turbidites, *in* Hartley, A. J. and Prosser, D. J., Eds., Characterization of Deep Marine Clastic Systems: Geological Society Special Publication, 51-62.

Hwang, X., Meister, L. and Workman, R., 1998, Improvement on the Quantitative Seismic History Matching: 68th Ann. Internat. Mtg., Soc. Expl. Geophys., Expanded Abstracts, 36-39.

Ivakin, B. N., 1966, Methods of seismic modelling: Studia Geophysica ey Geodaetica, **10,** 253-258.

Jack, I. G., 1998, Time-lapse seismic in reservoir management: Society of Exploration Geophysicists.

Jaeger, H. M., Nagel, S. R. and Behringer, R. P., 1996, The physics of granular materials: Physics Today, **49,** 4, 32-38.

Jaeger, J. C. and Cook, N. G. W., 1979, Fundamental Rock Mechanics: Cambridge University Press.

Johnson, D. L. and Plona, T. L., 1982, Acoustic slow waves and the consolidation transition: Journal of the Acoustical Society of America, **72,** 2, 556-565.

Johnstad, S. E., Uden, R. C. and Dunlop, K. N. B., 1993, Seismic reservoir monitoring over the Oseberg field: First Break, **11,** 5, 177-185.

Jones, S. M., Astin, T. R. and McCann, C., 1997, The effect of degree of saturation on ultrasonic velocity and attenuation in sandstones: 67th Ann. Internat. Mtg., Soc. Expl. Geophys., Expanded Abstracts, 1023-1026.

Jones, T. D., 1986, Pore fluids and frequency dependent wave propagation in rocks: Geophysics, **51,** 10, 1939-1953.

Kallweit, R. S. and Wood, L. C., 1982, The limits of resolution of zero-phase wavelets: Geophysics, **47,** 7, 1035-1046.

Katahara, K. W., 1996, Clay mineral elastic properties: 66th Ann. Mtg., Soc. Expl. Geophys., Expanded Abstracts, 1691-1694.

Kaufman, S. and Roever, W. L., 1951, Laboratory studies of transient elastic waves, *in* Ebrom, D. A. and McDonald, J. A., Eds., Seismic Physical Modeling: Society of Exploration Geophysics, 103-111.

Keary, P. and Brooks, M., 1991, An Introduction to Geophysical Exploration: Blackwell Scientific Publications.

Keep, M. and McClay, K. R., 1997, Analogue modelling of multiphase rift systems: Tectonophysics, **273,** 239-270.

Kerr, H. G. and White, N., 1992, Laboratory testing of an automatic method for determining normal fault geometry at depth: Journal of Structural Geology, **14,** 873-885.

Khaksar, A. and Griffiths, C., 1999, Acoustic velocities in partially saturated sandstones versus effective stress: 61st EAGE Conference and Technical Exhibition, EAGE, Expanded Abstracts, Paper 2-04.

Kimber, K. D. and Farouq Ali, S. M., 1991, Scaled physical modeling of steam-injection experiments: SPE Reservoir Engineering, Paper 18083, August 1991, 467-469.

Klimentos, T. and McCann, C., 1988, Why is the Biot slow compressional wave not observed in real rocks?: Geophysics, **53,** 12, 1605-1609.

Klimentos, T. and McCann, C., 1990, Relationships among compressional wave attenuation, porosity, clay content, and permeability in sandstones: Geophysics, **55,** 8, 998-1014.

Koefoed, O., 1981, Aspects of vertical seismic resolution: Geophysical Prospecting, **29,** 21-30.

Koopman, A., Speksnider, A. and Horsefield, W. T., 1987, Sandbox model studies of inversion tectonics: Tectonophysics, **137,** 379-388.

Kortekaas, T. F. M., 1983, Water/oil displacement characteristics in cross-bedded reservoir zones: Society of Petroleum Engineers, Paper 12112, 1-7.

Kowallis, B. J., Jones, L. E. A. and Wang, H. F., 1984, Velocity-porosity-clay content systematics of poorly consolidated sandstones: Journal of Geophysical Research, **89,** B12, 10355-10364.

Kowalski, M. B., Geller, J. T., Seifert, P. K., Nihei, K. T., Gritto, R., Peterson, J. E. J. and Myer, L., 1998, Acoustic visibility of immiscible liquids in poorly consolidated sand: 68th Ann. Internat. Mtg., Soc. Expl. Geophys., Expanded Abstracts, 1041-1044.

Krantz, R. W., 1991, Measurement of friction coefficients and cohesion for faulting and fault reactivation in laboratory models using sand and sand mixtures: Tectonophysics, **188,** 203-207.

Landro, M., 1999, Discrimination between pressure and fluid saturation changes from time-lapse seismic data: 68th Ann. Internat. Mtg., Soc. Expl. Geophys., Expanded Abstracts, 1651-1654.

Lemon, N. M. and Mahmood, T., 1994, Two and three dimensional analogue modelling of extensional fault systems with application to the North West Shelf, Western Australia: APEA Journal, **34,** 1, 555-565.

Leslie, D., 1998, The effects of high-velocity layering on seismic wave propagation: BSc. Hons. thesis, Curtin University of Technology.

Levin, F. K. and Robinson, D. J., 1968, Scattering by a random field of surface scatterers: Geophysics, **34,** 170-179.

Leurer, K. C. and Dvorkin, J., 1998, Intergranular squirt flow in unconsolidated sediment: Viscous cement model: 68th Ann. Internat. Mtg., Soc. Expl. Geophys., Expanded Abstracts, 1028-1031.

Lindsey, J. P., 1989, The Fresnel zone and its interpretive significance: The Leading Edge, **8,** 10, 33-39.

Liu, X. and Nur, A., 1996, A new experimental method for studying velocity dispersion in rocks: 66th Ann. Mtg., Soc. Expl. Geophys., Expanded Abstracts, 1683-1686.

Lorenz, J. C., 1999, Stress-sensitive reservoirs: Journal of Petroleum Technology, **51,** 1, 61-63.

Lumley, D., 1993, Seismic monitoring of fluid flow: Ph.D. thesis, Stanford University.

Lumley, D. E., Behrens, R. A. and Wang, Z., 1997, Assessing the technical risk of a 4-D seismic project: The Leading Edge, **16,** 9, 1287-1291.

Lynn, H. B. and Deregowski, S., 1981, Dip Limitations on migrated sections as a function of line length and recording time: Geophysics, **46,** 10, 1392-1397.

Macdonald, C., Davis, P. M. and Jackson, D. D., 1987, Inversion of reflection traveltimes and amplitudes: Geophysics, **52,** 5, 606-617.

MacLeod, M. K., Hadley, M. J., Reynolds, K. J. and Tura, A., 1999, Multicomponent analysis of ocean-bottom-cable data: Journal of Petroleum Technology, **51,** 6, 42-42.

Mahmood, T., 1996, ATLAS 3D Analogue Modelling of Extensional Fault Systems plus field applications: CDROM, University of Adelaide.

Mandl, G., 1988, Mechanics of Tectonic Faulting. Models and Basic Concepts: Elsevier.

Mandle, G., Jong, L. N. J. D. and Maltha, A., 1977, Shear zones in granular material: Rock Mechanics, **9,** 95-144.

Marion, D., 1990, Acoustical, mechanical and transport properties of sediments and granular materials: PhD thesis, Stanford University.

Marion, D. and Nur, A., 1991, Pore-filling material and its effect on velocity in rocks: Geophysics, **56,** 2, 225-230.

Marion, D., Mukerji, T. and Mavko, G., 1994, Scale effects on velocity dispersion: From ray to effective medium theories in stratified media: Geophysics, **59,** 10, 1613-1619.

Marion, D., Nur, A., Yin, H. and Han, D., 1992, Compressional velocity and porosity in sand-clay mixtures: Geophysics, **57,** 4, 554-563.

Mavko, G., 1998a, Rock physics for geophysical reservoir characterization and recovery monitoring: Course Notes, Stanford University.

Mavko, G. and Jizba, D., 1991, Estimating grain-scale fluid effects on velocity dispersion in rocks: Geophysics, **56,** 12, 1940-1949.

Mavko, G. and Mukerji, T., 1995, Seismic pore space compressability and Gassman's relation: Geophysics, **60,** 6, 1743-1749.

Mavko, G., Chan, C. and Mukerji, T., 1995, Fluid substitution: Estimating changes in Vp without knowing Vs: Geophysics, **60,** 6, 1750-1755.

Mavko, G., Mukerji, T. and Dvorkin, J., 1998b, The Rock Physics Handbook: Cambridge University Press.

McClay, K. and Dooley, T., 1995, Analogue models of pull-apart basins: Geology, **23,** 711-714.

McClay, K. R., 1989, Analogue Models of Inversion Tectonics., *in* Cooper, M. and Williams, G. D., Eds., Inversion Tectonics: Geological Society of London, 41-59.

McClay, K. R. and Buchanan, P. G., 1992, Thrust Faults in Extensional Basins, *in* McClay, K. R., Eds., Thrust Tectonics: Chapman and Hall, 93-104.

McGeary, R. K., 1961, Mechanical packing of spherical particles: Journal American Ceramics Society, **44,** 513-522.

Meckel, L. D., 1999, Exploration issues concerning stratigraphic onlap traps in turbidites: 61st EAGE Conference and Technical Exhibition, EAGE, Expanded Abstracts, Paper 5-49.

Medwin, H., 1975, Speed of sound in water: A simple equation for realistic parameters: Journal of the Acoustical Society of America, **58,** 6, 1318-1319.

Melia, P. J. and Carson, R. L., 1984, An experimental test of P-wave anisototropy in stratified media: Geophysics, **44,** 374-378.

Mese, A. I. and Tutuncu, A. N., 1996, An experimental investigation for relationship between physicohemical and acoustic properties of pure kaolinite and Pierre shale: 66th Ann. Mtg., Soc. Expl. Geophys., Expanded Abstracts, 1695-1698.

Meunier, J. and Huguet, F., 1998, Cere-la-Ronde: A laboratory for time-slice seismic monitoring in Paris Basin: The Leading Edge, **17,** 10, 1388-1394.

Mitchem, R. M. and Vail, P. R., 1977, Seismic stratigraphy interpretation procedure, *in* Payton, C. E., Ed., Seismic Stratigraphy - applications to hydrocarbon exploration. Memoir 26: American Association of Petroleum Geologists, 135-144.

Molyneux, J. B. and Schmitt, D. R., 1997, Semi-automatic transit time determination applied to ultrasonic laboratory measurements: 67th Ann. Mtg., Soc. Expl. Geophys., Expanded Abstracts, 1012-1015.

Morrow, N. R., 1971, Small-scale packing heterogeneity in porous sedimentary rocks: AAPG Bulletin, **55,** 3, 514-522.

Mueller, M. C., 1992, Using shear waves to predict lateral variability in vertical fracture intensity: The Leading Edge, **11,** 2, 29-35.

Mukerji, T., Mavko, G., Mujica, D. and Lucet, N., 1995, Scale-dependent seismic velocity in heterogeneous media: Geophysics, **60,** 4, 1222-1233.

Murphy, W. E., 1984, Acoustic measures at partial gas saturation in tight sandstones: Journal of Geophysical Research, **89,** B13, 11 549-11 559.

Murphy, W. F., Winkler, K. W. and Kleinberg, R. L., 1986, Acoustic relaxation in sedimentary rocks: Dependence on grain contacts and fluid saturation: Geophysics, **51,** 3, 757-766.

Nur, A., 1997, Rock Physics and 4D Seismic for Improved Oil Recovery: 67th Ann. Internat. Mtg., Soc. Expl. Geophys, Expanded Abstracts, 1009-1011.

Nur, A., Mavko, G., Dvorkin, J. and Galmudi, D., 1998, Critical porosity: A key to relating physical properties to porosity in rocks: The Leading Edge, **17,** 3, 357-362.

O'Brien, P. N. S., 1955, Model Seismology - The critical refraction of elastic waves: Geophysics, **20,** 227-242.

O'Brien, P. N. S. and Symes, M. P., 1971, Model seismology: Reports on Progress in Physics, **34,** 697-764.

Palmer, I. D. and Traviolia, M. L., 1980, Attenuation by squirt flow in undersaturated gas sands: Geophysics, **45,** 12, 1780-1792.

Palmer, N. C., 1999, A comparison of ocean-bottom seismic (OBS) with conventional marine seismic data: BSc. Hons. thesis, Curtin University of Technology.

Peraldi, R. and Clement, A., 1972, Digital processing of refraction data - study of first arrivals: Geophysical Prospecting, **20,** 529-548.

Peselnick, L. and Outerbridge, W. F., 1961, Internal friction in shear and shear modulus of Solenhofen limestone over a frequency range of 10^7 cycles per second: Journal of Geophysics Research, **66,** 581-588.

Pettingill, H. S., 1998, Lessons learned from 43 giant turbidite fields: Oil and Gas Journal, Oct 12, 93-95.

Plona, T. J., 1980, Observation of a second bulk compressional wave in a porous medium at ultrasonic frequencies: Applied Physics Letters, **36,** 4, 259-261.

Poet, B. F. and Rasolofosaon, P. N. J., 1993, Measurement of broad band intrinsic ultrasonic attenuation and dispersion in solids with laser techniques: Journal of the Acoustical Society of America, **97,** 1286-1292.

Prasad, M., 1997, Proposed use of acoustical microscopy to petrophysical studies of reservoir rocks: Stanford Rock Physics & Borehole Geophysics Project, Annual Report, Paper H1.

Pullin, N. E., Jackson, R. K., Mathews, L. W., Thornburn, R. F., Hirsche, W. K. and den Boer, L. D., 1987, 3-D Seismic Imaging of Heat Zones at an Athabasca Tar Sands Thermal Pilot: 57th Ann. Internat. Mtg., Soc. Expl. Geophys., Expanded Abstracts, 391-394.

Purnell, G. W., 1986, Observations of wave velocity and attenuation in two phase media: Geophysics, **51,** 12, 2193-2199.

Ramberg, H., 1967, Gravity, Deformation and the Earth's Crust: Academic Press.

Rapoport, L. A., Carpenter, C. W. J. and Leas, W. J., 1958, Laboratory studies of five-spot waterflood performance: Petroleum Transactions, American Institute of Mining, Metallurgical , and Petroleum Engineers, **213,** 113-120.

Rayleigh, L., 1945, The theory of sound: Dover Publcations.

Raynaud, S., Fabre, D., Mazerolle, F., Geraud, Y. and Latiere, H. J., 1989, Analysis of the internal structure of rocks and characterization of mechanical deformation by a non-destructive method: X-ray tomodensitometry: Tectonophysics, **159,** 149-159.

Richard, P. and Krantz, R. W., 1991, Experiments on fault reactivation in strike-slip mode: Tectonophysics, **188,** 117-131.

Richard, P., Naylor, M. and Koopman, A., 1995, Experimental models of strike-slip tectonics: Petroleum Geosciences, **1,** 71-78.

Richards, M. A., Jones, D. L., Duncan, R. A. and DePaolo, D. J., 1991, A mantle plume initiation model for the Wrangellia flood basalt and other oceanic plateaus: Science, **254,** 263-266.

Rimoldi, B., Alexander, J. and Morris, S., 1996, Experimental turbidity currents entering density-stratified water: analogues for turbidites in Mediterranean hypersaline basins: Sedimentology, **43,** 527-540.

Rio, P., Mukerji, T., Mavko, G. and Marion, D., 1996, Velocity dispersion and upscaling in a laboratory-simulated VSP: Geophysics, **61,** 2, 584-593.

Ross, C. P., Cunningham, G. P. and Weber, D. P., 1996, Inside the crossequalization black box: The Leading Edge, **15,** 11, 1233-1240.

Rossetti, F., Ranalli, G. and Faccenna, C., 1999, Rheological properties of paraffin as an analogue material for viscous crustal deformation: Journal of Structural Geology, **21,** 413-417.

Rozemond, H. J. and Simensen, G. W., 1999, Design and execution of the Gannet 4D time lapse survey: 61st EAGE Conference and Technical Exhibition, EAGE, Expanded Abstracts, Paper 1-33.

Savic, M., 1995, Ultrasonic scattering from a hydraulic fracture: Theory, Computation and Experiment: PhD thesis, Delft University of Technology.

Schmitt, D. R., 1999, Seismic attributes for monitoring of a shallow heated heavy oil reservoir: Geophysics, **64,** 2, 368-377.

Schruers, G., 1994, Experiments on strike-slip faulting and block rotation: Geology, **22,** 567-570.

Scott, C. R., 1980, An Introduction to Soil Mechanics and Foundations: Applied Science Publishers Ltd.

Sengputa, M. and Mavko, G., 1998, Reducing uncertainties in saturation scales using fluid flow models: 68th Ann. Internat. Mtg., Soc. Expl. Geophys., Expanded Abstracts, 1012-1015.

Shatilo, A., 1996, Relationship between ultrasonic P-wave attenuation and porosity, permeability and clay content in Glenn Pool Sandstone: 66th Ann. Internat Mtg., Soc. Expl. Geophys., Expanded Abstracts, 1679-1682.

Sheriff, R. E., 1977, Limitations on resolution of seismic reflections and geologic detail derivable from them, *in* Payton, C. E., Ed.., Seismic Stratigraphy - Application to Hydrocarbon Exploration: American Association of Petroleum Geologists, 3-14.

Sheriff, R. E., 1980, Seismic Stratigraphy: International Human Resources Development Corporation.

Sheriff, R. E., 1994, Encyclopedic Dictionary of Exploration Geophysics: Society of Exploration Geophysics.

Sheriff, R. E. and Geldart, L. P., 1982, Exploration seismology Volume 1; History, theory, and data acquisition: Cambridge University Press.

Sheriff, R. E. and Geldart, L. P., 1983, Exploration Seismology Volume 2: Data Processing and Interpretation: Cambridge University Press.

Sherlock, D. H., 1998, Seismic reflections without an acoustic impedance contrast: AAPG Annual Convention, Am. Assoc. Pet. Geol., Expanded Abstracts, A597.

Sherlock, D., McKenna, J. and Evans, B., 2000, Time-lapse 3-D seismic physical modelling: Exploration Geophysics, submitted.

Sherlock, D. H. and Evans, B. J., 1999, Time-lapse 3-D seismic with analogue sandbox models: 68th Ann. Internat. Mtg., Soc. Expl. Geophys., Expanded Abstracts, 1683-1686.

Shirley, D. J., 1978, An improved shear-wave transducer: Journal of the Acoustical Society of America, **63,** 5, 1643-1645.

Shirley, D. J. and Hampton, L. D., 1978, Shear-wave measurements in laboratory sediments: Journal of the Acoustical Society of America, **63,** 2, 607-613.

Shumway, G., 1958, Sound velocity vs. temperature in water-saturated sediments: Geophysics, **23,** 3, 494-505.

Sims, D., Ferrill, D. A. and Stamatakos, J. A., 1999, Role of a ductile decollement in the development of pull-apart basins: Experimental results and natural examples: Journal of Structural Geology, **21,** 533-554.

Sneider, R. M., 1997, Reservoir characterization for E & P: Course Notes, Robert M. Sneider Exploration, Inc.

Soucemarianandin, A., Bourlion, M. and Lenormand, R., 1989, Ultrasonic saturation mapping in porous media: SPE Reservoir Engineering, Paper 16953, May 1989, 194-200.

Spencer, J. W., 1981, Stress relaxations at low frequencies in fluid-saturated rocks: Attenuation and modulus dispersion: Journal of Geophysics Research, **86,** 1803-1812.

Stephen, K. D. and Clark, J. D., 1999, Outcrop based stochastic modelling of turbidite amalgamation and its effects on reservoir flow properties: 61st EAGE Conference and Technical Exhibition, EAGE, Expanded Abstracts, Paper 5-54.

Stoll, R. D., 1977, Acoustic waves in ocean sediments: Geophysics, **42,** 4, 715-725.

Stoll, R. D., 1989, Sediment Acoustics: Springer-Verlag.

Stoll, R. D., 1998, Comments on "Biot model of sound propagation in water-saturated sand": The Journal of the Acoustical Society of America, **103,** 5, 2723-2725.

Tadepalli, S., 1995, 3-D AVO Analysis - Physical Modelling Study: Ph.D thesis, University of Houston.

Talley, D. J., Davis, T. L., Benson, R. D. and Roche, S. L., 1998, Dynamic reservoir characterization of Vacuum Field: The Leading Edge, **17,** 10, 1396-1402.

Talwani, P., Nur, A. and Kovak, R. L., 1973, Compressional and shear wave velocities in granular materials to 2.5 kilobars: Journal of Geophysical Research, **78,** 29, 6899-6909.

Tatham, R. H., Goolsbee, D. V., Massell, W. F. and Nelson, H. R., 1983, Seismic shear-wave observations in a physical model experiment: Geophysics, **48,** 6, 688-701.

Thomas, M. M. and Clouse, J. A., 1995, Scaled Physical Model of Secondary Oil Migration: AAPG Bulletin, **79,** 1, 19-29.

Thompson, T., 1998, Stress-induced anisotropy: The effects of stress on seismic wave propagation: BSc. Hons. thesis, Curtin University of Technology.

Toksoz, M. N., Cheng, C. H. and Timur, A., 1976, Velocities of seismic waves in porous rocks: Geophysics, **41,** 4, 621-645.

Toksoz, M. N. and Johnston, D. H., Eds., 1981, Seismic Wave Attenuation: Society of Exploration Geophysics.

Toksoz, M. N., Johnston, D. H. and Timur, A., 1979, Attenuation of seismic waves in dry and saturated rocks: 1. Laboratory measurements: Geophysics, **44,** 4, 681-690.

Tron, V. and Brun, J., 1991, Experiments on oblique rifting in brittle-ductile systems: Tectonophysics, **188,** 71-84.

Tucker, P. M. and Yorston, H. J., 1973, Pitfalls in Seismic Interpretation: Society of Exploration Geophysicists.

Tura, A. and Lumley, D. E., 1999, Estimating pressure and saturation changes from time-lapse AVO data: 68th Ann. Internat. Mtg., Soc. Expl. Geophys., Expanded Abstracts, 1655-1658.

Uren, N. F., Gardener, G. H. F. and McDonald, J. A., 1991, Anisotropic wave propagation and zero offset migration: Exploration Geophysics, **22,** 405-410.

Urosevic, M., Evans, B. J., Juhlin, C. and McDonald, J. A., 1995, Subsurface imaging in the presence of anisotropy, fractures and associated gas pockets: 3rd SEGJ/SEG Internat. Symp. Geotomography, Expanded Abstracts, 408-415.

Van De Graaff, W. J. E. and Ealey, P. J., 1989, Geological modeling for simulation studies: AAPG Bulletin, **73,** 11, 1436-1444.

Vendeville, B. 1997, Personal Communication, University of Texas at Austin.

Vendeville, B. and Cobbold, P. R., 1988, How normal faulting and sedimentation interact to produce listric fault profiles and stratigraphic wedges: Journal of Structural Geology, **10,** 7, 649-659.

Vendeville, B., Cobbold, P. R., Davy, P., Broun, J. P. and Choukroune, P., 1987, Physical models of extensional tectonics at various scales, *in* Coward, M. P., Dewey, J. F. and Hancock, P. L., Eds., Continental Extensional Tectonics: Geological Society of London, Special Publication, 97-107.

Vestrum, R. W., 1994, Group- and phase-velocity inversions for the general anisotropic stiffness tensor: M.Sc. thesis, The University of Calgary.

Vinegar, H. J., 1986, X-ray CT and NMR imaging of rocks: Journal of Petroleum Technology, **38,** 257-259.

Wang, Z., Cates, M. E. and Langan, R. T., 1998a, Seismic monitoring of a CO_2 flood in a carbonate reservoir: A rock physics study: Geophysics, **63,** 5, 1604-1617.

Wang, Z., Hirsche, W. K. and Sedgewick, G., 1991, Seismic monitoring of water floods? - A petrophysical study: Geophysics, **56,** 10, 1614-1623.

Walton, C., 1996, Recovering the elastic parameters of multi-layered transversely isotropic media: B.Sc. Hons. thesis, Curtin University of Technology.

Wang, Z., Nur, A. M. and Batzle, M. M., 1990, Acoustic velocities in petroleum oils: Journal of Petroleum Technology, **45,** 2, 192-200.

Wang, Z., Wang, H. and Cates, M. E., 1998b, Elastic properties of solid clays: 67th Ann. Internat. Mtg., Soc. Expl. Geophys., Expanded Abstracts, 1045-1048.

Waters, K. H., 1987, Reflection Seismology: A tool for energy resource exploration: John Wiley and Sons, Inc.

White, N., 1992, A method for automatically determining normal fault geometry at depth: Journal of Geophysical Research, **97,** 1715-1733.

Widess, M. B., 1973, How thin is a thin bed?: Geophysics, **38,** 6, 1176-1180.

Williams, R. G., Leggott, R. and Skinner, M., 1999, Statistical repositioning of 4D seismic data for improved repeatability: 61st EAGE Conference and Technical Exhibition, EAGE, Expanded Abstracts, Paper 1-36.

Winkler, K., 1985, Dispersion analysis of velocity and attenuation in Berea Sandstone: Journal of Geophysical Research, **90,** B8, 6793-6800.

Winkler, K. W., 1983, Frequency dependent ultrasonic properties of high porosity sandstones: Journal of Geophysical Research, **88,** B11, 9493-9499.

Winkler, K. W., 1986, Estimates of velocity dispersion between seismic and ultrasonic frequencies: Geophysics, **51,** 1, 183-189.

Withjack, M. O., Islam, Q. T. and LaPointe, P. R., 1995, Normal faults and their hanging-wall deformation: an experimental study: AAPG Bulletin, **79,** 1, 1-18.

Wyllie, M. R. J., Gregory, A. R. and Gardener, L. W., 1956, Elastic wave velocities in heterogeneous and porous media: Geophysics, **21,** 1, 41-70.

Wyllie, M. R. J., Gregory, A. R. and Gardner, G. H. F., 1958, An experimental investigation of factors affecting elastic wave velocities in porous media: Geophysics, **23,** 3, 459-493.

Xiau, H. and Suppe, J., 1992, Origin of rollover: AAPG Bulletin, **76,** 509-529.

Zhang, M., Ebrom, D. A., McDonald, J. A. and Tatham, R. H., 1996, Comparison of experimental velocity measurements with theoretical results in a solid-solid composite material: Geophysics, **61,** 1429-1435.

Yilmaz, Ö., 1987, Seismic Data Processing: Soc. Expl. Geophys.

Yu, G., 1985, Offset-amplitude variation and controlled-amplitude processing: Geophysics, **50,** 12, 2697-2708.

APPENDIX

Summary of parameters that influence velocity in unconsolidated sand

Porosity	Velocity increases as porosity decreases
Permeability	Decrease in permeability shifts velocity dispersion to lower frequencies
Mineralogy	Minor influence in unconsolidated sand
Sorting	Poorer sorting increases velocity, decreases porosity
Packing	Tighter packing increases velocity, decreases porosity
Grain Shape	Angular grains have higher shear modulus, higher shear velocity (smaller grains tend to be more angular)
Clay Content	Small amount of clay causes small increase in Vp, large increase in Vs
Pressure:	
Confining	Increase in confining pressure increases velocity, reduces dispersion
Pore	Increase in pore pressure decreases velocity
Effective	= confining pressure – pore pressure
Temperature	Change in velocity parallels change in fluid velocity Water velocity increases with temperature up to 80°C Oil velocity decreases with increasing temperature
Oil	Increase in oil content decreases velocity, increases dispersion
Gas	Small amount of gas greatly decreases velocity, increases attenuation